Engineering
Library
620.5
U58
B91j

U. S. DEPARTMENT OF COMMERCE

BUREAU OF STANDARDS JOURNAL OF RESEARCH

Vol. 6 APRIL, 1931 No. 4

CONTENTS

RP. No.	TITLE AND AUTHOR	Page
292.	Variations caused in heating curves of glass by heat treatment. A. Q. Tool and C. G. Eichlin	523
293.	On the vibration of U bars. G. H. Keulegan	553
294.	Laundry "winter damage." John B. Wilkie	593
295.	The determination of the alpha cellulose content and copper number of paper. John O. Burton and Royal H. Rasch	603
296.	The structure of the arc spectrum of zirconium. C. C. Kiess and Harriet K. Kiess	621
297.	Radiation from metals bombarded by low-speed electrons. F. L. Mohler and C. Boeckner	673
298.	Pipe-line currents and soil resistivity as indicators of local corrosive soil areas. E. R. Shepard	683
299.	Two new crystalline difructose anhydrides from hydrolyzed inulin. Richard F. Jackson and Emma McDonald	709
300.	Measurement of fiber diameters by the diffraction method. H. J. McNicholas and H. J. Curtis	717
301.	Wind pressure on a model of a mill building. Hugh L. Dryden and George C. Hill	735
302.	Stabilization of boric acid buffers by aeration. Edna H. Fawcett and S. F. Acree	757

BUREAU OF STANDARDS JOURNAL OF RESEARCH

CONTENTS OF RECENT NUMBERS

October, 1930 (Vol. 5, No. 4)

RP234. Photo-ionization of cæsium vapor by absorption between the series lines. C. Boeckner and F. L. Mohler. Price 10 cents.

RP235. Efficiency of production of X rays. Warren W. Nicholas. Price 10 cents.

RP236. On the determination of the empirical formula of a hydrocarbon. Edward W. Washburn. Price 5 cents.

RP237. The importance of particle size in samples of certain metallurgical materials. J. A. Scherrer and G. E. F. Lundell. Price 5 cents.

RP238. A radiobeacon and receiving system for blind landing of aircraft. H. Diamond and F. W. Dunmore. Price 25 cents.

RP239. The isolation of the isomers of hexane from petroleum. Johannes H. Bruun and Mildred M. Hicks-Bruun. Price 10 cents.

RP240. Determination of carbon in high sulphur steels by direct combustion. H. A. Bright and G. E. F. Lundell. Price 5 cents.

RP241. Surface tension of soap solutions and its relation to the thickness of adsorbed films. Ronald Bulkley and F. G. Bitner. Price 5 cents.

RP242. The measurement of sound absorption. V. L. Christer and W. F. Synder. Price 10 cents.

November, 1930 (Vol. 5, No. 5)

RP243. Mechanism of heat flow in fibrous materials. J. L. Finck. Price 5 cents.

RP244. Compressibility and thermal expansion of petroleum oils in the range 0° to 300° C. R. S. Jessup. Price 15 cents.

RP245. Interference measurements in the first spectra of krypton. C. J. Humphreys. Price 5 cents.

RP246. Kennelly-Heaviside layer height observations for 4,045 and 8,650 kc. T. R. Gilliland. Price 10 cents.

RP247. A study of the method for titrating aldose sugars with standard iodine and alkali. G. M. Kline and S. F. Acree. Price 10 cents.

RP248. Properties of lead-bismuth, lead-tin, type metal, and fusible alloys. J. G. Thompson. Price 10 cents.

RP249. A study of the adsorption of sulphuric acid by leather. John Beck, jr. Price 5 cents.

RP250. A study of the so-called "over-reduced" condition in molten steel. J. V. McCrae, R. L. Dowdell, and Louis Jordan. Price 15 cents.

RP251. The constant occurrence of nonreducing disaccharides in hydrolyzed inulin. Richard F. Jackson and Emma McDonald. Price 5 cents.

RP252. Precision of color temperature measurements under various observing conditions; a new color comparator for incandescent lamps. Deane B. Judd. Price 10 cents.

RP253. The ring structure of mannose. The optical rotation of 4-glucoside-α-mannose. Horace S. Isbell. Price 5 cents.

December, 1930 (Vol. 5, No. 6)

RP254. Further study of paper-coating minerals and adhesives. Merle B. Shaw, George W. Bicking, and Martin J. O'Leary. Price 10 cents.

RP255. The structure of the spectrum of singly ionized zirconium. C. C. Kiess and Harriet K. Kiess. Price 10 cents.

RP256. A redetermination of the constant of gravitation. Paul R. Heyl. Price 15 cents.

RP257. The properties of pure nickel. Louis Jordan and Wm. H. Swanger, with collaboration of members of bureau staff as indicated. Price 10 cents.

RP258. The freezing point of nickel as a fixed point on the International Temperature Scale. H. T. Wensel and Wm. F. Roeser. Price 5 cents.

Research papers are available as separates for purchase from the Superintendent of Documents United States Government Printing Office, Washington, D. C.

U. S. DEPARTMENT OF COMMERCE
R. P. LAMONT, Secretary
BUREAU OF STANDARDS
GEORGE K. BURGESS, Director

BUREAU OF STANDARDS JOURNAL OF RESEARCH

April, 1931
Vol. 6, No. 4

UNITED STATES
GOVERNMENT PRINTING OFFICE
WASHINGTON : 1931

For sale by the Superintendent of Documents, Washington, D. C. - - Price 40 cents; $2.75 Per Year on Subscription

For a partial list of previous research papers appearing in BUREAU OF STANDARDS JOURNAL OF RESEARCH, see pages 2 and 3 of the cover.

VARIATIONS CAUSED IN HEATING CURVES OF GLASS BY HEAT TREATMENT [1]

By A. Q. Tool and C. G. Eichlin

ABSTRACT

This paper presents some of the variations that are produced in the heating curves of a glass by subjecting it previously to different heat treatments. The discussion incorporated shows that these variations are often fully indicative of the character of these previous treatments, and also that they bear a relation to the changes caused in numerous other characteristics of glass by the same means.

The differences in the curves presented arise from differences in the thermal properties of the glass, and especially from changes in the magnitude and character of the exothermic and endothermic effects. The physicochemical processes causing the latter effect are the reverse of those producing the exothermic; that is, the two effects are related as in the case of the similar and well-known phenomena observed at an inversion point, such as is found in many crystals. They are, however, not confined to the usual relatively narrow temperature ranges and are also much more subject to undercooling and superheating.

Apparently the resistance to the activity of the physicochemical processes causing these effects in glass increases very rapidly as the temperature is lowered. This makes it possible to suppress the exothermic processes to a great extent by rapid cooling and to prepare the way thereby for relatively large exothermic effects on subsequent heating. Since the preparatory exothermic activity is insufficient, the endothermic effects in the heating curves of chilled glasses are never pronounced, but they may become quite large in these curves after the glasses are annealed in a manner such that the exothermic processes have the opportunity to continue their activity into the range of relatively low annealing temperatures.

During annealing the exothermic activity progresses more and more slowly toward a limit which is determined by the annealing temperature employed, and reducing this temperature advances the limit. The physicochemical condition which the glass would have if the limit for any given annealing temperature were reached is termed "the equilibrium condition" of the glass for that temperature, and such an equilibrium is presumably kinetic in character. The continuous series made up of all these equilibrium conditions corresponding to the various temperatures in the annealing range is called the equilibrium sequence. It is shown that about any portion of such a sequence a glass may be made to follow any number of apparently closed cycles and that in traversing these cycles it passes through a series of intermediate conditions which, in general, do not coincide with the equilibrium sequence except when this is practically insured by very thorough annealing at constant temperatures. At ordinary atmospheric temperatures the usual type of glass is always in such an intermediate series, since in ordinary practice at least it is impossible to extend the realizable equilibrium sequence to temperatures much below the lower limit of the practical annealing range. In this range, however, very low rates of cooling or heating will cause a glass to follow its equilibrium sequence with relative closeness after coincidence has once been practically established.

In view of the present insufficient knowledge concerning the constitution of glass, the particular processes involved in these changes of physicochemical condition are presumably too complex and varied for analysis. Apparently, however, the activity of the exothermic type gives rise to a series of molecular readjustments which in many cases limit the ability of the glass to reach other conditions having possibly greater stability, especially at relatively low temperatures. In some cases these readjustments may insure a greater permanency to the vitreous state so long as the glass is not heated above the temperatures producing them. A relatively clear conception of these readjustments and of the general behavior

[1] This article includes many of the salient points discussed in a paper, Some Variations Caused in the Physical Properties of Glass by Heat Treatment, read at the meeting of the American Ceramic Society at Atlantic City, N. J., February, 1924. It also contains additional data bearing on those points.

of glass in the annealing range may be gained from a consideration of the changing conditions in any physicochemical system (for example, a solution) where the equilibrium condition depends upon the temperature, but normally does not change simultaneously with it. From the standpoint of investigating certain properties and characteristics, systems like glass yield advantages since their reaction rates are low and give opportunity for many observations during any change of importance and also since the thermal effects caused by superheating and undercooling are readily detectable.

The relation which the changes in physicochemical condition bear to certain problems in practical annealing is also considered, and from the discussion it will be evident that annealing procedures may often be manipulated so that the resultant changes in certain properties (notably the refractivity) will cause a glass to meet standards of requirement which it would normally fail to reach if annealed according to a fixed schedule prescribed for its general type. Although the tolerances of present-day standards are so lenient that adjustments of this character are seldom required or employed, it is believed that the time is rapidly approaching when an extended use will be made of them, especially in those cases where a highly standardized production of optical instruments of great precision is attempted. More important from the optical instrument standpoint, however, is the need of always annealing a glass in such a way that the physicochemical condition is fully uniform throughout the whole piece or blank from which an optical part is produced. In many cases gradients no greater than a small fraction of a degree will, if they exist during annealing, produce nonuniformities which cause greater disturbances than strains of considerable magnitude.

CONTENTS

		Page
I.	Introduction	524
II.	Method of obtaining and presenting the heating curves	527
III.	General characteristics of the heating curves	528
IV.	Annealing and "disannealing"	535
V.	Detailed exposition of the curves	539
VI.	General discussion and conclusions	548

I. INTRODUCTION

In a previous article[2] attention was called to the fact that the form of the heating curves obtained on glasses that have been chilled is different from that found on the same glasses after they have been well annealed, and also that this difference in curve form probably indicates the occurrence during annealing of some decided change involving physical and chemical readjustments in the glasses. Through deductions made from data secured by means of an extensive series of heating and cooling curve tests it was concluded that these readjustments, when induced by annealing, usually effect a shift of the physicochemical equilibrium of a glass to those conditions which are normal at lower temperatures, although it was found that displacements in the opposite sense can easily be accomplished by appropriate heat treatments. It was also noted that the equilibrium reached depended on the annealing temperature, and, as a consequence, it appeared that any temperature gradients that may exist during annealing will produce corresponding local variations in the physicochemical condition, and thereby cause the glass to be inhomogeneous. For this reason, as well as for the avoidance of strain, temperature gradients should be eliminated, in so far as practicable, when a glass intended for certain types of high precision instruments is being annealed.

For some of these instruments it is evident that glass besides possessing high degrees of structural homogeneity should also be in a physi-

[2] J. Op. Soc. Am., 4 p 340; 1920.

cochemical condition of considerable stability. This stability is increased when the temperature corresponding to the equilibrium is lowered; consequently, adequate annealing at temperatures somewhat lower than those usually employed is, at times, necessary. In the article mentioned it was pointed out, however, that in general it is unnecessary, if not practically impossible, to reduce the usual types of glass to conditions of equilibrium corresponding to those temperatures at which glass is ordinarily employed. This certainly holds for most glasses in common use because the rates at which the changes in equilibrium take place always become very low even at moderately low annealing temperatures; while at temperatures approaching those of ordinary service, these rates are almost always negligible even if the glass is rather poorly annealed.

Additional evidence is given in the present paper showing that from a practical standpoint it is not only impossible to reduce a glass of the usual type to any of the conditions which would constitute a vitreous equilibrium in the temperature range of ordinary service but that it is also difficult while cooling such a glass to maintain conditions which correspond [3] fully to any of the equilibrium conditions which may be easily reached at temperatures in the upper part of the annealing range. In other words, a piece of glass used at any temperature in the range below those temperatures at which it will deform at a perceptible rate under moderate stresses is seldom, if ever, in a condition of physicochemical equilibrium at the service temperature, since its actual condition even when it is used at temperatures relatively near this deformation range usually corresponds more closely, although never exactly, to an equilibrium that may be reached only by sufficiently long heat treatment at some other temperature which in some special cases may be lower, but which is ordinarily much higher than the service temperatures. The use of the glass, so long as the actual physicochemical condition is practically permanent and uniform throughout the whole piece, may, however, be continued indefinitely without detrimental effects arising from such differences between the actual and the equilibrium temperatures.

In a glass of homogeneous chemical composition the physicochemical condition, or constitution, and the lack of uniformity in this condition in any given specimen, or between different specimens from the same melt, are determined chiefly by the treatments to which the glass was subjected in the molding and annealing temperature ranges. Neither the physicochemical constitution nor its possible lack of uniformity, however, is materially affected by the magnitude of moderate elastic strains present at any time, although both are subject to changes whenever the glass is being annealed and although, in being changed, they affect both the distribution and the apparent relaxation rates of the strains. When these changes in the constitution of a glass are produced by means of a suitable annealing, the properties can, in certain cases, be made more desirable, especially since the resultant increase in uniformity often reduces much of the variation in properties sometimes found even within a single small piece of glass. It was consequently suggested in the article cited that annealing a

[3] Whenever it is said that the physicochemical condition at the actual temperature of the glass corresponds to another condition in which it may be found to exist at some other temperature, the word "correspond," as used here, is intended to convey the idea that the two conditions are the same in every respect except that the material has undergone those normal changes in density, heat content, etc., which accompany every such change in temperature, but which do not involve chemical reactions and changes in state or degrees of solution and aggregation.

glass intended for optical or other precision instruments involves much more, in general, than the removal of the stresses which cause the birefringence commonly used to indicate the quality of annealing.

In a later paper [4] in which the effects produced on the form of the heating curves obtained after treating a glass at different temperatures, but for equal periods of time, were fully discussed, it was stated that a gradual increase in the treating time at any given temperature produces a progressive change in this curve form until a physicochemical equilibrium for that particular treating temperature has been reached by the glass. It was also pointed out that the form of the curves, when obtained on samples in such equilibria, changes as the treating temperatures corresponding to the equilibria are varied; and that these variations in the treating procedure which are caused by varying either or both the temperature and period of treatment produce changes in certain physical properties of the glass that can be coordinated to a certain degree with the observed changes in form of the heating curves.

Since it was also found from these effects that the condition approached at any given treating temperature always appears to be practically the same regardless of whether the glass was originally in equilibrium at a higher or a lower temperature, it was concluded after testing many glasses that in most cases long and continuous series of equilibrium conditions which change with the temperature can be definitely established. (A section of such a series and certain possible cyclic changes about it are represented in fig. 2.) It was also concluded that by holding a glass successively, for a sufficient time, in every small temperature interval within the corresponding wide temperature range it may, when either heated or cooled, be made to follow its particular series of equilibrium conditions throughout this extensive temperature range. Such a range is often much wider than, and usually contains the whole of, the practical annealing range of a glass. Although the temperature limits between which this series of equilibrium conditions can be established in practice have not been definitely determined for any glass, it seems certain from the results so far obtained that in many cases such ranges extend from temperatures well above, to temperatures considerably below the commonly accepted limits of the seemingly anomalous effects observed in the expansion and the heating curves of the corresponding glasses.

Although some of the more interesting data and a few of the more illustrative curves have from time to time been published it has naturally been impossible to present more than a small portion of the results on which the above conclusions were based. In this paper, therefore, some additional data and a further discussion of the general subject are given. It is believed that all these new data are in full accord with the above conclusions and confirm, in part, some of the opinions advanced by other investigators, notably Marchis.[5] The chief object of this paper is, however, to show some of the changes appearing in the heating curves obtained on samples taken from time to time from a glass while it is, by continued treatment, being gradually advanced toward equilibrium at a given treating temperature from a condition of practical equilibrium corresponding to some other temperature.

---

[4] J. Opt. Sol. Am. and Rev. Sci. Int., 8, p. 419; 1924.
[5] L. Marchis, Les Modifications Permanentes du Verre et le Deplacement du Zero des Thermometres; Paris, 1898.

II. METHODS OF OBTAINING AND PRESENTING THE HEATING CURVES

As the methods and apparatus employed in obtaining these heating curves by the use of a differential thermocouple have been fully described in the articles already cited,[6] a complete discussion of them will be omitted here. It suffices to say that with the modified apparatus now used, the temperatures of both the glass and the neutral body, and the difference between these temperatures can be easily determined by separate measurements. The following more detailed information concerning the measurements and the resulting graphs is, however, necessary for a satisfactory interpretation of the data presented.

In curve *14* (fig. 3), for example, the difference between the ordinates for any two points on the curve represents the change observed in the temperature difference between a 1.5 g sample of granular glass [7] and a neutral body [8] having a volume about equal to that of the glass as both, packed in close contact, are heated at a steady rate of approximately 6° C. per minute [9] through the temperature range limited by the temperatures indicated by the abscissas of the two points being considered. Thus the abscissas represent the temperatures of the glass as it is being heated while the ordinates if their zero is established show the corresponding differences between the temperatures of the glass and neutral body.

It is, however, unnecessary to establish this zero in most cases, since under the conditions usually encountered in experiments of this sort the actual temperature of the glass body even in ranges free from abnormal heat effects may be either higher or lower than that of the neutral body because the direction of the heat flow in the furnace can never be fully controlled. By the use of a good thermocouple that has been properly placed in carefully packed bodies, this difference in temperature between the bodies can, however, be kept small in most cases, and it then shows no great variation from test to test on samples of the same glass. When this difference is small it appears that it is caused chiefly by the differences between the heat capacities and conductivities of the glass and neutral bodies—a view which is strengthened by the appearance of an appropriate change in the temperature difference whenever another glass with a different thermal capacity is tested under the same conditions.

Furthermore, in an investigation of this kind it is impossible to eliminate all the troublesome effects encountered in the use of differen-

[6] In addition to the articles mentioned, see B. S. Sci. Paper No. 358 (1920), entitled "Concerning the Annealing and Characteristics of Glass."

[7] Granules of glass having an average equivalent diameter of about 1 mm were used because the needed immersion and contact for the thermocouple were thus obtained with less difficulty than is encountered by using solid samples and with none of the peculiar effects found upon employing finely powdered glass.

[8] The neutral bodies used in these experiments were composed of fine granular alundum, although other materials have at times been employed and have usually been found suitable if they are free from disturbing heat effects in the required temperature ranges.

[9] This rate of heating has been found to give good results in determining the relative magnitudes of both the exothermic and the endothermic effects obtained with different samples. With all other conditions of the tests kept practically the same, it is possible by maintaining the heating rate reasonably constant throughout a series of tests, to compare the curves obtained for the various samples tested and to have a reasonable assurance that any differences in curve form noted are the result of differences in the previous heat treatments or in the character of the glasses. As shown in a previous paper (see footnote 4, p. 526) this method of comparison also makes it possible to determine the period of treatment required at a given treating temperature either to bring a glass into approximate equilibrium there or to cause it to show the heat effects corresponding to any of certain intermediate conditions through which the glass must pass in approaching equilibrium at this temperature and which may or may not be practically identical with approximate equilibrium conditions for certain other temperatures.

tial thermocouples, especially when a long series of tests is being made. If the couple has been used for some time and the wires have become contaminated or otherwise changed in character, the two parts of the differential thermocouple may become dissimilar and cause the introduction of possible errors which, although relatively insignificant in actual temperature determinations of these tests, become troublesome when they enter into the observed temperature differences whose magnitudes are never more than a few degrees. Such errors in these differences may reach a degree or more, although if care is taken they seldom become so large. Moreover, they never vary disturbingly in the temperature range covered by these particular tests during the time required for obtaining the data for limited series of curves; consequently the variability of the error in the differences between the ordinates of any comparable pairs of points on different curves is relatively small.

Since these ordinate differences are comparatively free from error and are at the same time fully indicative of the change in curve form when two curves are compared, it is possible for the purpose of this paper to ignore in most cases the actual magnitudes of the ordinates themselves which represent the differences in temperature between the neutral and glass bodies. Preferably, therefore, in considering a series of these heating curves they should all be made to coincide at a point corresponding to some temperature (see fig. 4) where it is probable that the glass has in every case reached practically the same physicochemical conditions; or, if this method of presentation causes confusion through the intermingling of a large number of curves, the curves may be presented one above another in some desirable order. (See fig. 3.) In the latter case, if critical intercurve comparisons seem desirable, reference points may be taken at some chosen and identical temperature on all of the curves. To determine the necessary ordinates at the temperatures where the comparisons are to be made, these ordinates should in every case be determined in relation to the reference point on the curve to which they belong. These relative ordinates for any curve may then be compared with those similarly determined for any other curve in its series.

III. GENERAL CHARACTERISTICS OF THE HEATING CURVES

The typical appearance of a heating curve for chilled glass (curve *27*, fig. 7) is radically different from that for one which has been annealed (curve *38*, fig, 9). Curve *27* shows the presence of an exothermic effect between 350° and 550° C., since in this range the curve rises rapidly from its initial level to a maximum and then, at somewhat higher temperatures, goes into a steep decline to a lower level. This decline indicates either or both of two effects: an endothermic effect, or a relatively rapid change in the specific heat and conductivity of the glass. Curve *38* shows no exothermic effect but the decline to a minimum is so marked that the presence of an endothermic effect is definitely established. Granting the presence of these effects, it appears that both the exothermic and endothermic effects must be associated with certain changes in the constitution of the glass, and

that these constitutional changes are to a great extent responsible for any change in the thermal properties that is indicated by the form of the curves. On these assumptions, a hypothesis concerning both the behavior of glass when heat-treated and the characteristics of the heating curves presented in this paper will be developed.

The exothermic effect occurs when a chilled glass is heated because this glass while being heated through the lower part of the temperature range of this effect is, from a physicochemical standpoint, in a series of very unstable conditions which correspond more nearly to the equilibria which are attainable at temperatures above the point where the curve maximum occurs than they do to those equilibrium conditions which the glass is approaching so long as it is in the temperature range below the point of this curve maximum.

In the consideration of these unstable conditions it is desirable to select some characteristic of a glass in a given condition that will differentiate that condition more or less definitely from all other conditions in which the glass may exist at the same actual temperature. A theoretical temperature corresponding to that equilibrium condition which most closely resembles the given condition is suitable for this purpose, since the glass assumes these unstable conditions because the chilling treatment produced an under cooling, the exceptional magnitude of which may be visualized in this way; that is, this equilibrium temperature in falling during the chilling treatment (see curves A' and B', fig. 1(b) lagged farther and farther behind the acutal temperature of the glass as the cooling progressed and became practically stationary much sooner (relatively speaking) than the latter and at a point which was well above the usual annealing range where equilibrium conditions are normally approximated as a result of ordinary annealing treatments.

On reheating the glass from room temperature, to procure a heating curve for example, this instability first becomes evident when the rise in actual temperature has proceeded far enough to allow (in view of the increased mobility of the glass and of the time lapse per degree increase in temperature) an appreciable activity of those exothermic processes in the glass which were suppressed by the chilling and which, under the favorable conditions of a sufficiently slow cooling and until too greatly hampered by the increasing rigidity of the glass and other unfavorable conditions, would ultimately have caused the equilibrium temperature to fall much farther and would have assisted correspondingly in the establishment of definite physicochemical equilibria in this temperature range of temporary instability. Owing to the increasing activity of these processes as the temperature rises, the constitution of the glass changes for a time more and more rapidly, and as a result the exothermic effect increases for a time. This continues until the changing condition of the glass approaches so closely to the equilibrium condition corresponding to the actual transient temperature attained that the process activity reaches its maximum while the exothermic effect and heating curve pass through their maxima. Beyond this point further heating soon causes the rising temperature of the glass to reach, pass, and, so long as its rise continues, to remain in advance of the more slowly changing equilibrium temperature which after the coincidence is also rising.

In other words, during the chilling treatment of the samples employed in this investigation this hypothetical equilibrium temperature was, in view of the undercooling, falling more slowly than the actual temperature of the glass (see fig. 1 (*b*)) and, when the glass was reheated

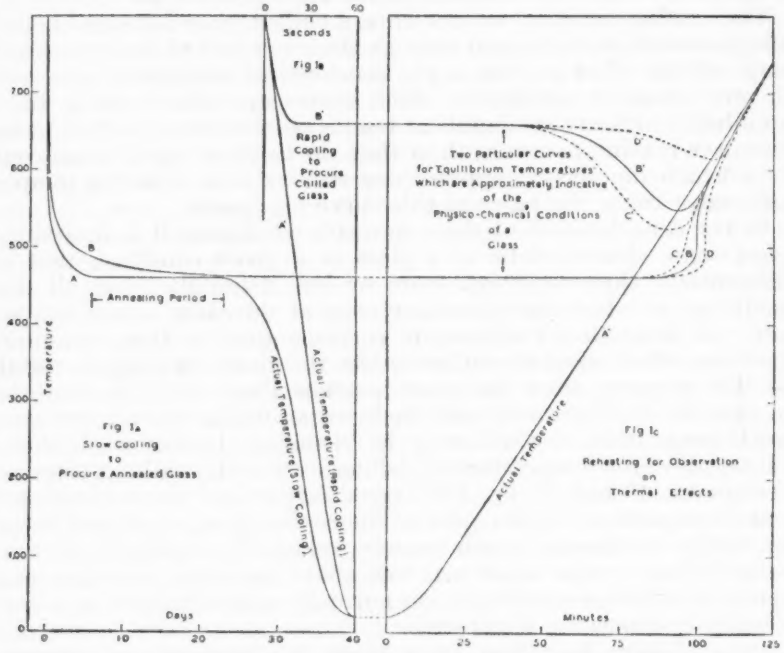

FIGURE 1.—*An approximate representation of the courses of the actual and equilibrium temperatures during the processes of annealing, chilling, and testing glass samples*

In part A of this figure, curve *A* is intended to represent roughly the course of the temperature of a sample of glass at all times during a relatively thorough annealing schedule in which the annealing temperature is chosen quite low in the practical annealing range. Curve *B* represents the course of the temperatures at which the glass would be found to be in equilibrium at various times; that is, if the temperature of the glass were at any time during the annealing raised quickly from curve *A* to *B* no further changes of a marked degree would be noted in the refractivity, density, etc., so long as the temperature remained constant.

Curves *A'* and *B'* in part B have a corresponding significance in a case where a glass sample is supposed to cool very rapidly.

In part C, curve *A''* represents the course of the temperature of either of these samples if they are heated at a normal rate for heating curve tests. Curves *B* and *B'* show the corresponding changes in the equilibrium temperatures of the two samples. Curves *C* and *C'* would represent the respective corresponding changes if the heating rate had been lower; while *D* and *D'* represent the same for an increased rate. For both the slower and faster rates it is evident that (as the curves are plotted) the abscissas must be multiplied by appropriate factors. It will also be evident that the magnitude and definiteness of the exothermic effects observed in the heating curves obtained on the chilled glass (curve 2, fig. 3 is an example) will depend primarily on the extent to which *B'*, *C'*, and *D'* drop below the original level of *B*, the quantity of heat thereby liberated, and the heat capacity of the test sample, although the samples' insulation is also a factor. The magnitude and definiteness of the endothermic effects in the heating curves of both the chilled and annealed samples (curves 2 and 14, fig. 3) will be controlled mainly by the lags of curves *B'*, *C'*, *D'*, *B*, *C*, and *D*, below the curve *A''* after crossing it. They will also be affected by the rapidity with which these curves regain their losses at higher temperatures and the quantity of heat absorbed per degree rise in the equilibrium temperature. The heat capacity and insulation of the samples as in the case of the exothermic effects are additional factors.

for testing, it resumed falling at an appreciable rate as soon as temperatures were reached that made the instability of the glass apparent. (Curve *B'*, fig. 1(*c*).) As the actual temperature of the glass continued to rise (curve A'', fig. 1(*c*)) this decrease in the equilibrium temperature continued until the two temperatures momentarily

coincided.[10] Presumably this occurred before the curves in Figure 4, for example, fell noticeably below the first level. After this coincidence of the two temperatures at the crossing of curve A'' by B' it is assumed that the actual temperature again led as it did during the chilling treatment, and that the glass at the moment of coincidence was changed from the undercooled to the superheated state; that is, if the actual temperature of a glass can be made to fall more rapidly than the equilibrium temperature and thereby cause undercooling it should also be possible to make it rise faster and cause superheating if all, or even a part, of the physicochemical processes involved in the undercooling of the glass are of a type which favor such a reversal.

This reversal and the attendant superheating, which are indicated in Figure 1(*c*) by the lag of the equilibrium temperature below the actual temperature of the glass after the coincidence, rapidly build up the condition for an endothermic effect which will occur as soon as a temperature range is reached where the mobility of the glass is such that the superheating can no longer be maintained without an excessive increase in the heating rate. The superheating then disappears so rapidly (as the equilibrium temperature gains on the actual) that an abnormal heat absorption becomes evident over a narrow temperature range. That is, whenever, in view of the quantity of heat required by the endothermic processes involved in its disappearance, this superheating and its rate of disappearance are large enough the resulting abnormal heat absorption will cause a steep decline of the heating curves shown in the last nine figures to a more or less well-defined minimum before the second or final level portion of the curve is attained in a temperature range which is usually located just below that of sintering. To a great extent these processes responsible for the endothermic effect are undoubtedly the reverse[11] of those that were previously moving the condition of the glass from approximate

[10] A lower heating rate than that chosen for the heating-curve test would have allowed the exothermic processes in the chilled sample to proceed further toward the equilibria of lower temperatures. (Curve C', fig. 1(*c*).) Such a test condition should increase the exothermic effect in a heating curve similar to No. 27 and might have increased the subsequent endothermic effect somewhat, although a low heating rate is unfavorable both to the building up of corresponding temperature differences and to superheating. If the heating rate is too low, an exothermic effect will not be found, since the heat liberated will be dissipated without a detectable rise in temperature and, for the same reason, an endothermic effect may not be observed; that is, the heating curve will drift gradually from the first into the second level. On the other hand, if the heating rate could be made great enough it should be possible as indicated by curve D' (fig. 1(*c*)), to suppress almost completely the exothermic effect shown by heating curve and to delay the endothermic effect (in a glass similar to melt 431, for instance) until temperatures higher than those of the maxima for this effect (see curves *27* and *28*) are reached. In reality heating at a rate equal to or greater than that of the cooling previously employed in chilling a glass should practically eliminate all trace of an exothermic effect and possibly most of the endothermic effect in the curves because that would allow so little time for those changes in condition which are necessary for these effects. With annealed glass, however, increasing the heating rate (see curve *D*, fig. 1(*c*)) should always increase the observable endothermic effect. It should also increase the temperature for the maximum of this effect but because of the rapid rate at which glass softens at high temperatures such a shift will never be large. Slight shifts which are not entirely traceable to errors in temperature measurements have, however, been observed. Decreasing this rate in the heating curve test of annealed glasses (curve *C*, fig. 1(*c*)) should decrease the endothermic effect and lower the temperature for its maximum somewhat.

[11] It is to be assumed, of course, that all the processes do not reverse at the same time and temperature and also that the reversal temperature of a given process is not at all times the same, since, in general, such a temperature will often depend not only on the process but also on the general condition of the glass and the degree to which the process had advanced. Some processes may first become active in a cooling glass when it has cooled to a certain temperature and, although they may continue active at still lower temperatures so long as they are not completed, the ultimate degree of completion may never exceed that which might have been attained at the starting temperature. The reversal temperatures of such processes will generally be as high as those of starting. Examples of such reversible processes would be the retarded crystallization and the liquefication of relatively insoluble components. With other processes the attainable degree of completion may increase continuously as the temperature of the glass falls (or rises), and in such cases the reversal temperatures of the processes will generally be lower on cooling and higher on heating than the starting points, and will be determined mainly by the advance the corresponding processes have made. This latter type of process is considered to be the chief cause of the heat effects observed. It is, of course, evident that at all temperatures there may be simultaneously active both exothermic and endothermic processes, especially when an unannealed glass is being heated. The observed heat effects are due, therefore, to a preponderance in either number of effectiveness of the one or the other type.

equilibrium at high temperatures toward those conditions which correspond more or less closely to equilibria at lower temperatures. Actually the vanishing exothermic effect probably overlaps the endothermic effect to a considerable extent if several types of processes are involved.

Since the temperature range of the endothermic effect as shown by the heating curves is much higher than that of the exothermic effect, it follows that the mobility of the glass is increasing at a much greater rate in the temperature range of the former. Consequently it is to be presumed that the endothermic processes have at these higher temperatures a much greater rate of increase in their activity than the exothermic processes have at the lower temperatures. This assumption gives an explanation for the relatively narrow temperature range of the endothermic effect as compared with that of the exothermic.

It will be noted that the minima for curves *27* and *38* both occur near 600° C., but that the one for the chilled glass is not so well defined as that for the annealed. The relative indefiniteness of the chilled-glass minimum (curve *27*) is generally observed in all chilled glasses and is to be ascribed to a reversal of a majority of the exothermic processes before they were completed to the extent required to produce even an approximate equilibrium at any temperature below that where the endothermic effect begins. (This is about 550° C. for the glass used in obtaining the curves now being considered.) That is, the reversals were brought about in reheating this chilled glass before the exothermic processes had time to produce the conditions necessary for a marked superheating. In fact, it is possible that some of the more important of these processes are so sluggish in their activity during the reheating that they had not reached a condition requiring their reversal until the actual temperature of the glass had reached or exceeded 600° C. Throughout the range of the endothermic effect in the curves for the chilled glasses such unreversed processes were therefore exothermically active and were reducing the observed endothermic effects caused in the curves by the more advanced process which were reversed at lower temperatures.

In the case of the annealed samples of this glass, however (see curve *38*), the previous annealing treatment gave all exothermic processes the opportunity to proceed much further toward establishing equilibria corresponding to temperatures below 500° C. Consequently, when these samples were reheated both the number of process reversals from neutral and exothermic to endothermic action at temperatures below 550° C. and the total effect of the resultant endothermic processes as the superheating began to diminish rapidly near this temperature were greatly increased, while the number of exothermic processes and their effect at temperatures near 600° C. were correspondingly reduced. Since it is here assumed that in any glass being heated the number of reversals is always larger in annealed than in chilled samples at those temperatures in a range just below a limit which corresponds in this particular glass to 550° C., and also that this increase is always gained from the relatively sluggish processes, it follows that on reheating the annealed samples to obtain heating curves a much greater superheating and a correspondingly larger endothermic effect with its maximum at slightly higher temper-

atures should always be expected as the thoroughness of annealing increases.

To a great extent an above-mentioned difference which exists between the first and second levels of these heating curves is doubtlessly attributable to changes in the specific heat and the thermal conductivity of the glass as its temperature and physicochemical condition are changed by heating from the lower to the higher corresponding temperature ranges. The specific heat, for example, may be changed rapidly and appreciably as the temperature changes if the exothermic and endothermic effects occurring between these ranges are associated with processes which so change the physical and chemical associations and arrangements of the molecules and ions that the types, numbers, degrees of freedom, etc., of these units, are rapidly decreased or increased. On this basis, it would appear that the second level, since it is in the higher temperature range where the specific heat is normally greater, should lie below the first as it actually does. Also it would seem that a chilled glass should have a higher specific heat in the temperature range of the lower level than an annealed glass. Acting alone this difference in specific heat, if it exists, should make the difference between the first and second levels greater for the annealed glasses than for the chilled. Actually, however, this condition is seldom observed, since these differences between the levels are (for a given glass) usually found to be almost equal for all samples regardless of their previous heat treatment except that in those cases where the samples have been very severely chilled they, contrary to the above deduction, yield differences which are relatively quite large. (See curves *2*, fig. 4, and *27* and *31*, fig. 8.) These results make it appear that in obtaining a heating curve the effect of the increased specific heat of a chilled glass is

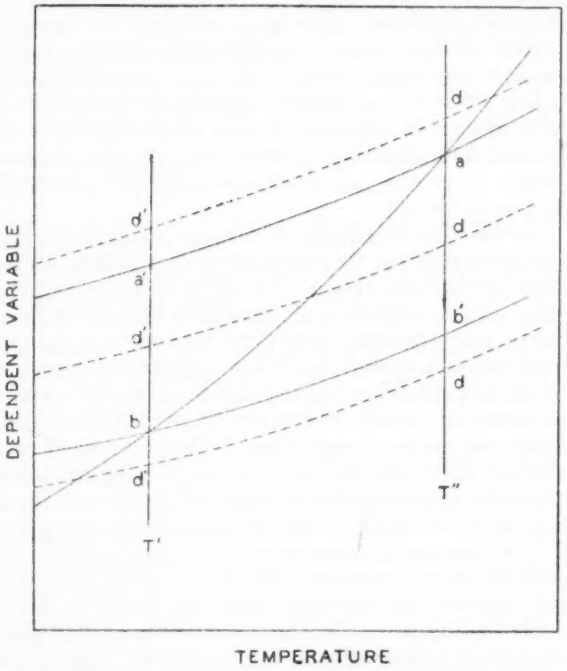

FIGURE 2.—*A representation of the cyclic changes in the physicochemical condition of a vitreous material.* (*See discussion in footnote 12, p. 534*)

With the possible exception of equilibrium curves, such as *ab*, lines drawn in a plane and representing the various possible sequences of conditions must be considered as mere projections of curves in a multidimensional space since, even with the pressure constant, one dependent variable determined on a single property of the material is presumably insufficient to determine the course of such changes in condition unless the equilibium sequence is being followed. For that reason, as indicated in the footnote, the lines *dd'* in particular must be considered as projections of curves which, in general, do not cut the line *ab*.

generally balanced and, in the case of severely chilled glasses, completely outweighed by the effect of an equally possible increase in the thermal conductivity. This would seem to indicate that the thermal diffusivities of such chilled glasses at atmospheric temperatures are relatively large. This comparatively large difference between the initial and final levels of a curve on severely chilled glass may, however, also be caused by some of the exothermic processes becoming active before the first observations are taken; that is, soon after the glass reaches 100° C. While this, for various reasons, seems relatively improbable as an explanation for all of the increase in the difference, it is evident that any heat released by such processes as might be active in this range would reduce the apparent specific heat by raising the curve level. At this point, it must also be noted that below 300° C. no really significant departure from the initial level by the curves referred to was observed; and while this may be considered as indicating that no exothermic processes were active in that range, it is also an obvious cause for overlooking such an activity if it were present.

In well-annealed glasses, on the other hand, it may be safely assumed that processes of this sort are so nearly completed or are so thoroughly inactive in this range of relatively low temperatures that the initial level of the curves is determined almost entirely by the real specific heats and thermal conductivities of the samples. At and near the final level, however, both the chilled and annealed glasses are assumed to be approaching the equilibria corresponding to each passing temperature so rapidly that very little difference is to be expected between their respective conditions. Their curve levels should consequently almost coincide in this range of higher temperatures. Until the sintering range is almost reached the curves on chilled samples should, however, be slightly higher since some vestige of activity on the part of the exothermic processes probably still exists while the activity of endothermic processes which are predominant at these temperatures has as yet not become quite so great as in the annealed samples. As in the range of the initial level for chilled glasses the activity of the processes again affects the apparent thermal capacity and conductivity; but since the predominant activity, especially in annealed glass, is now endothermic, the effect it has must be either an apparent increase in the specific heat or an apparent reduction in thermal conductivity which is the opposite of the effect of the exothermic activity at the initial level. As a result of the influence of these exothermic and endothermic effects the differences between these two levels probably always indicate a greater change in these two properties than that which actually occurs; that is, between these two temperature ranges the change in specific heat, for example, is generally greater than the corresponding change in the "true specific heat." [12]

[12] The terms "true" and "apparent" specific heats are used here merely for the purpose of making clear a distinction which exists between a specific heat that is not, and one that is, increased or decreased by endothermic or exothermic effects which are anomalous in the nature of this coefficient and whose presence, since they are often small and may not be confined to definite and narrow temperature ranges, is in many cases unsuspected. Such a clarification seemed desirable from the standpoint of promoting a better understanding of the variable results which are possible in all measurements on the different thermal coefficients of the various materials possessing indefinite effects of this sort. If these effects are caused by certain internal processes which in establishing equilibria consume considerable periods of time in reaching the required degrees of completion which, together with the velocities of the processes, are determined by the temperature and the general condition of the material, it follows that their relations to such variations in these coefficients can be very simply illustrated since the conceptions and facts involved are practically those

IV. ANNEALING AND "DISANNEALING"

In its application to the progressive change in form of the heating curves as the heat treatment of the glass is altered to increase the thoroughness of the annealing, the foregoing discussion, together with the conceptions it involves probably requires some elaboration which, to some extent, will be found in the following recapitulation:

1. As the temperature of a glass in the annealing range is reduced very slowly its physicochemical equilibrium changes correspondingly because of the activity of a number of slow exothermic processes which, in the case of a more rapid cooling, are suppressed and which after being suppressed will again resume activity, causing a detectable and an apparently abnormal exothermic effect, whenever the glass is reheated at a rate which is lower than that of cooling.

2. The indication of an exothermic effect usually observed on cooling curves of glass is caused by the cessation of the activity of these exothermic processes as undercooling begins.

---

discussed in the usual textbook presentation of The Influence of Temperature Upon the Heat of Reaction (See Nernst's Theoretical Chemistry, p. 599, English translation of the 6th ed., 1911.)

For instance, consider a sample of glass, having a mass of 1 g. and a length of 1 cm., which is in physicochemical equilibrium at the temperature, T'', where, although the changes are assumed to occur not too rapidly, such a condition can be reached in a reasonable time; that is T'' is chosen in the usual annealing range. If the glass is cooled at a sufficiently rapid rate from this temperature through an interval, $T''-T'$, there will be a contraction, C'', and a heat emission, S'', while the glass passes through that normal series of conditions, aa' in fig. 2, which in this interval "corresponds" to the equilibrium condition at T''. (See footnote 3, p. 525.) Under these circumstances S'' and C'' are changes caused entirely by processes which follow instantaneously any temperature change. If the glass is now held at T' until physicochemical equilibrium is established at that temperature there will occur a further contraction, c', and heat emission, s'. The particular values of the contractions and heats of reaction which may occur at T' are those, therefore, which accompany the specific change, $a'b$, from a condition corresponding at that temperature to the equilibrium, at T'' to equilibrium at T'.

If, however, the glass is cooled so slowly—in the upper part of the annealing range such a cooling may be made quite rapid but in the lower part it must be extremely slow—that it passes only through the series ab, of equilibrium conditions, the contraction and heat emission, C and S, respectively, will be observed for the interval, $T''-T'$; and in this case C and S are caused not only by the instantaneously responsive processes, but also by those which require time and which were responsible for c' and s'. Since the equilibrium conditions at T'' and also at T' are presumably the same for both cooling methods (except in certain causes not considered here) it follows that $C=C''+c'$ and that $S=S''+s'$.

If the glass now in physicochemical equilibrium at T' is heated with sufficient rapidity to T'' the resultant expansion and heat absorption will be C' and S', respectively, while the glass passes through the normal series of conditions, bb', which corresponds within this interval to the condition of equilibrium at T'. If the glass is then held at T'' until physicochemical equilibrium is established at that temperature by passing along $b'a$, a further expansion, c'', and heat absorption, s'', will occur. These are only particular values of the expansions and of the heats of absorption required in general by the reactions which may occur at T'' in producing equilibrium at that temperature, since they are those values associated with the specific change from a condition corresponding at that temperature to the equilibrium at T' to equilibrium at T''.

If the rate of heating is so low, however, that the series, ba, of equilibrium conditions is followed, an expansion and heat absorption will be observed which, disregarding signs, will equal the contraction, C, and heat emission, S, observed during the slow cooling over the same interval. Then since $C=C'+c''$ and $S=S'+s''$, it follows that $C''-C'=c''-c'$, and $S''-S'=s''-s'$.

In the above, therefore, $S''/(T''-T')$ and $S'/(T''-T')$ are, in general, different although both may be regarded as average true specific heats for the same interval $(T''-T')$. These particular values of the coefficient are to be obtained only by bringing the glass to equilibrium at the starting temperatures before the tests are begun. However, according to the general assumptions made, there must be at any temperature, T, a great number of other possible intermediate conditions such as are represented by various positions on $a'b$ or $b'a$, for example, which a glass might possess whenever a test is started. Corresponding to each of these initial intermediate conditions there is within any temperature interval beginning at T an average true specific heat which differs, in general, from those corresponding to all the others. These values of a thermal coefficient are met whenever a glass follows a series of intermediate conditions like that exemplified by any dd' in the interval, $T''-T'$. (It should be noted that such a series of intermediate conditions yielding a true specific heat may or may not correspond to some condition in the equilibrium series either within or without the section ab', that is, the coincidence of two such series which is indicated by an intersection of the representative lines in the accompanying diagram may be only apparent, since one dependent variable with the temperature is inadequate to determine such a coincidence.)

Likewise, the apparent specific heat, which in the above case is represented by $S/(T''-T')$, will vary depending on the initial condition, which is seldom one of equilibrium and is always conditioned by the mode of heating or cooling. It follows, therefore, that considerable variation may be expected in the results of tests made within intervals including temperatures in, or near, the annealing range. Although the methods of test ordinarily employed are generally favorable, a true specific heat can not, in general, be determined except within temperature intervals well below the softening range. If, however, the end temperatures of these intervals are low enough, the rate of heating, or cooling, has no appreciable effect, and the possibility of differences between true and apparent specific heats in such intervals need not be considered. Furthermore, since length of treatment at these temperatures causes no appreciable change in the condition of the glass, repeated tests on the same piece of glass should always give identical results; that is, the results can not be noticeably changed by varying the treatment preceding the measurements unless the glass was originally very severely chilled or unless the treatments include a heating of the glass to temperatures which rise almost to the annealing range.

3. All of those processes which may be retarded in glass by chilling and which are the cause of the relatively large exothermic effects observed in heating curves obtained on chilled glasses may be carried forward to such a degree by thorough annealing treatments, and especially by those given at low annealing temperatures, that they will no longer be sufficiently active to produce in the heating curves of annealed glasses any appreciable exothermic effect within the relatively short time allowed by the heating rates usually employed.

4. In annealing at any given temperature to reduce the activity of the exothermic processes during a reheating or a further annealing at lower temperatures, thoroughness is gained by increasing the duration of the treatment; and this activity is usually more completely reduced by treatments at low temperatures, provided the annealing periods can be made sufficiently long.

5. Since the exothermic processes tend, in general, to proceed much further at low annealing temperatures and since they, at the same time, meet increased resistance to their activity and consequently become much more sluggish, it follows that the annealing periods must be greatly increased as the annealing temperature of a glass is lowered if the thoroughness of annealing which corresponds to approximate equilibria at these low annealing temperatures is to be attained.

6. As this annealing proceeds the activity of the exothermic processes usually decreases progressively and it may happen that those processes which at first showed the greater activity gradually become less prominent in this respect than others—a result which may be caused either by differences in the rates of advance of the various original processes toward that degree of completion required of each for the establishment of equilibrium at the annealing temperature in question or, possibly also, by the appearance and growth in importance of secondary processes.

7. Heating a glass rapidly to sufficiently high temperatures either before or after equilibrium has been established at a given treating temperature will replace the activity of the exothermic processes by that of the reversed or endothermic processes.

8. The temperature at which any one of the more important exothermic processes is so reversed will, in general, not be a unique temperature which is characteristic of that process but it will be one which is determined chiefly by the progress which that process has individually made in contributing to the production of an equilibrium at the treating temperature employed before the temperature was increased; and since at any stage of this previous annealing treatment, except that of complete equilibrium, the degrees of progress of the various processes toward establishing such equilibrium may, in general, be considerably different, it follows that the reversal temperatures of the serveral processes may also be correspondingly different.

9. For simplicity consider that there is only one process that is affected by annealing, and that it is of the type having a variable exothermic to endothermic reversal point. Then, so long as the temperature of the glass is below this point, annealing will progress because the process will be exothermically active. As a consequence, the reversal point will be falling, although at a continually decreasing rate, until it finally coincides with the glass temperature and stops. Further, if the temperature of the glass is rising, "disannealing" will begin, just as soon as the reversal point is passed, because the reversed

process will then become endothermically active. In consequence, this point will begin to rise also, but the beginning rate will be relatively slow since it is controlled only indirectly by the rate of heating the glass.

10. This reversal temperature is equivalent to the equilibrium temperature and when once passed it will, on heating, as on cooling the glass, generally lag behind the actual temperature. (See fig. 1 (*c*).)

11. That is, if the actual temperature of the glass is still rising after the reversal temperature is passed, superheating will result because of the sluggishness of the endothermic process just as undercooling previously resulted because of a similar sluggishness on the part of the corresponding exothermic process during the cooling; but, as a consequence of the rapidly decreasing sluggishness of the endothermic process as the actual temperature continues to rise, this reversal temperature will soon greatly accelerate its rate of rise and regain much of the lost ground with the result that an abnormal endothermic effect will ultimately be detectable.

12. If there be only one process, or if the reversal temperatures of the possible several processes are all the same, as they would be in the case of equilibrium, the equilibrium temperature of a specimen of glass may be determined by finding that temperature in the annealing range at which a long heat treatment produces no change in its physical properties; while other similar treatments at temperatures somewhat higher and lower produce changes which, in the density, for example, are ordinarily decreases and increases respectively.

13. In general, it must be assumed, however, that there is, as previously stated, not one but a number of different processes active in a glass during a heat treatment, and that the reversal temperatures of these processes may all be considerably different after any period of treatment, such as the usual annealing schedules which are seldom capable of producing an equilibrium; consequently, it follows that an equilibrium temperature determined as above described does not necessarily coincide with any of these reversal temperatures, although it should always fall at some intermediate position between their extreme values.

14. While this intermediate temperature is therefore not strictly an equilibrium temperature it may be termed the "effective" annealing temperature of the previous heat treatments, since from the method of its determination it is evident that these treatments are capable of producing the same value for the property used in the determination as a thorough annealing treatment would normally have produced at this temperature.

15. Since any given physical property of a glass is presumably more sensitive to the activities of certain processes than to those of others and since this selectiveness probably changes with the property under consideration, it is to be expected that the effective annealing temperatures determined by observations on different properties will differ somewhat.

16. This possible difference in the reversal temperatures suggests that, in general, glass in proceeding to equilibrium or any other condition passes through a chain of conditions none of which is likely to be that of equilibrium at any temperature, and furthermore, that the number of such possible chains may be very large, although it

would appear possible by proper treatments of most glasses in their annealing ranges to make reasonably complete transitions from any one of such chains to any other chain.

17. Whenever a glass is subjected to a disannealing treatment at some constant temperature; that is, to a heat treatment at a temperature higher than the effective annealing temperature established by the preceding treatments, the endothermic activity of all the reversed processes decreases at a progressively decreasing rate as this new treatment is continued; and, for much the same reasons mentioned in connection with annealing, the processes initially taking a chief part in this activity may be replaced in this respect by others.

18. As in the case of annealing, the period required for a relatively thorough disannealing decreases rapidly as the treating temperature is raised.

19. In certain cases (usually in the less stable glasses) certain processes somewhat similar to devitrification may appear which have rather definite and unique reversal temperatures regardless of their degrees of advancement.

20. In other cases, treatments at certain temperatures may advance certain processes to such a degree that other processes which would be very active during treatments in other temperature ranges are partially or completely suppressed, and this suppression may continue unless it is possible to reverse the suppressing processes or otherwise to reduce their effect by some treatment of the glass.

21. Such suppressions make it possible to find, below certain temperatures, sets of chains of conditions about two or more apparently independent equilibrium chains which are more or less parallel and which may be connected only by treatments at relatively high temperatures. (All glasses tend to show similar characteristics below the annealing range while the glasses which exhibit them in this range are exceptions to the class considered under section 16.)

22. The annealing and disannealing under discussion do not take into account the relaxation and introduction of elastic stresses, although these effects may accompany certain of the treatments under consideration.

Because of the above-mentioned changes produced in glass by changing the character of the heat treatment, a comparison of a large number of heating curves obtained on samples that have been prepared by subjecting each of them to one of a properly chosen variety of treatments should show more or less clearly that some of the processes causing the changes are more sluggish than others and that this sluggishness and also the general character of the predominant processes which are active are affected by various conditions, among which are the temperature and the effective annealing temperature of the previous treatments of the samples. Such a comparison should also reveal that the reversal temperatures of the several processes active in any one sample are, in general, different except in the case of glasses which are thoroughly annealed at the chosen annealing temperature, and furthermore, that these reversal temperatures, although they may depend on the general condition of the glass are determined chiefly by the respective advances which the individual processes had made toward producing equilibrium conditions at low annealing temperatures during the sample's previous treatments, which naturally include a portion of the heating that was required in obtaining the curves.

V. DETAILED EXPOSITION OF THE CURVES

As already stated above, the purpose of these experiments was to trace the progressive changes produced in the heating curves as the period of treating a glass at a given temperature is gradually increased. These changes are well illustrated by the series of curves shown in Figure 3. Of these curves, *1* was obtained on a sample broken from a pot of "medium flint" glass, B. S. Melt No. 494.[13] As usual in the case of all glasses taken from pots that are not too quickly cooled, the sample, as the curve shows, was reasonably well annealed. This is evident from the form of the curve because an exothermic effect is lacking and the endothermic effect is quite pronounced. Another sample from the same source was broken into small fragments, and these, after being heated at 620° C., were chilled from that temperature by being plunged into cold water.[14] On treating a portion of this chilled sample, curve *2*, which shows the form usual for chilled glasses, was obtained. The remainder of the chilled sample was divided into several lots, some of which were heated quickly to 360° C.,[15]

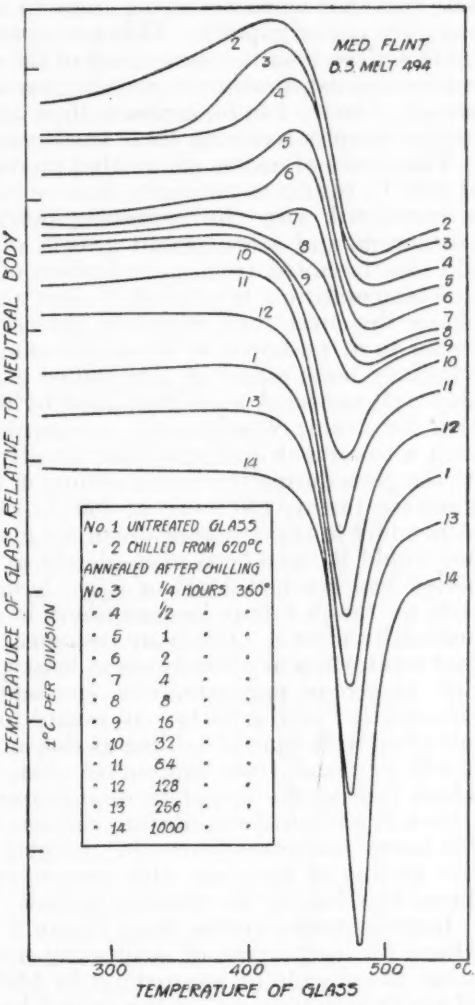

FIGURE 3.—*Heating curves obtained on samples of a flint glass where each sample was treated differently as indicated*

To make comparison easy the curves have been arranged one above another without reference to zero on the ordinate axis. In practically all cases the width of the lines cover all observed points, and observations were made at intervals of approximately 12°, 6°, 3°, or 1.5° C., the shorter intervals being employed between 450° and 550° C.

[13] An analysis of this glass gave the following composition: SiO_2, 50.55; Na_2O, 2.69; Al_2O_3, 0.65; CaO, trace; PbO, 40.14; K_2O, 5.93; Fe_2O_3, 0.02; MgO, not detected. See also Tool and Hill, Trans. Soc. Glass Tech., 9, p. 196; 1925. This glass and also melts Nos. 431 and 429 were produced under the direction of A. N. Finn at the Bureau of Standards.

[14] Water was used for quenching, since it is convenient and yields more uniform results than other quenchers, such as liquid air, mercury, etc. When the particles were not too fine the glass could be quickly and easily dried and showed no visible trace of deterioration due to its contact with the water.

[15] The heating temperatures are considered to have been correctly determined to within ±5° C., and the differences between two such temperatures are probably correct to less than that amount. During the long treatments the temperatures seldom fluctuated more than 5° C. and then for short intervals only. Naturally, in the 15-minute treatments almost two-thirds of the period was required for the glass to come to the required temperature.

held there for periods varying from 15 minutes to over 2,000 hours, and then cooled rapidly. This temperature was chosen because it is, for this glass, near the lower limit of the range in which an equilibrium can be established without exceeding a reasonable experimental treating period. Curves *3* to *15*, inclusive (figs. 3 and 4) are the results obtained on the samples receiving these treatments.

This series of curves shows that increasing the period of treatment at 360° C. results in producing a more fully annealed glass, since there is correlated with the increasing period a gradual erasure of the exothermic and a concurrent growth of the endothermic effects. It will also be noted from a comparison of curves *1*, *12*, and *13* that at this temperature a treatment of more than 150 hours is required [16] to obtain the curve form found on the original glass. After being subjected to a treatment of about the same period at this temperature relatively large pieces of this chilled glass were found to be reasonably well annealed when examined by one of the usual birefringence tests for strain; consequently, as regards the removal of stresses also, such a treatment does not differ greatly in effect from that received by the glass during the initial cooling in the pot. By such a relatively short treatment (150 hours at 360° C.) the equilibrium condition corresponding to this temperature of the glass was, however, not attained nor would it have been even closely approached unless the treating period had reached 2,000 or 3,000 hours. This conclusion is based both on the fact that the endothermic effect could still be increased materially after a 1,000-hour treatment and that it was later found that treatments of 3,000 hours at least were required at this temperature to secure approximately constant and stable values for the refractivity [17] and density. In regard to the growth of the endothermic effect with time of holding at this annealing temperature, 360° C., it will be noted from the curves that, after the 16-hour treatment which caused the complete disappearance of the exothermic effect (curve *9*) and until equilibrium was more closely approached through 256 hours' treatment (curve *13*), roughly equal increments in the relative cooling of the glass with respect to the neutral body were produced by doubling the treating periods.

Representative curves from Figure 3 are again shown in Figure 4 where, for the purpose of facilitating comparisons, they have all been made to coincide at approximately 550° C. which lies in the range where they flatten out on the second level. This point, or temperature, was chosen because the glass under the experimental conditions involved in obtaining such curves had not yet begun to sinter so far as could be noticed from a cursory examination and also because it appeared that on reaching this temperature the superheating, together with the resultant endothermic effects, had practically ceased. By discontinuing the heating a little above this point the erratic effects usually accompanying the softening of a glass were avoided, while as previously stated, it seemed safe to assume that a temperature had

[16] This does not signify that the pot of glass while being cooled was held for such a length of time in the immediate neighborhood of this temperature because, as a matter of fact, much shorter periods at somewhat higher temperatures will produce almost the same curve form. Furthermore, a moderate rate of cooling through the annealing range will cause practically the same result.

[17] This point was discussed in a paper by Tool, Tilton, and Hill, which was read at the Ithaca meeting of the Optical Society of America; October, 1925. (Abstract in J. Opt. Soc. and Rev. Sci. Inst., **12**, p. 490; 1926.)

been reached where the physicochemical conditions of all the variously treated samples were practically identical. That is, in this temperature range the conditions of the various samples may be considered as being practically independent of all previous heat treatments and as determined almost wholly by the temperatures attained in this final portion of the heating curves. That the effects of all previous heat treatments were eliminated by the required heating to these temperatures and that the conditions of all the samples on reaching the chosen reference temperature employed in these diagrams were practically identical was proved by retesting several of the samples after they were all cooled according to a common schedule from the maximum temperature reached in obtaining the data for this curve series. In every case the retest curves were identical in form; it was found that this form was entirely determined by the incidental annealing imposed on the samples by the cooling after the maximum temperature of the first tests was reached.

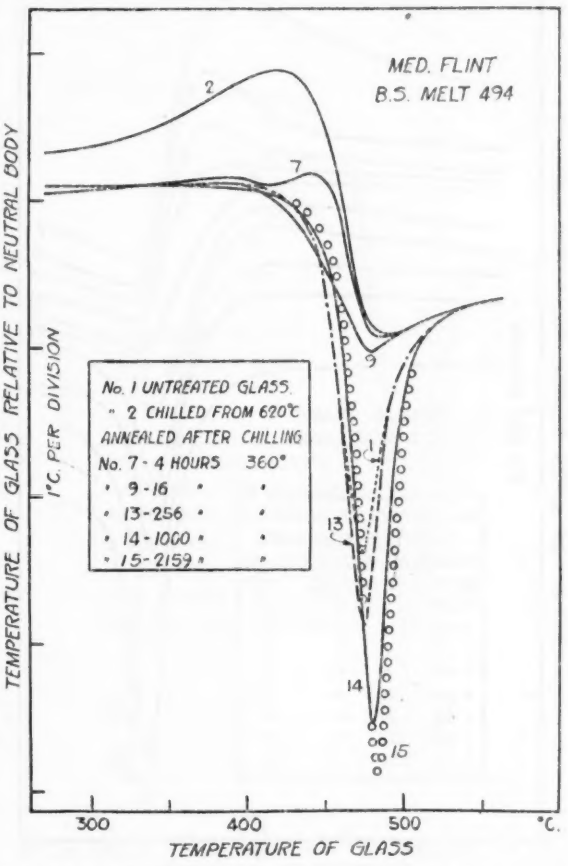

FIGURE 4.—*Representative curves chosen from Figure 3 and arranged on the basis of the assumption that all such curves for a given glass should have a common ordinate near the sintering range where it appears that the physicochemical conditions of the respective samples were almost identical*

In obtaining data showing the effect of changing the treating temperature, additional lots of the chilled sample were heated rapidly to 380° instead of 360° C.; held there for periods ranging from 15 minutes to over 1,000 hours, and then cooled very rapidly as before. Together with Nos. *1* and *2*, the heating curves, Nos. *16* to *24*, obtained on these lots of glass are shown in Figure 5. This series of curves shows much the same characteristics in the disappearance of the exothermic and in the growth of the endothermic effect as those found in the series of Figure 3. The changes, however, proceeded more rapidly at 380° than at 360° C. and less than 100 hours, instead of more than 150,

were required at the higher temperature to produce an endothermic effect of the magnitude found in curve *1*. The small increment in the relative cooling of the glass with respect to the neutral body shown by a comparison of curves *23* and *24* in which the holding periods differed by a factor of approximately 9, shows that the glass used to obtain curve *24* had (after the treatment of more than 1,100 hours) practically reached equilibrium at 380° C.

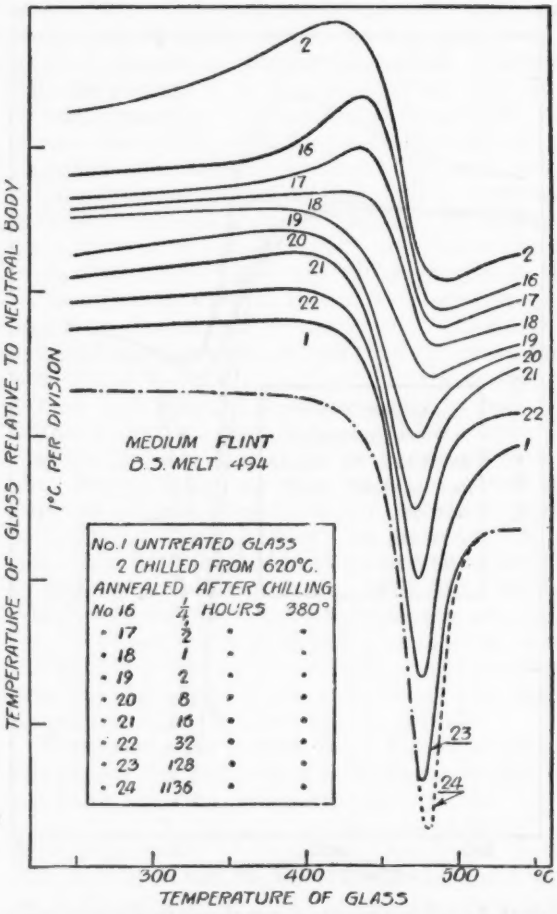

FIGURE 5.—*Heating curves obtained on samples of the same flint glass yielding the curves in Figure 3, but with the difference that the special annealing treatments were given at 380° instead of 360° C.*

That curve *24* corresponds to a practical equilibrium for this glass when treated at 380° C. is also indicated by comparing it with curve *25* (fig. 6), which was obtained after retreating, for more than 1,000 hours at 380° C., a part of the lot which was sampled in obtaining curve *15*. The previous treatment had caused this lot of glass to approach equilibrium at 360° C., and, consequently, the relative cooling indicated by curve *15* is, as should be expected, greater than that shown by curves *24* and *25*, which the comparison shows to be almost identical.[18] That is, after the treatment at 380° C., the relative cooling shown by curve *25* is, within the experimental error, the same as that shown by curve *24*. This procedure for establishing the maximum endothermic effect which corresponds to the equilibrium condition at any temperature can also be carried out over other temperature intervals and it demonstrates the reversibility of the processes involved. Experiments at this bureau have shown, however, that other characteristics of glass can be used with much greater facility

[18] In a paper previously cited (J. Opt. Sol. Am. and Rev. Sci. Inst., 8, p. 433; 1924) it was shown that decreasing the temperature of equilibrium of a glass increased the relative cooling shown by the heating curves, and that all samples of the same glass brought to equilibrium at the same temperature should give identical relative coolings.

in determining accurately [19] whether a glass has reached equilibrium at any given temperature, consequently this method is not recommended for other than special tests.

In Figures 7, 8, and 9, additional series of similar curves are given which were obtained on a borosilicate crown glass, B. S. Melt No. 431.[20] The samples furnishing these curves were prepared in the manner described above except that the glass in this case was chilled from 750° C. and then retreated or annealed at either 450° or 475° C., as indicated. Curve *26* was obtained on glass taken directly from the pot, while *27* (see figs. 7 and 8) shows the result on this glass after the chilling. The series in Figure 7 gives another exhibition of the gradual disappearance of the exothermic effect as the period of treatment is increased, while that in Figure 8 again makes apparent the large increase produced in the endothermic effect by lengthening the treating period. In the case of both series (figs. 7 and 8) the treating temperature was 450° C. which is near the lower limit of the range where equilibrium can be reached in a practicable time. Here it appears that approximately 250 hours are required to produce a relative cooling equal to that found on the original glass. (See footnote 16,

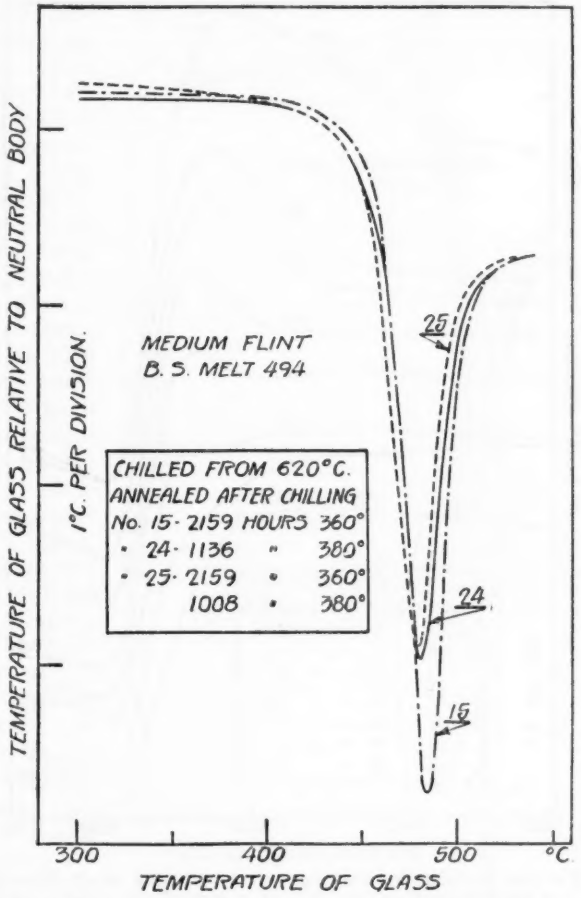

FIGURE 6.—*A comparison of the results of approximately thorough annealing treatments received by the chilled flint glass at 360° and 380° C.*

[19] This was demonstrated on the same glass by curves—shown at the Ithaca meeting of the Optical Society (see footnote 17, p. 540)—giving its change in refractivity with treating temperature. Lebedeff also (die Glas-Ind., **35**, p. 6; January, 1927) obtained similar results, but on a different glass and in a temperature range where the mobility was much higher. His curves in form and presentation are almost identical with those shown at the meeting mentioned and point to this same advantage of accuracy. See also, A. I. Stozarov, The Variation of Refractive Index of Glasses at High Temperatures, Trans. of the Opt. Inst. in Leningrad, **4** (No. 39), pp. 1-36; 1928. (Since the completion of this paper an article by E. Berger, Glastechn. Ber., **8**, p. 339; 1930; has appeared which to some extent discusses Stozarov's results and many of the views expressed in it are in full accord with the general trend of those presented here.)

[20] Analysis of this glass shows the following composition: SiO_2, 64.52; K_2O, 10.84; BaO, 2.56; R_2O_3, 0.35; B_2O_3, 11.93; Na_2O, 7.85; ZnO, 2.66. See article by Tool and Eichlin, J. Opt. Soc. Am. and Rev. Sci. Inst., **8**, p. 421; 1924.

p. 540.) From a comparison of curves *37* and *38*, it will be noted also that a treatment of somewhat more than 4,500 hours seems to have produced a condition of practical equilibrium at this temperature; however, a further slight increase would undoubtedly have been obtained if the period had been very greatly increased.

In obtaining curves *39* and *40* the method discussed above in describing curves *24* and *25* (fig. 6) was used to determine whether equilibrium had been established in the samples treated at 475° C. Thus curve *39* was obtained on a second sample taken from the lot that had been treated over 4,500 hours at 450° C. and had then furnished the sample yielding curve *38*.[21] Before yielding curve *39* this second sample was given an added treatment of more than 1,000 hours at 475° C. On comparing curve *39* with curve *40*, which was obtained on a sample that was taken from the unannealed chilled glass and then also treated over 1,000 hours at 475° C., it will be seen that the endothermic effects of the two curves are practically the same, although that of the former is somewhat larger, as should be expected. From this it may be inferred, as stated above, that both samples were in practical equilibrium at 475° C. when the treatments ended. This inference follows since for one sample the relative cooling caused by the endothermic effect increased, while for the other it decreased toward a common limit, which it appears was

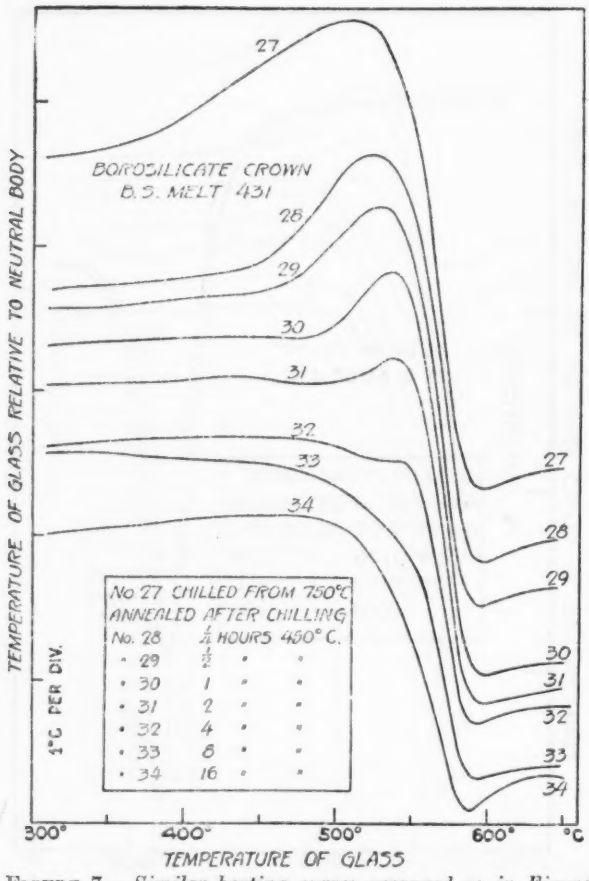

FIGURE 7.—*Similar heating curves arranged as in Figure 3, but obtained on samples of a borosilicate crown, each sample being differently treated as indicated*

In consideration of the low annealing temperature (450° C.) the annealing periods are all relatively short and failed to erase completely the effect of the previous chilling from 750° C.

[21] In this connection it should be mentioned that the magnitudes of the extreme dips of curves *38* and *39* below the first and second levels are not inconsistent with the conclusions drawn from the results given in Table 1, p. 430, and fig. 4, p. 433, of a previous paper (J. Opt. Soc. Am. and Rev. Sci. Inst., **8**, 1924). These conclusions concerned the increasing depth of such dips as the equilibrium temperature was decreased.

practically reached through the 1,000-hour treatments at this temperature.

The series of curves given in Figure 10 and obtained on a light barium crown, B. S. Melt No. 429 [22] was discussed in a paper [23] presented before the Optical Society of America, but is also included here to show that the manner in which the exothermic effect disappears with an increase in the treating period is much the same for a variety of glasses. Curve *41* resulted from a test on the glass as it came from the pot, while curve *42* was the result on a sample from a lot of the glass which had been chilled from 808° C. in the manner described above. The other curves were procured on samples from this chilled lot which were treated at 490° C. for periods indicated in the descriptive legend of the figure. The results obtained after longer periods of treatment are not included, but they were quite similar to those shown for the other glasses.

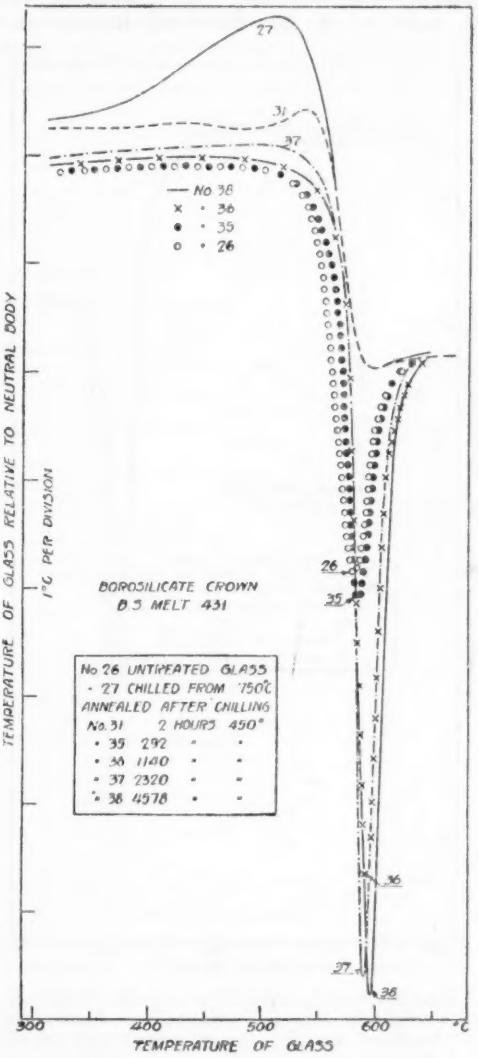

FIGURE 8.—*Selected heating curves for the same borosilicate crown showing the effectiveness of much longer annealing periods at 450° C. in removing the effect of chilling from 750° C.*

Those curves in Figures 3, 5, 7, and 10 that were obtained on glasses which were in the intermediate conditions that must be passed through as the activity of the various processes and reactions advances a glass toward equilibrium and before the last trace of the exothermic effect disappears, all show certain peculiar transitional changes in curve form which corresponds to certain differences in such intermediate conditions. Thus, on considering the region below the treating temperatures, it is seen that a 15-minute treatment reduced the first level of the curves to its normal height for an annealed glass and

[22] The composition of Melt No. 429 is approximately: SiO_2, 47.8; BaO, 27.1; MgO, 0.2; K_2O, 7.6; B_2O_3, 4.3; CaO, 2.5; ZnO, 8.2; Na_2 O2.1; R_2O_3, 0.2.

[23] Some Thermal Effects Observed in Chilled Glass, Tool and Eichlin, Rochester, N. Y.; Oct. 24-26, 1921.

thereby eliminated in this temperature range practically all trace of an exothermic effect, although it produced only a relatively small reduction in that effect at higher temperatures. As the length of treatment increased, the exothermic effect at these higher temperatures was gradually reduced, although a vestige of it may often be detected in curves obtained on samples which have received a treatment for many hours. Whenever tests of this nature are carried out it will be found that in almost every case some of the moderately short treatments, especially if they are given at low temperatures, result in curves having the form shown by curve 7 (fig. 3), where a slight but characteristic depression occurs in the curve in the temperature range corresponding to the beginning of the normal endothermic effect of a glass that is well annealed. This probably signifies that certain exothermic processes were practically completed by these moderately short treatments to the extent required for equilibrium at the low annealing temperature, but that they were reversed as soon as the glass was heated to higher temperatures and became endothermically active before the reversal temperatures of certain other more sluggish, but still exothermically potent processes had been reached.[24]

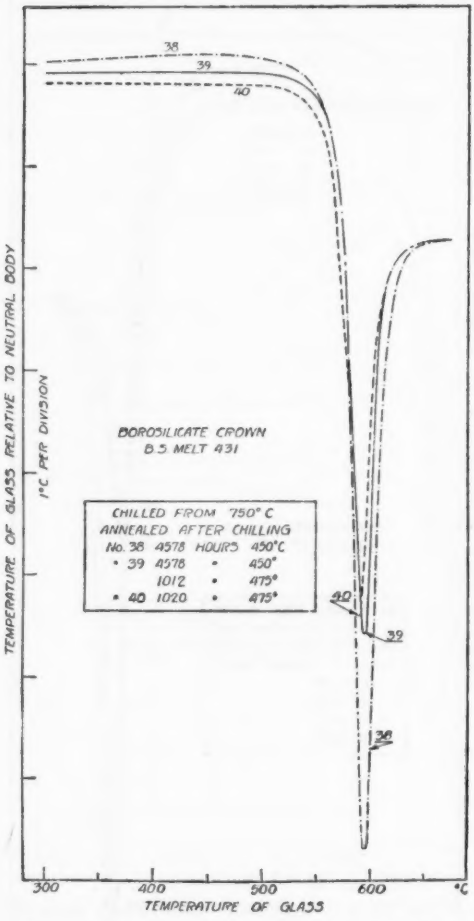

FIGURE 9.—*A comparison of the results of relatively thorough annealing treatments received by the chilled borosilicate crown at 450° and 475° C.*

A study of these curves also suggests that at times an exothermic process whose reversal temperature is found to be near that of the previous treatment may easily be more active in that range than one whose reversal temperature after the same previous treatment is

[24] A certain amount of evidence has been found showing that some of these exothermic processes in incompletely annealed glasses do not reach their maximum activity until temperatures near the upper limit of the usual endothermic effect are reached. In the case of the borosilicate investigated this would be in the neighborhood of 600° C. Such evidence is, however, difficult to obtain, since all exothermic effects in this range are masked by the greater endothermic effects arising from processes having lower reversal temperatures.

much higher, but whose activity might have been the greater and more potent of the two if the preceding treating temperature had been higher. Whenever there is any marked interference between such processes this change in relative activity with temperature makes it possible through a proper manipulation of treatments and cooling rates to aid either process in suppressing or hindering the other.

Some results on two other types of glass are presented in Figure 11. Of the fused germanium dioxide prepared in the laboratories of Cornell University only a limited sample was available for test. Expansivity measurements made on this glass by C. E. Merritt, of this bureau, indicated that it was unannealed, yet it will be noted that the exothermic effect shown by curve *48* for the untreated glass is small. Likewise the endothermic effect in curve *49* obtained after annealing the glass was not large, although it might have been increased possibly by choosing a more favorable heat treatment. As usual the annealing treatment did not change the difference between the first and second levels greatly.

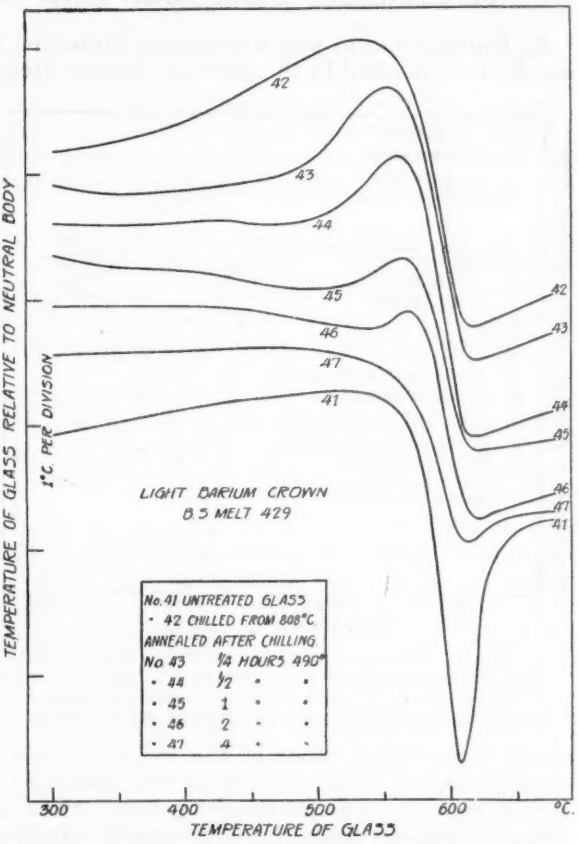

FIGURE 10.—*Heating curves obtained on samples (differently treated as indicated) of a barium crown*

These curves show that the forms of the curves presented in Figures 3, 5, and 7 and obtained after short periods of annealing chilled samples are typical results for chilled glasses that have been insufficiently annealed at low annealing temperatures.

This difference is, however, smaller than that ordinarily observed with other glasses tested. The relative smallness of the exothermic and endothermic effects before and after annealing, respectively, and of this difference between levels as compared with the corresponding effects in most other glasses may possibly be ascribable both to a smaller tendency toward intramolecular changes in this glass and to a greater sluggishness on the part of its processes.

The silicate of soda glass was a soluble commercial product of undetermined composition. Curve *50* was taken on some of the original

or untreated glass, while curve *51* is the result obtained on a sample after it had been treated over 600 hours at 380° C. It is evident from these curves that this treatment greatly increased the endothermic effect. In fact, so far as has been observed, this effect is always increased when any imperfectly annealed glass is reannealed in the range immediately below the temperature where the effect normally begins.

VI. GENERAL DISCUSSION AND CONCLUSIONS

1. From the data and discussions presented it is evident that the conclusions reached in the previous papers cited concerning the possibility of establishing equilibrium conditions in glass are well supported.

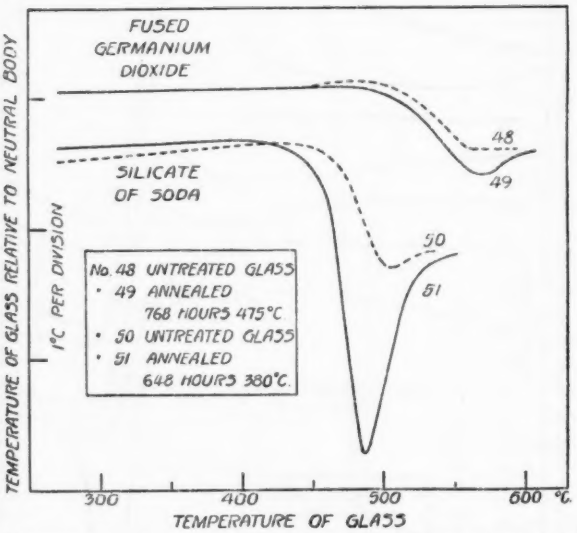

FIGURE 11.—*Heating curves of two glasses, one of which is rare and was produced for experimental purposes only, while the other, although produced commercially, is naturally not employed for the usual purposes of a glass*

2. With a given glass these conditions vary with the temperature and form a continuous chain of equilibrium conditions which generally extends throughout the practical annealing range and often to both higher and lower temperatures.

3. When a glass is treated at a chosen temperature the equilbrium for that temperature is approached at a constantly decreasing rate as the treatment is continued; that is, the reaction rates of the effective processes decreases exponentially as the treating time increases and the initial rate is correspondingly greater when the initial condition is farther removed from the equilibrium condition approached.

4. These reaction rates may also depend somewhat on the direction from which equilibrium is approached; that is, the initial rate of approaching equilibrium may depend on whether the difference between the effective annealing temperature of the initial condition and the treating temperature is positive or negative although the absolute magnitudes of these differences as measured by the changes in some characteristics of the glass may be equal.

5. Moreover, in the temperature ranges covered by these investigations and also by those on refractivity and density, both the velocity of these reactions, when the initial conditions, so far as can be determined, are about equally removed from equilbria, and the mobility of the glass appear to vary with the treating temperature in a manner which follows more or less closely the empirical rule

which has been derived from such compilations of data as that of van't Hoff [25] on the change of reaction velocity with temperature.

6. In general, both the stable condition toward which a glass of given composition [26] is advancing during treatment and the velocity of this reaction should be determined, not only by the treating temperature but also by the previous thermal history. So long, however, as this history is limited to treatments that are confined to the annealing range or still lower temperatures, most of the glasses so far tested do not show any marked effects of the previous history [27] which interfere with an almost perfect reversibility at all temperatures within the annealing range.

7. Some glasses, for example, some of the pyrex group,[28] are exceptional in this respect, since treatments in certain parts of the annealing range seem to induce conditions in these glasses which lead to different equilibrium chains or sequences at lower temperatures in that range.

8. These conditions developed in the annealing range are apparently induced by the excessive advancement of certain processes which causes an almost complete suppression of other processes which would lead to a different equilibrium sequence which may or may not be nearer that sequence followed when the cooling is extremely slow.

9. Reversing the suppressing processes by heating the glass to higher temperatures which are near or somewhat above the annealing range usually restores it again to conditions which are in the slow cooling sequence and are also common to the other equilibrium sequences involved.

10. While the glass may in many cases be carried through an indefinite number of cycles about each of these sequences there is at times some indication of a very slight drift from some of these possible sequences toward certain others which it would appear are usually those nearer the slow cooling sequence. This would seem to

---

[25] van't Hoff, Chemische Dynamik, p. 225; 1898. Ref. from Nernst's Theoretical Chem. van't Hoff, Chemical Dyanamics, p. 125; 1896. Translation by Ewan.

[26] In this connection the effect of ever-present impurities, dissolved gases, etc., can not be entirely neglected, but as so little is known, in general, concerning their action, an attempt at this time to analyze any possible relation they may have to the heat effects and the various changes caused by different heat treatments appears to be useless.

[27] It is evident from the foregoing discussion that any glass in common use can not be reduced to equilibria corresponding to ordinary or atmospheric conditions; and even at relatively high temperatures there is, with some glasses at least, a question concerning whether the condition actually developed is the ultimate condition of stability that would have been reached if the resistance met at various periods during the cooling from the molten state had not grown too great to allow a sufficiently rapid readjustment. This question remains even though a certain reversibility is later obtained when the temperature of treatment is raised and lowered repeatedly through various cycles in the annealing range. If the failure to reach a condition of ultimate stability can result from the previous heat history at relatively high temperatures as well as the temperatures in the annealing range, it may well happen in some cases that varying the number, length, and type of treatments in certain ranges (the molding range, for example) may bring such a condition considerably nearer and materially change the apparent equilibrium series of conditions at other, and especially at lower temperatures.

This effect of previous history at high temperatures leads to the possibility of more than one equilibrium series throughout the annealing range of a glass as well as in the still lower ranges previously mentioned. In part, this possibility is the basis for the feeling sometimes expressed that changes in the method of processing glass at high temperatures produce permanent differences in its properties without altering the compsoition; and it is a very good reason for experiments, such as those of Eckert (Zeit. f. Tech. Phys., p. 282; 1924). It has been found, however, that, as his results also indicate, irreversible effects of previous history at molding temperatures are probably small, since preheating most glasses to relatively high temperatures before reannealing will usually erase such differences in properties as may have been observed in a glass at lower temperatures unless the causes of such differences were originally produced at temperatures well above the annealing range (for example, by long treatments in the molding range or at even higher temperatures). In such cases the causes may have constituted a change in composition, something having the nature of a devitrification, or possibly a greater degree of segregation of the components as their mutual solubility decreased at temperatures below the melting range. Increasing devitrification caused by prolonged treatments at high temperatures will, for example, cause a gradual shift of the range in which the endothermic effect observed in heating curves is obtained.

[28] Tool and Hill, Trans. Soc. Glass Tech., p. 9, 196; 1925. Tool, Peffer, and Saunders, Toronto Meeting American Ceramic Soc., Toronto, Canada; February, 1930.

indicate that there is often a varying degree of approximate stability in these sequences and that the suppression of those processes whose lack of advancement caused the glass to enter the less stable sequence was not complete.

11. It may well be that the chief difference between glasses showing this effect and the apparently more common type which do not is chiefly a matter of the detectability of the effect and of the temperature range in which it occurs. That is, all glasses at temperatures below the annealing range may be made to follow a large number of different sequences about which it is possible to carry them through apparently closed cycles of conditions; but it may well be that these sequences constitute a series of only quasistable conditions, and that if the cycles about them are repeated a sufficiently large number of times a drift could be detected toward the sequence of equilibrium conditions which apparently can only be reached by a cooling treatment that would be so extremely slow that it would be impractical, if not impossible.[29]

12. The two glasses (B. S. Melts, Nos. 431 and 494) which yielded the greater part of the data given in this article and which with a number of others have been thoroughly investigated with regard to the refractivity and density changes [30] which are possible as a result of treatments in the annealing range,[31] each gave evidence of only a single equilibrium sequence in this range although at lower tempera-

[29] In annealing ordinary glassware it is not economically feasible to establish a fully stable condition at any point in the annealing range except possibly at the highest temperatures and from these, cooling can not be accomplished rapidly without the introduction of strain unless the articles are small. Since economy requires the shortest annealing procedure possible, the chief object, so far as the physicochemical condition is concerned, must be the obtaining of a reasonable uniformity in this condition throughout the piece of ware and the maintaining of this uniformity until comparatively low temperatures are reached where there is no danger that it will be disturbed materially. If the glass be heated to temperatures just below those where undesired deformations are to be feared, such a uniformity of condition within the glass is usually established very quickly if the temperature distribution in the ware is uniform. Furthermore, this uniformity of condition will generally be maintained to a sufficient degree throughout any cooling procedure that does not introduce undesirable strain. The physicochemical condition resulting from such a treatment will usually correspond, at least roughly, though not exactly, to one of equilibrium at some temperature which can be determined approximately. (See par. 14, Pt. IV.) If this temperature is fairly low in the annealing range, the changes in the condition of the glass will neither be noticeable over reasonably long periods nor markedly different in the various parts of the piece so long as it is always used at considerably lower temperatures and is not subjected to large and long-continued temperature differences between its parts.

This ordinary annealing is, however, not adequate for glass intended for precision apparatus even when there is no strain of an undesirable magnitude present. For example, it was shown in the paper cited in footnote 17 that a gradient of 1° per meter within the annealing furnace, while it is being held at the annealing temperature might easily cause such a lack of physicochemical homogeneity that variations of several units in the sixth decimal of the refractivity would result even within pieces of glass whose major dimension was not more than 10 cm.

[30] Tool and Hill, Trans. Soc. Glass Tech., **9**, p. 196: 1925. Annual Reports of the Director of the Bureau of Standards, U. S. Department of Commerce, pp. 11, 23, 21, and 25 of years 1925, 1927, 1928, and 1929, respectively.

[31] Since glass is employed chiefly at ordinary temperatures, data which are obtained on its refractivity and density under such conditions and which are serviceable in determining the effective annealing temperatures are more important from a practical standpoint than those obtained on the same properties at temperatures where the glass is being treated for the establishment of equilibrium conditions. Theoretically, however, it is also very important that data on these properties should be determined not only at a standard temperature in the range where glass is ordinarily used, but also at several temperatures in the range where equilibria can be attained. In fact, this should be done in every range where appreciable changes of any sort from heat treatment are likely. Only in this way can the relations between the properties of glass at different temperatures and in different conditions of equilibrium be satisfactorily determined, and the effects of annealing, of cooling at different rates, and of other variations in the treatments be fully evaluated.

Early in the progress of these investigations consideration was given to an interference method whereby the rate of approaching equilibrium could be studied and whereby other tests regarding this condition could be made through data simultaneously obtained on both the density and the refractivity changes which occur while the annealing, cooling, and heating treatments are being accomplished. So far, however, very little progress has been made on this project; and since such a method becomes tedious when the changes progress as slowly as they do at the lower temperatures of the annealing range which, from the standpoint of optical glasses, are the most important it was decided to use for that range of treating temperatures the less comprehensive method described in a previously mentioned paper. (See footnote 17, p. 540.) That the interference method could be used to advantage in the upper annealing range is shown by Lebedeff's (footnote 19 p. 543) data (obtained by another method) on the refractivity changes occurring during treatment.

tures there was the usual multiplicity of such sequences,[32] about which cyclic chains of "intermediate"[33] conditions may be established by suitable heat treatments at different points in a series of temperature cycles.

13. This tendency of glass to follow sequences of quasistability at relatively low temperatures is presumably due to the persistence of certain reversible processes after many of the important ones in the annealing ranges have been suppressed. Among the important processes which persist are those responsible for the true expansivities and contractivities as well as those which produce the modifications which result in the corresponding apparent coefficients.

14. Without taking into account the possible effects of the previous history of a glass at temperatures above the annealing range and considering only the great number of unstable sequences which it may be made to follow in the annealing range and which apparently become equilibrium series of conditions at still lower temperatures where they may be made to branch into a still greater number of such sequences because of certain unsuppressed processes, it will be seen that the apparently stable conditions in which a glass may be procured at room temperatures is unlimited and that any of its properties can be made to assume values anywhere within ranges of considerable breadth.

15. The density and refractivity, for example, can be varied in the neighborhood of 1 per cent, and roughly one-half of this may be procured by varying the treatments in the lower part of the annealing range which is that portion of the range utilizable for optical glass.

16. The various effects mentioned are also found in simple glasses; that is, those comprising only one oxide,[34] such as B_2O_3,[35] SiO_2, or GeO_2, as well as in the more complex.[36]

---

[32] Tool, Lloyd, and Merritt, B. S. Jour. Research, **5**, p. 627; 1930. J. Am. Ceramic Soc., **13**, p. 632; 1930.

[33] The term "intermediate condition" refers to one which arises, for example, during the transition from a condition of equilibrium at one temperature to that at another, but which may not be one of equilibrium at any temperature. (See footnote 12, p. 534.) The possibility that such conditions are produced in glass has been mentioned previously (see article by Tool and Hill, J. Soc. Glass Tech., **9**, 190; 1925), and it should be added that analogous conditions may arise even in very fluid solutions when the temperature is varied rapidly.

[34] It is possible that there may be several components in a glass with only one constituent oxide and that the equilibrium between these possible components may vary with the temperature. The processes involved in producing such an equilibrium condition might account for the thermal effects noted in the simple glasses mentioned as well as in the more complex. To some, these different components may appear to be caused by varying degrees of polymerization and the formation of complex molecules from groups of simple units as predicated by different theories. (For example, see theory of Asch and Asch, The Silicates in Chemistry and Commerce, Translation by Searle, Constable & Co., London; 1913.) Others may see a similarity between these effects in glass and the development of the more orderly molecular arrangements which have apparently been detected by means of X-ray studies of different liquids as they approach their congealing temperatures. It may also seem that the processes contemplated in both views may either be independent or related in their possible responsibility for the changes observed in glass, but in view of the data available at present it would appear inadvisable to speculate too deeply concerning the nature of the processes involved in the various unknown molecular rearrangements which probably occur.

[35] In view of the probable density changes coincident with changes in rate of cooling a B_2O_3 glass (in regard to the heat absorption effect in this glass see Tool and Valasek, B. S. Sci. Papers, No. 358; 1920) it would appear unsafe to base conclusions concerning the relative atomic weights of boron in different samples on density measurements made on this glass, as Briscoe, Robinson, and Stephenson (J. Chem. Soc., London, p. 70, pt. 1; 1926) appear to have done, unless great care is taken to cool the whole set of samples required in any one comparative test according to the same schedule.

[36] It would appear that similar effects should be found in glasses containing no silica or, for that matter, any of the other necessary acidic constituents common to ordinary commercial inorganic glasses. This leads to the assumption that they are probably present in all vitreous organic materials as well. Such a view is supported by the results of M. O. Samsoen, Contribution a L'étude de L'état Vitreux et de la Dilatation des Verres (1927) and also of G. S. Parks and various collaborators:

Gibson, Parks, and Latimer, J. Am. Chem. Soc., **42**, p. 1547; 1920.
Gibson and Giangue, J. Am. Chem. Soc., **45**, p. 93; 1923.
Parks, and Latimer, J. Am. Chem. Soc. **47**, 341; 1925.
Parks and Huffman, Sci., **64**, p. 364; 1926.
Parks and Huffman, J. Phys. Chem., **31**, p. 1842; 1927.
Parks, Huffman, and Cattoir, J. Phys. Chem., **32**, 1368; 1928.
Cattoir and Parks, J. Phys. Chem., **33**, p. 879; 1929.
Parks and Gilkey, J. Phys. Chem., **33**, p. 1428; 1929.

In these articles many other important references are noted which bear directly on the nature of the vitreous state.

17. This degree of possible variation emphasizes the need for great care in duplicating exactly the annealing conditions whenever it is necessary to produce a high degree of uniformity [37] in any property of a large piece or a large number of pieces of a glass.

18. It also suggests the use of variations in the annealing schedule for the purpose of compensating for small differences in certain properties where such differences result because of slight accidental variations between the compositions of different melts.

19. Furthermore, it shows the caution which must be exercised whenever it is desired to determine the effect a change in certain constituents of a glass will have on any property, such as density or refractivity. This follows since any change in composition also changes the annealing characteristics of a glass and usually makes it inadvisable to follow the same annealing schedule for all samples while at the same time there are no adequate clues as to what would be the equivalent schedules in the various cases.

WASHINGTON, September 1, 1930.

[37] Tilton, Finn, and Tool, B. S. Sci. Papers, **22** (No. 570), p. 719; 1928. Tilton, Finn, and Tool, J. Am. Ceramic Soc., **11**, 292; 1928.

ON THE VIBRATION OF U BARS

By G. H. Keulegan

ABSTRACT

A theoretical study has been made of elongated and short U bars with special reference to their use as vibrators in investigations on elastic hysteresis.

First, an expression for the frequency of the fundamental mode of vibration of the elongated U bar is derived by solving the differential equations of motion of the yoke and of the prongs through the use of an approximation. The physical basis of the approximation is the fact that the bar vibrates with a pitch differing slightly from that of the clamped-free bar of half the length.

Secondly, Ritz's method of approximation is developed for initially curved bars, the development being based on the principle of least action. In this connection a new proof is given of Rayleigh's method for determining the fundamental mode of vibration. As an illustration of Ritz's method, the example of the free-free bar is treated, and the results of the calculation are compared with the known solution of this problem. Next, the method is used to determine the fundamental mode of vibration of the short U bar, a short U bar being defined as one wherein the length of the curved portion, or the yoke, is equal to the sum of the lengths of the two parallel prongs.

Finally, Rayleigh's method is used to determine the static deformation of the short U bar, produced by the application of a single load so applied that the deformation is most nearly that present in the fundamental mode of vibration.

CONTENTS

	Page
I. Introduction	553
II. Formation of the equation of motion of a U bar	554
1. Displacements and stress components in curved bars	554
2. Equation of motion of a U bar	559
3. End conditions and conditions of continuity	561
4. Condition for the invariancy of the center of gravity	561
III. The frequency of vibration of an elongated U bar	562
1. Approximate values of the quantities n,a	562
2. Frequency of vibration in elongated U bars	565
3. The deformation of the circular yoke	569
IV. Ritz's method of approximation	571
1. Application of Ritz's method to curved bars	571
2. An illustration from a classical problem	575
V. Rayleigh's method for determining the fundamental mode of vibration	578
VI. Vibration of a short U bar	580
VII. Effect of the yoke on vibration	585
VIII. Reproduction by a single load of deformations due to vibration	586
IX. Acknowledgment	595

I. INTRODUCTION

Although hysteresis in elastic materials has engaged in recent times the attention of engineers and physicists alike, the information which is available on the subject is very fragmentary. Progress in this field is hindered by the lack of a proper technique for obtaining results quickly. For example, one of the more obvious methods of securing

data is that of making statical measurements. If, however, this method is used to determine the constants relating to hysteresis which are typical of a given material, it is necessary to test a multitude of samples of the material and to average the results, similarly as in determining the fatigue of materials. Accordingly, the method of statical measurements, being thus of a time-consuming nature, is not ideal.

In looking for a more rapid method, the damping of free oscillations readily suggests itself. Here, however, the choice of the vibrator must be made judiciously since two conditions must be fulfilled. First, the damping of the free oscillations must be due mainly to hysteresis, or internal friction. Second, the shape of the vibrator must be such that it can be used in securing statical measurements, with a view to effecting a comparison between statical and dynamical results.

To satisfy the first condition, the method of support must in no way contribute to the damping. When the nodal points of a vibrator executing vibrations of the fundamental type are in close proximity to each other, and the vibrator is suspended at these points, the damping may be assumed to be due principally to internal friction. It suffices, to see the truth of this statement, to point to the fact that during the motion, the distance between the nodal points varies periodically, and the smaller this distance, the less the effect of the supports on the vibration. In making statical measurements, it is advisable always to deal with deformations brought about by the application of a single load. A statical deformation so produced and duplicating as nearly as possible the dynamical deformation is chosen for direct comparison of the hysteresis during dynamical and statical tests. Only for the fundamental mode of vibration can this equivalence be accomplished by properly choosing the point of application of a single load.

The use of bars which are of U shape as possible vibrators for securing data on elastic hysteresis has many advantages. In this paper it is proposed to study the fundamental mode of vibration of two types of U bar, namely, one which is elongated, and one where the curve and the sum of the straight portions are of equal length. In all cases the yoke will be assumed to be of semicircular shape, and the prongs straight and parallel.

II. FORMATION OF THE EQUATION OF MOTION OF A U BAR

1. DISPLACEMENTS AND STRESS COMPONENTS IN CURVED BARS

Let E_1OE_2 represent the median line of a symmetrically curved bar. (See fig. 1.) The position of a point P on the median line is determined by the distance s of the point from the mid-point O of the curved bar, measured on the median line. s is positive when on the branch OE_1, negative when on the branch OE_2. Choose rectangular axes (x, y) having the mid-point O as origin and the x-direction midway between the prongs. The normal PC to the median line at the point P is drawn, making the angle α with the x-axis. The radius of curvature will be denoted by ρ. Draw the tangent PA making with the x-axis the angle i. The angle i will be spoken of as

the inclination of the bar at P. Expressing x, y as functions of s we have

$$\cos i = \frac{dx}{ds}$$

$$\sin i = \frac{dy}{ds} \tag{1}$$

and

$$\frac{1}{\rho} = -\frac{di}{ds}$$

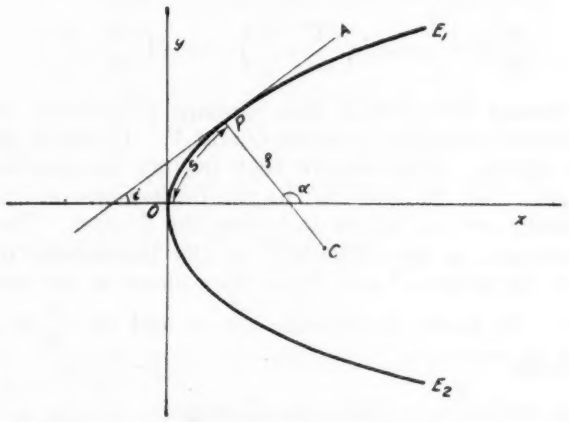

FIGURE 1.—*Median line of a symmetrically curved bar*

Let U and V be the normal and tangential displacements of the point P as it moves to the position P'. (See fig. 2.) U is measured along the normal and is regarded as positive when the displacement

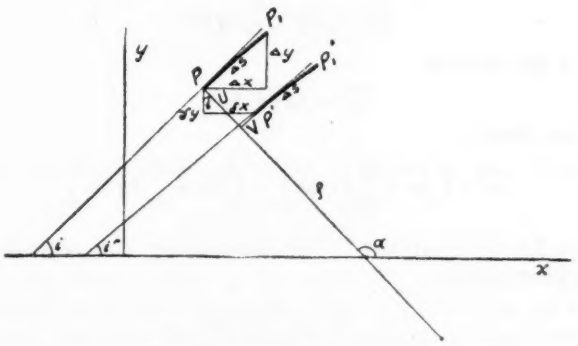

FIGURE 2.—*Displacements of a point on the median line*

is toward the center of curvature (when the normal is behind the tangent). V is measured on the tangent, and is regarded as positive when in the direction of increasing s. It will be assumed temporarily that these displacements are due to body forces and distributed

couples acting on the bar. Denoting by δx and δy the increments in the coordinates of the point P as it moves to the position P', we have

$$\begin{aligned} \delta x &= U \sin i + V \cos i \\ \delta y &= -U \cos i + V \sin i \end{aligned} \tag{2}$$

Differentiating with respect to s

$$\begin{aligned} \frac{d}{ds}\delta x &= \sin i\left(\frac{dU}{ds}+\frac{V}{\rho}\right)+\cos i\left(\frac{dV}{ds}-\frac{U}{\rho}\right) \\ \frac{d}{ds}\delta y &= -\cos i\left(\frac{dU}{ds}+\frac{V}{\rho}\right)+\sin i\left(\frac{dV}{ds}-\frac{U}{\rho}\right) \end{aligned} \tag{3}$$

During flexure the median line remains practically unextended. This establishes a relation between U and V. Consider the points P and P_1, Δs apart. After flexure they occupy the positions P′ and P_1', Δs apart. Let Δx and $\overline{\Delta x}'$ be the projections on the x-axis of this elementary arc Δs, before and after the flexure. The difference $\overline{\Delta x}' - \Delta x$ amounts to the difference in the increments of the x-coordinates of the points P and P_1 as they move to the new positions P' and P_1'. As these increments are δx and $\delta x + \frac{d}{ds}\delta x\ \Delta s$, respectively, we have

$$\overline{\Delta x}' - \Delta x = \frac{d}{ds}\delta x\,\Delta s$$

or

$$\overline{\Delta x}' = \Delta x + \frac{d}{ds}\delta x\,\Delta s$$

Similiarly

$$\overline{\Delta y}' = \Delta y + \frac{d}{ds}\delta y\,\Delta s$$

Since before the flexure

$$\overline{\Delta s}^2 = \Delta x^2 + \Delta y^2$$

and after the flexure

$$\overline{\Delta s}^2 = \left(\Delta x + \frac{d}{ds}\delta x\,\Delta s\right)^2 + \left(\Delta y + \frac{d}{ds}\delta y\,\Delta s\right)^2$$

one obtains by comparison, after neglecting the squares of small quantities, the relation

$$\frac{d}{ds}\delta x \cdot \frac{\Delta x}{\Delta s} + \frac{d}{ds}\delta y \cdot \frac{\Delta y}{\Delta s} = 0$$

which in view of equations (1) and (3) reduces to

$$\frac{dV}{ds} = \frac{U}{\rho} \tag{4}$$

the well-known condition for inextensibility of the median line.

If i and i' are the inclinations at the point P before and after the flexure, the change of inclination, H, is defined to be

$$H = i - i'$$

It also follows, since the change of inclination is small,

$$H = \sin\,(i - i')$$

Expanding

$$H = \sin\, i \cos\, i' - \cos\, i \sin\, i'$$

since

$$\cos\, i' = \frac{d}{ds}(x + \delta x) = \cos\, i + \frac{d}{ds}\delta x$$

and

$$\sin\, i' = \frac{d}{ds}(y + \delta y) = \sin\, i + \frac{d}{ds}\delta y$$

it follows that

$$H = \sin\, i \frac{d}{ds}\delta x - \cos\, i \frac{d}{ds}\delta y$$

This, in veiw of equations (3), reduces to

$$H = \frac{dU}{ds} + \frac{V}{\rho} \tag{5}$$

which is the expression for the change of inclination in terms of the displacements U and V.

If ρ and ρ' are the curvatures at the point P before and after the flexure, the change of curvature K is defined to be

$$K = \frac{1}{\rho'} - \frac{1}{\rho} \tag{6}$$

As a consequence of the definition of curvature, there is also obtained

$$K = -\frac{d}{ds}(i' - i)$$

or

$$K = \frac{dH}{ds} \tag{7}$$

Therefore, the change of curvature in terms of the displacements is

$$K = \frac{d}{ds}\left(\frac{dU}{ds} + \frac{V}{\rho}\right) \tag{8}$$

Imagine the bar broken at the point P. (Fig. 1.) In order that the deformation of the remaining portion of the bar in the direction of decreasing length s may be unaffected, it will be necessary to apply to the end section at P a bending moment G, a tension T, and a shear N. These are the stress components with which the portion of the bar in the direction of increasing s acts on the normal section at P. Using the Euler-Bernouli assumption; that is, neglecting

antielastic curvature and the effect of the curvature of the bar [1] on the stress distribution in the cross section, one writes

$$G=BK=B\frac{dH}{ds} \tag{9}$$

where B is the flexural rigidity, defined as the product of Young's modulus, E, and the moment of inertia of the section, I. The two remaining stress components T and N are secured as usual in the following manner from the relations of equilibrium obtained for an elementary portion of the bar under body forces.

Let F_n and F_t be the normal and tangential components of the body forces calculated per unit length of the bar. Let M be the distributed couple, applied externally, calculated likewise per unit length of the bar. The condition for equilibrium gives

$$\begin{aligned}\frac{dN}{ds}+\frac{T}{\rho}+F_n&=0\\ \frac{dT}{ds}-\frac{N}{\rho}+F_t&=0\\ \frac{dG}{ds}+N+M&=0\end{aligned} \tag{10}$$

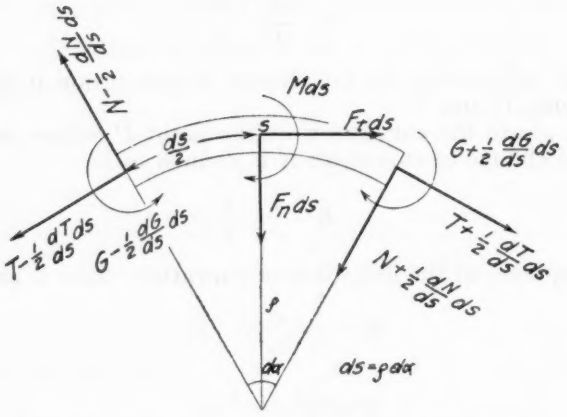

FIGURE 3.—*Stress components and body forces acting on an elementary portion of a curved bar*

These equations result readily from the normal and tangential resolution of the forces and couples, as shown in Figure 3.

For bars in vibration the body forces are taken to be the reverse of the effective forces. Accordingly

$$\begin{aligned}F_n&=-\omega\gamma\frac{d^2U}{dt^2}\\ F_t&=-\omega\gamma\frac{d^2V}{dt^2}\end{aligned} \tag{11}$$

[1] A discussion, dealing with the stress distribution in curved bars, will be found in Applied Elasticity, by Timoshenko and Lessels, Chap. IX. Westinghouse Technical Night School Press, East Pittsburgh, Pa., 1925.

where ω is the area of normal section and γ the density of the bar material. It is customary in problems of vibration to discard the rotational inertia. This is equivalent to supposing that M is negligible in comparison with N. Thus, from the third equation in (11), assuming that the bar is uniform in flexural rigidity, the value of the shear is

$$N = -B\frac{d^2H}{ds^2} \tag{12}$$

And from the first equation in (10), the expression for the tension is

$$T = B\rho\frac{d^3H}{d\ s^3} - F_n\rho \tag{13}$$

2. EQUATION OF MOTION OF A U BAR

The equation of motion of a bar of variable curvature in terms of the displacement follows directly from the second equation in (10), using equations (11), (12), and (13), and is, in fact,

$$\frac{Bd}{ds}\left(\rho\frac{d^3H}{ds_3}\right) + \frac{B}{\rho}\frac{d^2H}{ds^2} - \omega\gamma\frac{d^2V}{dt^2} + \omega\gamma\frac{d}{ds}\left(\rho\frac{d^2U}{dt^2}\right) = 0 \tag{14}$$

Set

$$H = \eta \cos kt$$
$$U = u \cos kt$$
$$V = v \cos kt$$

and

$$\mu^4 = \frac{\omega\gamma k^2}{B} \tag{15}$$

in equation (14), and there is obtained

$$\frac{d}{ds}\left(\rho\frac{d^3\eta}{ds^3}\right) + \frac{1}{\rho}\frac{d^2\eta}{ds^2} + \mu^4\left(v - \frac{d}{ds}[\rho u]\right) = 0 \tag{16}$$

with the auxiliary relations

$$\frac{dv}{ds} = \frac{u}{\rho} \qquad \eta = \frac{du}{ds} + \frac{v}{\rho} \tag{17}$$

Equation (15) defines the frequency of vibration, $\frac{k}{2\pi}$, in terms of μ and the constants of the bar B, the flexural rigidity, γ, the density, and ω the cross-sectional area. When μ is multiplied by a linear dimension, the product gives a dimensional number. We take s_1 the half length of the bar for this linear dimension for bars curved symmetrically in a plane. For bars with one end clamped and the other end free, this dimension is s_1 the total length of the bar. In subsequent pages μs_1 will be occurring constantly, and will be referred to as the frequency characteristic.

When the bar is of uniform curvature, there is but one fundamental equation of the type of (16) to consider. Where there are different curvatures, as in a U bar, the differential equation (16) assumes

different forms for different portions of the bar. In the present case, it is assumed that the yoke is a semicircle of radius a and of length $2s_o$. The prongs are straight and parallel to each other. The total length of the U bar is $2s_1$. (See fig. 4.) Accordingly, the distribution of curvature is

$$\frac{1}{\rho}=\frac{1}{a}, \text{ when } 0\leq s\leq s_0$$

$$\frac{1}{\rho}=0, \text{ when } s_o\leq s\leq s_1$$

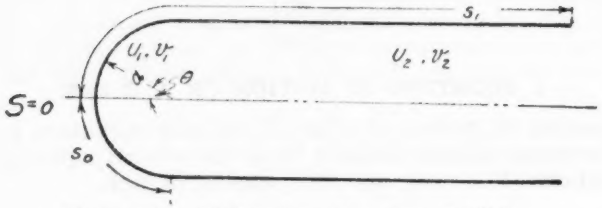

FIGURE 4.—*Median line of an elongated* U *bar*

Denoting the longitudinal and the normal displacements in the yoke by v_1 and u_1, equation (16) yields, by putting $\rho=a$

$$a^6\frac{d^6v_1}{ds^6}+2a^4\frac{d^4v_1}{ds^4}+(1-\mu^4a^4)a^2\frac{d^2v_1}{ds^2}+\mu^4a^4v_1=0 \tag{18}$$

Hence, if $\pm in_1$, $\pm in_2$, and $\pm in_3$ are the roots of the equation

$$a^6x^6+2a^4x^4+(1-a^4\mu^4)\,a^2x^2+a^4\mu^4=0 \tag{19}$$

the displacements v_1 and u_1 are given by

$$\begin{aligned} v_1&=\sum_{i=1}^{3}A_i\cos n_is+\Sigma\, B_i\sin n_1s \\ u_1&=a\frac{dv_1}{ds} \end{aligned} \tag{20}$$

Denoting the longitudinal and the normal displacements in the prongs by v_2 and u_2 there results from equation (16), by putting $\rho=\infty$

$$\frac{d^4u_2}{ds^4}-\mu^4u_2=0 \tag{21}$$

Accordingly

$$v_2=c_1a \text{ constant}$$

and

$$\begin{aligned} u_2=&D(\cos\ \mu s+\cosh\ \mu s)+E(\cos\ \mu s-\cosh\ \mu s) \\ &+F\ (\sin\ \mu s+\sinh\ \mu s)+G(\sin\ \mu s-\sinh\ \mu s) \end{aligned} \tag{22}$$

It is of interest to note that equation (21) also follows directly from (13). Since T is a finite quantity, the multiplier of ρ must approach the limit zero as ρ becomes infinite.

3. END CONDITIONS AND CONDITIONS OF CONTINUITY

The application of equation (20) to the vibration of a circular arc and of equations (22) to the vibrations of a straight bar are well known. Here the two sets are to be taken together, as the U bar considered here is partly circular and partly straight. This means merely that the constants of integration in (20) and (22) bear definite relations to one another. There are altogether 11 constants to be considered. All the A's drop out when the modes of vibration are symmetrical with respect to the axis of the U bar. The fundamental mode of vibration, which is of practical interest, is of this type. The U bar having free ends,

$$\frac{d^2u_2}{ds^2}=0, \text{ when } s=s_1$$
$$\frac{d^3u_2}{ds^3}=0, \text{ when } s=s_1 \tag{23}$$

Since the displacements, the change of inclination, the bending moment, and the shear are continuous

$$v_1=v_2$$
$$u_1=u_2$$
$$\frac{du_1}{ds}+\frac{v_1}{a}=\frac{du_2}{ds} \tag{24}$$
$$\frac{d}{ds}\left(\frac{du_1}{ds}+\frac{v_1}{a}\right)=\frac{d^2u_2}{ds^2}$$

and

$$\frac{d^2}{ds^2}\left(\frac{du_1}{ds}+\frac{v_1}{a}\right)=\frac{d^3u_2}{ds^3}$$

all when $s=s_0$.

4. CONDITION FOR THE INVARIANCY OF THE CENTER OF GRAVITY

One more condition is needed. It is obtained under the supposition that the center of gravity of the whole U bar experiences no displacement during the vibration. This is necessarily true, as no external forces are acting. Since the mode of vibration to be considered (the fundamental) is one of symmetry with respect to the axis of the U bar (that is, the x-axis), the y coordinate of the center of gravity is always zero. The x coordinate, however, since the bar is of uniform cross section and of uniform density, is given by

$$\bar{x}=\frac{1}{s_1}\int_0^{s_1} x\,ds$$

when there is no flexure. On the other hand, when flexure exists, as during vibration,

$$\bar{x}=\frac{1}{s_1}\int_0^{s_1} (x+\delta x)\,ds$$

Thus the condition for the invariancy of the center of gravity resolves into

$$\int_0^{s_1} \delta x ds = 0 \tag{25}$$

From equation (2)

$$\delta x = u_1 \sin i + v_1 \cos i \quad \text{when } o \leq s \leq s_0$$

$$\delta x = v_2 \quad \text{when } s_0 \leq s \leq s_1$$

Substituting these values of the increment αx in equation (25), there results

$$\int_0^{s_0} (u_1 \sin i + v_1 \cos i)\, ds + \int_{s_0}^{s_1} v_2 ds = 0$$

Since in the curved portion we have

$$\frac{di}{ds} = -\frac{1}{a}$$

$$u_1 = -\frac{dv_1}{di}$$

and

$$v_2 = v_1 (s_o)$$

the above equation may be written also as

$$a\int_{\frac{\pi}{2}}^{0} \left(-\sin i \frac{dv_1}{di} + v_1 \cos i\right) di + v_1 (s_o) \int_{s_0}^{s_1} ds = 0$$

or

$$a\int_{\frac{\pi}{2}}^{0} \frac{d}{di}(v_1 \sin i)\, di + 2a\int_{\frac{\pi}{2}}^{0} v_1 \cos i\, di + v_1 (s_o) \int_{s_0}^{s_1} ds = 0$$

The first integral vanishes; for v is equal zero when $i = \frac{\pi}{2}$. Thus the condition for the invariancy of the center of gravity becomes, replacing i by $\frac{\pi}{2} - \theta$

$$v_1 (s_o) = -\frac{2a}{s_1 - s_o}\int_0^{\frac{\pi}{2}} v_1 \sin \theta d\theta \tag{26}$$

where $\theta = s/a$.

III. THE FREQUENCY OF VIBRATION OF AN ELONGATED U BAR

1. APPROXIMATE VALUES OF THE QUANTITIES $n_i a$

The expressions of the tangential and radial displacements, as given in equations (20) involve the quantities $n_i a$ when s is replaced by νa, a being the radius of the circular yoke. The quantities $n_i a$, however, depend on the frequency characteristic μs_1. It, therefore, becomes necessary to express them as explicit functions of μa.

Setting

$$a^2\mu^2=\phi^2$$

and

$$a^2x^2=y \tag{27}$$

in equation (19), the resultant cubic is

$$y^3+2y^2+y+\phi^4(1-y)=0 \tag{28}$$

with the roots y_1, y_2, y_3, say. The roots of equation (19) being $\pm in_1$, $\pm in_2$, and $\pm in_3$, it follows that

$$\begin{aligned} y_1&=-n_1^2a^2 \\ y_2&=-n_2^2a^2 \\ y_3&=-n_3^2a^2 \end{aligned} \tag{29}$$

If the bar is sufficiently long the quantities n_ia can be developed into series of ascending powers of μ^2a^2, or θ^2, since μ^2a^2 is a small quantity. The smallness of μ^2a^2 follows from the fact that the frequencies of vibration of an elongated U-bar of length $2s_1$ and of a clamped-free bar of length s_1 are nearly equal. Now, the frequency characteristic of a clamped-free bar satisfies the equation [2]

$$\cosh \mu s_1 \cos \mu s_1=-1$$

To obtain the frequency characteristic for the fundamental we take the smallest root; that is, $\mu s_1=1.8751$. Hence, for the elongated U bar, we put, since its fundamental frequency is nearly the same, $\mu s_1=1.8751+x$, where x is a small quantity. Hence

$$\mu a=(1.8751+x)\frac{a}{s_1}$$

and, therefore, can be made as small as it is desired by taking a small enough while s_1 is kept constant.

The series for n_ia will now be derived. The reduced cubic

$$z^3+pz+q=0 \tag{30}$$

follows, when $y=z-\frac{2}{3}$ is set in equation (28). The explicit expressions for p and q are

$$\begin{aligned} p&=-1/3(1+3\phi^4) \\ q&=-\frac{2+45\phi^4}{27} \end{aligned} \tag{31}$$

The reduced cubic will have three distinct roots, all real, when the discriminant is negative. The discriminant is negative as long as the quantity ξ^2, defined as the ratio

$$\xi^2=\frac{1}{4}\,\frac{(-2+45\phi^4)^2}{(1+3\phi^4)^3} \tag{32}$$

[2] Rayleigh. The Theory of Sound, **1**, 2d ed., p. 278.

is smaller than unity. Accordingly, when $3\phi^4<0.34$ we may adopt the trigonometric form of solution, and pass over the roots z_1, z_2, z_3, to the roots y_1, y_2, y_3, writing

$$y_1=-\frac{2}{3}-\frac{2}{3}\sqrt{1+3\phi^4}\cos\frac{\psi}{3}$$

$$y_2=-\frac{2}{3}-\frac{2}{3}\sqrt{1+3\phi^4}\left(\frac{1}{2}\cos\frac{\psi}{3}-\sqrt{\frac{3}{2}}\sin\frac{\psi}{3}\right) \tag{33}$$

$$y_3=-\frac{2}{3}-\frac{2}{3}\sqrt{1+3\phi^4}\left(\frac{1}{2}\cos\frac{\psi}{3}-\sqrt{\frac{3}{2}}\sin\frac{\psi}{3}\right)$$

where $\cos\psi=\xi$.

The trigonometric expressions in equation (33) require that $3\phi^4$ shall be smaller than unity if the quantities y_1, y_2, y_3 are to be developed into series of ascending powers of ϕ^2 or μ^2a^2. With the criterion of convergence thus established [$3\phi^4<0.34$] we shall proceed as explained below, instead of working with the above trigonometric expressions, to obtain the desired series. Setting separately in the original cubic equation (28)

$$y=\sum_{n=1}^{n=\infty}b_n\phi^2$$

$$y=1+\sum_{n=1}^{n=\infty}a_n\phi^2$$

and then equating to zero in the separate series thus obtained the coefficients of like powers of ϕ, we have

$$y_1=-n_1^2a^2=-\phi^4-3\phi^8-\ \ldots$$

$$y_2=-n_2^2a^2=-1-\sqrt{2}\,\phi^2+\frac{1}{2}\,\phi^4-\frac{9\sqrt{2}}{16}\,\phi^6+\frac{3}{2}\,\phi^8-\ \ldots\ . \tag{34}$$

$$y_3=-n_3^2a^2=-1+\sqrt{2}\,\phi^2+\frac{1}{2}\,\phi^4+\frac{9}{16}\sqrt{2}\,\phi^6+\frac{3}{2}\,\phi^8+\ \ldots$$

It is now apparent that the treatment of the vibration of the U bar by the method of differential equations is exceedingly complicated. Unless the treatment deals with long bars, the method must be discarded. With a view to introducing an approximation, it will be required that $\pi\phi^4$ be negligible in comparison with unity. Mathematically,

$$A(1+g\phi^4)=A$$

where (35)

$$g\leqslant\pi$$

The corresponding approximations for nia, therefore, follow:

$$n_1a=\phi^2$$

$$n_2a=1-\frac{\sqrt{2}}{2}\,\phi^2-\frac{1}{2}\,\phi^4 \tag{36}$$

$$n_3a=1+\frac{\sqrt{2}}{3}\,\phi^2-\frac{1}{2}\phi^4$$

2. THE FREQUENCY OF VIBRATION OF AN ELONGATED U BAR

As stated before, v_1, u_1, and v_2, u_2 are the tangential and normal displacements in the yoke and in the prong, respectively. For the fundamental mode of vibration

$$\begin{aligned} v_1 &= B_1 \sin n_1 s + B_2 \sin n_2 s + B_3 \sin n_3 s \\ u_1 &= n_1 a B_1 \cos n_1 s + n_2 a B_2 \cos n_2 s + n_3 a B_3 \cos n_3 s \end{aligned} \tag{37}$$

The conditions of continuity, equations (24) require that

$$\begin{aligned} &\sum_{i=1}^{3} n_i a\ B_i \cos n_i s_0 = C_0 \phi^2 \\ &\sum_{i=1}^{3} (1 - n_i^2 a^2)\ B_i \sin n_i s_0 = C_1 \phi^2 \\ &\sum_{i=1}^{3} n_i a\ (1 - n_i^2 a^2)\ B_i \cos n_i s_0 = C_2 \phi^2 \\ &\sum_{i=1}^{3} n_i^2 a^2\ (1 n_i^2 a^2)\ B_i \sin n_i s_0 = -C_3 \phi^2 \end{aligned} \tag{38}$$

where

$$\begin{aligned} C_0 \phi^2 &= (u_2)_{s_0} \\ C_1 \phi^2 &= a \left(\frac{du^2}{ds} \right)_{s_0} \\ C^2 \phi^2 &= a^2 \left(\frac{d^2 u_2}{ds^2} \right)_{s_0} \\ C_3 \phi^3 &= a^3 \left(\frac{d^3 u_2}{ds^3} \right)_{s_0} \end{aligned} \tag{39}$$

On forming the approximations

$$\cos \mu s_0 = 1 - \frac{\pi^2}{8} \phi^2 \qquad \sin \mu s_0 = \frac{\pi}{2} \phi$$

$$\cos h\mu s_0 = 1 + \frac{\pi^2}{8} \phi \qquad {}^2\sin h\mu s_0 = \frac{\pi}{2} \phi$$

on the basis of equation (35), and setting them in equations (39), there result

$$\begin{aligned} C_0 &= 2d - \frac{\pi^2}{4} E + \left(\pi f - \frac{\pi^3}{24} G \right) \phi \\ C_1 &= -E + \left(2f - \frac{\pi^2}{4} G \right) \phi \\ C_2 &= -2E - \pi G \phi \\ C_3 &= -2G + \left(\pi d - \frac{\pi^3}{24} E \right) \phi^3 \end{aligned} \tag{40}$$

where

$$D=d\phi^2$$
$$F=f\phi^2 \tag{41}$$

In the left-hand members of equations (38) occur various products of $n_i a$ and trigonometric functions of $n_i s_0$. Quantities of the type $n_i a\ (1-n_i^2 a^2)$ are to be evaluated on the basis of the approximate values of $n_i a$ given in equations (36). As regards the trigonometric functions, we put immediately, since $n_i s_0=\frac{\pi}{2} n_i a$, the approximations

$$\sin n_1 s_0=\frac{\pi}{2}\phi^2 \qquad \cos n_1 s_0=1$$

$$\sin n_2 s_0=1 \qquad \cos n_2 s_0=\frac{\pi}{4}\sqrt{2}\phi^2$$

$$\sin n_3 s_0=1 \qquad \cos n_3 s_0=-\frac{\pi}{4}\sqrt{2}\phi^2$$

Thus, the various equations (38), now become

$$B_1+\frac{\pi}{4}\sqrt{2}(B_2-B_3)-\frac{\pi}{4}(B_2+B_3)\phi^2=C_0$$

$$\frac{\pi}{2}B_1+\sqrt{2}(B_2-B_3)+\frac{1}{2}(B_2+B_3)\phi^2=C_1 \tag{42}$$

$$B_1-\frac{\pi}{8}\sqrt{2}(B_2-B_3)\phi^4+\frac{\pi}{2}(B_2+B_3)\phi^2=C_2$$

$$\frac{\pi}{2}B_1\phi^4+\sqrt{2}(B_2-B_3)-\frac{3}{2}(B_2+B_3)\phi^2-C_3\phi$$

The condition of the constancy of the center of gravity, equation (26), yields, putting $s_1-s_0=qa$

$$\sum_{i=1}^{3} B_i\left(q\sin n_i s_0+\frac{2\cos n_i s_0}{1-n_i^2 a^2}\right)=0$$

which, in virtue of the approximations adopted, becomes

$$B_2+B_3=-\frac{q\pi+4}{2q+\pi}B_1\phi^2+\frac{3\sqrt{2}\,\pi}{4(2q+\pi)}(B_2-B_3)\phi^2 \tag{43}$$

Our immediate purpose is to obtain two relations among the C_3'. To accomplish this, first, the following equations

$$2B_1+\frac{\pi}{4}\sqrt{2}(B_2-B_3)+\frac{\pi}{4}(B_2+B_3)\phi^2=C_0+C_2$$

$$\underline{\quad 0\quad}+\frac{\pi}{4}\sqrt{2}(B_2-B_3)-\frac{3\pi}{4}(B_2+B_3)\phi^2=C_0-C_2$$

$$\frac{\pi}{2}B_1+\qquad 0\qquad +2(B_2+B_3)\phi^2=C_1+C_3\phi \tag{44}$$

$$\frac{\pi}{2}B_1+2\sqrt{2}(B_2-B_3)-(B_2+B_3)\phi^2=C_1-C_3\phi$$

are derived from equations (42) with a view of eliminating the terms containing ϕ^4. We remark that in equations (44) the (B_2+B_3) terms can be neglected in virtue of the equation (43). Accordingly

$$\begin{aligned} 2B_1+\frac{\pi}{4}\sqrt{2}(B_2-B_3) &= C_0+C_2 \\ \frac{\pi}{4}\sqrt{2}(B_2-B_3) &= C_0-C_2 \\ \frac{\pi}{2}B_1 &= C_1+C_3\phi \\ \frac{\pi}{2}B_1+2\sqrt{2}(B_2-B_3) &= C_1-C_3\phi \end{aligned} \tag{45}$$

from which the two desired relations

$$\begin{aligned} C_1-\frac{\pi}{2}C_2+C_3\phi &= 0 \\ C_1-C_2+\frac{\pi}{4}C_3\phi &= 0 \end{aligned} \tag{46}$$

follow. Substituting in equation (46) the expressions for the C's as given in equations (40), there result

$$\begin{aligned} 2d+\pi f\phi &= \left(\frac{\pi^2}{4}-2\right)E+\left(\frac{\pi^3}{24}-\frac{\pi}{2}\right)G\phi \\ 2d+\pi d\phi^3 &= \left(2-\frac{\pi^2}{4}\right)G+\frac{\pi^3}{24}E\phi^3 \end{aligned} \tag{47}$$

Solving for f and d, and setting the values of f and d thus secured in equations (41), there is finally obtained

$$\begin{aligned} D &= \delta_1 E\phi^2+\delta_2 G\phi^2 \\ F &= -\delta_1 G\phi^2 \end{aligned} \tag{48}$$

where

$$\delta_1=\frac{\pi^2}{8}-1,\quad \delta_2=\frac{\pi^3}{12}-\frac{3\pi}{4}$$

To establish a relation between E and G there remains to be considered the end conditions given in equations (23). Accordingly, after substituting the values of F and D as expressed above, there result

$$\begin{aligned} &E[-\cos\mu s_1-\cosh\mu s_1+\delta_1\phi^2(-\cos\mu s_1+\cosh\mu s_1)] \\ &+G[-\sin\mu s_1-\sinh\mu s_1-\delta_1\phi^2(-\sin\mu s_1+\sinh\mu s_1) \\ &\qquad +\delta_2\phi^3(-\cos\mu s_1+\cosh\mu s_1)]=0 \\ &E[\sin\mu s_1-\sinh\mu s_1+\delta_1\phi^2(\sin\mu s_1+\sinh\mu s_1)]+ \\ &G[-\cos\mu s_1-\cosh\mu s_1-\delta_1\phi^2(-\cos\mu s_1+\cosh\mu s_1) \\ &\qquad +\delta_2\phi^3(\sin\mu s_1+\sinh\mu s_1)]=0 \end{aligned} \tag{49}$$

Hence, the condition of compatibility, which is the equation for determining μs_1, is found to be

$$\cos \mu s_1 \cosh \mu s_1 + 2 \delta_1 \mu^2 a^2 \sin \mu s_1 \sinh \mu s_1 - \delta_2 a^3 \mu^3 (\cosh \mu s_1 \sin \mu s_1 + \sinh \mu s_1 \cos \mu s_1) = -1 \tag{50}$$

Now the smallest root of the equation

$$\cos m \cosh m = -1$$

is $m = 1.8751$. Accordingly, we put

$$\mu s_1 = m + x \tag{51}$$

and substitute in the equation (50). This gives, neglecting powers of x higher than the first,

$$x = \frac{2\delta_1 m^2 \left(\frac{a}{s_1}\right)^2 \sin m \sinh m - \delta_2 m^3 \left(\frac{a}{s_1}\right)^3 (\cosh m \sin m + \cos m \sinh m)}{\sin m \cosh m - \cos m \sinh m} \tag{52}$$

Introducing the numerical values of m, δ_1, and δ_2 from above, and expressing a, the radius of the circular yoke in terms of s_0, the expression for x further becomes

$$x = 0.49\left(\frac{s_0}{s_1}\right)^2 - 0.2\left(\frac{s_0}{s_1}\right)^3 \tag{53}$$

where $\frac{s_0}{s_1}$ is the ratio of the length of the circular yoke to the total length of the bar measured on the median line.

We are now ready to give the frequency of vibration of the fundamental mode, N. This, from equation (15), is

$$N = \frac{k}{2\pi} = \frac{1}{2\pi}\sqrt{\frac{B}{\omega\gamma}}\frac{m^2}{{s_1}^2}\left(1 + \frac{2x}{m}\right) \tag{54}$$

where B is the flexural rigidity, ω the cross-sectional area, γ the density, s_1, half the length of the U bar, measured on the median line, m equals 1.8751, and x which gives the effect of the yoke on the vibration, is given by equation (53).

It is now evident from equation (54), that an elongated U bar of length $2s_1$ and a clamped-free bar of length s_1 will vibrate with nearly the same frequency. In fact, when $\frac{s_0}{s_1}$ equals one-tenth the frequency of vibration of the U bar will be only 0.5 per cent higher than the frequency of vibration of a clamped-free bar.

3. THE DEFORMATION OF THE CIRCULAR YOKE

According to equations (37), the tangential and the radial displacements of points in the yoke are

$$v_1(s) = B_1 \sin n_1 s + B_2 \sin n_2 s + B_3 \sin n_3 s$$

$$u_1(s) = n_1 a B_1 \cos n_1 s + n_2 a B_2 \cos n_2 s + n_3 a B_3 \cos n_3 s$$

In elongated U bars the trigonometric functions are readily expressed as functions of ϕ^2. The method is, as before, to introduce the approximate expressions of $n_i a$, as given in equations (36). In fact, putting $s = \nu a$, we obtain,

$$\sin n_1 s = \nu\phi^2$$

$$\sin n_2 s = \sin \nu - \frac{\sqrt{2}}{2} \nu \cos \nu \phi^2$$

$$\sin n_3 s = \sin \nu + \frac{\sqrt{2}}{2} \nu \cos \nu\phi^2$$

$$\cos n_1 s = 1$$

$$\cos n_2 s = \cos \nu + \frac{\sqrt{2}}{2} \nu \sin \nu \phi^2$$

and

$$\cos n_3 s = \cos \nu - \frac{\sqrt{2}}{2} \nu \sin \nu\phi^2$$

Adopting these values of the trigonometric functions of $n_i s$, the above expressions for the tangential and radial displacements now become

$$v_1(s) = B_1\nu\phi^2 + (B_2 + B_3)\sin\nu - \frac{\sqrt{2}}{2}(B_2 - B_3)\nu\cos\nu\phi^2$$

$$u_1(s) = B_1\phi^2 + (B_2 + B_3)\cos\nu - \sqrt{2}\,\frac{(B_2 - B_3)}{2}[\cos \nu - \nu \sin \nu]\phi^2 \qquad (55)$$

The numerical values of the constants B, etc., depend on the end deflection. We write, from equations (43) and (45),

$$B_1 = C_2$$

$$\sqrt{2}(B_2 - B_3 = -C_3\phi$$

$$B_2 + B_3 = -\frac{q\pi + 4}{2q + \pi} C_2\phi^2 - \frac{3\pi}{4(2q + \pi)} C_3\phi^3$$

The expression for $B_2 + B_3$ can be simplified still more.

Since

$$qa = s_1 - s_0$$

$$\phi = \mu s_1 \frac{a}{s_1}$$

and

$$\mu s_1 = 1.8751 + x$$

where x is a small quantity, we can show that, also,

$$B_2 + B_3 = -(1.571 - 0.25\phi)C_2\phi^2 - 0.62\phi^4$$

Equations (40) determine C_2 and C_3 in terms of G and E. The values of G and E follow from equations (49), and, in fact, prove to be

$$G = 0.367\alpha$$

$$E = 0.500\alpha$$

when terms involving ϕ^2 are discarded. α is the amplitude of the end excursions or deflections. Thus, we write, from equations (40)

$$C_2 = (1 - 1.153\phi)\alpha$$

$$C_3 = -0.734\alpha$$

Accordingly, we have in terms of α

$$B_1 = (1 - 1.153\phi)\alpha$$

$$\sqrt{2}(B_2 - B_3) = 0.734\phi\alpha$$

$$B_2 + B_3 = -(1.571 - 2.06\phi)\phi^2\alpha \qquad (56)$$

As an example, we shall evaluate the displacements of points in the yoke of a particular bar. Let the total length of the bar be ten times as great as the length of the circular yoke; that is, s_0/s_1 equals 0.1. This makes $\mu s_1 = 1.880$, and, therefore, μa or ϕ equals 0.1194. Using this value of ϕ and reckoning the end deflection α as unity, we have from (56)

$$B_1\phi^2 = 0.01232$$

$$B_2 + B_3 = -0.01895$$

$$\frac{\sqrt{2}}{2}(B_2 - B_3)\phi^2 = 0.00063$$

Substituting these in equations (55) the numerical values of the tangential and radial displacements result. These are plotted in Figure 5.

An important observation, which is of value in practice, will be made presently. It appears from Figure 5 that the radial displacement u_1 vanishes at $s = 0.05s_1$, whereas the tangential displacement v_1 at the same value of s is about (0.4 per cent) of the end deflection. We infer from this that, if the bar is held vertical, the points of the

yoke corresponding to $s = 0.05 s_1$ will have maximum vertical and horizontal amplitudes of equal value and of amount 0.003 mm, when the amplitude of the end deflections is 1 mm. This deduction follows from equation (2). Accordingly, to minimize the resistance of the supports to the vibratory motion of the bar, it is sufficient that the supports be introduced at the point $s = \pm 0.05 s_1$.

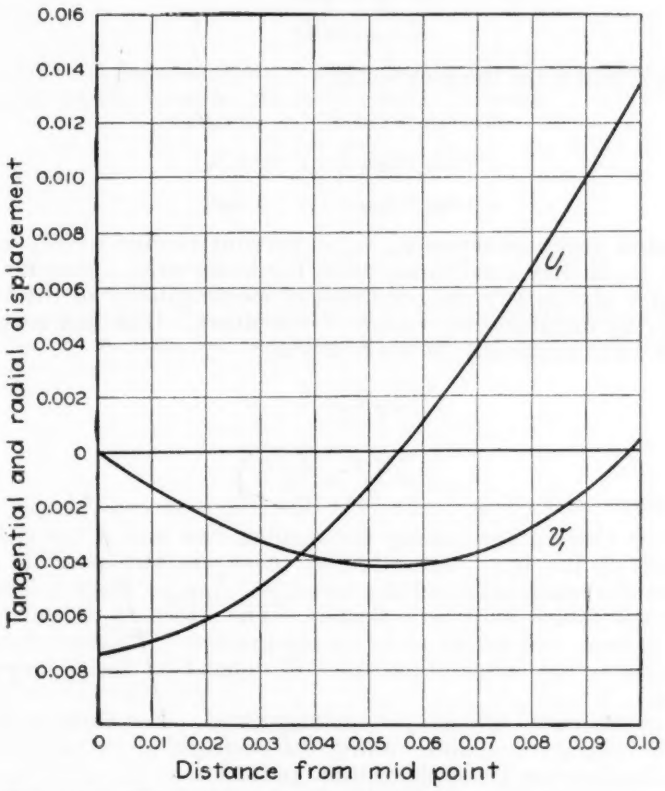

FIGURE 5.—*Tangential and radial displacement, v_1 and u_1, respectively, of the yoke of an elongated U bar of ratio $s_0/s_1 = 0.10$*

Displacements are expressed as fractions of the end displacement. Distance from mid-points, measured on the median line, are expressed as fractions of the half length, s_1, of the bar.

IV. RITZ'S METHOD OF APPROXIMATION

1. APPLICATION OF RITZ'S METHOD TO CURVED BARS

In the cases where the method of representing the motion of curved bars by differential equations leads to lengthy calculations in evaluating the required displacements, it is preferable to use Ritz's method of approximation. The advantage of using the differential equations is that they result in the formulation of normal functions. If, however, the interpretation of the differential equations is not clear, no real information is secured. After all, all that is necessary for practical purposes in vibration problems is an approximate evaluation

of the deformation for the fundamental mode of vibration. This information is always obtainable by Ritz's method.

Following Ritz,[3] the displacements U and V, and the change of curvature K, will be expressed as

$$U = u \cos kt$$

$$V = v \cos kt$$

$$K = \kappa \cos kt$$

where u, v, and κ are the polynomials

$$\begin{aligned} u &= c_1u_1 + c_2u_2 + \cdots + c_nu_n \\ v &= c_1v_1 + c_2v_2 + \cdots + c_nv_n \\ \kappa &= c_1\kappa_1 + c_2\kappa_2 + \cdots + c_n\kappa_n \end{aligned} \tag{57}$$

The related group of terms u_r, v_r, κ_r by construction satisfy all the end and continuity conditions, when the latter exist. Among themselves they also satisfy the condition of inextensibility of the median line and the definition of change of curvature. The last statement amounts mathematically to the following:

$$u_r = \rho \frac{dv_r}{ds}$$

$$\kappa_r = \frac{d^2u_r}{ds_2} + \frac{d}{ds}\left(\frac{v_r}{\rho}\right)$$

where s is the distance along the median line and ρ the radius of curvature of the bar. Accordingly, there are two possible procedures for the construction of the terms (u_r, v_r, κ_r). Once v_r is chosen, the rest will follow by differentiation. The alternate procedure is to choose κ_r first, and arrive at v_r by integration. Whether to choose the former or the latter procedure will depend on the nature of the problem.

The constants c_r are as yet undetermined. For their evaluation two principles are available—either the principle of virtual velocities, or the Hamiltonian principle of least action.

The latter one will be used here. Representing the potential energy of deformation by W, and the kinetic energy by T, Hamilton's principle states that

$$\delta \int_{t_1}^{t_2} (W - T)\, dt = 0 \tag{58}$$

In the case at hand, the required variation will be produced through varying the constants c_r.

Since at the instants t_1 and t_2 the system must be in its natural configuration, we take

$$\begin{aligned} t_1 &= (2m+1)\frac{\pi}{2k} \\ t_2 &= (2m+5)\frac{\pi}{2k} \end{aligned} \tag{59}$$

[3] Walter Ritz, Uber eine neue Methode zur Lösung gewisser Variations probleme der mathematischen physik; J. für die reine und angewandte Mathematik; Band 135; 1909.

where m is a positive integer. The potential energy of deformation and the kinetic energy in a vibrating bar are given by the expressions

$$W=\frac{1}{2}\int_{-s_1}^{s_1} B\,K^2\,ds$$

$$\mathrm{T}=\frac{1}{2}\int_{-s_1}^{+s_1}\omega\gamma\,(U^2+V^2)\,ds$$

where B is the flexural rigidity, γ the density and ω the cross-sectional area, and $2s_1$ the total length of the bar. Defining

$$W_c=\frac{1}{2}\int_{-s_1}^{+s_1}\kappa^2\,ds$$

$$\mathrm{T}_c=\frac{1}{2}\int_{-s_1}^{+s_1}(u^2+v^2)\,ds \tag{60}$$

and, assuming that the quantities B, γ, ω are uniform throughout the bar, the expressions for the potential and the kinetic energies now become

$$W=BW_c\,\mathrm{cas}^2\,kt$$

$$T=\omega\gamma k^2 T_c\sin^2 kt \tag{61}$$

In view of equations (59) and (61), the Hamiltonian equation (58) gives

$$\delta\int_{(2m+1)\frac{\pi}{2k}}^{(2m+\delta)\frac{\pi}{2k}}(BW_c\cos^2 kt-k^2\,\omega\gamma\,T_c\sin^2 kt)\,dt=0$$

which after integration is

$$\delta\,(BW_c-k^2\,\omega\gamma\,T_c)=0$$

or

$$\delta\,(W_c-\mu^4\,T_c)=0 \tag{62}$$

since,

$$\mu^4=\frac{k^2\omega\gamma}{B}$$

according to the equation (15). Expanding equation (62), since W_c and T_c are functions of c_s,

$$\delta\,(W_c-\mu^4 T_c)=\Sigma\frac{d}{dc_s}(W_c-\mu^4 T_c)\,\delta c_s=0 \tag{63}$$

As all the values of c_s are independent of each other, it suffices, in order to produce the variation required in equation (63), to put $c_s=0$ for all values of s except where $s=r$. Thus,

$$\frac{d}{dc_r}(W_c-\mu^4 T_c)=0,\quad (r=1,\,2\,\cdots\,n) \tag{64}$$

Now, W_c and T_c are each quadratic in the c_s. In fact, when the definitions

$$T_{sr}=\int_0^{s_1}(u_r\,u_s+v_r\,v_s)\,ds$$

$$W_{sr}=\int_0^{s_1}\kappa_r\,\kappa_s\,ds$$

are written, equations (60) yield

$$W_c=\sum_{s=1}^{n}\alpha_{rs}\,c_r\,c_s\,W_{rs}+W_1$$

$$T_c=\sum_{s=1}^{n}\alpha_{rs}\,c_r\,c_s\,T_{rs}+T_1$$

$$\begin{pmatrix}\alpha_{rs}=2, \text{ when } r\pm s\\ \alpha_{rs}=1, \text{ when } r=s\end{pmatrix}$$

where W_1 and T_1 both are free from the particular constant C_r. Accordingly, the differentiation in (64) gives the following n homogeneous equations.

$$\sum_{r=1}^{n}c_s\,(W_{rs}-\mu^4\,T_{rs})=0\ (s=1\cdots n) \tag{65a}$$

Introducing the dimensional quantities

$$w_{rs}=s_1\,W_{sr}$$

$$t_{rs}=s_1^{-3}\,T_{sr}$$

the n homogeneous equations now become

$$\sum_{r=1}^{r=n}c_s\,[w_{rs}-(\mu s_1)^4 t_{rs}]=0\ (s=1,\,2\,\cdots,\,n) \tag{65b}$$

The condition of compatibility among these n equations leads to the determinant:

$$\begin{vmatrix} w_{11}-(\mu s_1)^4 t_{11} & w_{12}-(\mu s_1)^4 t_{12} & \cdots & w_{1n}-(\mu s_1)^4 t_{1n}\\ \cdot & \cdot & \cdots & \cdot\\ w_{n1}-(\mu s_1)^4 t_{n1} & w_{n2}-(\mu s_1)^4 t_{n2} & \cdots & w_{nn}-(\mu s_1)^4 t_{nn}\end{vmatrix}=0 \tag{66}$$

which is an algebraic equation of the n^{th} degree in $(\mu s_1)^4$ the frequency characteristics. Theoretically, the number n ought to be increased indefinitely. Physically, the number of degrees of freedom of the vibrating bar ought to be made correspondingly large. In practice, a determinant of rank 2 or an algebraic equation of the second degree in $(\mu s_1)^4$ suffices amply to determine the particular value of μs_1 which relates to the fundamental mode of vibration.

2. AN ILLUSTRATION FROM A CLASSICAL PROBLEM

The modes of vibration of a straight bar, both ends free, are well known. A new solution will be worked out as an illustration of the preceding theory. This particular example has been chosen since a straight bar may be thought of as a limiting case of a U bar. Here, only the symmetrical (that is, fundamental) vibration will be considered.

Let the straight bar be of length $2s_1$. Let U be the transversal displacement.

$$U = u \cos k\,t \tag{67}$$

As before, let B, ω, γ be the flexural rigidity, the cross-sectional area, and the density of the bar, respectively. Putting $s = s_1 x$, we choose for the change of curvature the polynomial series

$$\kappa = \frac{d^2u}{ds^2} = \frac{d^2u}{s_1^2 dx^2} = \frac{1}{s_1^2}\left[c_1(1+\cos \pi x) + c_2\,(1-\cos 2\pi x) + \cdots\right] \tag{68}$$

since the bending moment G and the shear N vanish at $x = \pm 1$. To point out the analogy with the third of equations (57), equation (68) may also be written

$$\kappa = \frac{1}{s^2}\,(c_1\kappa_1 + c_2\kappa_2 + \cdots + c_n\kappa_n) \tag{68a}$$

Integrating equation (68) with respect to x,

$$\frac{du}{dx} = c_1\left(x + \frac{\sin \pi x}{\pi}\right) + c_2\left(x - \frac{\sin 2\pi x}{2\pi}\right) + \cdots \tag{69}$$

The constant of integration vanishes by virtue of the fact that the bar experiences no change of inclination at the mid-point $s = 0$, or $x = 0$. A further integration with respect to x gives

$$u = c_1\left(a_1 + \frac{x^2}{2} - \frac{\cos \pi x}{\pi^2}\right) + c_2\left(a_2 + \frac{x^2}{2} + \frac{\cos 2\pi x}{4\pi^2}\right) + \cdots \tag{70}$$

To determine the constants of integration, a_s, the condition for the conservation of the center of gravity is employed, which in the present example will be expressed by the relation

$$\int_0^1 u\,dx = 0$$

As this is to be satisfied whatever the value of the constants a_s, individually

$$\int_0^1 \left(a_1 + \frac{x^2}{2} - \frac{\cos \pi x}{\pi^2}\right) dx = 0$$

and

$$\int_0^1 \left(a_2 + \frac{x^2}{2} + \frac{\cos 2\pi x}{4\pi^2}\right) dx = 0$$

from which

$$a_1 = a_2 = -\frac{1}{6}$$

So, finally, the expression for the displacement assumes the form

$$u = c_1\left(-\frac{1}{6}+\frac{x^2}{2}-\frac{\cos \pi x}{\pi^2}\right)+c_2\left(-\frac{1}{6}+\frac{x^2}{2}+\frac{\cos 2\pi x}{4\pi^2}\right)+\ldots \tag{71}$$

which may also be written, in analogy with the first of equations (57),

$$u = c_1u_1+c_2u_2+\ldots. \tag{71a}$$

Rewriting the definitions

$$t_{rs}=\int_0^1 u_r u_s dx$$

$$w_{rs}=\int_0^1 \kappa_r \kappa_s dx$$

the quantities t_{11}, w_{11}, etc., on the basis of equations (68a) and (71a) emerge with the following numerical values:

$$t_{11}=\left(\frac{\pi^4}{45}+\frac{5}{2}\right)\frac{1}{\pi^4}=4.66462\,\frac{1}{\pi^4},\ w_{11}=\frac{3}{2}$$

$$t_{12}=\left(\frac{\pi^4}{45}+\frac{17}{16}\right)\frac{1}{\pi^4}=3.22712\,\frac{1}{\pi^4},\ w_{12}=1 \tag{71}$$

$$t_{22}=\left(\frac{\pi^4}{45}+\frac{5}{32}\right)\frac{1}{\pi^4}=2.32087\,\frac{1}{\pi^4},\ w_{22}=\frac{3}{2}$$

Thus, neglecting the constants c_r, r larger than 2, the system of homogeneous equations corresponding to equation (65b) becomes in this example

$$\begin{aligned} c_1[w_{11}-(\mu s_1)^4 t_{11}]+c_2[w_{12}-(\mu s_1)^4 t_{12}]&=0 \\ c_1[w_{12}-(\mu s_1)^4 t_{12}]+c_2[w_{22}-(\mu s^1)^4 t_{22}]&=0 \end{aligned} \tag{72}$$

The condition of compatibility leads to the characteristic relation, expressed as a determinant

$$\begin{vmatrix} w_{11}-(\mu s_1)^4 t_{11} & w_{12}-(\mu s_1)^4 t_{12} \\ w_{12}-(\mu s_1)^4 t_{12} & w_{22}-(\mu s_1)^4 t_{22} \end{vmatrix}=0$$

which when expanded yields, after introducing the numerical values for t_{11}, etc., indicated in equation (71), the quadratic equation

$$1.646704\left(\frac{\mu s_1}{\pi}\right)^8-16.09600\left(\frac{\mu s_1}{\pi}\right)^4+5.00000=0 \tag{73}$$

with the roots

$$(\mu s_1)_1 = 2.36506$$
$$(\mu s_1)_2 = 5.50895 \tag{74}$$

The smaller root gives the frequency characteristic of the fundamental mode of vibration. The larger, that of the next overtone. To determine the ratio of c_2 to c_1, we substitute $\mu s_1 = 2.36506$, in the first or the second of the equations (72). The substitution in the first gives for c_2/c_1 the value 0.07; in the second, the value 0.05. In view of the smallness of this ratio, it is sufficient to take

$$u = c_1\left(-\frac{1}{6} + \frac{x^2}{2} - \frac{\cos \pi x}{\pi^2}\right) \tag{75}$$

as the expression for the transverse displacement of the bar when vibrating in its fundamental mode.

In order to effect a comparison with the classical theory of the bar with free ends, the consideration of the latter will be restricted to the solution for the case of symmetrical vibration. As $u(s) = -u(-s)$, it follows from equation (22) that

$$u = D(\cos\mu s + \cosh \mu s) + E(\cos\mu s - \cosh \mu s)$$

As the ends of the bar are free,

$$D(-\cos\mu s_1 + \cosh \mu s_1) + E - \cos\mu s_1 - \cosh \mu s_1) = 0$$

$$D(-\sin\mu s_1 + \sinh \mu s_1) + E(\sin\mu s_1 - \sinh \mu s_1) = 0$$

with the condition of compatibility

$$\cot\mu s_1 \tanh \mu s_1 = -1$$

The two smallest roots of this equation are

$$(\mu s_1)_1 = 2.3650204$$
$$(\mu s_1)_2 = 5.4978039 \tag{76}$$

which are in good agreement with the values already found by the approximate method of Ritz and given in equations (74). The values in equations (76) are taken from Rayleigh[4] and are the results of dividing his values of m_1 and m_3 by 2.

To compare the displacements obtained by the two methods, Ritz's and the classical, Table 1 has been prepared, in which the results in the second column have been calculated on the basis of the classical solution and those in the third have been calculated on the basis of equation (75). The end deflections were chosen to be the same for both methods. The agreement appears to be good, the deviations of the results in the two cases being less than 1 per cent of the end deflection.

[4] Rayleigh The Theory of Sound, 5, 2d ed., p. 278.

TABLE 1.—*The lateral displacements in a free-free bar computed by the classical and by Ritz's method*

Distance from mid-point	Displacements	
	Classical method	Ritz's method
0.0	−0.6078	−0.6167
.1	−.5857	−.5937
.2	−.5202	−.5260
.3	−.4142	−.4169
.4	−.2720	−.2714
.5	−.0992	−.0959
.6	+.0977	+.1027
.7	+.3120	+.3172
.8	+.5372	+.5413
.9	+.76775	+.7469
1.0	+1.0000	+1.0000

V. RAYLEIGH'S METHOD FOR DETERMINING THE FUNDAMENTAL MODE OF VIBRATION

If in equation (57) the displacements u_r, v_r are those due to the r^{th} overtone in the r^{th} mode of vibration, the quantities T_{rs} and W_{rs} vanish and the determinant (66) reduces to

$$\prod_{r=1}^{r=\infty}(W_{rr}-\mu^4 T_{rr})=0$$

where

$$T_{rr}=\int_0^{s_1}(U_r^2+V_r^2)ds$$

$$W_{rr}=\int_0^{s_1}\kappa_r^2 ds$$

κ_r being the change of curvature. The roots μ_r^4 now are

$$\mu_r^4=\frac{W_{rr}}{T_{rr}};\quad(\mu_1^4<\mu_2^4<\ldots) \tag{77}$$

Suppose that for the fundamental mode of vibration a radial displacement u, is assumed which is a slight modification of u_1, the actual value, and with the same end conditions as in u_1. The quantities T_{11} and W_{11} are evaluated on the basis of u, and the ratio

$$\overline{\mu}^4=\frac{\overline{W}_{11}}{\overline{T}_{11}}$$

is formed. Is the approximate value $\overline{\mu}_1$ thus formed, larger or smaller than the true value μ_1? To answer this question we again resort to Ritz's method of approximation. Since u_1 is only slightly in error, it is sufficient to put

$$u_1=c_1u_1+c_2u_2$$

where u_2 gives the displacement for the mode of vibration next higher than the fundamental. The quantities v_1 and κ_1, the tangential displacement and the change of curvature, respectively, follow from u_1.

The quantities W_{12}, T_{12}, etc., are formed which give rise, as in equation (66), to the determinant

$$\begin{vmatrix} \overline{W}_{11}-\mu^4\overline{T}_{11} & W_{12}-\mu^4 T_{12} \\ W_{12}-\mu^4 T_{12} & W_{22}-\mu^4 T_{22} \end{vmatrix}=0$$

which expands into

$$\overline{W}_{11}-\mu^4\overline{T}_{11}=\frac{(W_{12}-\mu^4 T_{12})^2}{W_{22}-\mu^4 T_{22}} \tag{78}$$

To determine the smallest root μ_1^4, we write

$$\mu_1^4=\overline{\mu}_1^4+\Delta\mu=\frac{\overline{W}_{11}}{\overline{T}_{11}}+\Delta\mu$$

and set it in equation (78), with the result that

$$-\Delta\mu\overline{T}_{11}=\frac{(W_{12}-\mu_1^4 T_{12})^2}{(W_{22}-\mu_1^4 T_{22})} \tag{79}$$

It is easily seen, by virtue of equation (77), that the denominator in the right member of equation (79) is positive. The numerator, being a squared quantity, is also positive. Accordingly $\Delta\mu$ is a negative quantity, since $\overline{T}_{11}$ is positive. Hence, any assumed configuration for the fundamental mode of vibration which is a departure from the actual configuration will give a larger value for μ_1^4 calculated on the basis of

$$\overline{\mu}_1^4=\frac{\overline{W}_{11}}{\overline{T}_{11}} \tag{80}$$

where

$$\overline{W}_{11}=\int_0^{s_1}(u^2+v^2)ds)$$

$$\overline{T}_{11}=\int_0^{s_1}\kappa^2 ds$$

The above result, which we obtain by means of Ritz's method, was stated, originally, by Rayleigh as a corollary to a general theorem on vibrations.[5] In Rayleigh's method, therefore, μ_1, will be made to depend on a parameter β. Then, to obtain the configuration which is the nearest to the actual configuration present during the fundamental mode of vibration, we choose that value of β which makes the right-hand member in (80) a minimum.

[5] Rayleigh, Some General Theorems Relating to Vibrations. London Math. Soc. Proc. IV, pp. 357–368; 1873 (sci. papers, **1**, p. 21)

VI. VIBRATION OF A SHORT U BAR

The bar to be considered now is of length $2s_1$. The yoke is a semicircle of radius a and of length $2s_0$. The ratio $\frac{s_1}{s_0}=2$. (See fig. 6.) Hence,

$$\rho=a \qquad \text{when } o\leqq s\leqq s_0$$

$$\rho=\infty \qquad \text{when } s_0\leqq s\leqq s_1$$

$$s_0=\frac{s_1}{2} \qquad \frac{s_1}{a}=\pi$$

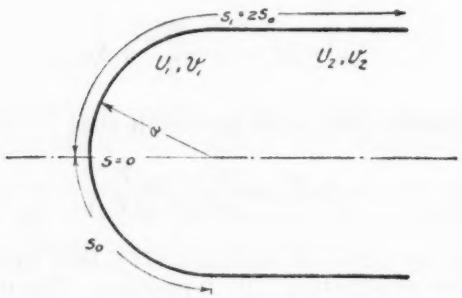

FIGURE 6.—*Median line of the short* U *bar*

The frequency characteristic of vibration of the fundamental mode and the displacements present will be determined by Ritz's method.

The shear is assumed to be given by a sine series, as in the case of the straight bar previously considered. Accordingly,

$$\frac{d\kappa}{ds}=\frac{d^2}{ds^2}\left(\frac{du}{ds}+\frac{v}{\rho}\right)=\sum_{q=1}^{n}\frac{A_2}{s_1^2}\sin q\pi\frac{s}{s_1} \tag{81}$$

Putting $s=s_1x$, a first integration with respect to x gives

$$\kappa=\kappa s_1=\frac{d}{dx}\left(\frac{du}{ds}+\frac{v}{\rho}\right)=\sum_{q=1}^{n}\pi A_q(C_q+\cos_q\pi x) \tag{82}$$

As the bending moment vanishes at $s=\pm s_1$, or $x=\pm 1$, C_q has the value $+1$ or -1 depending on q. Thus, introducing new constants a_q, equation (82) becomes

$$\begin{aligned}\kappa=\kappa s_1=\frac{d}{dx}\left(\frac{du}{ds}+\frac{v}{\rho}\right)=a_1(1+\cos\pi x)+\\ \sum_n a_n(1+\cos n\pi x)+\\ \sum_m a_m(1-\cos m\pi x)\end{aligned} \tag{83}$$

$$n=3,\ 5,\ 7\ \ldots$$

$$m=2,\ 4,\ 6\ \ldots$$

Integrating equation (83) with respect to x,

$$\frac{du}{ds}+\frac{v}{\rho}=a_1\left[x+\frac{\sin\ \pi x}{\pi}\right]+$$
$$\sum_n a_n\left[x+\frac{\sin\ n\pi x}{n\pi}\right]+$$
$$\sum_m a_m\left[x-\frac{\sin\ m\pi x}{m\pi}\right]+ \qquad (84)$$
$$n=3,\ 5,\ 7\ \ldots$$
$$m=2,\ 4,\ 6\ \ldots$$

The constant of integration vanishes, since the inclination of the bar at the mid-point of the yoke, or at $x=0$, experiences no change. Next, putting

$$\bar{u}=\frac{u}{s_1},\quad \bar{v}=\frac{v}{s}$$

the condition for the inextensibility of the median line gives, for the curved portion

$$\frac{du}{ds}=\frac{1}{\pi}\frac{d^2\bar{v}}{dx^2}$$

Also, in the curved portion, from equation (84)

$$\frac{d^2\bar{v}}{dx^2}+\pi^2\bar{v}=a_1\pi(x+\sin\ \pi x)+$$
$$\sum_n a_n\pi\left(x+\frac{\sin\ n\pi x}{n\pi}\right)+$$
$$\sum_m a_m\pi\left(x-\frac{\sin\ m\pi x}{m\pi}\right)+$$
$$n=3,\ 5,\ 7\ \ldots$$
$$m=2,\ 4,\ 6\ \ldots$$

Solving for $\bar{v}$ in the usual manner, we obtain for the curved portion

$$\bar{v}=\frac{a_1}{\pi^2}\left(\pi x-\frac{\pi x\cos\ \pi x}{2}+b_1\sin\ \pi x\right)+$$
$$\sum_n \frac{a_n}{\pi^2}\left(\pi x-\frac{\sin\ n\pi x}{n(n^2-1)}+b_n\sin\ \pi x\right)+\ldots \qquad (85)$$
$$\sum_m \frac{a_m}{\pi^2}\left(\pi x+\frac{\sin\ m\pi x}{m(m^2-1)}+b_m\sin\ \pi x\right)+\ldots$$
$$n=3,\ 5,\ 7\ \ldots$$
$$m=2,\ 4,\ 6\ \ldots$$

since the tangential displacement v vanishes at $x=0$. The constants b_1, b_n, and b_m are evaluated on the basis of the condition that the

center of gravity of the bar remains at rest independently of a_1, a_n, and a_m. Accordingly, we have, from equation (26),

$$b_1 = -\frac{2}{\pi} - \frac{\pi}{4} + \frac{1}{8}$$

$$b_n = -\frac{2}{\pi} - \frac{\pi}{4} + \frac{\sin \frac{n\pi}{2}}{2n(n^2-1)}$$

$$b_m = -\frac{2}{\pi} - \frac{\pi}{4} + \frac{2}{\pi}\frac{\cos \frac{m\pi}{2}}{(m^2-1)^2}$$

$$n = 3, 5, 7 \ldots$$

$$m = 2, 4, 6 \ldots$$

The radial displacement u divided by s_1 in the curved portion follows from the condition of inextensibly, and, therefore, is

$$\bar{u} = \frac{a_1}{\pi^2}\left(1 - \frac{\cos \pi x}{2} + \frac{\pi x \sin \pi x}{2} + b_1 \cos \pi x\right) +$$

$$\sum_n \frac{a_n}{\pi^2}\left(1 - \frac{\cos n\pi x}{n^2-1} + b_n \cos \pi x\right) + \ldots$$

$$\sum_m \frac{a_m}{\pi^2}\left(1 + \frac{\cos m\pi x}{m^2-1} + b_m \cos \pi x\right) + \ldots \qquad (86)$$

$$n = 3, 5, 7 \ldots$$

$$m = 2, 4, 6 \ldots$$

The expression which gives the change of inclination in the straight portion of the bar simplifies to

$$\frac{d\bar{u}}{dx} = a_1[x + \sin \pi x] +$$

$$\Sigma a_n\left[x + \frac{\sin n\pi x}{n\pi}\right] + \ldots$$

$$\Sigma a_m\left[x - \frac{\sin m\pi x}{m\pi}\right] + \ldots$$

$$n = 3, 5, 7 \ldots \qquad (87)$$

$$m = 2, 4, 6 \ldots$$

since the radius of curvature ρ is infinite. Accordingly, the lateral displacement in the straight portion is given by

$$\bar{u} = \frac{a_1}{\pi^2}\left(\frac{\pi^2 x^2}{2} - \cos \pi x + c_1\right) +$$

$$\Sigma \frac{a_n}{\pi^2}\left(\frac{\pi^2 x^2}{2} - \frac{\cos n\pi x}{n^2} + c_n\right) + \ldots$$

$$\Sigma \frac{a_m}{\pi^2}\left(\frac{\pi^2 x^2}{2} + \frac{\cos m\pi x}{m^2} + c_m\right) + \ldots$$

$$n = 3, 5, 7 \ldots$$

$$m = 2, 4, 6 \ldots$$

The normal displacement is continuous everywhere. Consequently, the different expressions (86) and (87) for u give the same numerical value when x is put equal to 1/2. This determines the constants c_1, c_n, and c_m, with the following values:

$$c_1 = 1 + \frac{\pi}{4} - \frac{\pi^2}{8}$$

$$c_n = 1 - \frac{\pi^2}{8}$$

$$c_m = 1 - \frac{\pi^2}{8} + \frac{\cos \frac{m\pi}{2}}{m^2(m^2-1)}$$

$$m = 2, 4, 6 \ldots$$

The tangential displacement in the straight portion of the bar is constant. Since the tangential displacement is continuous everywhere, it follows from equation (85) that

$$\bar{v} = \sum_{r=1}^{n+1} \frac{a_r}{\pi^2}\left(\frac{\pi}{2} + b_r\right) \tag{88}$$

We next write, in analogy with equation (57)

$$u = (a_1\bar{u}_1 + a_2\bar{u}_2 + a_3\bar{u}_3 + \ldots)\frac{s_1}{\pi^2}$$

$$v = (a_1\bar{v}_1 + a_2\bar{v}_2 + a_3\bar{v}_3 + \ldots)\frac{s_1}{\pi^2}$$

$$\kappa = (a_1\bar{\kappa}_1 + a_2\bar{\kappa}_2 + a_3\bar{\kappa}_3 = \ldots)\frac{1}{s_1}$$

where the expressions for the typical terms u_r, v_r, κ_r are obtained by comparison with equations (85), (86), (87), (88), and (83).

Introducing the definitions

$$T_{rs} = s_1^2 \int_0^{s_1} (\bar{v}_r\bar{v}_s + \bar{u}_r\bar{u}_s)\, ds = s_1^3 \int_0^{\pi} (\bar{v}_r\bar{v}_s + \bar{u}_r\bar{u}_s) dx$$

$$W_{rs} = \frac{1}{s_1^2}\int_0^{s_1} \bar{\kappa}_r\bar{\kappa}_s d_s = \frac{1}{s_1}\int_0^{\pi} \bar{\kappa}_r\bar{\kappa}_s dx$$

the quantities T_{11}, W_{11}, etc., prove to have the numerical values

$$T_{11} = 9.64721\frac{s_1^3}{\pi^4}, \quad W_{11} = \frac{3}{2}s^{-1}$$

$$T_{12} = 6.17078\frac{s_1^3}{\pi^4}, \quad W_{12} = s_1^{-1} \tag{89}$$

$$T_{22} = 4.09341\frac{s_1^3}{\pi^4}, \quad W_{22} = \frac{3}{2}s^{-1}$$

Neglecting in the expansion for the displacement the terms with the coefficients a_g, where g is larger than 2, the system of homogeneous equations in a_g corresponding to equations (65) reduce to

$$a_1(W_{11}-\mu^4 T_{11})+a_2(W_{12}-\mu^4 T_{12})=0$$
$$a_1(W_{12}-\mu^4 T_{12})+a_2(W_{22}-\mu^4 T_{22})=0$$

with the condition of compatibility

$$\begin{vmatrix} W_{11}-\mu^4 T_{11} & W_{12}-\mu^4 T_{12} \\ W_{12}-\mu^4 T_{12} & W_{22}-\mu^4 T_{22} \end{vmatrix}=0$$

which, with the numerical values of W_{11}, etc., given above, reduces to

$$1.41146\left(\frac{\mu s_1}{\pi}\right)^8-8.25937\left(\frac{\mu s_1}{\pi}\right)^4+1.25=0. \tag{90}$$

To find the root of the smallest value; that is, the frequency characteristic of the fundamental mode, we take first

$$W_{11}-\mu^4 T_{11}=0$$

or, with numerical values substituted,

$$\left(\frac{\mu s_1}{\pi}\right)^4=0.15548.$$

Next, we take

$$\left(\frac{\mu s_1}{\pi}\right)^4=0.15548+z$$

and substitute in the equation (90). The substitution gives,

$$z=0.000006.$$

Accordingly, the first approximations give a value for the frequency characteristic μs_1 of 1.97275, which is sufficiently accurate for practical purposes. We also infer that there is no need to keep the terms containing a_2 in the expressions for the displacements for the fundamental mode of vibration.

Hence, the radial and tangential displacements, u and v, in the fundamental mode of vibration of the short U bar, may be written

$$u=a_1\left[1-\frac{\cos\pi x}{2}+\frac{\pi x\sin\pi x}{2}+\left(\frac{1}{8}-\frac{2}{\pi}-\frac{\pi}{4}\right)\cos\pi x\right],\ \text{when } 0\leqq x\leqq\tfrac{1}{2}$$

$$v=a_1\left[\pi x-\frac{\pi x\cos\pi x}{2}+\left(\frac{1}{8}-\frac{2}{\pi}-\frac{\pi}{4}\right)\sin\pi x\right]\ \text{when } 0\leqq x\leqq\tfrac{1}{2}$$

$$u=a_1\left[\frac{\pi^2x^2}{2}-\cos\pi x+1+\frac{\pi}{4}-\frac{\pi^2}{8}\right]\ \text{when } \tfrac{1}{2}\leqq x\leqq 1 \tag{91}$$

$$v=a_1\left[\frac{1}{8}-\frac{2}{\pi}+\frac{\pi}{2}\right]\ \text{when } \tfrac{1}{2}\leqq x\leqq 1$$

where $x=\frac{s}{s_1}$, s_1 is the half length of the bar, s is the distance of a point from the mid-point of the yoke, measured on the median line. As for the frequence of vibration, N,

$$N=\frac{3.8917}{2\pi}\sqrt{\frac{B}{\omega\gamma}}\cdot\frac{1}{s_1^2}$$

where B is the flexural rigidity, ω the cross-sectional area, and γ the density of the bar.

The numerical values of the displacements, evaluated from the formula (91) are given in Table 2. The radial or the lateral displacement of the ends is assumed to be unity. It now appears from this table that the radial displacement vanishes at the point $s=0.244s_1$. Also, that the tangential displacement is 0.0594. We infer from this that, when the short U bar is held vertical, the point $s=0.24s_1$ executes maximum vertical and horizontal displacements of equal value and of amount 0.042 mm when the amplitude of the end deflections is 1 mm. This follows from equation (2).

TABLE 2.—*The tangential and radial displacements of a vibrating short* U *bar*

Fractional distance from mid-point	Radial displacement	Tangential displacement
0.0	−0.1229	0.0000
.1	−.1018	−.0365
.2	−.0415	−.0599
.3	+.0501	−.0591
.4	+.1761	−.0264
.5	+.2752	+.0422
.6	+.4065	+.0422
.7	+.5487	+.0422
.8	+.6966	+.0422
.9	+.8479	+.0422
1.0	+1.0000	+.0422

VII. EFFECT OF THE YOKE ON VIBRATION

It was shown by Lamb [6] that when a straight bar is curved slightly the frequency of vibration is lowered and the nodal points are brought together slightly. The same effects are illustrated here. As one passes from the example of the straight bar, to the short U bar, defined above, and then to the elongated U bar with a length ten times as great as that of the yoke, the frequency characteristic μs_1 takes the values 2.365, 1.973, 1.880, successively. With regard to the variation of displacements in these examples, as effected by the presence of a yoke, we refer to Figure 7, where the radial displacements are plotted against the fractional distances from the mid-point. This figure illustrates two important effects, as resulting from increased length of the yoke, while the total length of the bar is kept the same; that is, the points, where the radial displacements vanish, are brought nearer to the mid-point of the yoke, and the ratio of the radial displacement at the mid-point of the yoke to the end deflection is made smaller.

[6] Horace Lamb, On the Flexure of a Curved Bar Proc. London Math. Soc., **14**, p. 367; 1888.

VIII. REPRODUCTION BY A SINGLE LOAD OF DEFORMATIONS DUE TO VIBRATION

Theoretically, to reproduce in static tests the strained form of the vibrating U bar, a continuous distribution of externally applied forces is required. In practice, however, it is sufficient to have the form obtained under the action of a single load. If the point of application of the single load is properly chosen, the form thus secured will not differ very much from the dynamic form during vibration. This is true only for the fundamental mode of vibration, of course. For the determination of the proper location of the single load Rayleigh's method is of great value.

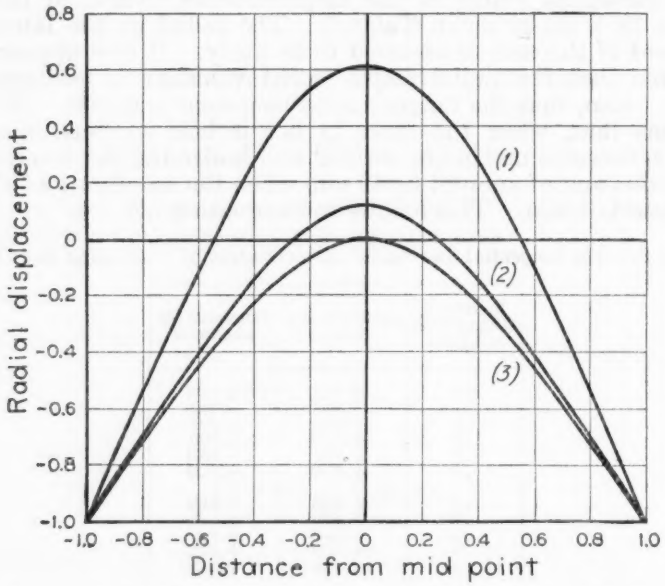

FIGURE 7.—*Effect of the presence of the yoke on the radial displacement u*

Curve (1) refers to a straight bar; curved (2) to the short U bar; curve (3) to an elongated U bar of ratio $s_0/s_1=0.10$. The apex of the curve (3) is slightly above the zero line of the radial displacement. The distance from the mid-point is given as the fractional value of the half length of the bar, measured on the median line and the radial displacement as the fractional value of the end displacement.

Let s_2 be the distance measured on the median line of the point of application of the single load X from the mid-point of the yoke. (See fig. 8.) Also let $2s_1$ be the total length of the bar and $2s_0$, the length of the semicircular yoke of radius a. Denote the radial and tangential displacements in the yoke by u_1 and v_1; in the portion from $s=s_0$ to $s=s_2$ by u_2 and v_2; and in the portion $s=s_2$ to $s=s_1$ by u_3 and v_3.

It is clear that the bending moment G at s, when s is in the yoke, is given by

$$G=X\left(s_2-s_0+a\cos\frac{s}{a}\right)$$

and the change of curvature κ_1, by

$$\kappa_1 = \frac{d}{ds}\left(\frac{du_1}{ds} + \frac{v_1}{a}\right)$$

Hence

$$\frac{d}{ds}\left(\frac{du_1}{ds} + \frac{v_1}{a}\right) = \frac{X}{B}\left(s_2 - s_0 + a \operatorname{cas}\frac{s}{a}\right)$$

where B represents the flexural rigidity of the bar, uniform throughout. Making the substitutions

$$s = a\theta$$

$$\frac{s_2 - s_0}{a} = n$$

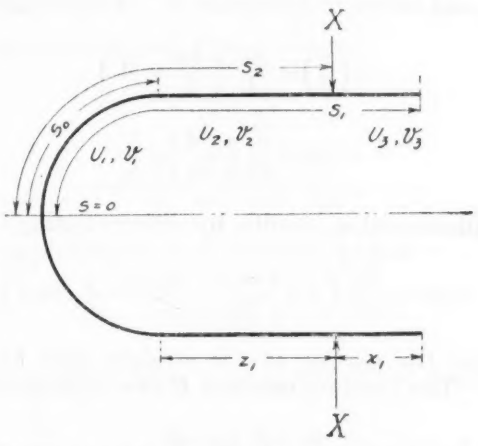

FIGURE 8.—*Position of the point of application of a single load acting on a U bar*

the equation (91) becomes

$$\frac{d}{d\theta}\left(\frac{du_1}{d\theta} + v_1\right) = \frac{X}{B}a^3(n + \cos\theta)$$

the integration of which, with respect to θ, gives, since there is no change of inclination at the mid-point of the yoke ($\theta = 0$)

$$\frac{du_1}{d\theta} + v_1 = \frac{X}{B}a^3(n\theta + \sin\theta)$$

Or, introducing the condition of inextensibility,

$$\frac{d^2v_1}{d\theta} + v_1 = \frac{X}{B}a^3(n\theta + \sin\theta)$$

Solving for v_1, in the usual manner

$$v_1(\theta) = \frac{X a^3}{B}\left(n\theta - \frac{\theta\cos\theta}{2} + A\sin\theta\right) \qquad (92)$$

since v_1 vanishes for $\theta=0$. The term $\frac{AXa^3}{B}\sin\theta$ represents a rigid displacement. In fact, it will be the displacement caused by moving the bar along its axis by an amount $\frac{AXa^3}{B}$. As the present analysis is for the purpose of finding the static deformation as nearly as possible like the deformation during vibration, it is evident that the determination of the constants of integration should be made by using the appropriate conditions implied by the dynamic deformation. As will be remembered, the condition of constancy of the center of gravity

$$v_1\left(\frac{\pi}{2}\right)=-\frac{2a}{s_1-s_0}\int_0^{\frac{\pi}{2}} v_1\sin\theta\,d\theta$$

is one of these, and serves to determine A. Accordingly

$$v_1\left(\frac{\pi}{2}\right)=\frac{Xa^3}{B}\left(\frac{\pi n}{2}+A\right)$$

and, hence

$$A=-\frac{n}{2}\left(\frac{\pi}{2}+\frac{4}{\pi}\right)+\frac{1}{8} \tag{93}$$

The radial displacement u_1 results, by differentiating v_1, and is

$$u_1(\theta)=\frac{Xa^3}{B}\left(n+\frac{\theta\sin\theta}{2}-\frac{\cos\theta}{2}+A\cos\theta\right) \tag{94}$$

Next consider the portion in the straight part of the bar, from $s=s_0$ to $s=s_2$. The bending moment G at s is given by

$$G=X\,(s_2-s)$$

and the change of curvature κ_2 by

$$\kappa_2=\frac{d^2u_2}{ds^2}$$

Hence,

$$\frac{du_2}{ds}=\frac{X}{B}(s_2-s)$$

which, after making the substitution

$$z=s_2-s$$

becomes

$$\frac{du_2}{dz}=\frac{X}{B}z$$

Two successive integrations with respect to z give

$$u_2=\frac{X}{B}\left(\frac{z^3}{6}+\alpha z_1^2 z+\beta z_1^3\right) \tag{95}$$

where

$$z_1=s_2-s_0$$

The constants of integration α and β are to be determined from the conditions of continuity of the radial displacement and the change of inclination at $s = s_0$:

$$(u_1)_{\theta=\frac{\pi}{2}} = (u_2)_{z=z1}$$

$$\left(\frac{du_1}{ds}+\frac{v_1}{a}\right)_{\theta=\frac{\pi}{2}} = -\left(\frac{du_2}{dz}\right)_{Z=z1}$$

Accordingly

$$a^2\left(n+\frac{\pi}{4}\right) = z_1^3\left(\frac{1}{6}+\alpha+\beta\right)$$

$$a^2\left(\frac{n\pi}{2}+1\right) = z_1^2\left(\frac{1}{2}+\alpha\right)$$

As $na = z_1$, the constants α and β prove to be

$$-\alpha = \frac{1}{2}+\frac{1}{n^2}+\frac{\pi}{2n}$$

$$\beta = \frac{1}{3}+\frac{2}{n^2}+\frac{\pi}{4n^3}+\frac{\pi}{2n}$$

The tangential displacement v_2 is constant, and is

$$v_2 = v_1\left(\frac{\pi}{2}\right) \tag{96}$$

Finally, for the portion from s_2 to s_1, the radial displacement u_3 is given by

$$u_3 = \frac{X}{B}(-\alpha z_1^3 x+\beta z_1^3) \tag{97}$$

where

$$x = s - s_2$$

The displacement in this portion is a rigid displacement and fulfills the conditions

$$(u_3)_{x=0} = (u_2)_{z=0}$$

$$\left(\frac{du_3}{dx}\right)_{x=0} = -\left(\frac{du_2}{dz}\right)_{z=0}$$

The tangential displacement is constant, and is

$$v_3 = v_1\left(\frac{\pi}{2}\right) \tag{97}$$

The quantities n, x_1 and z_1, enter variously in the separate expressions of the displacements. The quantities x_1 and z_1 depend on n

$$na = z_1$$

$$x_1/z_1 = \frac{\pi}{2n}\left(\frac{s_1}{s_0}-1\right)$$

Accordingly when n is given, x_1 and z_1 follow. To determine n, we remark that if the same bar is put in vibration the deformations will be given by

$$u=u_1 \cos kt \qquad v=v_1 \cos kt$$

$$u=u_2 \cos kt \qquad v=v_2 \cos kt$$

$$u=u_3 \cos kt \qquad v=v_3 \cos kt$$

when

$$0 \leqq s \leqq s_0$$

$$s_0 \leqq s \leqq s_2$$

$$s_2 \leqq s \leqq s_1$$

and proceed according to Rayleigh's method.

Introducing the definitions (given in connection with equation (80)).

$$\overline{T}_{11}=\int_0^{s_1}(u^2+v^2)ds$$

$$\overline{W}_{11}=\int_0^{s}\kappa^2 ds$$

and substituting the appropriate value of the displacements and of the change of curvature from above, it is found that

$$\overline{T}_{11}=\frac{X^2}{B^2}(a^7e_1+a^7e_2+z_1^7e_3+z_1^7e^4)$$

$$\overline{W}_{11}=\frac{X^2}{B^2}(a^3w_1+z_1^3w_2)$$

where

$$e_1=n^2\left(\frac{\pi}{2}+\frac{\pi^3}{24}\right)+n\left(2-\frac{\pi^2}{4}+4A\right)+A_2\frac{\pi}{2}-A\frac{\pi}{4}+\frac{\pi^3}{96}$$

$$e_2=\frac{\pi}{2}\left(\frac{n\pi}{2}+A\right)^2$$

$$e_3=\frac{1}{252}+\frac{\alpha^2}{3}+\beta^2+\frac{\alpha}{15}+\frac{\beta}{12}+\alpha\beta$$

$$e^4=\frac{\alpha^2}{3}\left(\frac{x_1}{z_1}\right)^3-\alpha\beta\left(\frac{x_1}{z_1}\right)^2+\beta^2\frac{x_1}{z_1}$$

$$w_1=\frac{n^2\pi}{2}+2n+\frac{\pi}{4}$$

$$w_2=\frac{1}{3}$$

We require the ratio of W_{11} to T_{11}. This is from the above

$$\frac{\overline{W}_{11}}{\overline{T}_{11}}=\frac{a^3w_{11}+z_1^3w_2}{a^7(e_1+e_2)+z_1^7(e_3+e_4)}$$

Also, since $z_1 = na$ and $s_0 = \frac{\pi}{2} a$

$$\frac{\overline{W}_{11}}{\overline{T}_{11}} = \left(\frac{\pi}{s_1}\right)^4 \left(\frac{s_1}{2s_0}\right)^4 \frac{N_1(n)}{N_2(n)} \tag{99}$$

where

$$N_1(n) = w_1 + n^3 w_2$$

$$N_2(n) = e_1 + e_2 + n^7(e_3 + e_4)$$

Thus, for the frequency characteristic, we obtain from equation (99) the expression

$$\left(\frac{\mu s_1}{\pi}\right)^4 = \left(\frac{s_1}{2s_0}\right)^4 \frac{N_1(n_1)}{N_2(n_1)} \tag{100}$$

where n_1 is the root of the equation

$$\frac{d}{dn} \frac{N_1(n)}{N_2(n)} = 0$$

as is required by Rayleigh's method. This particular value of $n = n_1$, then, determines the position s_2

$$s_2 = \left(n_1 + \frac{\pi}{2}\right) a$$

of the point of application of the single load to obtain a statical deformation reproducing the deformation present during vibration.

We shall now determine the value of $n = n_1$, for the example of the short U bar $\left(\frac{s_1}{s_0} = 2\right)$, already treated by Ritz's method. The value of n_1 is best obtained graphically. Selecting various values for n, the quantities $N_1(n)$ and $N_2(n)$ are calculated and also the ratios of $N_1(n)$ to $N_2(n)$. These calculated values are given in Table 3. Plotting in Figure 9 the ratio $N_1(n)$ to $N_2(n)$ against n, we find that the minimum value of the ratio occurs nearly at $n = 1$. Accordingly when the single load is applied at the point

$$s_2 = 0.815 s_1$$

the resulting static deformation will for the short U bar most closely approximate the deformation realized during vibration.

This particular value gives for the frequency characteristic the value

$$\left(\frac{\mu s_1}{\pi}\right)^4 = 0.15600$$

which is only slightly higher than the value obtained by Ritz's method ($= 0.15548$).

Similarly as for the short U bar (fig. 8), let s_2 be the point of application on an elongated U bar of a single load which gives the same form of deformation as that when the bar is in vibration.

TABLE 3.—*Evaluation of the ratio $N_1(n)$ to $N_2(n)$*

n	$N_1(n)$	$N_2(n)$	$\frac{N_1(n)}{N_2(n)}$
1.5708	9.0948	56.938	0.15973
1.3090	6.8383	43.519	.15714
1.0472	4.9852	31.950	.15604
1.0000	4.6895	30.061	.15600
.9500	4.3888	28.131	.15601
.7854	3.4866	22.265	.15659
.5236	2.3111	14.497	.15942

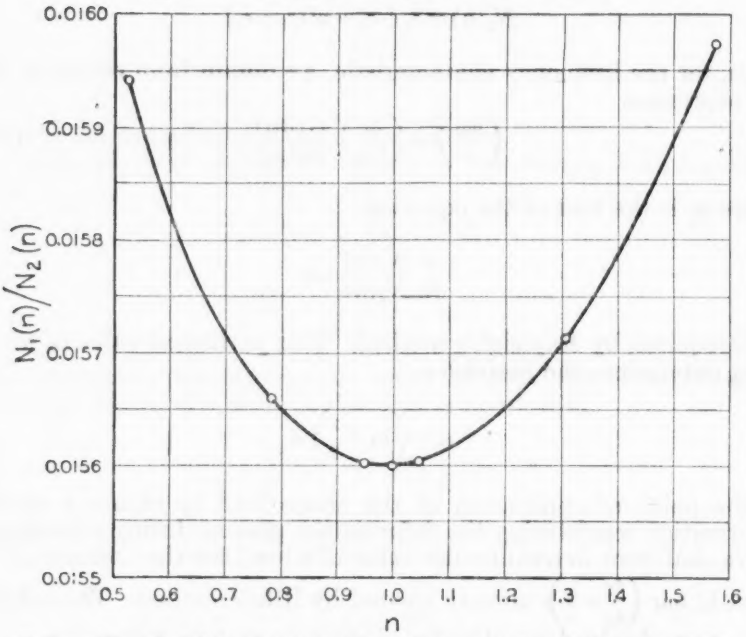

FIGURE 9.—*Graph to determine the minimum value of the ratio $N_1(n)$ to $N_2(n)$*

n is given by the relation $s_2 - s_0 = na$, where s_2 is the distance of the point of application of the single load X from the mid-point of the yoke, measured on the median line; $2s_0$ is the length of the yoke; a is the radius of the yoke.

Rayleigh,[7] as an illustration of his method, has considered the example of clamped-free bar of length s_1 and found that when the single load is applied at a point whose distance from the clamped end is 3/4 s_1, the deformation thus obtained approximates the form of the vibrating bar. Now, it was shown in the treatment of the elongated U bar of length $2s_1$, that the frequency of vibration is practically that of a clamped-free bar of length s_1. Accordingly, to obtain in statical tests on elongated U bars a deformation which approximates most closely that when the same bar is vibrating, it suffices to apply the load at a point $s_2 = 0.75S_1$.

IX. ACKNOWLEDGMENT

It is a pleasure to acknowledge the encouragement and assistance of Prof. F. D. Murnaghan in the preparation of this paper.

WASHINGTON, December 11, 1930.

[7] Rayleigh, The Theory of Sound. 1, 2d ed., p. 284.

R P294

LAUNDRY "WINTER DAMAGE"

By John B. Wilkie

ABSTRACT

When laundered cotton fabrics are dried out of doors in the winter time in New England, they frequently undergo excessive deterioration of a type called "winter damage." This paper is concerned with an investigation of the causes of "winter damage" and with its prevention.

Analyses of damaged fabrics and experimental work in the laundries and in the laboratory showed that the damage is caused by sulphuric acid which is formed in the damp fabric by the oxidation of atmospheric sulphur dioxide. The oxidation is accelerated and the damage is increased by small amounts of certain substances which may occur in laundered fabrics. Traces of iron, of spent bleach liquor, and of acetic acid were found to have this effect.

A small amount of calcium bicarbonate in the final rinse water of the wash materially reduced the damage, and is recommended as a satisfactory remedy. Precautions should be taken to eliminate iron and spent bleach liquor from the laundered fabrics, and the drying time should be made as short as possible. Antioxidants showed promise of giving protection.

CONTENTS

	Page
I. Introduction	593
1. Nature of the problem	593
2. Outline of the investigation	594
II. Determination of the cause of winter damage	594
1. Study of laundry practice	594
2. Study of individual cases	595
3. Theoretical explanation of winter damage	597
4. Artificial winter damage	598
III. Remedies suggested	600
1. Alkaline rinses	600
2. Reducing agents	601
3. The remedy recommended	601
4. Statements from the laundries	602
IV. Patent	602
V. Acknowledgment	602

I. INTRODUCTION

1. NATURE OF THE PROBLEM

For some years past, residents of New England have been harassed by a peculiar kind of disintegration of laundered cotton goods. The outstanding peculiarities are that this kind of deterioration is of general occurrence only in New England and only in the winter. This latter fact has given rise to the name "winter damage." Examples of winter damage are shown in the photographs reproduced in Figures 1, 2, and 3.

Winter damage is unlike other types of deterioration in that its occurrence is largely unpredictable. One garment out of a number

in the same wash may be attacked. A new garment is just as liable to be attacked as an old one. Our present experience indicates that the attack of winter damage is limited to cotton, and occurs only when garments are hung outdoors to dry.

Garments laundered in the home are attacked in the same manner as those washed in commercial laundries and sent home to be dried and ironed—the regular "wet wash" service. Probably it is because the laundrymen are organized that the request for assistance in solving this problem came from the Laundryowners' National Association.

2. OUTLINE OF THE INVESTIGATION

Some months were spent in New England studying laundry practice. Through the cooperation of several laundries, many cases of winter damage with their complete histories were examined. Damaged fabrics were analyzed in the laboratory. The rate of deterioration of cotton cloth when laundered and dried outdoors was compared with the rate when the cloth was dried indoors.

On the basis of the information thus obtained, an explanation of how winter damage occurs was developed. This explanation was corroborated by the production of winter damage under artificial conditions in the laboratory. Based on these results a remedy was suggested and put into use in four laundries, where its effectiveness has been indicated by the practical experience of these laundries during the past two winters.

II. DETERMINATION OF THE CAUSE OF WINTER DAMAGE

1. STUDY OF LAUNDRY PRACTICE

While many minor variations were noted at the different plants visited, laundry practice has been pretty well standardized. The "wet wash" is processed in the following steps: Wash with warm alkalized soap suds, wash three times with hot alkalized soap suds, rinse, bleach, rinse four times, sour,[1] blue.

It was found that the water used by New England laundries is relatively pure. The bicarbonate (HCO_3) content was only 6 to 15 parts per 1,000,000, and the calcium carbonate hardness was 0.2 to 2.3 grains per gallon. Occasionally the water was noticeably contaminated with iron,[2] which probably came from corrosion of the heaters and pipes in the laundry.

The odor of chlorine was frequently noticeable in the wash room during the bleaching process. If garments which had been washed and extracted were stored in this room, they might absorb enough chlorine to cause trouble when they are being dried. It will be shown that strong oxidizing agents like chlorine are liable to increase winter damage.

The souring step is introduced in the laundry practice because experience has shown that if a cotton fabric is ironed when in an

[1] The sour is an acid bath used in one of the last rinses to neutralize traces of alkali remaining in the cloth. It is also claimed by some manufacturers of proprietary sources that their products will remove rust stains.

[2] Iron has been found in water of heating systems of New England laundries between 3.6×10^{-5} molar and 1.4×10^{-3} molar. These conditions are sufficient to effect catalytic action. Even in the cold tap water of Massachusetts 0.4×10^{-5} molar iron has been reported. F. S. Cook, Rôle of Certain Metallic Ions as Oxidation Catalysts, J. Biol. Chem. **10**, p. 289; 1926.

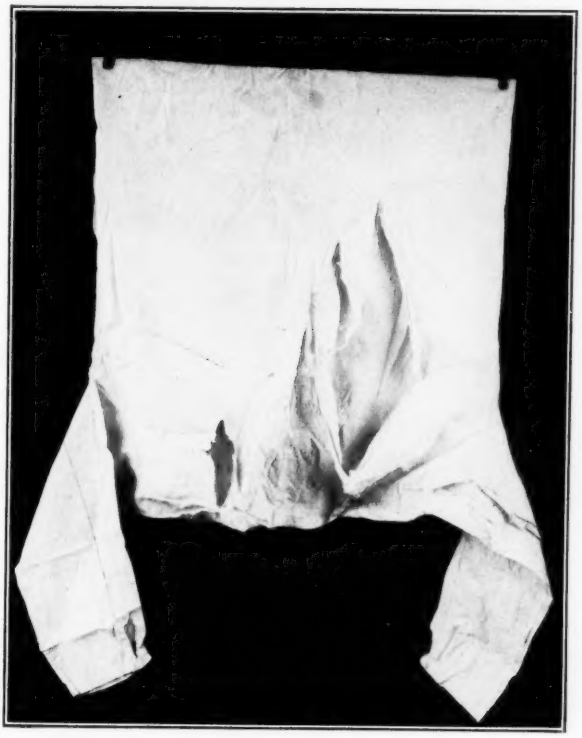

FIGURE 1.—*Typical example of winter damage*

FIGURE 2.—*Advanced case of winter damage showing discoloration in the region of failure*

alkaline condition, it will eventually turn yellow. A weakly acid [3] (sour) rinse is therefore given to remove the last trace of alkali. Unfortunately, most laundries do not operate under strict technical control, so that, in about half the cases observed, too little sour was added, and the clothes remained slightly alkaline.

2. STUDY OF INDIVIDUAL CASES

The 10 cooperating laundries sent in 907 cases of winter damage, each accompanied with its history. Ten per cent of these proved to be other kinds of deterioration and not winter damage. A study of the authentic cases brought out the fact that winter damage occurs in spots; one or more parts of the garment are seriously weakened or destroyed, but the rest of it remains strong. This strong portion furnished a very convenient blank for analysis.

Winter damage does not necessarily occur all at once. A slight amount of damage may be done at one time, and the final destruction of the goods may not occur until the conditions which cause this type of damage reappear, perhaps, some weeks or months later.

There is a slight, but important,[4] weakening of cotton fabrics every time they are laundered. This "natural deterioration" may add to the deterioration caused by incipient winter damage and thus bring about a failure which will have all the appearance of having been caused by winter damage alone.

In order to get some information about the magnitude of this regular deterioration, and also to ascertain the rôle played by the atmosphere, a bolt of cotton toweling was cut into a number of specimens which were sent to five laundries. The laundries were requested to wash the towels by their customary procedures, to dry half of the specimens with a regular laundry flat-work ironer and the other half by hanging them on a line outdoors, to iron them, and then to repeat the process a number of times. Individual towels were returned to the laboratory after 10, 20, 30, 40, and 50 washings and were tested for tensile strength. The results are shown in Figure 4.

These results show that the treatment given the towels in some laundries is much more severe than in others, but that in every case, drying the towels outdoors results in greater deterioration than when the drying is done on the usual laundry flat-work ironer. Evidently the rôle played by the atmosphere is important.

Chemical examination of garments sent to the laboratory showed several characteristics of winter damage. The badly damaged portion of the garment is practically always more acid in reaction than the remainder, and often it contains a higher proportion [5] of iron in the ash. In no case could the slightest trace of free chlorine be detected. However, the damaged goods usually possessed an odor

[3] By a weak acid is meant one with a low degree of dissociation, such as acetic acid. However, acids as strong as oxalic are used, but such an acid would usually be buffered to decrease the H-ion concentration.

[4] A report prepared by the Research Laboratory of Applied Chemistry of Massachusetts Institute of Technology indicates that the loss in strength by laundering of collars is distributed as follows: Bleach 40 per cent, soap and soda and rinsing 25 per cent, loss in drying 20 per cent, loss by sour and blue 5 per cent, loss by molder 5 per cent, loss in hot tube 5 per cent. This loss, as well as the losses incurred through normal outside drying, would have to be regarded largely as chemical in nature.

It is well known that a fabric is deteriorated by the action of light, especially between the wave lengths of 400 and 295 μ. Undoubtedly this factor enters where outside drying is concerned. F. W. Aston, Report on the Action of Sunlight on Aeroplane Fabric: Its Nature and Prevention. Advisory Committee for Aeronautics (British) Memoranda 396, pp. 2-5; 1917.

[5] This higher proportion of iron in the ash indicates the possibility of increased catalytic activity. The catalytic action of iron is made use of in industry in the contact process for preparing sulphuric acid from sulphur dioxide and water.

resembling spent bleach liquor, and freshly damaged pieces were found which contained oxidizing material.[6]

In every case of winter damage where the garment had not been laundered subsequent to the occurrence of the damage, the fabric around the obviously affected parts was distinctly more acid than the other parts of the fabric. The damaged portion was so acid as to give a yellow color when treated with a dilute solution (0.0135 g per liter) of brom-phenol blue (indicating a pH of about 3). This high degree of acidity can not be accounted for by the absorption of carbon dioxide from the air.[7] The only other strongly acidic material likely to be extensively present in the atmosphere is sulphur dioxide which in the presence of moisture, may be oxidized to sulphuric acid.

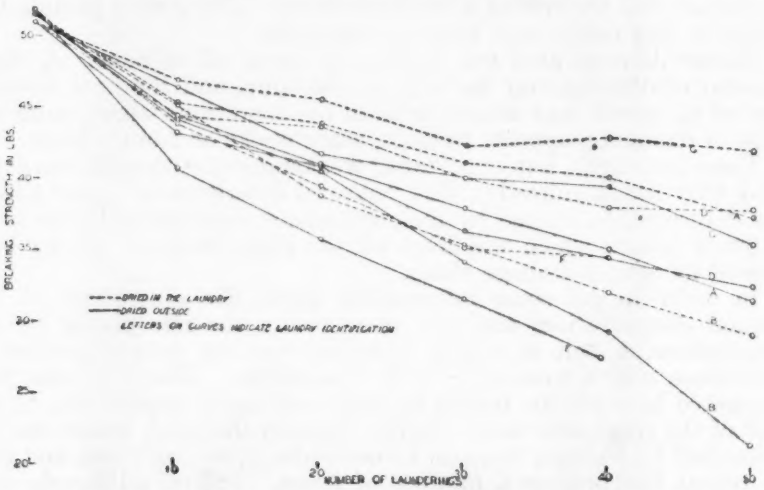

FIGURE 4.—*Effect of laundering on the strength of cotton toweling*

The badly damaged portions of these garments were, therefore, analyzed for sulphuric acid by titration with methyl orange and phenolphthalein, and for sulphates gravimetrically.[8] In practically every case they were found to have a higher content both of free sulphuric acid and combined sulphates than had other portions of the same garments.

In Figure 5 are given the results of typical analyses for free sulphuric acid. It will be seen that the badly damaged portions contain much more acid than the other portions. The amount of sulphuric acid present is small, often between 0.01 and 0.04 per cent, though it may be more than 0.12 per cent. The difference in sulphate content calculated to sulphuric acid between the more damaged and the less damaged portions of affected garments lies between 0.004 and

[6] Free chlorine may be detected by the use of orthotolidine indicator. The active oxidizing material was not free chlorine but chlorates, ferrates, or ferric salts or even oxidized soap. No free chlorine is present at the time of extraction normally but only the less active oxidized or chlorinated material, as soap, which laboratory experiment has demonstrated as being responsible for the odor of spent bleach liquor.

[7] The pH of moist air subjected to CO_2 of the atmospheric concentration is about 5.7. H. Edna Fawcett and S. F. Acree, The Problem of Dilution in Colorimetric H-Ion Measurements, J. Bacteriology **17**, p. 163; 1929.

[8] No free acid could be found in samples of new fabrics similar to those which underwent winter damage deterioration.

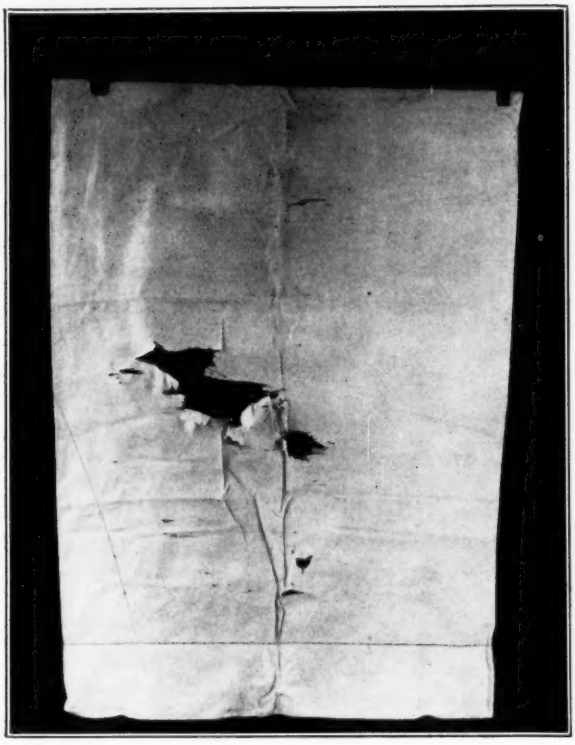

FIGURE 3.—*Most advanced type of winter damage in which damaged regions crumble*

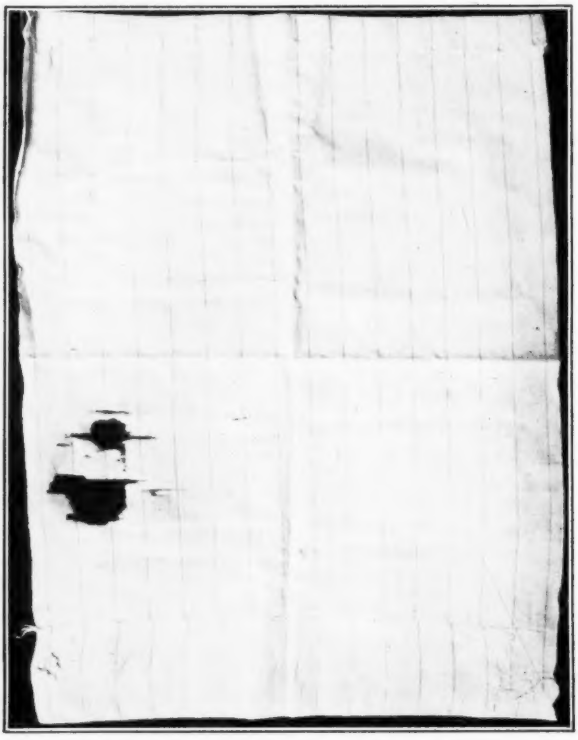

FIGURE 6.—*Failure resembling winter damage caused by exposure of an iron-impregnated towel to air containing 1 part per 1,000,000 sulphur dioxide*

0.4 per cent. Barr and Hadfield [9] have shown that even much smaller [10] quantities of sulphuric acid can cause damage to cotton fabrics when they are dried at temperatures such as exist during ironing.

The presence of sulphur dioxide in the atmosphere has been noted by many investigators.[11] The average of more than 1,500 determinations of the concentrations of sulphur dioxide in the vicinity of New York City was 0.265 part per 1,000,000 and a concentration as high as 1.3 parts per 1,000,000 existing for 15-minute intervals has also been found in this vicinity. It has also been established that many metallic salts, particularly those of iron, act as catalysts which accelerate the oxidation of sulphur dioxide to sulphur trioxide, especially in the

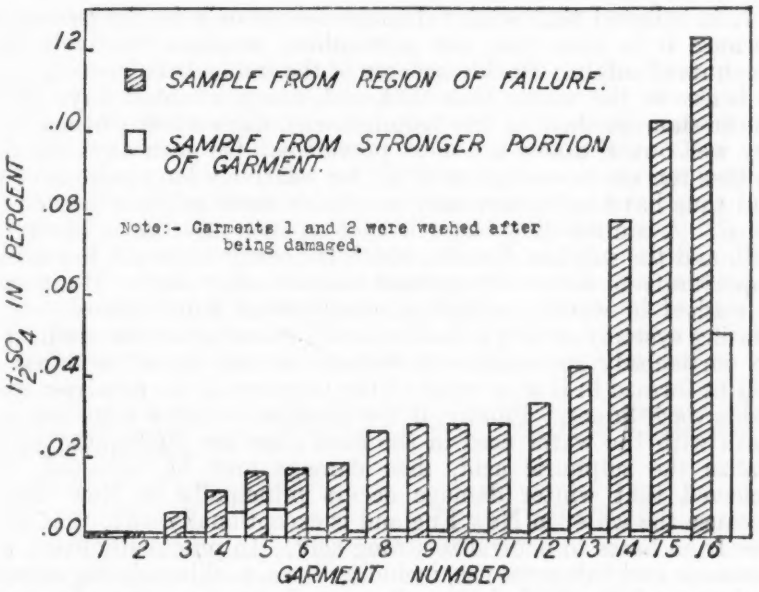

FIGURE 5.—*Typical analyses of winter damaged garments for sulphuric acid*

presence of moisture.[12] [13] [14] Damp cotton cloth absorbs sulphur dioxide from the air and becomes more and more acid in reaction with time of exposure.

3. THEORETICAL EXPLANATION OF WINTER DAMAGE

The following explanation of how winter damage takes place may be given on the basis of the facts set forth above. The chemical facts may be summarized as follows: Damp cotton absorbs sulphur dioxide

[9] Barr, Guy, and Isabel H. Hadfield. The Effect of Minimal Amounts of Acid on the Strength of Cotton and Linen, Tech. Rept. Advisory Committee for Aeronautics (British), **2**, pp. 609–615; 1919–20.

[10] Solutions of N/8,000 H_2SO_4 were found to cause deterioration upon fabrics immersed in them and subsequently heated.

[11] Office of Industrial Hygiene and Sanitation, U. S. Public Health Service, Partial List of References on Pollution of Air by Smoke, Mimeograph Report No. E688.

[12] Cook, S. F., Rôle of Certain Metallic Ions as Oxidation Catalysts, J. Biol. Chem., **10**, pp. 289–312; 1926.

[13] Wilson, L. P., Catalytic Action in the Oxidation of Cellulose, J. Soc. Chem. Ind., **39**, p. 177T; 1920.

[14] Baudisch, O., and Davidson, D., Catalytic Oxidation by Means of Complex Iron Salts, J. Biol. Chem., **71**, pp. 501–508; 1927; C. A. p. 914; 1927.

present in the atmosphere. In the presence of the moisture in the cloth this sulphur dioxide is oxidized to sulphuric acid, rapidly when small amounts of iron or other catalytic agents are present. As the cloth dries, the sulphuric acid becomes concentrated in the regions which dry last.[15] When the cloth is ironed rapid deterioration of the cotton takes place and the cloth becomes weak. In extreme cases it becomes yellowish in color and powders when handled.

Winter damage may be expected to occur, even when there is less sulphur dioxide in the atmosphere than 1 part per 1,000,000, especially (1) when the cloth remains damp and in contact with the atmosphere for a relatively long time, (2) when iron has been absorbed by the cloth, (3) when there are no substances in the cloth which will neutralize the sulphuric acid formed.

It is believed that winter damage occurs only in the winter time because it is then that the atmosphere contains relatively larger amounts of sulphur dioxide because of the smoke from heating plants. It is also in the winter time that cool, damp, overcast days (typical winter-damage days of the laundrymen), days when clothes do not dry well out of doors, are most prevalent. On such days the damp clothes remain in contact with air for relatively long periods of time and thus have an opportunity to absorb more sulphur dioxide than usual. A contributing factor is that on such days air is likely to be still, and the sulphur dioxide, which is heavier than air, has a better opportunity to sink to the ground than on other days. If a garment is washed in water containing iron (derived from corrosion of the heating system) or if it is inadequately rinsed after the wash, it will be particularly susceptible to damage because more sulphuric acid will be formed in it as a result of the presence of the catalysts iron or spent wash liquor. Finally, if the alkaline or buffer salts left in the cloth with the water used in the final rinse are inadequate to neutralize the sulphuric acid, then damage may be expected. It is believed that winter damage occurs principally in New England because the water in New England is exceptionally soft; that is, it is free from bases to neutralize strong acid. In practically every other domestic and industrial use, including the actual laundering operation exclusive of the final rinse, soft water is very much to be desired. Buffer salts which are usually either unnecessary or objectionable serve a useful purpose in the final rinse of "wet wash."

4. ARTIFICIAL WINTER DAMAGE

Further evidence in support of the explanation given above was obtained in the following experiments in which winter damage was produced under artificial conditions. A bolt of cotton toweling was cut into towels which were washed thoroughly and rinsed in distilled water to remove sizing and other superfluous impurities. Towels impregnated with various substances were exposed in a cabinet in air containing 1 part per 1,000,000 of sulphur dioxide when the towels were introduced.[16] A fan kept the air in the cabinet in circulation. All towels were removed from the cabinet once each day, moistened with

[15] The action of the sulphuric acid is first one of hydrolysis in which a number of products, such as dextrins and sugars, are formed. Continued action of the sulphuric acid removes water from the sugars previously formed and thus results in carbonization or charring. Textbook of Cellulose Chemistry, Heuser, West & Esseln, pp. 142–143; 1924.

[16] The effective concentration was much less than 1 part per 1,000,000 because of the absorption by the towels and condensed moisture present on the walls of the case.

distilled water (with calcium chloride-sodium bicarbonate solution in the case of the towels treated with this material), ironed (temperature of iron about 438° F. decreasing about 30° F. during each ironing), again moistened and returned to the cabinet. At the end of 10, 30, and 50 treatments a towel representing each treatment was tested for tensile strength, sulphate content, and free acidity.

The impregnating treatments were: (1) Blanks, towels simply wet with distilled water; (2) towels immersed in a solution of 1.25 g of ferric chloride in 5 liters of water and then in a 0.1 per cent solution of sodium carbonate to precipitate the iron in the towels; (3) towels treated with iron as in (2) and then with a solution of 15 g of sodium bicarbonate and 10 g of calcium chloride in 2.5 liters of water which reacts as a calcium bicarbonate solution; (4) towels bleached with sodium hypochlorite solution containing 0.045 per cent available chlorine at 70° C.

The effect of these treatments on the strength of the toweling is shown in Table 1. The blank retained 60 per cent of its original strength after 50 treatments. The presence of a small amount of iron greatly accelerated the damage to the toweling caused by exposure to sulphur dioxide, the strength being completely gone after 14 treatments. Considerable protection was afforded the iron-impregnated towel by treating it with a calcium chloride-sodium bicarbonate solution (compare experiment 2 and 3 in the table). The towels impregnated with calcium chloride-sodium bicarbonate solution alone deteriorated faster than the blank, but not nearly so fast as the towel containing iron. The bleached toweling (experiment 5 in the table) was not quite so resistant as the unbleached (experiment 1).

TABLE 1.—*Breaking strength of toweling treated with various substances when moistened and exposed to air containing 1 part per 1,000,000 of sulphur dioxide for 24 hours and ironed*

Experiment No.	Towels treated with (see text)—	Breaking strength in per cent of original after: Number of exposures—		
		10	30	50
1	Nothing	96	87	60
2	Iron	91	0	0
3	Iron and calcium bicarbonate	95	80	45
4	Calcium bicarbonate	100	76	37
5	Bleach	91	74	54

The sulphate and the free acid content of the exposed towels was observed to increase with number of exposures. The blank contained 0.02 per cent free acid and 0.59 per cent sulphates (reported as H_2SO_4), after 50 exposures, The iron-impregnated towel contained 0.03 per cent free acid and 0.3 per cent sulphates after only 10 exposures. The iron-impregnated towel which was given the additional treatment with calcium bicarbonate solution contained 0.02 per cent free acid after 50 treatments and 0.54 per cent sulphates.

The damage to the toweling in these experiments is in every way like winter damage occurring under natural conditions. Figure 6 shows the failure of an iron-impregnated towel after exposure to air containing 1 part per 1,000,000 sulphur dioxide.

Similar experiments to those described above were carried out exposing the fabrics on the roof of the Industrial Building, National Bureau of Standards. The results were, in general, similar to those obtained in the cabinet exposures though the decrease in strength was much less, and smaller amounts of acid and sulphates accumulated in the fabrics.

Another series of experiments was carried out in which towels containing small amounts of soap, bleach liquor, etc., were exposed in the cabinet to air containing 1 part per 1,000,000 of sulphur dioxide according to the procedure already described.

The treatments were: (1) Blank, toweling simply wet with distilled water, (2) towels immersed in water containing 0.25 per cent tallow soap, then in a sodium hypochlorite bleach solution containing 0.025 per cent available chlorine, and wrung out; (3) towels treated as in (2) and then rinsed in a 2 per cent solution of acetic acid; (4) towels immersed in a solution of 10 g of sodium chlorate (an oxidizing agent) in 3 liters of water; (5) towels immersed in a 0.026 per cent solution of ferric chloride, then in a 0.1 per cent solution of sodium carbonate to precipitate the iron in the towels, and finally in a 0.33 per cent solution of sodium chlorate.[17]

The effect of these treatments on the strength of the toweling after 17 exposures, each followed by moistening and ironing, is shown in Table 2. The laundryowners' attention is particularly called to experiments 2 and 3 which indicate that traces of soap and bleach liquor in the towel decrease its ability to withstand the action of sulphur dioxide and that a final rinse with acetic acid makes matters very much worse. The results of experiments 4 and 5 are further evidence that strong oxidizing agents increase the action of sulphur dioxide.

TABLE 2.—*Breaking strength of toweling treated with various substances when moistened and exposed to air containing 1 part per 1,000,000 of sulphur dioxide for 24 hours and ironed*

Experi- No.	Towels treated with (see text)—	Breaking strength in per cent of original after 17 exposures
1	Nothing	92
2	Soap and bleach	44
3	Soap, bleach, and acetic acid	9
4	Sodium chlorate	[1] 30
5	Iron and sodium chlorate	20

[1] The sodium chlorate-treated towel would have been weakened more if it had been made distinctly acid before exposure because the sodium chlorate would then have been a more active oxidizing agent. This principle is demonstrated in experiments 2 and 3 in above table.

III. REMEDIES SUGGESTED

1. ALKALINE RINSES

This work indicates that it should be possible to materially decrease or prevent winter damage by introducing an alkali into the cloth after each laundering, in order that any sulphuric acid may be

[17] Concentrations of soap and bleach correspond to laundry practice. The concentration of iron was sufficient to insure catalytic action. Arbitrary amounts of the other chemicals were used. In all cases objectionable excesses were avoided.

neutralized. Practical experience has shown that sodium carbonate left in the garments makes it impossible to produce that brilliant whiteness which is so generally desired. Although the "yellowing" produced by such alkalies, as sodium carbonate, may have little effect on the strength of the fabric, it has such an important effect on the appearance that they must be carefully avoided. To this end, general laundry practice calls for a final rinse with a mild acid (sour), and many of the types of bluing in general use will work only in a weakly acid solution.

The use of sodium silicate to keep iron from the fabric and to exert a neutralizing action in the fabric was first tried as a possible preventive of winter damage. However, it was found in the case of the particular silicate being tried, that if an adequate quantity was used to be effective, discoloration occurred. Hence, more extensive trials with this material were discontinued.

A mixture formed by adding to the rinse calcium chloride and then sodium bicarbonate was found to be effective. It is very mildly alkaline in reaction, is soluble at the dilution prepared, and apparently does not cause discoloration if used properly. There is no cumulative building up of the carbonate in the fabric as there is of sodium silicate when this latter material is used.

2. INHIBITING AGENTS

The above explanation of winter damage suggests that the damage would be prevented by impregnating the garment with an inhibiting agent. By means of such a chemical, it would be possible to keep the sulphur dioxide from becoming oxidized to sulphur trioxide, and, since sulphur dioxide is a gas having only a limited solubility in water, the drying and ironing of the garment would not concentrate the sulphurous acid (formed when sulphur dioxide dissolves in water) to the point where it could attack cotton.

Many different inhibiting agents were tried. Towels impregnated with iron as in the previous experiments were dipped in solutions of inhibiting agents (adjusted to the same pH with methyl red), exposed to the action of sulphur dioxide, ironed, and the process repeated. Several chemicals were found which afforded protection to the fabric. Sodium oxalate and resorcinol were among the best.

This is one more bit of evidence in substantiation of the cause of winter damage, and the laboratory work as completed indicates that further study with inhibiting agents might result in formulating the most efficient means of decreasing winter damage. Inasmuch as the calcium chloride-sodium bicarbonate treatment has practical advantages and fewer possible complications, it was selected for trial in the laundries.

3. THE REMEDY RECOMMENDED

Certain conclusions having been reached as a result of the laboratory work, it was appropriate to try them out on a practical scale. Cooperative arrangements were made with four laundries in New England, and the following procedure was put into effect, under carefully controlled conditions:

After the garments have been washed, rinse thoroughly.

If a sour is used, follow it with at least one rinse with plain water.

Apply the bluing in the usual way, running the wheel (washing machine) for three mintues. The dye Colour Index No. 246 [18] is a satisfactory bluing for use in alkaline solution. Bring the water level to 6 to 8 inches for a 42 by 84 inch wheel. Add 2 pounds of calcium chloride dissolved in a pail of water, and run for two mintues. Add 3 pounds of sodium bicarbonate dissolved in a pail of water and run for five minutes.[19] Remove the goods, and extract in the centrifuge in the usual way. Caution the customer to dry the garments quickly, and particularly not to let them hang out of doors over night.

The quantities of reagents given above are approximately correct for the size of wheel mentioned. Since too great alkalinity is almost as bad as not enough, the use of this process requires careful control of the amounts of reagents used. The final alkalinity should be such that not less than 6 nor more than 10 drops (20 drops = 1 ml.) of tenth normal sulphuric acid are required to neutralize 5 ml of the rinsing water using methyl red as the indicator.

4. STATEMENTS FROM THE LAUNDRIES

Statistics were received weekly during the winter of 1928–29 from eight laundries not using this treatment as well as from one using it. The laundry having the greatest damage reported an average of 50 pieces (approximate weight per piece = 0.4 pound) per 5,000 pounds of goods and the average for all laundries not using the treatment was 10 pieces for every 5,000 pounds of goods. In the laundry where the calcium bicarbonate final rinse was used, the average for the season was only one piece for every 5,000 pounds of goods. The opinion of the three other laundries using the treatment, but not sending in weekly reports concerning this rinse is given in one production manager's report in which he states that "the treatment materially and immediately reduced" his winter damage claims and "continued to be effective as long as used."

IV. PATENT

It will be noted from the above that the final stage of this investigation was completed during April, 1929. On April 9, 1929, a patent for a method of protecting fabric was granted to Robert A. Pahir and assigned to H. Kohnstamm & Co. (Inc.). The patent number is 1708519, and the application was filed on March 9, 1925. Without assuming any legal responsibility for the statement, it would seem that the calcium bicarbonate treatment recommended herein is covered by this patent.

V. ACKNOWLEDGMENT

The author gratefully acknowledges the cooperation of the Massachusetts Laundryowners' Association and its member laundries. He is especially indebted to the Massachusetts Institute of Technology for laboratory space and for chemicals and to H. O. Forest and H. J. MacMillan, of the institute staff, for helpful information. F. H. Guernsey, of the Cowles Detergent Co., and R. A. Phair, of the H. Kohnstamm Co., furnished much valuable data.

WASHINGTON, January 26, 1931.

[18] "Colour Index" of the British Society of Dyers and Colourist; 1928. See the current Yearbook of the American Association of Textile Chemists and Colorists for the American Manufacturers of this dye and the names under which they sell it.

[19] The ratio is approximately that of the equivalent weights of the chemicals used. The amounts used correspond to the concentrations of bicarbonates and calcium salts frequently found in natural waters.

THE DETERMINATION OF THE ALPHA-CELLULOSE CONTENT AND COPPER NUMBER OF PAPER

By John O. Burton and Royal H. Rasch [1]

ABSTRACT

In determining the permanence of a paper it is important to know the purity of the cellulose composing it. The tests most commonly used for the determination of the purity of cellulosic materials are the alpha cellulose and copper number tests. The alpha-cellulose test is based upon the assumption that unmodified cellulose is insoluble in a mercerizing caustic solution. This insoluble portion is termed "alpha cellulose." The copper-number test is based upon the quantitative reduction of an alkaline copper solution by the degraded celluloses of the sample. The copper number is the weight of copper so reduced by a definite weight of the sample.

Both of these tests have been highly developed for the analysis of cellulosic materials in a loose, fibrous form, such as paper pulp. But the fibers of paper are packed into a dense, compact sheet and, hence, methods which can be applied to other forms of cellulose can not be applied to paper. Also, papers contain several noncellulosic constituents which must be taken into account. Methods which have been proved reliable for the analysis of other forms of cellulosic materials have been modified by the bureau to make them applicable to paper testing. The modification considered of prime importance is the reduction of the sample to a cotton-like form by means of mechanical disintegration. It is also important to correct the results for the amounts of sizing and loading materials in the paper. Several minor details of the methods have been altered for purposes of simplicity and increased accuracy. By the use of the alpha-cellulose method duplicate determinations of the percentage of alpha cellulose agree within 0.3. Duplicate results obtained with the copper-number method seldom vary more than 1 per cent from their mean.

CONTENTS

		Page
I.	Introduction	603
II.	Preparation of the sample	605
III.	The determination of the alpha-cellulose content of paper	606
	1. Definition of alpha cellulose and origin of the method	606
	2. Preparation of the mercerizing solution	606
	3. Procedure	606
	4. Discussion of the method	607
IV.	The determination of the copper number of paper	613
	1. Definition of the copper number and origin of the method	613
	2. Preparation of the solutions	614
	3. Procedure	615
	4. Discussion of the method	616
V.	Conclusion	619

I. INTRODUCTION

The determinations of the alpha-cellulose content and copper number are used to a considerable extent in evaluating the purity of cellulose materials. The alpha-cellulose content of a cellulosic material is that part which is insoluble in a sodium hydroxide solution

[1] Research Associate of the Brown Co., Berlin, N. H.

of mercerizing strength under certain specified conditions. The copper number is the weight of copper in grams, reduced as cuprous oxide from an alkaline copper solution by a given amount of the cellulosic material. The purer forms of cellulose are characterized by a high content of alpha cellulose and a low copper number. The alpha-cellulose content is regarded as the amount of unmodified cellulose which the material contains. The remainder of the cellulose material may be composed of several substances, such as naturally occurring waxes and resins, lignin, pentosans, and modified forms of cellulose, but the chief constituents are the modified forms of cellulose. These modified celluloses are characterized by their power to reduce copper from alkaline copper solutions. The quantity of copper which they will reduce depends upon their amount and the extent to which they have been modified. Thus the copper number arises from these modified forms of cellulose and simultaneously measures their amount and degree of modification.

These determinations are used as a matter of routine procedure in testing the raw cellulose materials, such as cotton and wood fibers, used in the manufacture of rayon, lacquers, guncotton and other cellulose products. The viscose industry has long realized the close connection between the purity of the cellulose materials and the quality of the product. There is without doubt a similar relation in the manufacture of paper. The stability of paper, and in many cases its strength, appears to be directly related to its cellulosic purity as measured in terms of alpha cellulose and copper number. The use of these determinations for judging the quality of fibrous raw materials used for paper making and for testing the probable permanence of papers is rapidly increasing. As the cellulose of paper-making fibers is usually degraded to some extent in the paper-making process, such as by oxidation or hydration in the cooking, bleaching, and beating, determinations of alpha cellulose and copper number are also used to some extent as control tests. As these modified celluloses are considered to be quite impermanent and a possible cause of deterioration, it is important to know not only the content of unmodified cellulose in a paper or a paper-making material, but also to know the degree of the modification as expressed by the copper number.

In its research on the permanence of paper the National Bureau of Standards makes extensive use of the alpha cellulose and copper number determinations. In the course of this work the methods described in the literature for these determinations were found unsuitable for the analysis of paper, having been designed more particularly for soft, readily-absorbent materials such as are used for viscose products. They could not be successfully applied to more compact and resistant materials such as paper and certain paper-making fibers.

Experimental study of the methods available resulted in the development of modified testing procedures which appear to be more satisfactory for the analysis of paper and paper-making fibers. Following are descriptions of the modified methods as they are now being used by the bureau, and of the experimental studies made in connection with their development.

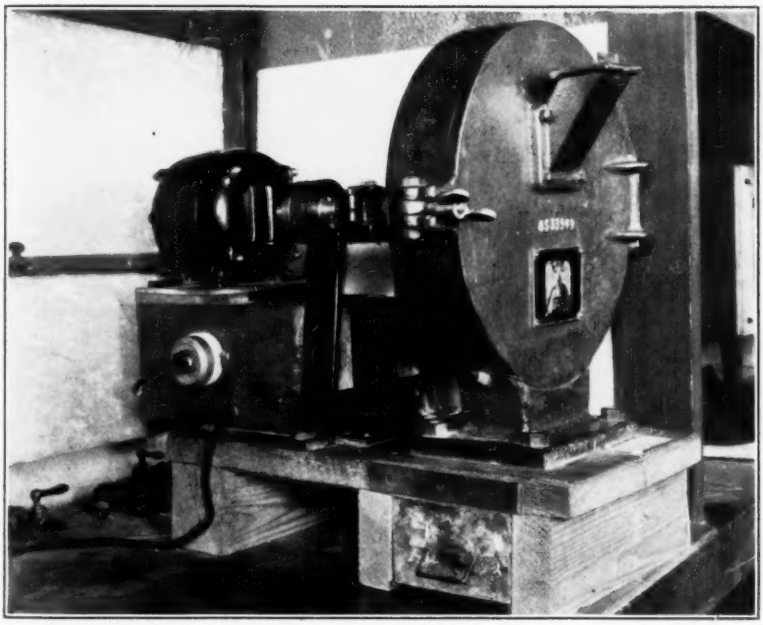

FIGURE 1.—*Paper disintegrator*

UNIV. OF MICH.

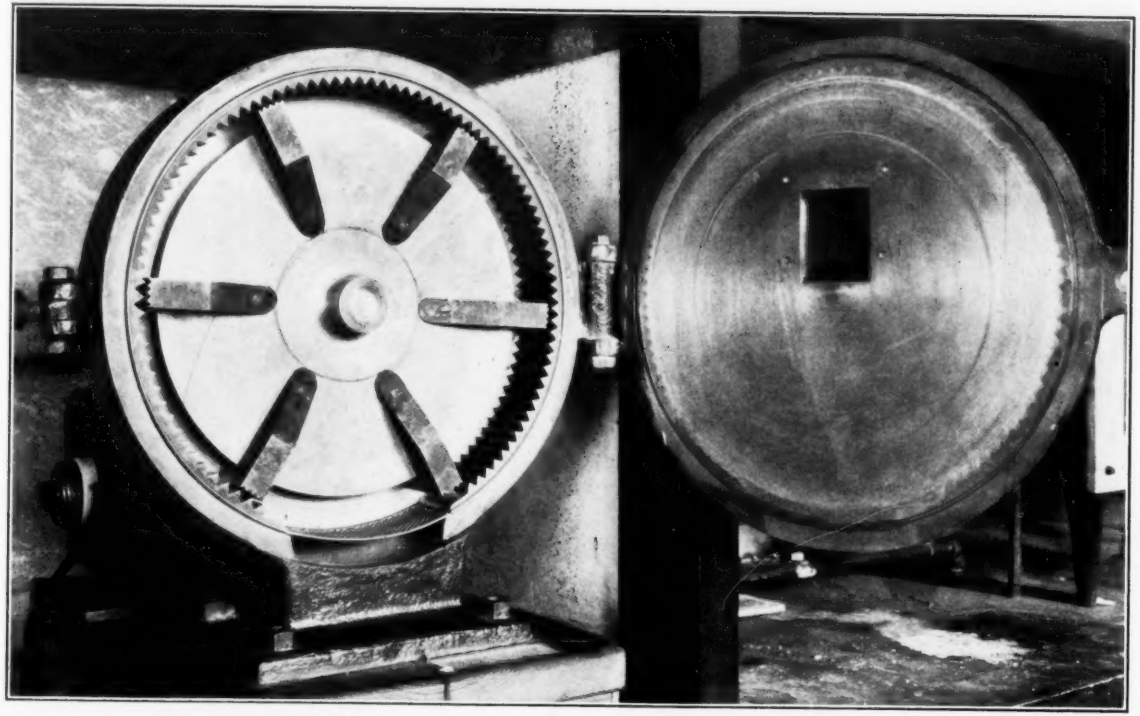

FIGURE 2.—*Paper disintegrator showing construction of grinding parts*

II. PREPARATION OF THE SAMPLE

The basic constituent of papers is cellulose, but in a determination of their chemical properties they differ markedly from most other cellulosic materials in that the fibers are closely packed into a dense, compact sheet and are protected from the action of chemical agents by a covering of rosin. For this reason the bureau has adopted the suggestion of Kohler and Hall [2] and for chemical determinations such as these, reduces all paper to a uniform fibrous condition by the use of a grinder.

The grinder used was designed by Gösta Hall, and is similar to the one used at the Swedish Government Testing Institute. (See figs. 1 and 2.) Several of these grinders are in use in this country and abroad. The grinder consists of a 12-inch rotor revolving inside a steel housing at a speed of 1,700 revolutions per minute. The rotor is fitted with six serrated steel lugs, and the inner circumference of the steel housing is also serrated. The rotor teeth clear those of the housing by a sixteenth of an inch. The paper is introduced in the form of ½-inch strips through a hopper and is then carried by centrifugal force to the space between the rotor teeth and those of the steel housing where it is disintegrated. The cotton-like material thus formed is ejected through a 10-mesh wire screen and collected in a receptacle in the base of the apparatus. This method of grinding possesses the advantages of rapidity, and absence of a noticeable rise in temperature and of contamination. Most of the grinding is done by impact, the paper being thrown against the teeth of the steel housing with sufficient force for disintegration. Thus there is no sustained action on the fibers and excessive bruising and crushing are avoided.

The disintegrated paper is spread loosely in trays and allowed to attain equilibrium with the moisture of the atmosphere in the vicinity of the balance upon which the sample is to be weighed. Samples should be exposed to this atmosphere for at least six hours. This procedure has been found to be superior to conditioning the sample in a closed container as in many cases the relative humidity of the atmosphere in the container and that of the atmosphere in which the sample must be weighed differ sufficiently to cause the sample to continually change in weight during the weighing. A constant temperature and humidity room in which weighings can be made is very useful for conditioning samples.

Papers containing sizing or loading materials must be analyzed for the amounts of these materials, as the results are based on the weight of the fibrous material in the paper and not on the weight of the paper itself. The analysis of the paper for sizing materials may be made on either the sheet or disintegrated form of the sample. The analysis for loading materials should be made on the disintegrated paper, as the amount of loading materials in this form may differ from the amount in the original paper because of loss during the grinding operation. The grinding tends to free the filler from the fibers so that it is rather loosely held. Although some of the filler is usually lost, that which is retained by the fibers will remain quite uniformly distributed throughout the sample if care is taken to avoid excessive shaking and handling of the disintegrated paper. This is true if the filler content is less than about 12 per cent. If it is greater than this it may be difficult

[2] Kohler and Hall, Acidity in Paper, The Paper Ind., 7, No. 7; October, 1925.

to obtain a uniform sample. The moisture content of the sample is also determined. The analyses for sizing materials, filler, and moisture are made by the methods of the Technical Association of the Pulp and Paper Industry.[3]

The weights of the samples used in the alpha-cellulose and copper-number determinations are corrected for moisture content, ash, and sizing materials, and the results are calculated on this corrected weight. Table 4 shows the magnitude of the correction for the sizing materials in the sample.

III. THE DETERMINATION OF THE ALPHA-CELLULOSE CONTENT OF PAPER

1. DEFINITION OF ALPHA-CELLULOSE AND ORIGIN OF THE METHOD

By alpha cellulose is meant that part of cellulosic materials which is insoluble in a solution of sodium hydroxide of mercerizing strength under definite conditions for a definite time. Cross and Bevan [4] first mentioned the analytical use of mercerizing caustic for the isolation of "normal cellulose." Data were later produced to show that no so-called pure cellulose was entirely insoluble in mercerizing caustic, but the principle used by Cross and Bevan for isolating normal cellulose was found to be applicable to the testing of cellulosic materials for unmodified cellulose or "alpha cellulose." Many methods have been devised for the determination of alpha cellulose, but the one most commonly used is that of Jentgen [5] or some modification thereof. The method described here is based on that of Jentgen and modifications of his method suggested by Parsons [6] and Ross.[7]

2. PREPARATION OF THE MERCERIZING SOLUTION

The mercerizing solution consists of an aqueous solution of sodium hydroxide (cp grade) containing 17.5 per cent sodium hydroxide by weight, having a specific gravity of 1.197 at 15° C. The c. p. grade of sodium hydroxide usually contains 1 to 2 per cent sodium carbonate, which must be removed. This is accomplished according to directions given by Clark.[8] The required weight of sodium hydroxide sticks is dissolved in an equal weight of water and the solution allowed to stand in a closed vessel for several days, during which time the sodium carbonate will precipitate. The solution is filtered through a thick mat of asbestos or a hardened filter paper and diluted to the correct concentration with distilled water, which has been recently boiled to expel carbon dioxide. Care must be taken when handling the solution that it is exposed to the atmosphere as little as possible to prevent the absorption of carbon dioxide.

3. PROCEDURE

Weigh accurately approximately 5 g of the sample, prepared in the manner previously described, in a weighing bottle. Calculate the corrected weight of sample by subtracting from the original air-dry weight the weights of mositure, ash, and sizing materials. Transfer

[3] Paper Testing Methods, published for the Technical Association of the Pulp and Paper Industry, New York, Lockwood Trade Journal Co.; 1928.
[4] Cross and Bevan, Researches on Cellulose, **3**, p. 22; 1905–1910.
[5] Jentgen, Kunststoffe, **1**, p. 165; 1911.
[6] Parsons, Paper Trade Jour., **82**, No. 8, p. 211 (Technical Section, p. 105); 1926.
[7] Ross, Research Notes, Canadian Pulp and Paper Association, **1**, pp. 37–57; 1926.
[8] Clark, The Determination of Hydrogen Ions, Baltimore, The Williams & Wilkens Co., p. 195; 1928.

the accurately weighed sample to a 400 ml beaker of resistant glass, such as Pyrex, and place the beaker in a constant temperature bath at 20° C. After the beaker has attained the temperature of the bath add by means of a pipette 50 ml of the sodium hydroxide solution, the temperature of which has been adjusted to 20° C. Note the time immediately after the addition of the mercerizing solution. Macerate the sample well with a flattened glass stirring rod. Add another 50 ml portion of the sodium hydroxide solution and repeat the maceration. Allow the solution to stand for 30 minutes from the time of the first addition of caustic soda solution. In the meantime fit a filter flask with a 7.5 cm Büchner funnel containing a circular piece of cloth as a filtering medium. Use a high-grade cotton cloth of fine texture for this purpose. Nainsook has been found to be satisfactory. Dry the cloth in an oven at 105° C. until the weight is constant and record the dry weight.

At the end of the 30-minute period dilute the contents of the beaker with 250 ml of distilled water and filter through the cloth, using mild suction. Pack the mat thus formed with the stirring rod and wash with an additional 125 ml of distilled water. Return the filtrate to the mat and refilter to retain any fine fibers which may have passed through when the mat was first formed. Then wash with 625 ml of distilled water added in small portions, packing the mat occasionally to prevent the formation of a channel around its edges. All of the wash water is used at 20° C. After the washing, disconnect the suction and add 100 ml of 20 per cent acetic acid, allowing it to soak through the mat for five minutes. Remove the acetic acid by means of suction and complete the washing with 1 liter of boiling distilled water, added in small portions. Place the mat and filter cloth on a watch glass or Petri dish and dry at 50° to 60° C. until most of the moisture has been removed. Then transfer them to a glass-stoppered weighing bottle and dry to constant weight at 105° C.

If no filler were present in the paper this weight, less that of the filter cloth, would be the weight of the alpha cellulose. If the paper contained filler, determine the amount retained in the alpha-cellulose residue by igniting the residue and weighing the ash. The ignition is carried out in the manner described in the method of the Technical Association of the Pulp and Paper Industry for the quantitative determination of filler in paper.[9] Subtract the weight of the ash from the weight of the alpha-cellulose residue. The alpha cellulose is reported as the percentage of the corrected weight of the sample.

4. DISCUSSION OF THE METHOD

In common with all other test methods, the value of a method for determining the alpha-cellulose content of a material depends upon the accuracy and reproducibility of the measurements. Also, because of the use of the determination as a control test in several industries where a large number of samples must be analyzed, the analysis should be as simple and rapid as possible.

The accuracy of the method is difficult to determine because of the empirical and arbitrary definition of alpha cellulose. As was stated before, alpha cellulose is that part of cellulosic materials which resists the action of mercerizing caustic under definite conditions for a specified time. With a definition such as this the only criterion

[9] See footnote 3, p. 606.

of accuracy appears to be reproducibility. If the conditions specified in the definition are fulfilled in every detail and the results of an analysis can be duplicated, those results are, by definition, the accurate value of the alpha-cellulose content of the material. Thus, providing the details of the procedure are followed, the value of the method is determined by the reproducibility of the results. It may be seen from Table 1 that consistent results are obtained by the use of this method. Two analysts were able to duplicate their own and each other's results satisfactorily on a wide variety of papers. These papers were representative of several of the more common papermaking fibers. Some were sized with rosin, some with both glue and rosin, while others were unsized. Sample 6 contained 8 per cent of clay filler. Sample 1, an unsized paper made in the bureau mill from new unbleached cotton rags, which were a quite pure form of cellulose, had an alpha-cellulose content commensurate with its purity.

TABLE 1.—*Accuracy and reproducibility of the alpha-cellulose method*

Sample No.	Fiber composition	Sizing material	Analyst No. 1			Analyst No. 2			Difference between analysts
			Alpha cellulose	Average	Difference	Alpha cellulose	Average	Difference	
			Per cent	*Per cent*	*Per cent*	*Per cent*	*Per cent*	*Per cent*	*Per cent*
1	100 rag	Unsized	98.26 98.17	98.21	0.09	97.97 98.21	98.09	0.24	0.12
2	do	Rosin and glue	89.15 89.23	89.19	.08	89.46 89.23	89.34	.23	.15
3	100 purified wood fiber.	Unsized	91.65 91.82	91.74	.17	92.20 92.05	92.12	.15	.38
4	do	Rosin and glue	88.14 88.43	88.29	.29	88.34 88.57	88.45	.23	.16
5	100 sulphite	Rosin	80.21 80.23	80.22	.02	79.87 80.14	80.00	.27	.22
[1] 6	40 sulphite; 60 soda	do	65.33 65.30	65.32	.03	66.03 66.06	66.04	.03	.72
	Average				.11			.19	.20

[1] This paper contained clay filler.

The method is quite rapid. Two determinations on a given sample may be made in parallel. The mercerizing solution may be added to the next two samples during the 5-minute immersion of the first two in acetic acid. This procedure may be repeated, thus completing two determinations about every 45 minutes, exclusive of the time required for the weighing and drying operations. The method is quite simple, but close attention to detail is required throughout the analysis. This is especially true of the control of the temperature.

Several details of the method were investigated. One of these was the effect of mechanical grinding upon the value obtained for the alpha-cellulose content. The data in Table 2 show that the determined value of the alpha-cellulose content of a paper is dependent upon the form in which the paper is analyzed, ½-inch squares giving a higher value than is obtained when the paper is disintegrated. This difference is found in all papers, but it is not constant for all, being less for the softer papers. Providing the sample is disintegrated without heating, this difference may be due to the difference in the amount of surface exposed in the two cases. When the paper is analyzed in the ground form the measured value of the alpha-cellulose content may be

FIGURE 3.—*Fibers from unground rag bond paper.* × *100*

FIGURE 4.—*Fibers from rag bond paper after being ground in paper disintegrator.* × *100*

FIGURE 5.—*Fibers from unground sulphite bond paper.* × *100*

UNIV. OF MICH.

FIGURE 6.—*Fibers from sulphite bond paper after being ground in paper disintegrator.* × *100*

low because of reduced particle size and consequent increased rate of solution in the alkali; and when the squares are used, the measured value may be high because of incomplete reaction with the alkali. Photomicrographs of rag and wood fibers, after being subjected to the action of the grinder, showed that the fibers were well separated from one another, but that there was no excessive crushing and breaking of the fibers. (See figs. 3, 4, 5, and 6). On the other hand, the data given in Table 2 show that the incomplete reaction of the alkali with the sample in the form of cut squares is the cause of the difference.

If incomplete reaction between the cellulose and alkali were the cause, the difference between the measured alpha-cellulose contents of samples in the form of squares and in the ground form should increase as the hardness of the paper increases. This point was investigated by making by hand papers of varying degrees of hardness from three kinds of pulps. The beating process results in the formation of a gelatinous form of the cellulose material which, when dried, imparts to the finished paper such properties as resistance to liquids, increased density, smoother texture, and other properties usually associated with hardness in paper. As continued beating results in greater hardness, varying the length of the beating period is a convenient method of obtaining papers of different degrees of hardness from the same stock. The three kinds of fibers—kraft, sulphite, and highly purified wood fiber—were beaten in a 2-pound beater until they were well hydrated. Samples were removed from the beater at four different intervals—before any appreciable hydration had taken place, twice during the beating, and at the end of the beating period—and made into hand sheets on a sheet mold.[10] Thus papers of varying degrees of hardness were obtained from each kind of fiber, the hardness increasing with the time of beating. Each set was divided into two lots, one lot being cut into one-half inch squares and the other being mechanically disintegrated. An alpha-cellulose determination was then made on all of the sets of hand sheets in the two forms The results are given in Table 2.

TABLE 2.—*Effect of the hardness and the form of the paper on the alpha-cellulose determination*

Sample[a]	Time of beating	Alpha-cellulose content		
		½-inch squares	Disintegrated	Difference
Kraft sulphate wood fiber:	*Hours*	*Per cent*	*Per cent*	*Per cent*
A	0	89.13	87.66	1.47
B	2¼	89.35	87.66	1.89
C	4¼	89.80	87.39	2.41
D	7¼	89.57	87.20	2.37
Sulphite wood fiber:				
A	0	84.26	81.80	2.46
B	2¼	86.08	80.39	5.69
C	4¼	87.99	80.19	7.80
D	6¼	88.77	80.21	8.56
Highly purified wood fiber:				
A	0	93.71	91.38	2.33
B	2½	94.39	90.70	3.69
C	5	94.81	90.75	4.06
D	7½	95.25	90.67	4.58

[a] The sample designations of A, B. C, and D refer to the same stock beaten different lengths of time as indicated.

[10] M. B. Shaw, G. W. Bicking, and L. W. Snyder. The Preparation of Fiber Test Sheets, B. S. Jour. Research, 5, (RP 190), pp. 105–114; July, 1930.

These results show that as the hardness of the paper increases the difference between the values obtained as the alpha-celulose contents of the two forms of the sample increases. The measured value of the alpha-cellulose content of the paper in the ground form changes very little as the hardness of the paper increases. This change is toward a decrease of the value of the alpha-cellulose content, and probably results from chemical changes in the fiber during the beating process. On the other hand, the value obtained for the alpha-cellulose content of the paper in the form of squares increases to a marked extent as the paper increases in hardness. This large increase could hardly be ascribed to any other cause than incomplete reaction of the reagents with the paper. Inasmuch as the fibers of most papers are hydrated to some extent, and as the hardness and resistance to liquids are further increased by engine and surface sizing, these data show that papers must be reduced to a fibrous condition by some such means as grinding to insure maximum reaction in the alpha-cellulose determination.

A grinder similar to the one described under "Preparation of the Sample" is recommended. However, there are several forms of grinders in use, and any of them which will reduce the paper to a fibrous condition without the formation of lumps,without heating the paper, and without excessively bruising and crushing the fibers should be satisfactory.

The solubility of the nainsook filter cloth in the alkali was investigated. In the alpha-cellulose determination the 100 ml of 17.5 per cent sodium hydroxide used for the mercerization are diluted with 250 ml of water before the mixture is filtered. Thus the concentration of the strongest alkali coming in contact with the filter cloth is about 5.7 per cent. Alkali of this concentration is in contact with the filter cloth for a few minutes only. To find the change of the weight of the filter cloth during a determination, a piece of the nainsook of the size used in the determination was thoroughly washed with warm water and dried to constant weight at 105° C. It was then treated for 10 minutes with 6 per cent sodium hydroxide solution at 20° C. The cloth and alkali were thrown on a Büchner funnel, and the cloth washed with 750 ml of water at 20° C., then allowed to soak in 25 per cent acetic acid for five minutes, and finally washed with 1 liter of boiling distilled water. The cloth was then dried in an oven at 105° C. to constant weight. The original weight of the cloth, the weight after this treatment, and the difference between the weights are given in Table 3. The change in weight is the solubility of the cloth under these conditions. A and B refer to two different samples of nainsook. The solubility of B is higher than that of A, showing that different samples vary. For this reason it is recommended that the cloth be analyzed, as outlined here, before it is used, and that a cloth having a solubility approximately that of A be selected. If a cloth such as A were used an error of about 0.03 per cent, based upon a 4 gr. alpha-cellulose residue, would be introduced into the alpha-cellulose determination. An error of this magnitude may be neglected.

TABLE 3.—*Change of the weight of the filter cloth during the alpha-cellulose determination*

Sample[1] No.	Weight of the cloth before treatment	Weight of the cloth after treatment	Change of the weight of the cloth during the treatment	Sample[1] No.	Weight of the cloth before treatment	Weight of the cloth after treatment	Change of the weight of the cloth during the treatment
	g	*g*	*g*		*g*	*g*	*g*
A1	0.3174	0.3161	0.0013	B1	0.2806	0.2772	0.0034
A2	.3172	.3160	.0012	B2	.2742	.2706	.0036
A3	.3123	.3107	.0016	B3	.2778	.2751	.0027

[1] Samples A and B were two different pieces of nainsook. Three analyses of each were made.

To make the value obtained for the alpha-cellulose content independent of the amount of sizing and filling materials, it is necessary to correct the weight of the sample analyzed by subtracting the weights of these materials which the sample contains. The difference between the value of the alpha-cellulose content obtained when corrections are made for these materials and the value obtained when they are disregarded is given in the eighth column of Table 4. This difference is appreciable and shows that the basis of calculation of the alpha-cellulose content should be the weight of the fibrous material in the paper and not the weight of the paper itself. If the weight of the paper is used as the basis of calculation the measured alpha-cellulose content will vary as the amount of filler and sizing material in the paper varies. When the calculation of the alpha-cellulose content is made in this manner the assumption is made that the sizing materials are completely removed by the reagents. This assumption is not strictly valid, as the data in Table 4 show that small amounts of rosin and glue remain in the alpha-cellulose residues. The difference between the calculated value of the alpha-cellulose content when the weight of the residue is corrected for the sizing materials it contains and the value calculated when they are disregarded is given in the last column of Table 4. This difference is small, varies but slightly among the different samples, and for most purposes may be neglected. If a high degree of accuracy is desired, the residues may be analyzed for sizing materials and the corrections applied. However, the alpha-cellulose residues of loaded papers must always be analyzed for mineral matter and the weights of the residues corrected, owing to the large amount of loading material present in the residues.

TABLE 4.—*Data showing magnitude of corrections for sizing materials in papers and in alpha-cellulose residues from them*

Sample No.	Rosin in sample	Glue in sample	Rosin[1] in alpha-cellulose residues	Glue[1] in alpha-cellulose residues	Alpha-cellulose content				
					Not corrected for sizing materials in sample or residue	Corrected for sizing materials in sample but not in residue	Difference due to correction for sizing materials in sample	Corrected for sizing materials in sample and residue	Difference due to corrections for sizing in residue
	Per cent	*Per cent*	*Per cent*	*Per cent*	*Per cent*	*Per cent*	*Per cent*	*Per cent*	*Per cent*
2	2.50	3.68	0.11	0.16	83.78	89.34	5.56	89.06	0.28
4	1.20	2.19	.08	.16	85.44	88.45	3.01	88.19	.26
5	1.70	------	.10	------	78.63	80.00	1.37	79.68	.32

[1] Percentages of rosin and glue in the alpha-cellulose residues were calculated on the oven-dry weight of the sample before mercerization.

In 1929, the cellulose division of the American Chemical Society published a tentative standard method for the determination of alpha cellulose.[11] This method gives very satisfactory results when applied to pulps, but it is unsuitable for the analysis of papers because of the form in which the sample is used. This method comes from an authoritative source, and will probably be used to a large extent by cellulose investigators. There will, therefore, be many instances when it will be necessary to compare the results obtained by the use of the American Chemical Society method with those obtained by the use of a more specialized method, such as the one described in this article for the analysis of papers, and it is desirable that the two methods give results in close agreement. The greatest difference between the bureau procedure and that recommended by the American Chemical Society is the difference in the form of the sample. The American Chemical Society method specifies that the material be analyzed in the form of one-half-inch squares, whereas the bureau method specifies that the material be reduced to a fibrous condition before analysis for reasons previously discussed. Otherwise the differences between the two methods are slight. The ratio of alkali to sample in the two methods does not differ sufficiently to cause much difference in the results. The mercerization periods differ, being 30 minutes in the bureau procedure and 45 minutes in the American Chemical Society method. Most methods have a 30-minute mercerization period, and this time was chosen for the bureau procedure so that it would conform as far as practicable with the existing methods. In developing the American Chemical Society method the committee at first suggested a period of 30 minutes, but later changed this to 45 minutes in order to allow more time for the maceration of troublesome materials. Such difficulties are not encountered when the bureau procedure is used, as all materials macerate readily after being ground. The greater length of the mercerization period of the American Chemical Society method should not cause any considerable difference in the results obtained with it and those obtained with the bureau method, but the time required for a determination is somewhat longer. The methods of filtering used in the two procedures differ, but both are rapid and efficient and should cause no difference in the results. The method used in the bureau procedure, filtering through a fine cotton cloth on a Büchner funnel, is the more rapid of the two. The removal of the alkali is accomplished in much the same manner in the two methods. Both specify that water at 20° C. shall be used and that the mat shall soak in dilute acetic acid for five minutes. The volume and concentration of the acetic acid are greater in the bureau method, but this should cause no difference in the results. The method for the removal of the acetic acid used in the bureau procedure, washing with 1 liter of boiling water, is as efficient as the method used in the American Chemical Society procedure, washing with water at 20° C. until the filtrate is no longer acid to litmus, and is much less time consuming. A comparison of the results obtained with the two methods is given in Table 5. One variation was made in the American Chemical Society method in that the sample was ground before use. Otherwise the two methods

[11] Determination of Alpha-Cellulose, Report of Work of Subcommittee 2 of the Division of Cellulose Chemistry of the American Chemical Society, George J. Ritter, chairman, Ind. and Eng. Chem. Analytical Section, 1, p. 52; 1929.

were followed in detail. The data in Table 5 show that results obtained by the two methods agree very well when the determinations are made on ground samples. The bureau method, however, is somewhat more simple and more rapid than the American Chemical Society method.

TABLE 5.—*Comparison of the Bureau of Standards method with the tentative method of the American Chemical Society*

Sample No.	Bureau of Standards method			American Chemical Society method			Difference between methods
	Alpha cellulose	Average	Variation	Alpha cellulose	Average	Variation	
	Per cent	*Per cent*	*Per cent*	*Per cent*	*Per cent*	*Per cent*	*Per cent*
11	98.43 98.25	98.34	0.18	98.54 98.44	98.49	0.10	0.15
12	90.70 90.82	90.76	.12	90.51 90.74	90.63	.23	.13
13	90.71 90.77	90.74	.06	90.67 90.71	90.69	.04	.05
14	85.30 85.11	85.21	.19	84.83 84.98	84.91	.15	.30

The bureau procedure is equally applicable to the analysis of pulps, although designed primarily for paper testing. If pulps are to be analyzed the sample should be ground in the same manner as are papers, if the alpha-cellulose contents of pulps and papers made therefrom are to be compared.

IV. THE DETERMINATION OF THE COPPER NUMBER OF PAPER

1. DEFINITION OF THE COPPER NUMBER AND ORIGIN OF THE METHOD

The copper number is defined as the number of grams of copper in the cuprous oxide precipitated from an alkaline solution of cupric hydroxide under certain specified conditions by 100 g of cellulose material. The method for the determination of the reducing action of cellulose materials on alkaline copper solutions was originated by Schwalbe.[12] His method employed Fehling solution and the reduced copper was determined electrolytically after being dissolved in nitric acid. Later this method was modified to include a correction for the bivalent copper absorbed by the cellulose and to exclude as far as possible the correction necessary for the autoreduction of the Fehling solution.[13] To avoid the correction for the bivalent copper absorbed by the cellulose Hägglund,[14] and Knecht and Thompson [15] further modified Schwalbe's method by determining the reduced copper directly. The reduced copper is dissolved in an acidified solution of ferric alum and the copper determined by oxidizing the resulting ferrous solution back to the ferric state by means of standardized potassium permanganate. Staud and Gray [16] stated that the auto-

[12] Schwalbe, Ber., **40**, p. 4523; 1907.
[13] Schwalbe, Robinoff, and Schulze, in Robinoff's Dissertation, Darmstadt, 1912, and Schulze's Dissertation, Darmstadt, 1910.
[14] Hägglund, Papierfabrikant, **17**, p. 301; 1919.
[15] Knecht and Thompson, J. Soc. Dyers and Colorists, **36**, p. 255; 1920.
[16] Staud and Gray, Ind. and Eng. Chem., **17**, p. 741; 1925.

reduction of the Fehling solution can be reduced to a negligible amount, and that a minimum blank is obtainable if certain proportions of the copper sulphate and alkaline tartrate solutions are used. They also studied the effect of time and temperature of heating, and proposed a modification of the Schwalbe method which has found wide applicability. Later Scribner and Brode [17] developed modifications especially applicable to the determination of the copper number of paper using a modification of the Staud and Gray method for reducing the solution and the method of Gault and Mukerji [18] for determining the precipitated cuprous oxide. They also subjected the sample to mechanical grinding in order to obtain uniform reaction.

All of the methods described above employ Fehling solution as the copper-containing reagent, all are subject to the inaccuracy caused by the autoreduction of the solutions, and all involve great care and skill to reduce this to a minimum. In 1921 Braidy,[19] and Koehler and Marqueyrol [20] described a method in which the alkalinity of the solution is obtained by the use of a sodium carbonate-sodium bicarbonate solution instead of the alkaline tartrate. The lower alkalinity of this solution is designed to prevent the alteration of the cellulose and autoreduction of the solution. Clibbens and Geake [21] thoroughly investigated this method and found it to be very satisfactory in determining the extent of oxidation of cotton by acids and oxidizing agents. They recommended its use because of the almost negligible blank obtained on the reagents, because of its accuracy and the reproducibility of the results and because the solution is less alkaline than Fehling solution and is therefore less likely to alter the reducing substances in the cellulose.

After the work of Scribner and Brode in 1927, the Bureau of Standards employed their method for the determination of the copper number of papers. The method was used for some time, but considerable trouble was experienced with the autoreduction of the solution and in duplicating results. (See Table 6 and 7.) Various means were tried to avoid these difficulties, such as using carefully purified reagents, agitating the reaction mixture in various ways during the heating, and using carefully regulated temperature baths. Although some of these were advantageous there was still an appreciable blank determination and the desired accuracy could not always be obtained. It was finally decided to use the method of Braidy.

This method has been successfully adapted, with a few minor modifications, to the determination of the copper number of paper. The method is thoroughly described by the authors and by Clibbens and Geake,[22] but will be repeated here. The cuprous oxide is determined by the method of Gault and Mukerji.[23]

2. PREPARATION OF THE SOLUTIONS

The alkaline copper solution is made up in two parts, which are mixed just before use.

---

[17] Scribner and Brode, B. S. Tech. Papers, **22**, No. 354; 1927.
[18] Gault and Mukerji, Comp. rend., **178**, p. 711; 1924.
[19] Braidy, Rev. gén. Mat. Col., **25**, p. 35; 1921.
[20] Koehler and Marqueyrol, Mém. Poudres, **18**, p. 73; 1921.
[21] Clibbens and Geake, J. Textile Inst., **15**, p. T31; 1924.
[22] See footnote 21.
[23] See footnote 18.

	g
Solution A:	
Copper sulphate ($CuSO_4.5H_2O$)	100
Distilled water (make up to 1 liter).	
Solution B:	
Sodium bicarbonate	50
Sodium carbonate ($Na_2CO_3.10\ H_2O$)	350
Distilled water (make up to 1 liter).	

The reagents should be of cp grade and the solutions filtered before using.

For the determination of the cuprous oxide a solution of phosphomolybdic acid is used, which is made up as follows:

Sodium molybdate ($Na_2MoO_4.2H_2O$)	g	100
Phosphoric acid, 83 per cent	ml	75
Sulphuric acid, 95 per cent	ml	275
Distilled water	ml	1,750

3. PROCEDURE

Weigh accurately approximately 1.5 g of the paper sample, prepared as described in Section II, and place in a 125 ml Pyrex Erlenmeyer flask. Run 5.0 ml of solution A from a burette into 95 ml of solution B, shake well and bring the mixture to a boil. Pour the boiling solution over the sample and stir thoroughly. Stopper the flask with a loosely fitting glass bulb. A flat-topped glass stopper, the stem of which is slightly smaller than the neck of the flask, is suitable for this purpose. Place the flask in a steam bath or some other constant temperature bath at about 100° C. and allow it to remain there three hours. The contents of the flask should be shaken occasionally during this period. At the end of the heating period filter the contents of the flask through a good grade of filter paper having a low porosity,[24] using a Büchner funnel and suction. Wash with 100 ml of 5 per cent sodium carbonate solution and then with 250 ml of boiling distilled water. Transfer the fiber and filter paper to a 400 ml beaker, add 25 ml of the phosphomolybdic acid solution and macerate well with a flattened glass rod. Allow the acid to act for a few minutes, then add 100 ml of cold distilled water and filter again on a Büchner funnel with suction. Wash the fiber with distilled water until all of the blue color has been removed. To avoid an excessive volume of wash water, the washing is best accomplished by disconnecting the suction, adding a small volume of water and allowing the fiber to soak in it for a few minutes. This is then removed by means of the suction and the washing repeated with another small volume of water. Titrate the blue filtrate with $N/20$ potassium permanganate to a faint pink.

The copper number may be calculated from the following formula:

$$\text{Copper number} = \frac{6.357 \times (\text{total ml } KMnO_4 - \text{ml } KMnO_4 \text{ for blank}) \times N}{W}$$

where N is the normality of the potassium permanganate and W is the weight in grams of the sample used after corrections have been applied for noncellulosic constituents as described in Section II. The blank correction is the volume of $KMnO_4$ necessary to color the solution a faint pink.

[24] A Whatman No. 42 filter paper is suitable for this purpose.

4. DISCUSSION OF THE METHOD

A complete study of the method has been made by Clibbens and Geake. For this reason the work described in this article was limited to a study of the application of the Braidy method to paper analysis and a comparison of the Braidy method with a method employing Fehling solution as the copper containing reagent. The results of the comparison are given in Tables 6 and 7. These results show that if the duplicate analyses on one sample are made at different times the Braidy method has an average error only one-eighth as large as the method employing Fehling solution. If duplicate analyses are made at the same time the Braidy method has an average error one-third as large as the Fehling solution method. The ratios of the Braidy values to the Fehling solution values average approximately 1.3. This ratio has been given values from 1.15 to 1.5 by various investigators. Considering the wide variety of papers studied the ratios agree rather well, and as an approximation it may be said that:

Copper number (Braidy method) = 1.3 × copper number (Fehling solution method).

TABLE 6.—*Copper number of papers; duplicate analyses made at different times*

Sample No.	Fiber composition [1]	Copper number; Fehling solution method [2]				Copper number; Braidy method				Ratio B : F. S.
		I	II	Average	Deviation from average	I	II	Average	Deviation from average	
	Per cent				*Per cent*				*Per cent*	
Blank				0.47				0.03		
106–O	100 P. W. F.	1.11	1.08	1.10	1.4	1.30	1.32	1.31	0.8	1.2
106–H	100 P. W. F.	1.22	1.20	1.21	.8	1.65	1.67	1.66	.6	1.4
109–O	100 S	3.13	3.44	3.29	4.8	4.61	4.60	4.61	.1	1.4
109–H	100 S	3.75	3.94	3.85	2.5	5.08	5.12	5.10	.4	1.3
118–O	100 R	.68	.78	.73	6.9	.82	.81	.82	.6	1.1
119–O	100 R	.94	1.02	.98	4.1	1.23	1.25	1.24	.8	1.3
119–H	100 R	1.36	1.42	1.39	2.2	1.71	1.68	1.70	.9	1.2
120–O	100 R	.53	.62	.58	7.8	1.07	1.05	1.06	.9	1.8
120–H	100 R	.94	.94	.94	0	1.32	1.32	1.32	0	1.4
126–O	100 R	.85	.90	.88	2.9	1.13	1.12	1.13	.5	1.3
126–H	100 R	1.03	1.20	1.12	7.6	1.56	1.48	1.52	2.6	1.4
127–O	100 R	.86	.66	.76	[3] 13.1	.90	.90	.90	0	1.2
127–H	100 R	1.39	.93	1.16	[3] 19.8	1.66	1.70	1.68	1.2	1.4
Average					5.7				.7	1.3

[1] The fiber composition is denoted as follows: R = rag, P. W. F. = highly-purified wood fiber, S = sulphite wood fiber.
[2] The Fehling solution method was that described by Scribner and Brode. (See footnote 17, p. 614.)
[3] Despite the unusually wide deviations it was decided to include these results in the average.

TABLE 7.—*Copper number of papers; duplicate analyses made at the same time*

Sample No.	Fiber composition [1]	Copper number; Fehling solution method [2]				Copper number; Braidy method				Ratio B : F. S.
		I	II	Average	Deviation from average	I	II	Average	Deviation from average	
	Per cent				*Per cent*				*Per cent*	
1-O	100 R	1.77	1.81	1.79	1.1	2.55	2.52	2.53	0.6	1.4
2-O	50 S–50 So	2.52	2.25	2.38	5.7	3.24	3.23	3.23	.2	1.4
3-O	100 R	1.66	1.51	1.59	4.7	2.10	2.10	2.10	0	1.3
4-O	100 S	3.54	3.53	3.53	.2	4.56	4.37	4.47	2.1	1.3
5-O	100 S	2.27	2.19	2.23	1.8	3.02	2.91	2.96	1.9	1.3
6-O	50 R–50 So	1.09	1.12	1.11	1.4	2.31	2.31	2.31	0	2.1
7-O	100 R	1.55	1.40	1.47	5.1	1.79	1.81	1.80	.6	1.2
8-O	100 R	1.11	1.13	1.12	.9	1.41	1.39	1.40	.7	1.3
11-O	40 S–60 So	4.04	3.83	3.93	2.6	4.66	4.75	4.70	.9	1.2
12-O	100 R	3.53	3.56	3.54	.4	4.38	4.30	4.34	.9	1.2
13-O	100 R	4.32	4.24	4.28	.9	5.61	5.70	5.65	.8	1.3
14-O	100 R	2.19	2.08	2.13	2.6	2.54	2.55	2.55	.2	1.2
Average					2.3				.7	1.3

[1] The fiber composition is denoted as follows: R=rag; S=sulphite wood fiber; So=soda wood fiber
[2] The Fehling solution method was that described by Scribner and Brode. (See footnote 17, p. 614.)

The results obtained on the papers tested showed no relation between the type of fiber and the value of this ratio.

Three modifications of the Braidy method, as described by Clibbens and Geake, were made so that the method would be more applicable to paper analysis. The form of the sample was not specified by these investigators, doubtlessly because they were working with raw cotton which may be analyzed in its natural form. A specification for the form in which the sample must be used has been included in the present procedure. A second modification is a change of the weight of the sample from 2.5 to 1.5 g. The third modification is the use of phosphomolybdic acid instead of ferric alum for the determination of the cuprous oxide.

As was the case in the alpha-cellulose determination the greatest departure from the usual methods is the disintegration of the sample. Such a procedure appears to be necessary in the copper number determination for the same reason that it is necessary in the alpha-cellulose determination; that is, to insure complete reaction. The copper numbers of papers in the form of squares are usually lower than those obtained when the paper is disintegrated, although this is not always the case. Jonas [25] recommends the use of beaten cellulose. Other investigators recommend the squares. The copper number depends upon the number of reducing groups in the material and the completeness of the reaction between these groups and the reagents. Therefore, the method of preparation of the sample should be immaterial if it does not alter the number of reducing groups, and if it produces a form of the sample which will insure complete reaction. Grinding the sample as described in Section II reduces the material to such a condition that it can all be acted upon by the reagents, and if the grinding is done without heating the material the number of reducing groups should remain unaltered. Also, the precipitated

[25] Jonas, Z. angew. Chem., 41, pp. 960-961; 1928. Abstracted in The Paper Makers' Monthly J., 11, Nov. 15, 1928.

cuprous oxide is much more easily removed from a disintegrated sample than it is from hard, compact squares.

The Braidy method, as described by Clibbens and Geake, uses 2.5 g of sample, but in the method described here for the analysis of paper the weight of the sample is changed to 1.5 g. This is because there is insufficient copper in the volume of solutions used to account for all of the reducing power of some papers when the weight of the sample is 2.5 g. Clibbens and Geake showed that there was a slight increase in copper number as the weight of the sample was increased. However, as the 2.5 g sample is an arbitrary weight another arbitrary weight was used which would give the desired range for the method. This is suggested by Clibbens and Geake.

The determination of the cuprous oxide by means of phosphomolybdic acid is used because of the assurance of complete washing by the removal of all of the blue color and because of the very definite end point when the blue solution is titrated with potassium permanganate. The blue color changes from dark blue, to green, to colorless and finally to pink as the potassium permanganate is added. Ferric alum is equally good as an oxidizing agent for the cuprous oxide, but we believe the phosphomolybdic acid is easier to work with. The two give practically the same results, as is shown in Table 8.

TABLE 8.—*Comparison of methods for determining the cuprous oxide in the copper number determination*

Sample No.	Copper number	
	Phosphomolybdic acid	Ferric alum
Blank	0.03	0.12
1	.31	.30
2	.37	.38
3	3.75	3.77

A variation of the temperature at which the reduced phosphomolybdic acid is titrated between 10° and 40° C. has no effect on the results. Cuprous oxide was dissolved in 125 ml of the phosphomolybdic acid solution and the solution made up to 250 ml with water in a volumetric flask. Fifty ml portions of this solution were made up to 300 ml with water of different temperatures and titrated with potassium permanganate. The results are given in Table 9.

TABLE 9.—*Effect of temperature on the titration in the copper number determination*

Temperature of solution titrated (° C.)	Titre in ml $KMnO_4$
10	10.34
27	10.36
40	10.32

Clibbens and Geake studied the effect of small changes of the temperature of the reaction upon the copper number. They found that a difference of 1.5° C. caused a difference of 5 to 10 per cent in

the copper number. For this reason it is important to control the temperature of the constant temperature bath very carefully. A bath of steam or boiling water is the usual form of constant temperature bath, but the temperature of such a bath varies with the atmospheric pressure, causing a variation in the copper number. For accurate work or when results obtained at different times must be compared, a bath which is not subject to these variations, such as an oil bath with thermostatic control capable of maintaining a temperature constant within $\pm 0.1°$ C., should be used.

If pure reagents are used no couprous oxide will be precipitated from them when they are heated for three hours at the temperature of the steam bath. This is clearly shown by the fact that no blue color is formed when reagents treated in this manner are filtered and phosphomolybdic acid is added to the filter paper. However, if the phosphomolybdic added to the filter paper is washed out and filtered as is done when copper numbers are being determined, the resulting filtrate will require about 0.15 ml of $N/20$ potassium permanganate to color it a faint pink. This volume of potassium permanganate accounts for the blank correction in the formula given in Section IV, part 3.

V. CONCLUSION

The methods described in this article for the determination of the alpha-cellulose content and copper number of paper are the methods now being used at the Bureau of Standards. It is not claimed that they are new, but rather that they are further developments of existing methods designed to make them more suitable for paper testing. While it is recognized that several steps in the procedures might be further investigated to advantage, the methods described herein give results which can be readily duplicated, and they are less time consuming than the methods formerly used. Grinding the sample, as recommended herein, is particularly important when analyzing paper.

WASHINGTON, January 27, 1931.

THE STRUCTURE OF THE ARC SPECTRUM OF ZIRCONIUM

By C. C. Kiess and Harriet K. Kiess

ABSTRACT

Nearly 1,600 lines have been measured in the arc spectrum of zirconium between 2,085 A in the ultra-violet and 9,300 A in the infra-red. Approximately 80 per cent of these lines, which includes all but 7 for which temperature classes have been determined, have been classified as combinations between terms of the singlet, triplet, and quintet systems. The terms, without exception, are those required by Hund's theory, and many of them have been confirmed by Zeeman effect observations. Many pairs of terms of nearly the same value, with the same inner quantum number, and arising from the same electron configuration, mutually perturb one another with the result that lines originating in them exhibit abnormal intensities and Zeeman effects. The lowest term of the spectrum, a^3F, and the lowest term of the quintet system, a^5F, both form Rydberg series with higher terms, from which the distance separating the ground states of Zr I and Zr II proves to be 56,077 cm^{-1}, giving an ionization potential of 6.92 volts for the neutral Zr atom. The resonance lines are given by the combination $a^3F-z^5G°$, whereas the raies ultimes are given by $a^3F-z^3G°$. More than 200 Zr lines have been identified with dark lines in the solar spectrum, of which nearly half represent term combinations which do not appear in emission spectra observed in the laboratory.

CONTENTS

	Page
I. Introduction	621
II. Experimental	622
1. Wave lengths and intensities	622
2. Zeeman effects	623
III. Structure of the arc spectrum	623
1. The term systems	623
2. The Zeeman effects	660
3. The intensities	662
4. Interpretation of the observed terms	664
5. Series and ionization potential	667
IV. Zirconium in the sun	669
V. Conclusion and acknowledgments	671

I. INTRODUCTION

For more than a decade the spectra of zirconium, as emitted by arcs and condensed spark discharges, have been under investigation at the National Bureau of Standards not only to obtain as accurate a description of them as possible, but also for the purpose of finding the series relationships underlying their structure. Various steps in the completion of this problem have been described in three earlier papers, of which the first,[1] by one of us (C. C. K.), gives tables of wave lengths observed in the arc and spark spectra between 9,300 A and 2,100 A; the second, by Kiess and Lang,[2] describes the structure of Zr III and Zr IV; and the third,[3] by the present writers, presents

[1] B. S. Sci. Papers, No. 548, **22**, p. 47; 1927.
[2] B. S. Jour. Research (RP. 202), **5**, p. 305; 1930.
[3] B. S. Jour. Research (RP. 255), **5**, p. 1205; 1930.

an analysis of the first spark spectrum, Zr II. In this paper we present a similar analysis of the arc spectrum, Zr I.

The work on both Zr I and Zr II was carried on at the same time, and our earliest efforts at disentangling these spectra centered about the groups of strong lines in the ultra-violet and infra-red. From these we detected the wave-number differences which are characteristic of the low [4] F term of Zr II and the low [5] F term of Zr I. However, as stated in our paper on Zr II, we laid aside the Zr problem while we endeavored to work out the structure of the titanium spectrum in which we sought a small scale pattern of the structure to be expected in Zr. That our expectation in this respect was justified has been verified by our subsequent progress with the Zr spectra; for we have, indeed, found that the spectral structures of Zr closely parallel those which our own [4] and the more complete investigation of Russell [5] have revealed in Ti.

When we resumed our work on the Zr spectra we had acquired from Dr. A. S. King, of the Mount Wilson Observatory, a set of plates copied from his furnace spectra of Zr, supplemented later with an advance copy of the temperature classifications of the Zr lines made by him and Miss Carter.[6] And from the late Prof. B. E. Moore, of the Brace Laboratory, University of Nebraska, we had obtained the films on which he had recorded the Zeeman effect of Zr out to 7,000 A in the red. With these aids we were able to identify most of the stronger lines of Zr I as members of the quintet and triplet systems.

II. EXPERIMENTAL

1. WAVE LENGTHS AND INTENSITIES

When the Zr wave-length tables, presented in the first paper referred to above, were published in 1927, it was decided to terminate the list of arc lines at approximately 4,900 A because it seemed unnecessary to duplicate Vahle's [7] excellent description of the spectrum from this point onward to the ultra-violet. However, we found it desirable to have for inspection a map of the spectrum covering the range of the published wave lengths. New observations of the arc spectrum have, therefore, been made at the National Bureau of Standards with both the concave grating and the Hilger E_1 quartz prism spectrographs. The plates secured with the prism spectrograph cover the region from 2,000 to 3,050 A. The first order of the grating, with a dispersion of 3.7 A per mm. was used for the region from 2,200 to 2,900 A. For the region 2,900 to 4,900 A the second order of the grating was employed giving a dispersion of 1.8 A per mm. At least two plates of each region were secured. The material used as electrodes in the arcs was metallic Zr obtained from three different sources. Although these samples are of high purity from the chemical point of view yet they were found to contain traces of other elements, of which the more conspicuous are Fe, Ti, and Si. Each of them contains traces of Hf also; and, in addition, the sample used for the ultra-violet observations with the prism spectrograph contains traces of Ni, Cb, Al, Pb, and Sn.

[4] J. Opt. Soc. Am. & Rev. Sci. Inst., **8**, p. 607; 1924.
[5] Astrophys. J., **66**, pp. 283 and 347; 1927.
[6] Astrophys. J., **65**, p. 86; 1927.
[7] Zeit. für Wiss. Phot., **18**, p. 84; 1918.

Most of these newer spectrograms have been measured for wave-length determinations and intensity estimates, since it was noted that many of Vahle's faintest lines appear on our plates with increased strength. The wave lengths and intensities which appear in Table 3, therefore, are derived entirely from measurements made at the National Bureau of Standards. The compilation of these wave lengths afforded opportunity to revise the earlier tabulation of the spectrum in the range from 4,900 to 9,300 A and, accordingly, in the list as presented in this paper, a few lines have been added, but others have been omitted as not belonging to Zr I. We believe that the wave lengths as given in Table 3 are characteristic of the arc spectrum of zirconium, but the possibility of eliminating other lines from the list, especially in the ultra-violet where most of the unclassified lines of Zr I occur, is recognized. At the present time, however, it is not possible to make thorough comparisons with other elements owing to the inadequate descriptions of their spectra.

2. ZEEMAN EFFECTS

When Landé's quantum theoretical interpretation of the anomalous Zeeman effect [8] was published we found Moore's [9] observations of Zr of great service not only in confirming the classifications of Zr I lines we had already made, but in leading to the classification of additional lines. However, only a few of Moore's observations referred to lines of wave length longer than 4,900 A. When his attention was directed to the fact that the arc spectrum of Zr contains many strong lines in the red and near infra-red he generously offered, as stated above, to secure additional observations for our investigation with the equipment of the Brace Laboratory. These observations and the results obtained from them have been described in our paper on Zr II cited above, and to which the reader is referred for the details. Here also will be found a description of our preliminary observations of the Zeeman effect of Zr obtained with the magnet and spectrographs at the National Bureau of Standards.

III. STRUCTURE OF THE ARC SPECTRUM

1. THE TERM SYSTEMS

The terms on which the arc spectrum of Zr is built belong to the singlet, triplet, and quintet systems. Of these, the quintet system is simplest, having as its lowest term a^5F, with the characteristic $\Delta\nu$'s 348.4, 291.5, 225.7, 152.9. It was these wave-number differences that were found first, separating the strong infra-red lines in the group lying between 7,849 and 8,498 A, and also those in the blue-green group containing the lines which de Gramont [10] has described as specially sensitive for visual spectrochemical analysis. After the stronger lines, which were linked by these $\Delta\nu$'s had been assigned to multiplets, several fragmentary groups remained which were suspected as intersystem combinations with triplet terms. This view proved to be correct, and led to the identification of the low and metastable terms of the triplet system. The triplet system

[8] Zeit. für Physik, **15**, p. 189; 1923.
[9] Astrophys. J., **28**, p. 15; 1908.
[10] Compt. Rend., **166**, p. 367; 1918.

is by far the most complex and contains more observed terms than the singlet and quintet systems combined. Although the singlet system is much less complex than the triplet system, yet it proved to be the most difficult to unravel owing to the lack of term combinations with distinctive wave-number differences and the uniform character of the Zeeman effects.

The terms which have been established for Zr I are presented in Tables 1 and 2. The relative positions of these terms are shown in Figures 1, 2, and 3, the black dots representing the even terms of Table 1 and the open circles the odd terms of Table 2. The combinations between the terms, which are usually shown in diagrams of this kind, are omitted because of the confusion that would result

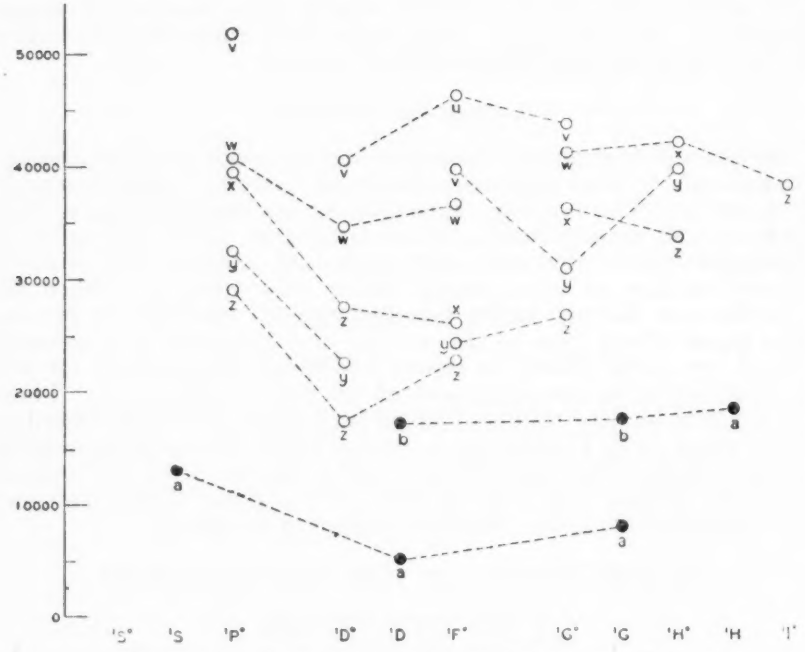

FIGURE 1.—*Term diagram of the singlet system of Zr I*

from drawing in so many lines. The visual representation of the term combinations is supplied to some extent, however, by Table 4, which contains the key numbers of the classified lines of Table 3 and shows at a glance all the combinations which occur. It is of interest to note that there are about 20 combinations between terms of the singlet and quintet systems. An explanation of their appearance in the spectrum is offered in a subsequent paragraph. The symbols used in defining the terms are those proposed in the report of Russell, Shenstone, and Turner. [11]

All the quintet terms and most of those of the triplet system are regular. The triplet terms that depart from regularity show only partial inversion. The most conspicuous of these is a^3P, of which

[11] Phys. Rev., **33,** p. 900; 1929.

the component a^3P_2 lies 10.7 cm^{-1} below a^3P_0. It exhibits a close affinity with the lowest term of the singlet system, a^1D_2, the mean of their term values being very nearly that which a^3P_2 would have if it occupied its normal position as determined by the interval rule. These two terms are almost identical in their behavior, with the result that many combinations into which they enter show abnormal intensities and Zeeman effects. The properties of these terms in the magnetic field will be discussed in a subsequent paragraph. Other terms which are partially inverted are c^3P, $z^3I°$, $x^3H°$, $y^3F°$, $t^3D°$, $z^3P°$, and $y^3P°$. With these may be included such terms as a^3G, $x^3G°$, $v^3G°$, $w^3F°$, $v^3D°$, etc., which show marked deviations from the interval

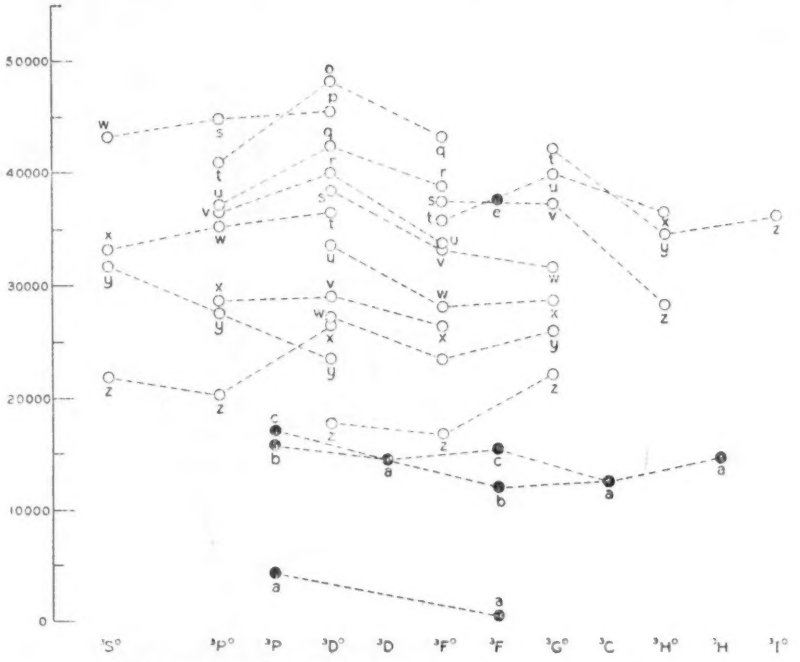

FIGURE 2.—*Term diagram of the triplet system of Zr I*

rule. In fact, very few of the complex terms of Zr I have separations which follow the interval rule closely.

Of the nearly 1,600 lines recorded in Table 3 approximately 80 per cent have been classified as combinations between the terms of Tables 1 and 2. Each classified line is provided with a key number giving the number of the multiplet of which it is a member. For comparison with our intensity estimates we give those of King and Miss Carter, and also their temperature classifications. Inspection of the table shows that all but seven of the lines observed in the furnace spectra have been classified. The lowest term, a^3F, and the two related terms, a^3P and a^1D, each enter into combination with about 60 of the 80 odd terms comprising the middle group, while a^5F combines with 40 of them. These combinations account for nearly all of the strong arc lines of Temperature Classes I and II.

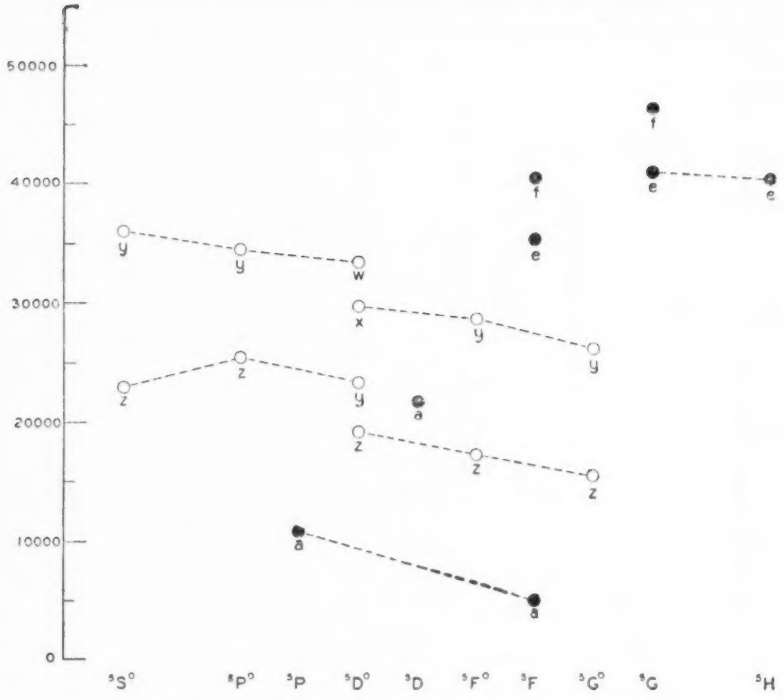

FIGURE 3.—*Term diagram of the quintet system of Zr I*

TABLE 1.—*Even terms of Zr I*

Term	*a*	*b*	*c*	*e*	*f*
$^5H_7$				42,086.82	
				643.29	
$^5H_6$				41,443.53	
				806.48	
$^5H_5$				40,637.05	
				700.35	
$^5H_4$				39,936.70	
$^5H_3$				?	
$^5G_6$				41,940.86	47,698.29
				402.63	*563.79*
$^5G_5$				41,538.23	47,134.50
				358.93	*493.08*
$^5G_4$				41,179.30	46,641.42
				291.69	*446.27*
$^5G_3$				40,887.61	46,195.15
				226.96	*396.67*
$^5G_2$				40,660.65	45,798.48
$^5F_5$	5,888.93			36,360.20	41,068.00
	348.39			*499.37*	*218.80*
$^5F_4$	5,540.54			35,860.83	40,849.70
	291.47			*384.76*	*196.29*
$^5F_3$	5,249.07			35,476.07	40,653.41
	225.66			*265.77*	
$^5F_2$	5,023.41			35,210.30	?
	152.88			*163.35*	
$^5F_1$	4,870.53			35,046.95	?
$^5D_4$	22,398.00				
	252.69				
$^5D_3$	22,145.31				
	201.57				
$^5D_2$	21,943.74				
	142.53				
$^5D_1$	21,801.21				
	74.93				
$^5D_0$	21,726.28				
$^5P_3$	11,258.38				
	241.73				
$^5P_2$	11,016.65				
	131.29				
$^5P_1$	10,885.36				
$^3H_6$	15,119.66				
	131.15				
$^3H_5$	14,988.51				
	197.23				
$^3H_4$	14,791.28				
$^3G_5$	12,772.78				
	12.12				
$^3G_4$	12,760.66				
	257.22				
$^3G_3$	12,503.44				
$^3F_4$	1,240.84	12,342.37	15,699.86	38,101.09	
	670.43	*386.04*	*242.46*	*400.01*	
$^3F_3$	570.41	11,956.33	15,457.40	37,701.08	
	570.41	*315.61*	*310.92*	*241.48*	
$^3F_2$	0.00	11,640.72	15,146.48	37,459.60	
$^3D_3$	14,697.03				
	348.25				
$^3D_2$	14,348.78				
	225.77				
$^3D_1$	14,123.01				
$^3P_2$	4,186.11	15,932.10	17,142.72		
	−190.17		*82.90*		
$^3P_1$	4,376.28	?	17,059.82		
	179.43		*−261.70*		
$^3P_0$	4,196.85	?	17,321.52		
$^1H_5$	18,738.94				
$^1G_4$	8,057.30	17,752.73			
$^1F_3$	?				
$^1D_2$	5,101.68	17,228.42			
$^1P_1$	?				
$^1S_0$	13,141.76				

TABLE 2.—*Odd terms of Zr I*

Term	z	y	x	w	v	u	t	s	r	q	p	o
$^5G_6^0$	16,978.29	27,214.89										
	661.83	*449.23*										
$^5G_5^0$	16,316.96	26,765.66										
	596.60	*423.13*										
$^5G_4^0$	15,720.36	26,342.53										
	519.10	*370.82*										
$^5G_3^0$	15,201.26	25,971.71										
	417.78	*341.23*										
$^5G_2^0$	14,783.54	25,630.48										
$^5F_5^0$	18,276.92	29,535.48										
	444.19	*412.77*										
$^5F_4^0$	17,832.73	29,122.71										
	410.56	*304.69*										
$^5F_3^0$	17,422.17	28,818.02										
	362.56	*222.99*										
$^5F_2^0$	17,059.61	28,595.03										
	272.68	*148.11*										
$^5F_1^0$	16,786.93	28,446.92										
$^5D_4^0$	19,833.78	24,376.37	30,384.50	34,287.49								
	208.20	*487.34*	*297.17*	*376.40*								
$^5D_3^0$	19,625.58	23,889.03	30,087.33	33,912.09								
	201.74	*399.60*	*239.84*	*279.61*								
$^5D_2^0$	19,323.84	23,489.43	29,847.49	33,632.48								
	227.81	*243.10*	*170.35*	*187.61*								
$^5D_1^0$	19,096.53	23,246.33	29,677.14	33,444.87								
	120.17	*124.04*	*89.07*	*95.31*								
$^5D_0^0$	18,976.36	23,122.29	29,588.07	33,349.56								
$^3P_2^0$	25,898.16	35,090.90										
	252.19	*329.38*										
$^3P_1^0$	25,645.97	34,761.52										
	156.10	*144.52*										
$^3P_0^0$	25,489.87	34,617.00										
$^4S_2^0$	23,085.06	35,990.21										
$^3I_7^0$	36,152.85											
	−20.18											
$^3I_6^0$	36,173.03											
	391.26											
$^3I_5^0$	35,781.67											

$^{2}H^{\frac{7}{2}}$	28,608.62	35,135.07	36,840.59									
	396.80	*429.17*	*243.11*									
$^{2}H^{\frac{5}{2}}$	28,211.82	34,705.90	36,597.48									
	305.54	*255.30*	*−10.93*									
$^{3}H^{\frac{4}{2}}$	27,908.28	34,450.60	36,608.41									
$^{2}G^{\frac{9}{2}}$	22,563.89	26,433.72	29,001.65	32,152.16	37,422.36	40,178.44	42,834.96					
	419.81	*422.17*	*251.85*	*457.64*	*192.82*	*244.30*	*562.55*					
$^{2}G^{\frac{7}{2}}$	22,144.08	26,011.55	28,749.80	31,694.52	37,229.54	39,934.14	42,272.41					
	294.75	*281.59*	*345.54*	*367.71*	*287.89*	*544.85*	*169.85*					
$^{2}G^{\frac{5}{2}}$	21,849.33	25,729.96	28,404.26	31,326.81	36,941.65	39,389.29	42,102.56					
$^{2}F^{\frac{9}{2}}$	17,556.26	24,006.30	26,938.42	28,528.36	33,688.23	33,559.34	36,001.35	37,920.96	39,174.44	43,276.00		
	712.33	*439.18*	*494.54*	*370.94*	*496.37*	*138.87*	*195.72*	*452.09*	*292.64*	*7.76*		
$^{2}F^{\frac{7}{2}}$	16,843.93	23,567.12	26,443.88	28,157.42	33,191.86	33,420.47	35,805.63	37,468.87	38,881.80	43,268.24		
	547.42	*−30.35*	*382.18*	*281.26*	*219.56*	*256.49*	*291.10*	*345.45*	*315.80*	*562.24*		
$^{2}F^{\frac{5}{2}}$	16,296.51	23,597.47	26,061.70	27,876.16	32,972.30	33,163.98	35,514.53	37,123.42	38,566.00	42,706.00		
$^{2}D^{\frac{5}{2}}$	18,243.56	23,660.97	27,111.16	27,482.26	29,274.82	34,239.82	36,220.45	38,435.88	40,346.35	42,799.20	45,710.29	48,713.44
	429.92	*341.11*	*553.95*	*360.30*	*216.98*	*475.70*	*−74.42*	*109.16*	*579.88*	*865.55*	*122.67*	*579.80*
$^{2}D^{\frac{3}{2}}$	17,813.64	23,319.86	26,557.21	27,121.96	29,057.84	33,764.12	36,294.87	38,326.72	39,766.47	42,433.65	45,587.62	48,133.64
	583.78	*300.94*	*403.08*	*219.51*	*257.33*	*277.30*	*169.71*	*55.91*		*136.85*	*182.52*	*368.08*
$^{2}D^{\frac{1}{2}}$	17,429.86	23,018.92	26,154.13	26,902.45	28,800.51	33,486.82	36,125.16	38,270.81	?	42,296.80	45,405.30	47,765.56
$^{2}P^{\frac{3}{2}}$	20,466.83	27,673.35	28,909.57	35,456.25	37,008.40	37,450.23	41,787.62	45,017.13				
	−52.57	*100.83*	*199.69*	*250.73*	*519.30*	*479.58*	*815.68*	*134.83*				
$^{2}P^{\frac{1}{2}}$	20,519.20	27,572.52	28,709.88	35,205.52	36,489.10	36,970.65	40,973.94	44,882.30				
	885.23	*−27.72*	*77.13*		*454.56*	*432.38*	*457.56*					
$^{2}P^{\frac{0}{2}}$	20,233.97	27,600.24	28,632.75	?	36,034.54	36,538.27	40,536.38	?				
$^{2}S^{\frac{1}{2}}$	21,974.18	31,850.77	33,113.80	43,182.96								
$^{1}I^{\frac{11}{2}}$	38,475.82											
$^{1}H^{\frac{9}{2}}$	33,839.20	39,855.22	42,309.29									
$^{1}G^{\frac{7}{2}}$	26,931.35	31,050.48	36,336.48	41,319.96								
$^{1}F^{\frac{5}{2}}$	22,862.02	24,387.52	26,226.97	36,759.90	39,803.73	46,328.16						
$^{1}D^{\frac{3}{2}}$	17,511.78	22,750.53	27,515.38	34,850.96	40,557.65							
$^{1}P^{\frac{1}{2}}$	28,999.46	32,722.80	39,704.10	40,931.60	51,899.40							
$^{1}S^{0}$	?											

TABLE 3.—*Wave lengths in the arc spectrum of Zr*

Key No.	λ I. A.	Intensities, temperature class, and notes		Wave No.	Term combinations	Observed Zeeman effects	Theoretical Zeeman effects
		B. S.	King				
1	9, 276. 94	1		10, 776. 46	a^5F_4–$z^5G^0_5$		
2	9, 139. 33	1		10, 938. 72	a^3H_4–$y^3G^0_5$		
3	9, 099. 90	0		10, 986. 12	a^3G_3–$y^5D^0_2$		
2	9, 069. 40	2		11, 023. 06	a^3H_5–$y^3G^0_4$		
1	9, 015. 13	5		11, 089. 43	a^5F_5–$z^5G^0_6$		
4	9, 011. 31	1		11, 094. 12	a^3G_3–$y^3F^0_2$		
5	8, 941. 74	1		11, 180. 45	a^3H_4–$y^3G^0_3$		
6	8, 930. 10	1		11, 195. 01	a^1D_2–$z^3F^0_2$		
7	8, 925. 04	1		11, 201. 36	a^3D_3–$z^5P^0_3$		
2	8, 910. 05	1		11, 220. 20	a^3H_4–$y^3G^0_4$		
8	8, 906. 33	1		11, 224. 89	b^3F_4–$y^3F^0_3$		
4	8, 899. 52	6		11, 233. 48	a^3G_5–$y^3F^0_4$		
	8, 894. 01	0		11, 240. 44			
9	8, 844. 50	0		11, 303. 36	a^5F_4–$z^3F^0_3$		
2	8, 836. 09	8		11, 314. 12	a^3H_6–$y^3G^0_5$		
5	8, 804. 98	3		11, 354. 06	a^3H_5–$y^5G^0_4$		
10	8, 786. 23	2		11, 378. 32	b^3F_2–$y^3D^0_1$		
11	8, 778. 48	0		11, 388. 37	c^3P_0–$x^3P^0_1$		
	8, 771. 02	0		11, 398. 05			
	8, 762. 93	1		11, 408. 58			
9	8, 749. 48	5		11, 426. 12	a^5F_1–$z^3F^0_2$		
12	8, 742. 11	1		11, 435. 75	a^3H_4–$x^1F^0_3$		
2	8, 734. 86	4		11, 445. 24	a^3H_5–$y^3G^0_5$		
13	8, 709. 24	1		11, 478. 91	c^3P_0–$z^3D^0_1$		
7 18	8, 656. 04	0		11, 549. 35	a^3D_2–$z^5P^0_3$ $y^3D^0_3$–c^5F_2		
5	8, 654. 59	0		11, 551. 39	a^3H_4–$y^5G^0_4$		
11	8, 642. 76	2		11, 567. 20	c^3P_2–$x^3P^0_1$		
	8, 641. 01	3		11, 569. 55			
11	8, 638. 51	1		11, 572. 90	c^3P_1–$x^3P^0_0$		
14	8, 627. 71	1		11, 587. 38	$y^5D^0_3$–c^5F_3		
3	8, 615. 66	1		11, 603. 58	a^3G_5–$y^5D^0_2$		
15	8, 614. 16	0		11, 605. 61	b^3F_2–$y^5D^0_1$		
8	8, 610. 24	2		11, 610. 89	b^3F_3–$y^3F^0_3$		
8	8, 587. 84	4		11, 641. 17	b^3F_3–$y^3F^0_2$		
17	8, 585. 90	0		11, 643. 81	a^5D_1–$w^5D^0_1$		
5	8, 584. 21	6		11, 646. 10	a^3H_6–$y^5G^0_5$		
11	8, 581. 22	1		11, 650. 16	c^3P_1–$x^3P^0_1$		
16	8, 579. 47	1		11, 652. 53	a^3H_4–$x^3F^0_3$		
13	8, 575. 69	1		11, 657. 67	c^3P_2–$b^3D^0_1$		
8	8, 571. 05	4		11, 663. 98	b^3F_4–$y^3F^0_4$		
9	8, 568. 54	4		11, 667. 40	a^5F_5–$z^3F^0_4$		
19	8, 558. 64	2		11, 680. 90	b^1D_2–$z^3P^0_2$		
	8, 554. 42	2		11, 686. 66			
	8, 536. 22	1		11, 711. 57			
20	8, 535. 13	1		11, 713. 07	a^3D_2–$x^3F^0_2$		
18	8, 524. 99	1		11, 727. 00	$y^3D^0_2$–c^5F_1		
13	8, 515. 06	3		11, 740. 68	c^3P_1–$z^3D^0_1$		
6	8, 513. 78	3		11, 742. 44	a^1D_2–$z^3F^0_3$		
20	8, 510. 38	1		11, 747. 13	a^3D_3–$x^3F^0_3$		
	8, 502. 77	2		11, 757. 65			
21	8, 498. 44	10		11, 763. 64	a^5F_2–$z^5F^0_1$		
11	8, 495. 98	4		11, 767. 04	c^3P_2–$z^3P^0_2$		
21	8, 464. 65	10		11, 810. 59	a^5F_3–$z^5F^0_2$		
9	8, 457. 50	4		11, 820. 58	a^5F_2–$z^3F^0_3$		
22	8, 453. 17	10		11, 826. 63	a^5P_3–$z^5S^0_2$		
23	8, 429. 14	0		11, 860. 35	a^3D_3–$x^3D^0_2$		
24	8, 416. 91	1		11, 877. 59	a^3D_2–$x^1F^0_3$		
21	8, 414. 00	7		11, 881. 69	a^5F_4–$z^5F^0_3$		
17	8, 408. 50	1		11, 889. 47	a^5D_4–$w^5D^0_4$		
13	8, 390. 18	2		11, 915. 43	c^3P_2–$b^3D^0_2$		
21	8, 389. 42	8		11, 916. 50	a^5F_1–$z^5F^0_1$		
25	8, 386. 70	3		11, 920. 37	a^3P_1–$z^3F^0_2$		
8	8, 382. 79	1		11, 925. 93	b^3F_2–$y^3F^0_2$		
21	8, 370. 21	10		11, 943. 85	a^5F_5–$z^5F^0_4$		
16	8, 365. 98	2		11, 949. 86	a^3H_5–$x^3F^0_4$		

TABLE 3.—*Wave lengths in the arc spectrum of Zr*—Continued

Key No.	λ I. A.	Intensities, temperature class, and notes		Wave No.	Term combinations	Observed Zeeman effects	Theoretical Zeeman effects
		B. S.	King				
8	8, 361. 17	2		11, 956. 77	b^3F_2–$y^3F_2^\circ$		
26	8, 360. 17	0		11, 958. 20	a^1D_2–$z^3F_2^\circ$		
14	8, 350. 45	0		11, 972. 12	$y^5D_3^\circ$–e^5F_4		
	8, 345. 99	0		11, 978. 52			
14	8, 342. 10	0		11, 984. 10	$y^5D_4^\circ$–e^5F_5		
13	8, 332. 44	6		11, 997. 99	c^3P_1–$v^3D_2^\circ$		
	8, 328. 54	1		12, 003. 61			
9	8, 320. 12	5		12, 015. 76	a^5F_4–$z^3F_4^\circ$		
10	8, 316. 97	1		12, 020. 31	b^3F_2–$y^3D_3^\circ$		
23	8, 309. 50	4		12, 031. 11	a^3D_1–$x^3D_1^\circ$		
21	8, 305. 94	15	8, III	12, 036. 27	a^5F_2–$z^5F_2^\circ$		
27	8, 299. 79	4		12, 045. 19	b^3F_4–$y^1F_3^\circ$		
8	8, 296. 54	2		12, 049. 91	b^3F_3–$y^3F_4^\circ$		
22	8, 283. 84	10		12, 068. 38	a^5P_2–$z^5S_2^\circ$		
13	8, 240. 36	8		12, 132. 06	c^3P_2–$v^3D_3^\circ$		
21	8, 212. 59	18	10, III	12, 173. 07	a^5F_3–$z^5F_3^\circ$		
21	8, 201. 73	10		12, 189. 20	a^5F_1–$z^5F_2^\circ$		
18	8, 194. 64	6	20, V	12, 199. 75	$y^3D_3^\circ$–e^5F_4		
22					a^5P_1–$z^5S_2^\circ$		
23	8, 188. 76	3		12, 208. 51	a^3D_2–$x^3D_2^\circ$		
28	8, 174. 63	1		12, 229. 61	a^5P_2–$y^5D_1^\circ$		
28	8, 169. 72	2		12, 236. 96	a^5P_1–$y^5D_0^\circ$		
29	8, 152. 59	4		12, 262. 67	a^5F_3–$z^1D_2^\circ$		
21	8, 133. 00	20	15, III	12, 292. 21	a^5F_4–$z^5F_4^\circ$		
30	8, 125. 84	1		12, 303. 04	a^5P_2–$y^3D_2^\circ$		
31	8, 120. 15	6		12, 311. 66	a^1H_5–$y^1G_4^\circ$		
26	8, 114. 29	4		12, 320. 55	a^1D_2–$z^3F_3^\circ$		
32	8, 109. 23	2		12, 328. 24	a^1D_2–$z^3D_1^\circ$		
	8, 107. 5υ	1		12, 330. 87			
28	8, 087. 79	2		12, 360. 92	a^5P_1–$y^5D_1^\circ$		
21	8, 070. 12	25	20, III	12, 387. 99	a^5F_5–$z^5F_5^\circ$		
21	8, 063. 10	10	3, V	12, 398. 77	a^5F_2–$z^5F_3^\circ$		
33	8, 058. 14	7		12, 406. 41	a^5F_3–$z^3D_3^\circ$		
34	8, 055. 73	5		12, 410. 12	a^1D_2–$z^1D_2^\circ$		
35	8, 055. 32	4		12, 410. 75	a^3P_1–$z^5F_1^\circ$		
23	8, 053. 08	4		12, 414. 20	a^3D_3–$x^3D_3^\circ$		
36	8, 046. 08	1		12, 425. 00	a^3D_3–$w^3D_3^\circ$		
23	8, 040. 12	2		12, 434. 21	a^3D_1–$x^3D_2^\circ$		
28	8, 015. 22	3		12, 472. 84	a^5P_3–$y^5D_2^\circ$		
29	8, 005. 28	5		12, 488. 33	a^5F_2–$z^1D_2^\circ$		
36	7, 963. 69	5		12, 553. 54	a^3D_2–$w^3D_1^\circ$		
33	7, 960. 01	7	2, V	12, 559. 35	a^5F_1–$z^3D_1^\circ$		
33	7, 956. 69	7	2, IV	12, 564. 59	a^5F_3–$z^3D_3^\circ$		
21	7, 944. 65	15	6, V	12, 583. 63	a^5F_3–$z^5F_4^\circ$		
35	7, 940. 46	5		12, 590. 27	a^3P_0–$z^5F_1^\circ$		
28	7, 931. 76	3		12, 604. 08	a^5P_1–$y^5D_2^\circ$		
37	7, 924. 17	3		12, 616. 15	a^3D_3–$y^5P_2^\circ$		
28	7, 915. 17	3		12, 630. 50	a^5P_2–$y^5D_3^\circ$		
29	7, 908. 46	6		12, 641. 21	a^5F_1–$z^1D_2^\circ$		
30	7, 906. 55	2		12, 644. 27	a^5P_2–$y^3D_3^\circ$		
25	7, 897. 98	5		12, 657. 99	a^3P_2–$z^3F_3^\circ$		
37	7, 888. 52	3		12, 673. 17	a^3D_2–$y^5P_1^\circ$		
35	7, 882. 15	6		12, 683. 41	a^3P_1–$z^5F_2^\circ$		
37	7, 876. 24	6		12, 692. 93	a^5D_4–$y^5P_3^\circ$		
33	7, 870. 00	12	4, III	12, 702. 99	a^5F_4–$z^3D_3^\circ$		
38	7, 868. 34	3		12, 705. 67	a^5D_3–$w^1D_2^\circ$		
39	7, 864. 37	3		12, 712. 08	a^5P_1–$y^3F_2^\circ$		
32					a^1D_2–$z^3D_2^\circ$		
21	7, 849. 38	15	5, III	12, 736. 35	a^5F_4–$z^5F_5^\circ$		
27	7, 842. 93	2		12, 746. 84	b^3F_2–$y^1F_3^\circ$		
23	7, 833. 36	2		12, 762. 41	a^3D_2–$x^3D_2^\circ$		
36	7, 826. 75	9	2, V	12, 773. 19	a^3D_2–$w^3D_2^\circ$		
36	7, 822. 96	8	2, V	12, 779. 37	a^3D_1–$w^3D_1^\circ$		
36	7, 819. 36	15	5, V	12, 785. 26	a^3D_3–$w^3D_3^\circ$		
33	7, 816. 31	5		12, 790. 25	a^5F_2–$z^3D_1^\circ$		

TABLE 3.—*Wave lengths in the arc spectrum of Zr*—Continued

Key No.	λ I. A.	Intensities, temperature class, and notes		Wave No.	Term combinations	Observed Zeeman effects	Theoretical Zeeman effects
		B. S.	King				
37	7,800.73	4		12,815.79	a^5D_1–$y^5P^\circ_1$		
37	7,799.51	2		12,817.80	a^5D_2–$y^5P^\circ_2$		
28	7,766.54	5		12,872.21	a^5P_2–$y^5D^\circ_3$		
35	7,765.67	4		12,873.65	a^3P_2–$z^3F^\circ_3$		
37	7,755.39	2		12,890.72	a^5D_0–$y^5P^\circ_1$		
38	7,745.43	2		12,907.29	a^5D_2–$w^1D^\circ_2$		
	7,744.05	2		12,909.59			
33	7,723.70	5		12,943.60	a^5F_1–$z^3D^\circ_2$		
37	7,722.48	4		12,945.65	a^5D_3–$y^5P^\circ_3$		
40	7,721.72	1		12,946.92	c^3F_3–$x^3G^\circ_4$		
41	7,708.38	6		12,969.33	a^3G_4–$y^3G^\circ_3$		
42	7,704.24	7		12,976.30	a^3D_3–$y^3P^\circ_2$		
33	7,693.45	2		12,994.50	a^5F_3–$z^3D^\circ_3$		
36	7,690.81	7	1, V	12,998.96	a^5D_1–$w^3D^\circ_2$		
40	7,660.75	1		13,049.97	c^3F_4–$x^3G^\circ_4$		
43	7,658.62	8	3, IV	13,053.60	a^3P_1–$z^3D^\circ_1$		
	7,654.40	2		13,060.79			
	7,650.50	1		13,067.45			
	7,646.71	2		13,073.93			
44	7,621.60	3		13,117.00	a^3H_4–$z^3H^\circ_4$		
28	7,621.16	7	1, V	13,117.76	a^5P_3–$y^5D^\circ_4$		
45	7,615.74	4		13,127.09	a^3G_3–$y^5G^\circ_2$		
46	7,614.48	2		13,129.27	a^5P_3–$y^1F^\circ_3$		
36	7,612.08	7		13,133.40	a^3D_2–$w^3D^\circ_3$		
47	7,610.89	5		13,135.45	a^3P_1–$z^1D^\circ_2$		
48	7,609.69	3		13,137.53	a^3G_4–$z^5P^\circ_3$		
32	7,607.19	15	8, III	13,141.85	a^1D_2–$z^3D^\circ_3$		
33	7,562.17	6		13,219.91	a^5F_2–$z^3D^\circ_3$		
44	7,560.31	4		13,223.33	a^3H_5–$z^3H^\circ_5$		
42	7,560.04	5		13,223.80	a^3D_2–$y^3P^\circ_1$		
41	7,558.47	9	2, V	13,226.55	a^3G_3–$y^3G^\circ_3$		
43	7,554.73	10	5, III	13,233.10	a^3P_0–$z^3D^\circ_1$		
49 / 35	7,552.99	5		13,236.15	$z^3S^\circ_1$–e^3F_2 / a^3P_2–$z^5F^\circ_3$		
41	7,551.50	10	2, V	13,238.76	a^3G_5–$y^3G^\circ_4$		
41	7,544.62	8	1, V	13,250.83	a^3G_4–$y^3G^\circ_4$		
40	7,540.65	8	1, V	13,257.82	c^3F_3–$x^3G^\circ_3$		
40	7,521.03	6		13,292.40	c^3F_3–$z^3G^\circ_4$		
	7,519.34	2		13,295.38			
50	7,517.97	6		13,297.81	b^1G_4–$y^1G^\circ_4$		
40	7,515.74	8	1, V	13,301.75	c^3F_4–$x^3G^\circ_5$		
	7,506.56	6		13,318.02			
42	7,502.91	6	1, V	13,324.49	a^3D_2–$y^3P^\circ_2$		
47	7,502.25	1		13,325.68	a^3P_2–$z^1D^\circ_2$		
51	7,479.61	8		13,366.00	a^3H_6–$w^3F^\circ_4$		
52	7,467.57	8	1, V?	13,387.56	b^3F_4–$y^3G^\circ_3$		
43	7,439.89	20	10, III	13,437.36	a^3P_1–$z^3D^\circ_2$		
42	7,433.12	6		13,449.60	a^3D_1–$y^3P^\circ_1$		
53	7,423.83	2		13,466.44	a^3G_4–$z^1F^\circ_3$		
45	7,422.77	6		13,468.35	a^3G_3–$y^5G^\circ_3$		
42	7,417.91	5		13,477.18	a^3D_1–$y^3P^\circ_0$		
	7,414.24	1		13,483.85			
44	7,411.42	4		13,488.98	a^3H_6–$z^3H^\circ_5$		
41	7,400.89	6	tr, V	13,508.17	a^3G_3–$y^3G^\circ_4$		
	7,399.33	4		13,511.02			
51	7,383.64	7	1, V	13,539.73	a^3H_5–$w^3F^\circ_4$		
	7,379.19	1		13,547.90			
42	7,377.85	1		13,550.35	a^3D_1–$y^3P^\circ_2$		
54	7,374.80	3		13,555.96	b^3F_4–$z^5P^\circ_3$		
55	7,373.51	6	1, V	13,558.33	a^3G_3–$x^3F^\circ_4$		
45	7,367.22	3		13,569.91	a^3G_3–$y^5G^\circ_3$		
45	7,360.66	2		13,582.01	a^3G_4–$y^5G^\circ_4$		
	7,358.60	1		13,585.80			
	7,353.34	1		13,595.52			
56	7,343.98	8	4, III	13,612.85	a^3H_4–$z^3G^\circ_3$		

TABLE 3.—*Wave lengths in the arc spectrum of Zr*—Continued

Key No.	λ I. A.	Intensities, temperature class, and notes		Wave No.	Term combinations	Observed Zeeman effects	Theoretical Zeeman effects
		B. S.	King				
44	7,340.03	1		13,620.18	a^3H_5–$z^3H_6^\circ$		
43	7,336.03	8	4, II	13,627.60	a^3P_2–$z^3D_2^\circ$		
	7,332.73	1		13,633.74			
	7,327.84	4		13,642.83			
	7,323.75	2		13,650.45			
41	7,318.15	9	8, III	13,660.90	a^3G_5–$y^3G_5^\circ$		
	7,317.32	2		13,662.45			
52	7,313.73	7	2, V	13,669.15	b^3F_4–$y^3G_4^\circ$		
41	7,311.68	7	2, V	13,672.99	a^3G_4–$y^3G_3^\circ$		
	7,307.38	3		13,681.03			
55	7,306.24	5	1, V	13,683.17	a^3G_4–$x^3F_3^\circ$		
53	7,284.76	3		13,723.51	a^3G_3–$x^1F_3^\circ$		
	7,284.02	2		13,724.91			
56	7,264.79	8	4, V	13,761.24	a^3H_5–$x^3G_4^\circ$		
52	7,258.23	5		13,773.67	b^3F_3–$y^3G_3^\circ$		
57	7,248.50	3		13,792.16	a^1G_4–$z^3G_3^\circ$		
45	7,223.87	2		13,839.19	a^3G_5–$y^3G_4^\circ$		
56	7,201.67	8	4, V	13,881.85	a^3H_6–$x^3G_5^\circ$		
58	7,193.37	3		13,897.87	a^3D_3–$y^3F_2^\circ$		
	7,179.59	3		13,924.54			
	7,177.26	2		13,929.05			
59	7,169.14	40	150, II	13,944.84	a^3F_3–$z^5D_4^\circ$	(0.00) 1.16	(**0.00**, 0.10, 0.20, ---) **1.00**, 1.10, 1.20, ---
56	7,162.12	2		13,958.51	a^3H_4–$x^3G_4^\circ$		
60	7,161.02	2		13,960.65	a^3F_4–$z^3G_3^\circ$		
	7,157.88	3		13,966.77			
61	7,146.11	2		13,989.78	b^3F_2–$y^5G_2^\circ$		
45	7,144.48	5		13,992.97	a^3G_5–$y^5G_3^\circ$		
	7,143.87	3		13,994.16			
62	7,143.43	3		13,995.03	a^1D_2–$z^5D_1^\circ$		
61	7,140.74	4		14,000.29	b^3F_4–$y^5G_4^\circ$		
54, 45	7,138.30	5		14,005.08	b^3F_2–$z^5P_2^\circ$; a^3G_4–$y^5G_3^\circ$		
61	7,132.98	5		14,015.53	b^3F_3–$y^5G_3^\circ$		
63	7,113.54	5	1, V	14,053.83	a^5G_3–$x^5D_2^\circ$		
52	7,112.83	8	4, IV?	14,055.23	b^3F_3–$y^3G_4^\circ$		
43	7,111.71	12	20, II	14,057.45	a^3P_2–$z^5D_3^\circ$		
59	7,103.77	18	40, II	14,073.16	a^3F_2–$z^5D_1^\circ$	(0.00) 0.00 *w*	(**0.00**, 0.50) **0.50**, **1.00**, 1.50
59	7,102.95	20	80, II	14,074.78	a^3F^5–$z^5D_2^\circ$		
59	7,097.78	25	150, II	14,085.04	a^5F_4–$z^5D_3^\circ$	(0.00 *w*) 1.10	(**0.00**, 0.15, 0.30, 0.45) **0.90**, 1.05, 1.20, ---
52	7,095.66	8	5, V	14,089.24	b^3F_2–$y^3G_3^\circ$		
52	7,094.61	7	3, IV	14,091.33	b^3F_4–$y^3G_3^\circ$		
64	7,092.82	3		14,094.88	$y^5F_4^\circ$–e^3F_4		
	7,091.27	2		14,097.96			
65	7,089.50	5	1, V	14,101.49	b^3F_4–$x^3F_3^\circ$		
59	7,087.35	20	20, III	14,105.76	a^5F_1–$z^5D_0^\circ$	(0.00) 0.00	(0.00) 0.00
66	7,060.84	3		14,158.72	a^3G_5–$z^1G_4^\circ$		
	7,057.99	4	1, V	14,164.44			
55	7,057.38	7	3, V	14,165.66	a^3G_5–$x^3F_4^\circ$		
59	7,027.40	15	30, III	14,226.10	a^5F_1–$z^5D_1^\circ$	(1.48) 0.00, 1.55	(1.50) 0.00, 1.50
67	7,005.46	4		14,270.65	b^1F_3–$x^1F_3^\circ$		
59	6,994.38	12	15, IV?	14,293.25	a^5F_4–$z^5D_4^\circ$	(0.51) 1.51	(--- 0.45, **0.60**) --- 1.20, **1.35**, **1.50**, 1.65, ---
59	6,990.86	18	50, III	14,300.45	a^5F_2–$z^5D_2^\circ$	(0.93) 0.80, 1.77	(0.50, **1.00**) 0.50, **1.00**, **1.50**, 2.00
61	6,975.94	4		14,331.04	b^3F_2–$y^5G_2^\circ$		
63	6,966.49	12	15, III	14,350.48	a^5G_4–$x^5D_3^\circ$	(0.00) 0.64	(**0.00**, 0.28, ---) **0.20**, 0.48, 0.77, ---
59	6,953.87	20	60, III	14,376.52	a^5F_3–$z^5D_3^\circ$	(0.68) 1.53	(0.25, 0.50, **0.75**) ---, 1.00, **1.25**, **1.50**, 1.75, ---
68	6,948.51	8	4, V	14,387.61	a^5P_3–$z^5P_3^\circ$		
65	6,932.41	6	2, V	14,421.03	b^3F_2–$x^3F_3^\circ$		
66	6,929.09	3		14,427.93	a^3G_3–$z^1G_4^\circ$		
55	6,925.71	2		14,434.98	a^3G_3–$x^3F_4^\circ$		
45	6,922.23	3		14,442.23	a^3G_5–$y^5G_5^\circ$		
59	6,916.90	7	2, III	14,453.36	a^5F_1–$z^5D_2^\circ$		
68	6,907.40	8	3, IV	14,473.24	a^5P_2–$z^5P_1^\circ$		

TABLE 3.—*Wave lengths in the arc spectrum of Zr*—Continued

Key No.	λ I. A.	Intensities, temperature class, and notes		Wave No.	Term combinations	Observed Zeeman effects	Theoretical Zeeman effects
		B. S.	King				
60	6,904.40	7	2, III	14,479.53	a^5F_4–$z^5G^\circ_4$		
65	6,900.59	8	2, IV	14,487.52	b^3F_3–$x^3F^\circ_3$		
69	6,888.30	15	20, IV	14,513.37	b^3F_2–$x^3D^\circ_1$	(0.00) 0.66	(**0.00,** 0.17) 0.50, 0.67, **0.83**
	6,885.20	3		14,519.91			
62	6,883.27	4		14,523.98	a^1D_2–$z^1D^\circ_2$		
70	6,857.93	3		14,577.64	a^3D_3–$v^3D^\circ_3$		
59	6,854.63	3		14,584.66	a^5F_3–$z^5D^\circ_4$		
67	6,853.85	3		14,586.32	b^3F_2–$x^1F^\circ_3$		
71	6,852.59	4		14,589.00	b^3F_4–$z^1G^\circ_4$		
65	6,849.29	8	4, V	14,596.03	b^3F_4–$x^3F^\circ_4$		
72	6,847.34	2		14,600.19	a^3P_1–$z^3D^\circ_0$		
69	6,847.03	18	25, V	14,600.85	b^3F_3–$z^3D^\circ_2$	(0.00) 0.85	(**0, 00,** 0.08, 0.17) **0, 92,** 1.00, 1.08, ---
59	6,846.42	5		14,602.15	a^5F_2–$z^5D^\circ_3$		
68	6,845.30	5		14,604.54	a^5P_1–$z^5P^\circ_1$		
63	6,843.76	2		14,607.83	a^3G_3–$x^3D^\circ_3$		
73	6,838.69	3		14,618.65	a^3G_3–$w^3D^\circ_2$		
68	6,833.69	4		14,629.35	a^5P_2–$z^5P^\circ_2$		
60	6,832.93	12	12, III	14,630.98	a^3F_3–$z^5G^\circ_3$		
68	6,828.82	10	10, V	14,639.80	a^5P_3–$z^5P^\circ_3$	(0.00) 1.66	(0.00) 1.67
	6,812.66	3		14,674.51			
70	6,811.32	2		14,677.40	a^3D_1–$p^3D^\circ_1$		
70	6,796.71	4		14,708.95	a^3D_2–$e^3D^\circ_2$		
74	6,794.66	2		14,713.38	a^3P_2–$y^3G^\circ_3$		
75					a^5P_2–$y^5G^\circ_3$		
73	6,790.89	10	4, V	14,721.55	a^3G_4–$w^3D^\circ_3$		
68	6,772.92	8	3, V	14,760.61	a^5P_1–$z^5P^\circ_2$		
69	6,769.16	20	40, V	14,768.81	b^3F_4–$x^3D^\circ_3$	(0.00w) 0.72	**0, 00,** 0.08, ---) **1. 00,** 1.08, 1.17, ---
60	6,762.38	20	30, III	14,783.62	a^3F_2–$z^5G^\circ_3$	(0.55) 0.58	(0.33, **0. 67**) 0.00, **0. 33,** 0. 67, 1.00
76	6,752.73	10	4, V	14,804.74	a^1G_4–$z^1F^\circ_3$	(0.00) 0.90	(0.00) 1.00
68	6,717.89	8	3, III	14,881.53	a^5P_2–$z^5P^\circ_3$	(0.00w) 1.25	(**0, 00,** 0.17, 0.33) **1. 33,** 1.50, 1. 67, ---
72	6,709.61	7	2, IV	14,899.89	a^3P_0–$z^5D^\circ_1$		
69	6,702.13	6	1, V	14,916.52	b^3F_2–$z^3D^\circ_2$		
	6,698.50	2		14,924.60			
70	6,697.94	3		14,925.85	a^3D_2–$v^3D^\circ_3$		
70	6,693.95	3		14,934.75	a^3D_1–$v^3D^\circ_2$		
72	6,688.19	7	2, V	14,947.61	a^3P_1–$z^5D^\circ_2$	(0.00) 1.44	(0.00) 1.50
77	6,678.81	3		14,968.60	a^5P_3–$x^1F^\circ_3$		
78	6,645.16	3		15,044.40	a^5P_3–$x^3F^\circ_3$		
81	6,620.62	5	1, V	15,100.16	a^1H_5–$z^1H^\circ_5$	(0.00) 1.08	(0.00) 1.00
	6,617.28	2		15,107.78			
	6,616.40	2		15,109.79			
80	6,603.27	8	4, V	15,139.84	b^3F_4–$w^3D^\circ_3$	(0.00w) 0.78	(**0, 00,** 0.08, 0.17, 0.25) **1. 00,** 1.08, 1.17, ---
82	6,599.89	2		15,147.59	a^3G_4–$z^3H^\circ_4$		
60	6,598.86	3		15,149.95	a^3F_3–$z^5G^\circ_4$		
69	6,596.75	3		15,154.80	b^3F_3–$x^3D^\circ_3$		
80	6,592.02	8	4, V	15,165.68	b^3F_3–$w^3D^\circ_2$	(0.00) 0.82	(**0, 00,** 0.08, 0.17) **0. 92,** 1.00, 1.08, ---
78	6,583.61	2		15,185.05	a^5P_2–$x^3F^\circ_3$		
60	6,576.57	3	1, V	15,201.30	a^3F_2–$z^5G^\circ_3$		
79	6,569.43	4	1, V	15,217.82	a^5F_2–$z^1P^\circ_1$		
80	6,550.57	5	3, V	15,261.64	b^3F_2–$w^3D^\circ_1$	(0.00) 0.72	(**0, 00,** 0.17) 0.50, 0.67, **0. 83**
83	6,506.39	4	6, IV?	15,365.27	a^1D_2–$z^3P^\circ_2$	(0.46) 1.46	(0.50, **1. 00**) 0.50, **1. 00,** 1.50, 2.00
84	6,503.31	5	5, IV?	15,372.55	a^3G_3–$w^3F^\circ_2$	(0.00) 0.92	(**0, 00,** 0.08, 0.17) --- 0.75, 0. 83, **0. 92**
85	6,493.12	4	1, V?	15,396.67	a^3H_5–$x^3D^\circ_4$		
84					a^3G_4–$w^3F^\circ_3$		
82	6,489.68	10	25, IV	15,404.83	a^3G_3–$z^3P^\circ_1$	(**0.00**) **0. 84**	(**0. 00,** 0. 05, 0. 10, 0. 15) --- 0. 85, 0. 90, **0. 95**
83	6,484.35	2		15,417.49	a^1D_2–$z^3P^\circ_1$		

TABLE 3.—*Wave lengths in the arc spectrum of Zr*—Continued

Key No.	λ I. A.	Intensities, temperature class, and notes		Wave No.	Term combinations	Observed Zeeman effects	Theoretical Zeeman effects
		B. S.	King				
82	6,470.25	10	15, IV	15,451.09	a^3G_4–$z^3H^0_5$	(0.00) 0.79	(**0.00**, 0.02, 0.03, ---) **0.97**, 0.98, 1.00, ---
80	6,457.60	3	1, V	15,481.36	b^3F_3–$w^3D^0_3$		
79	6,451.62	3		15,495.71	a^5F_2–$z^3P^0_1$		
86	6,445.76	8	10, IV	15,509.80	a^1G_4–$y^3F^0_3$	(0.00) 0.90	½(**0.00**, 0.08, ---) **0.75**, 0.83, 0.92, ---
80	6,439.01	4		15,526.05	b^3F_2–$w^3D^0_3$		
87	6,434.40	4	1, V	15,537.18	$z^3G^0_5$–e^3F_4	(0.00) 1.14	
87	6,426.20	2		15,557.00	$z^3G^0_4$–e^3F_3	(0.00) 1.04	
88	6,407.03	5	4, V	15,603.55	a^1G_4–$y^3D^0_3$		
89					a^3F_4–$z^3F^0_3$		
87	6,404.27	2		15,610.28	$z^3G^0_3$–e^3F_2		
90	6,390.61	2		15,643.64	a^3G_4–$x^3G^0_3$		
84	6,386.40	2		15,653.96	a^3G_3–$w^3F^0_3$		
84	6,345.23	15	8, IV	15,755.52	a^3G_5–$w^3F^0_4$		
84	6,340.39	4	1, V	15,767.55	a^3G_4–$w^3F^0_4$	(0.00 *w*) 1.18	(---, 0.60, **0.80**) --- 0.85, **1.05**, **1.25**, 1.45, ---
	6,324.55	2		15,807.04			
91	6,321.37	6	2, V	15,814.99	b^3F_4–$w^3F^0_3$	(0.00 *w*) 1.54	(**0.00**, 0.17, ---) --- 1.42, 1.58, **1.75**
92	6,314.71	2		15,831.67	a^1G_4–$y^5D^0_3$		
82	6,313.05	12	50, V	15,835.83	a^3G_5–$z^3H^0_6$	(0.00) 1.12	(**0.00**, 0.03, 0.07, ---) **1.00**, 1.03, 1.07, ---
93	6,304.35	3		15,857.69	a^1S_0–$z^1P^0_1$	(0.00) 1.44	(0.00) 1.50
94					a^3P_1–$z^3P^0_0$		
95	6,299.72	7	12, V	15,869.34	b^3F_4–$z^3H^0_5$	(0.00) 0.78	(**0.00**, 0.22, 0.43, ---) **0.17**, 0.38, 0.60, ---
96	6,282.66	2		15,912.43	c^3P_1–$e^3F^0_2$		
91	6,279.77	1		15,919.76	b^3F_3–$w^3F^0_2$		
95	6,267.09	4		15,951.97	b^3F_3–$z^3H^0_4$		
90	6,257.28	5	8, V	15,976.98	a^3G_5–$x^3G^0_4$	(0.00) 1.27	(**0.00**, 0.15, 0.30 ---) --- 1.50, 1.65, **1.80**
97	6,224.22	2		16,061.83	b^3F_4–$x^3G^0_3$		
98	6,220.86	2		16,070.51	$z^5D^0_0$–e^5F_1		
99	6,214.72	8	6, V	16,086.39	b^1G_4–$z^1H^0_5$	(0.00) 1.00	(0.00) 1.00
94	6,213.06	8	8, IV?	16,090.68	a^3P_1–$z^3P^0_2$	(0.00) 1.49	(0.00) 1.50
98	6,204.13	3		16,113.85	$z^5D^0_1$–e^5F_2		
94	6,192.96	7	5, III	16,142.91	a^3P_1–$z^3P^0_1$	(0.00) 1.51	(0.00) 1.50
98	6,189.38	3		16,152.25	$z^5D^0_2$–e^5F_3		
100	6,178.26	3		16,181.32	a^3F_4–$z^5F^0_5$	(0.00) 1.26	(0.00) 1.25
90	6,160.27	2		16,228.57	a^3G_5–$x^3G^0_5$	(0.00) 1.22	(0.00) 1.20
98	6,157.75	6	20, IV	16,235.22	$z^5D^0_3$–e^5F_4	(0.00) 0.80	(0.00) 0.67
91					b^3F_2–$w^3F^0_2$		
90	6,155.56	2		16,240.99	a^3G_4–$x^3G^0_5$	(0.00) 1.36	(**0.00**, 0.15, 0.30, ---) --- 1.50, 1.65, **1.80**
101	6,149.94	1		16,255.83	a^5F_5–$z^3G^0_4$		
89	6,143.23	30	150, II	16,273.59	a^3F_3–$z^3F^0_3$	(0.00) 1.10	(0.00) 1.08
94	6,140.50	10	15, II	16,280.82	a^3P_2–$z^3P^0_2$	(0.48) 1.44	(0.00) 1.50
89	6,134.58	25	125, II	16,296.53	a^3F_2–$z^3F^0_2$	(0.00) 0.69	(0.00) 0.67
89	6,127.49	35	200, II	16,315.39	a^3F_4–$z^3F^0_4$	(0.00) 1.26	(0.00) 1.25
94	6,124.86	10	5, III	16,322.39	a^3P_0–$z^3P^0_1$	(0.00) 1.50	(0.00) 1.50
102	6,121.95	12	20, II	16,330.16	a^1G_4–$y^1F^0_3$	(0.00) 0.74 A^1	(0.00) 1.00
94	6,120.86	5	3, IV	16,333.06	a^3P_2–$z^3P^0_1$	(0.00) 1.15	(0.00) 1.50
100	6,062.88	7	12, II	16,489.26	a^3F_3–$z^5F^0_2$	(0.00) 1.17	(**0.00**, 0.08, 0.17), --- 1.08, 1.17, **1.25**
91	6,052.84	4		16,516.61	b^3F_2–$w^3F^0_3$		
98	6,049.29	6	3, IV	16,526.30	$z^5D^0_4$–e^5F_5	(0.00) 1.14	(**0.00**, 0.10, 0.20, ---) **1.00**, 1.10, 1.20, ---
103	6,045.89	7	4, IV	16,535.59	a^3H_4–$w^3G^0_3$	(0.00) 0.88	(**0.00**, 0.05, ---) --- 0.85, 0.90, **0.95**
91	6,032.62	7	5, IV	16,571.96	b^3F_3–$w^3F^0_4$	(0.00) 1.45	(**0.00**, 0.17, ---) --- 1.42, 1.58, **1.75**
100	6,025.41	3		16,591.80	a^3F_4–$z^5F^0_4$		
104	6,014.69	1		16,621.37	c^3P_2–$u^3D^0_2$		
	6,002.66	2		16,654.68			
97	6,001.03	4		16,659.20	b^3F_4–$x^3G^0_5$	(0.00) 1.36	(**0.00**, 0.05, ---) **1.00**, 1.05, 110, ---
101	5,995.41	2		16,674.82	a^3F_5–$z^3G^0_5$		
104	5,984.82	2		16,704.32	c^3P_1–$u^3D^0_2$		

TABLE 3.—*Wave lengths in the arc spectrum of Zr*—Continued

Key No.	λ I. A.	Intensities, temperature class, and notes		Wave No.	Term combinations	Observed Zeeman effects	Theoretical Zeeman effects
		B. S.	King				
103	5, 984. 24	6	5, V	16, 705. 94	a^3H_5–$w^3G_4^1$	(0.00) 1.02	(**0. 00,** 0.02, **0.03,** ---) **0. 97,** 0.98, 1.00, ---
105	5, 969. 29	2		16, 747. 78	a^1D_2–$z^3G_3^1$		
100	5, 955. 37	12	12, II	16, 786. 93	a^3F_2–$z^3F_1^1$	(**0. 00,** 0.52) 0.68, **1. 14**	(**0. 00,** 0.67) 0.00, 0.67, **1. 33**
89	5, 935. 23	10	10, II	16, 843. 89	a^3F_2–$z^3F_3^1$	(**0. 00,** 0.42, 0.87) 1.52, **1. 96**	(**0. 00,** 0.42, 0.83) --- 1.08, 1.50, **1. 92**
106	5, 925. 17	7	12, III	16, 872. 49	a^1D_2–$z^3S_1^1$	(**0. 00,** 0.71) **0. 49,** 1.30	(**0. 00,** 1.00) **0. 00,** 1.00, 2.00
107	5, 901. 09	4	2, III	16, 941. 34	a^3F_3–$z^1D_2^1$	(0.00) 1.25	(**0. 00,** 0.08, **0.17**) --- 1.08, 1.17, **1. 25**
89	5, 885. 61	10	8, II	16, 985. 90	a^3F_3–$z^3F_4^1$	(0.00 *w*) 1.29, **1. 74**	(**0. 00,** 0.17, ---) --- 1.42, 1.58, **1. 75**
108	5, 879. 79	25	40, II	17, 002. 71	a^3F_4–$z^3D_3^1$	(0.00) 1.12	(**0. 00,** 0.08, ---) **1. 00,** 1.08, 1.17, ---
101	5, 872. 62	1		17, 023. 47	a^5F_1–$z^3G_2^1$		
103	5, 869. 51	8	4, IV	17, 032. 49	a^3H_6–$w^3G_5^1$	(0.00) 1.10	(**0. 00,** 0.03, **0.07,** ---) **1. 00,** 1.03, 1.07, ---
100	5, 868. 28	4		17, 036. 07	a^3F_4–$z^5F_5^1$		
104	5, 847. 33	5		17, 097. 09	c^3P_2–$u^3D_3^1$	(0.00) 1.20	(**0. 00,** 0.17, 0.33) **1. 00,** 1.17, 1.33, ---
109	5, 818. 48	2		17, 181. 87	b^3P_2–$x^3S_1^1$		
	5, 809. 15	2		17, 209. 46			
110	5, 801. 31	2		17, 232. 72	$z^3D_3^0$–e^5F_3		
108	5, 797. 76	12	25 II	17, 243. 27	a^3F_3–$z^3D_2^1$	(0.00) 1.03	(**0. 00,** 0.08, 0.17) **0. 92,** 1.00, 1.08, ---
111	5, 791. 30	2		17, 262. 50	a^1H_5–$t^3F_4^1$		
100					a^3F_3–$z^5F_4^1$		
110	5, 746. 59	2		17, 396. 81	$z^3D_3^0$–e^3F_3		
108	5, 735. 70	12	20, II	17, 429. 84	a^3F_2–$z^3D_1^1$	(0.00) 0.90 A[3]	(**0. 00,** 0.17) 0.50, 0.67, **0. 83**
107	5, 708. 88	4	2, III	17, 511. 73	a^3F_3–$z^1D_2^1$	(0.66) 0.77	(0.33, **0. 67**) 0.33, **0. 67,** 1.00, 1.33
112	5, 685. 47	3		17, 583. 83	$z^5F_5^0$–e^5F_4		
113					a^3G_3–$z^5D_3^0$		
114	5, 680. 93	12	15, II	17, 597. 88	a^1H_5–$z^1G_4^1$	(0.50) 1.47, 2.01	(0.50) 1.50, 2.00
115					a^3P_1–$z^3S_1^1$		
110	5, 674. 76	2		17, 617. 02	$z^3D_1^0$–e^5F_1		
110					$z^3D_2^0$–e^5F_4		
112	5, 666. 28	2		17, 643. 38	$z^3F_4^0$–e^5F_3		
116	5, 664. 55	12	25, II	17, 648. 77	a^1D_2–$y^1D_2^1$	(0.51) 1.09	(0.00) 1.00
117	5, 659. 83	3		17, 663. 49	a^3P_2–$z^3G_3^1$		
118	5, 629. 02	4		17, 760. 16	a^1D_2–$z^1F_3^1$		
115	5, 623. 56	5	3, V	17, 777. 41	a^3P_0–$z^3S_1^1$	(0.00) 1.97	(0.00) 2.00
112	5, 620. 16	10	15, IV	17, 788. 16	$z^5F_5^0$–e^5F_2	(**0. 00,** 0.75) **0. 44,** 1.27, 2.00	(**0. 00,** 0.50) **1. 00,** 1.50, 2.00
115					a^3P_2–$z^3S_1^1$		
108	5, 612. 11	3		17, 813. 68	a^3F_2–$z^3D_2^1$		
112	5, 557. 91	2		17, 987. 39	$z^5F_2^0$–e^5F_1		
119	5, 555. 38	2		17, 995. 58	a^5F_2–$y^5D_1^1$		
120	5, 550. 34	2		18, 011. 88	$y^5F_4^1$–f^5G_5		
112	5, 545. 42	8	3, V	18, 027. 90	$z^5F_4^0$–e^5F_4	(0. 00) 1. 35	(0. 00) 1. 35
112	5, 537. 45	5	2, V	18, 053. 85	$z^5F_3^0$–e^5F_3	(0. 00) 1. 23	(0. 00) 1. 25
	5, 536. 67	3		18, 056. 39			
119	5, 532. 30	4		18, 070. 66	a^5F_3–$y^5D_2^1$		
112	5, 528. 44	10	8, V	18, 083. 28	$z^5F_5^0$–e^5F_5	(0. 00) 1. 40	(0. 00) 1. 40
	5, 523. 88	3		18, 098. 20			
121	5, 522. 78	2		18, 101. 81	a^1H_5–$z^3H_6^1$		
122	5, 518. 06	2		18, 117. 29	a^5F_3–$y^5F_4^1$		
119	5, 517. 12	4	2, V	18, 120. 38	a^5F_4–$y^5D_4^1$		
112	5, 507. 96	3		18, 150. 51	$z^5F_5^0$–e^5F_2		
120	5, 504. 22	1		18, 162. 84	$y^5F_5^1$–f^5G_6		
123	5, 502. 16	12	15, V	18, 169. 65	a^1G_4–$x^1F_3^1$	(0. 00) 0. 90	(0. 00) 1. 00
124	5, 487. 52	2		18, 218. 12	a^1D_2–$y^3D_3^1$		
125	5, 486. 09	4	2, IV	18, 222. 87	a^5F_2–$y^5D_1^1$		
	5, 481. 17	3		18, 239. 23			
125	5, 480. 82	5	2, IV	18, 240. 39	a^5F_3–$y^5D_4^1$		
126	5, 478. 34	5	3, III	18, 248. 65	b^1G_4–$t^3F_4^1$		

TABLE 3.—*Wave lengths in the arc spectrum of Zr*—Continued

Key No.	λ I. A.	Intensities, temperature class, and notes		Wave No.	Term combinations	Observed Zeeman effects	Theoretical Zeeman effects
		B. S.	King				
125	5,477.40	3		18,251.78	a^5F_1–$y^5D_0^1$		
127	5,475.55	2		18,257.95	a^5P_2–$v^5D_3^3$		
112	5,474.94	2		18,259.98	$z^5F_1^1$–e^5F_1		
	5,474.39	2		18,261.81			
119	5,464.02	1		18,296.47	a^5F_2–$y^5D_2^2$		
128	5,460.71	3		18,307.56	b^5P_2–$u^5D_3^3$		
122	5,457.58	1		18,318.06	a^5F_3–$y^5F_3^3$		
125 / 122	5,448.55	5	3, III	18,348.42	a^5F_4–$y^5D_3^3$ / a^5F_3–$y^5F_3^3$		
	5,447.94	2		18,350.48			
129	5,443.16	2		18,366.59	$z^5F_3^3$–e^5F_2		
125	5,440.41	4		18,375.87	a^5F_1–$y^5D_1^1$		
130	5,437.74	5	2, IV	18,384.89	a^3F_4–$z^5D_4^4$		
131	5,437.26	3		18,386.52	a^1G_4–$z^3F_3^3$		
132	5,436.91	3		18,387.70	a^1D_2–$y^3D_2^2$		
112	5,428.42	4		18,416.46	$z^5F_2^2$–e^5F_3		
112	5,426.36	3		18,423.45	$z^5F_1^1$–e^5F_2		
	5,423.50	2		18,433.17			
112	5,421.86	3		18,438.74	$z^5F_3^3$–e^5F_4		
119	5,418.73	2		18,449.39	a^5F_1–$y^5D_2^2$		
133 / 122	5,413.92	3		18,465.79	a^1D_2–$y^3F_2^2$ / a^5F_4–$y^5F_4^4$		
125	5,407.63	10	7, II	18,487.26	a^5F_5–$y^5D_4^4$	(0.00) 1.22	(**0.00**, 0.10, 0.20, ---) **1.00**, 1.10, 1.20, ---
133	5,405.13	4	2, III	18,495.82	a^1D_2–$y^3F_3^3$		
112	5,395.88	3		18,527.52	$z^5F_4^4$–e^5F_5		
122	5,391.18	3		18,543.67	a^5F_3–$y^5F_3^3$		
124	5,386.65	3		18,559.27	a^1D_2–$y^3D_3^3$	(0.00) 1.32	(**0.00**, 0.33, 0.67) --- 1.33, 1.67, **2.00**
134	5,385.14	15	40, II	18,564.47	a^3P_2–$y^1D_2^2$	(0.45) 1.10	(0.50, **1.00**) **0.50**, **1.00**, **1.50**, 2.00
122	5,382.36	3		18,574.06	a^5F_2–$y^5F_2^2$		
135	5,379.54	3		18,583.80	b^1G_4–$x^1G_4^4$		
	5,372.43	2		18,608.39			
125	5,369.39	4		18,618.92	a^5F_1–$y^5D_2^2$		
125	5,363.35	3		18,639.89	a^5F_3–$y^5D_3^3$		
136	5,362.56	8	6, III	18,642.64	a^3P_1–$y^3D_1^1$	(0.97) **0.50**, 1.53	(1.00) 0.50, **1.50**
	5,351.92	5		18,679.70			
137	5,350.89	4		18,683.30	a^1H_5–$e^1G_4^4$		
138 / 139	5,343.59	2		18,708.82	a^3P_1–$z^5S_2^2$ / a^1G_4–$y^5G_3^3$		
122	5,338.41	4		18,726.97	a^5F_1–$y^3F_2^2$		
129	5,331.74	3		18,750.40	$z^5F_2^2$–e^5F_1		
130	5,330.83	5		18,753.60	a^3F_3–$z^5D_3^3$		
122	5,329.83	3		18,757.12	a^5F_3–$y^3F_4^4$		
	5,321.81	2		18,785.39			
132	5,321.27	4		18,787.30	a^1D_2–$y^5D_2^2$		
140	5,319.98	2		18,791.85	a^3P_1–$x^5D_1^1$		
141	5,316.75	1		18,803.27	c^3P_0–$t^3D_1^1$		
136	5,311.42	8	6, III	18,822.13	aP_0–$y^3D_1^1$	(0.00) **0.54**	(0.00) 0.50
142	5,310.97	2		18,823.73	a^3G_3–$w^3G_3^3$		
140	5,309.64	2		18,828.45	a^5P_3–$x^5D_3^3$		
140	5,308.94	2		18,830.93	a^5P_3–$x^5D_2^2$		
136	5,308.38	2		18,832.91	a^3P_2–$y^3D_1^1$		
125	5,307.62	2		18,835.61	a^5F_1–$y^5D_0^1$		
143	5,305.50	2		18,843.14	a^3D_2–$v^3F_3^3$		
143	5,303.80	2		18,849.18	a^3D_1–$v^3F_2^2$		
144	5,303.36	1		18,850.74	a^3H_5–$z^1H_5^5$		
145	5,301.98	7		18,855.65	b^1G_4–$x^3H_4^4$	(0.00*w*) 0.98	(---, 0.60, **0.80**) --- 0.60, **0.80**, **1.00**, **1.20**, ---
146	5,300.11	3		18,862.30	a^3D_3–$u^3F_4^4$		
	5,299.53	3		18,864.36			
125	5,299.20	3		18,865.54	a^5F_2–$y^5D_2^2$		
147	5,296.78	10	5, III	18,874.21	a^1G_4–$z^1G_4^4$	(0.19) 1.04	(0.00) 1.00
131	5,294.82	7	2, V	18,881.14	a^1G_4–$z^3F_4^4$		
	5,292.52	3		18,889.35			
142	5,280.06	10	2, V	18,933.92	a^3G_4–$w^3G_4^4$	(0.00) 1.54	(0.00) **1.05**

TABLE 3.—*Wave lengths in the arc spectrum of Zr*—Continued

Key No.	λ I. A.	Intensities, temperature class, and notes		Wave No.	Term combinations	Observed Zeeman effects	Theoretical Zeeman effects
		B. S.	King				
136	5,277.40	12	8, III	18,943.47	a^3P_1–$y^3D_2^0$	(**0.00**, 0.34) **0.70**, 1.13	(**0.00**, 0.33) **0.83**, 1.17, 1.50
140	5,272.15	2		18,962.33	a^5P_1–$x^5D_2^0$		
143	5,264.04	4		18,991.55	a^3D_3–$z^3F_4^0$		
	5,263.74	1		18,992.63			
146	5,250.33	2		19,041.14	a^3D_1–$u^3F_2^0$		
144	5,248.51	3		19,047.74	a^3H_4–$z^1H_5^0$		
148	5,248.03	3		19,049.48	a^3P_0–$y^3D_1^0$		
141	5,243.46	5		19,066.09	c^3P_1–$t^3D_1^0$		
140	5,242.19	2		19,070.71	a^5P_2–$x^5D_3^0$		
146	5,241.93	1		19,071.65	a^3D_2–$u^3F_3^0$		
130	5,235.07	3		19,096.64	a^3F_3–$z^3D_2^0$		
148	5,230.55	4		19,113.14	a^3P_1–$y^5D_2^0$		
140	5,227.00	3		19,126.12	a^5P_3–$x^5D_4^0$		
136	5,224.94	9	6, III	19,133.66	a^5P_2–$y^3D_2^0$	(0.00*w*) 1.18	(0.33, **0.67**) 0.83, **1.17**, **1.50**, 1.83
149	5,223.62	2		19,138.50	a^5F_3–$y^1F_3^0$		
150	5,215.58	2		19,168.00	c^3P_0–$v^3P_1^0$		
142	5,209.31	8	4, V	19,191.07	a^3G_3–$w^3G_4^0$	(**0.00** *w*, 0.55) 1.29, **1.70**	(**0.00**, 0.30, ---) --- 1.35, 1.65, **1.95**
151	5,201.17	8	4, III	19,221.11	a^3P_1–$y^3F_2^0$	(**0.00**, 0.59) 0.00, 0.98	(**0.00**, 0.83) **0.17**, 0.67, 1.50
152	5,187.04	4		19,273.46	b^3P_2–$w^3P_1^0$		
153	5,184.55	2		19,282.72	a^3D_2–$w^5D_2^0$		
154	5,183.71	8	6, III	19,285.85	a^1D_2–$y^1F_3^0$	(0.00) 1.02	(0.00) 1.00
148	5,178.99	3		19,303.42	a^3P_2–$y^5D_2^0$		
153	5,174.31	2		19,320.88	a^3D_1–$w^5D_1^0$		
155	5,165.97	8	4, V	19,352.07	b^3F_4–$w^3G_4^0$		
	5,164.71	3		19,356.80			
155	5,161.01	7	3, V	19,370.67	b^3F_3–$w^3G_3^0$		
142	5,158.68	6		19,379.42	a^3G_5–$w^3G_5^0$		
156	5,158.02	12	7, V	19,381.90	$z^5G_6^0$–e^5F_5	(0.00) 1.10	(**0.00**, 0.07, **0.13**, ---) 1.00, 1.07, 1.13, ---
142	5,155.46	15	12, V	19,391.53	a^3G_4–$w^3G_5^0$	(0.00) 1.30	(**0.00**, 0.15, 0.30, ---) --- 1.50, **1.65**, **1.80**
151	5,150.22	1		19,411.25	a^3P_2–$y^3F_2^0$		
150	5,145.46	1		19,429.21	c^3P_1–$v^3P_1^0$		
157	5,140.42	1		19,448.26	a^3H_4–$u^3D_3^0$		
158	5,136.78	3		19,462.04	a^3H_5–$y^3H_4^0$		
	5,136.16	4		19,464.39			
	5,135.16	2		19,468.18			
	5,134.43	1		19,470.95			
136	5,133.42	10	6, V	19,474.78	a^3P_2–$y^3D_3^0$	(0.00) 1.23	(**0.00**, 0.17, 0.33) **1.00**, 1.17, 1.33, ---
159	5,132.88	3		19,476.83	b^1G_4–$v^3G_4^0$		
	5,128.16	2		19,494.76			
	5,126.06	3		19,502.74			
152	5,120.44	7		19,524.15	b^3P_2–$w^3P_2^0$	(0.00) 1.46	(0.00) 1.50
	5,119.44	2		19,527.96			
156	5,115.27	15	5, V	19,543.88	$z^5G_5^0$–e^5F_4	(0.00) 1.13	(**0.00**, 0.08, **0.17**, ---) 0.93 1.02, 1.10, ---
	5,113.69	1		19,549.92			
	5,112.82	1		19,553.24			
153	5,110.17	2		19,563.39	a^3D_2–$w^5D_3^0$		
160	5,105.56	5		19,581.05	a^1S_0–$y^1P_1^0$		
158	5,104.23	2		19,586.15	a^3H_6–$y^3H_5^0$		
	5,102.54	1		19,592.64			
	5,098.56	2		19,607.93			
	5,089.62	2		19,642.37			
158	5,085.26	10	3, V	19,659.21	a^3H_4–$y^5H_4^0$	(0.00) 0.80	(0.00) 0.80
	5,082.02	2		19,671.75			
	5,080.00	4		19,679.57			
	5,079.01	2		19,683.40			

TABLE 3.—*Wave lengths in the arc spectrum of Zr*—Continued

Key No.	λ I. A.	Intensities, temperature class, and notes		Wave No.	Term combinations	Observed Zeeman effects	Theoretical Zeeman effects
		B. S.	King				
155	5,078.28	20	20, V	19,686.23	b^3F_2–$w^3G_3^0$	(0.00) 0.82	(**0.00**, 0.08, 0.17) --- 0.75, 0.83, **0.92**
	5,075.23	3		19,698.06			
148	5,074.00	10	2, V	19,702.84	a^3P_2–$y^3D_3^0$		
	5,073.14	2		19,706.18			
	5,072.29	2		19,709.48			
	5,071.82	1		19,711.31			
158	5,070.27	12	3, V	19,717.33	a^3H_5–$y^3H_5^0$	(0.00) 1.02	(0.00) 1.03
161	5,065.25	12	4, V	19,736.87	a^1H_5–$z^1H_5^0$	(0.00) 1.00	(0.00) 1.00
155	5,064.92	35	15, V	19,738.16	b^3F_3–$w^3G_4^0$	(0.00) 1.06	(**0.00**, 0.03, 0.07, 0.10) **0.95**, 0.98, 1.02, ---
156	5,060.42	12	3, V	19,755.71	$z^5G_4^0$–e^5F_3	(0.60*w*) 1.08	(**0.00**, 0.10, 0.20, 0.30) **0.85**, 0.95, 1.05, ---
	5,059.89	1		19,757.78			
	5,056.10	3		19,772.59			
155	5,046.61	25	10, V	19,809.77	b^3F_4–$w^3G_3^0$	(0.00) 1.25	(**0.00**, 0.05, 0.10 ---) **1.00**, 1.05, 1.10, ---
	5,037.43	1		19,845.87			
162	5,034.45	4		19,857.62	$z^3D_3^0$–e^3F_4		
150	5,032.42	2		19,865.63	c^3P_2–$v^3P_2^0$		
162	5,026.91	2		19,887.41	$z^3D_2^0$–e^3F_3		
150	5,011.47	4		19,948.67	c^3P_1–$v^3P_2^0$		
	5,002.16	2		19,985.80			
156	4,996.35	10	2, V	20,009.65	$z^5G_3^0$–e^5F_2	(0.00) 0.92 A[1]	(**0.00**, 0.08, 0.17), **0.75**, 0.83, 0.92, ---
158	4,994.77	12	5, IV	20,015.38	a^3H_6–$y^3H_6^0$	(0.00) 1.16	(0.00) 1.17
	4,992.45	1		20,024.68			
162	4,991.19	2 +Ti		20,029.74	$z^3D_1^0$–e^3F_2		
156	4,987.83	4		20,043.22	$z^5G_5^0$–e^5F_5		
	4,980.59	2		20,072.36			
163	4,968.17	2		20,122.54	a^5F_5–$y^7G_4^0$		
156	4,963.74	5		20,140.50	$z^5G_4^0$–e^5F_4		
158	4,962.30	5		20,146.34	a^3H_5–$y^3H_6^0$	(0.00*w*) 1.25	(**0.00**, 0.13, 0.27, ---) --- 1.57, 1.70, **1.83**
164	4,960.31	2		20,154.42	a^1G_4–$z^3H_5^0$		
	4,960.10	2		20,155.28			
	4,959.12	2		20,159.26			
165	4,956.90	2		20,168.29	$y^5G_2^0$–f^5G_2 / b^1G_4–$s^3F_4^0$		
166							
163	4,951.73	3		20,189.34	a^5F_4–$y^5G_3^0$		
	4,950.83	2		20,193.01			
	4,949.94	2		20,196.66			
167	4,948.77	6	2, V	20,201.42	a^3P_2–$y^1F_3^0$	(0.00) 1.06	(**0.00**, 0.50, 1.00) **0.00**, 0.50, 1.00, ---
165	4,943.48	1		20,223.04	$y^5G_3^0$–f^5G_3		
	4,939.93	3		20,237.57			
156	4,933.66	7	3, V	20,263.29	$z^5G_2^0$–e^5F_1		
168	4,932.45	1		20,268.26	a^3D_2–$y^5P_1^0$		
156	4,930.88	5		20,274.71	$z^5G_3^0$–e^5F_3		
165	4,925.03	1		20,298.80	$y^5G_4^0$–f^5G_4		
169	4,922.92	2		20,307.50	c^3P_2–$u^3P_2^0$		
170	4,922.23	4		20,310.34	a^3P_2–$w^3G_3^0$		
171	4,913.07	1		20,348.21	c^3F_3–$t^3F_3^0$		
	4,911.60	2		20,354.30			
172	4,910.78	3		20,357.70	a^5F_4–$z^5P_3^0$		
171	4,908.29	1		20,368.02	c^3F_2–$t^3F_2^0$		
	4,908.10	2		20,368.81			
173	4,905.09	4		20,381.31	a^5F_3–$y^5G_2^0$	(**0.00**, 0.86, 1.74)?	(**0.00**, 0.92, **1.83**) --- 1.25, 2.17, **3.08**
169	4,902.89	1		20,390.46	c^3P_1–$u^3P_2^0$		
156	4,894.18	4		20,426.74	$z^5G_2^0$–e^5F_2		
174	4,893.12	6	2, IV	20,431.18	a^3G_4–$v^3F_3^0$ / a^5F_4–$y^5G_3^0$		
173							
173	4,887.72	2		20,453.74	a^5F_5–$y^5G_4^0$		

TABLE 3.—*Wave lengths in the arc spectrum of Zr*—Continued

Key No.	λ I. A.	Intensities, temperature class, and notes		Wave No.	Term combinations	Observed Zeeman effects	Theoretical Zeeman effects
		B. S.	King				
165 174	4, 884. 12	3		20, 468. 82	$\left\{\begin{matrix} y^5G^0_5\text{–}f^5G_5 \\ a^3G_3\text{–}v^3F^0_2 \end{matrix}\right\}$		
163	4, 883. 61	8	5, II	20, 470. 96	$a^5F_4\text{–}y^5G^0_4$	(0. 96) 1. 10	(---, 0. 90, **1. 20**) ---, 0. 75, **1. 05, 1. 35**, 1. 65, ---
163	4, 881. 25	8	4, III	20, 480. 85	$a^5F_2\text{–}y^5G^0_3$	(0. 78, **1. 21**) 1. 14	(0. 50, 1. 00, **1. 50**) ---, 0. 25, **0. 75, 1. 25, 1. 75**, ---
165	4, 880. 66	1		20, 483. 33	$y^5G^0_6\text{–}f^5G_6$		
163 175	4, 866. 07	10	5, II	20, 544. 74	$\left\{\begin{matrix} a^5F_5\text{–}y^5G^0_5 \\ z^3F^0_4\text{–}e^3F_4 \end{matrix}\right\}$	(0. 87) 1. 25	(---, 0. 80, **1. 00**) ---, 1. 00, **1. 20, 1. 40**, 1. 60, ---
173	4, 851. 36	12	12, II	20, 607. 04	$a^5F_2\text{–}y^5G^0_2$	(0. 61, **1. 24**) **0. 31**, 0. 95, 1. 59	(0. 67, **1. 33**) **0. 33**, **1. 00**, 1. 67
	4, 850. 10	1		20, 612. 39			
172	4, 847. 67	1		20, 622. 72	$a^5F_2\text{–}z^5P^0_2$		
176	4, 846. 35	2		20, 628. 34	$a^1D_2\text{–}y^3G^0_3$		
156	4, 843. 84	1		20, 639. 02	$z^5G^0_4\text{–}e^5F_5$		
172	4, 841. 45	1		20, 649. 21	$a^5F_3\text{–}z^5P^0_3$		
177 156	4, 838. 99	4	2, V	20, 659. 71	$\left\{\begin{matrix} a^3G_4\text{–}u^3F^0_3 \\ z^5G^0_2\text{–}e^5F_4 \end{matrix}\right\}$ (0. 00) 1. 20		(0. 00, 0. 03, ---) **0. 95**, 0. 98, 1. 02, ---
177	4, 838. 77	5	4, IV	20, 660. 64	$a^3G_3\text{–}u^3F^0_2$	(0. 00) 0. 80	(**0. 00**, 0. 08, 0. 17) ---, 0. 75, **0. 83, 0. 92**
178	4, 832. 75	2		20, 686. 37	$a^5F_4\text{–}x^1F^0_3$		
163	4, 828. 05	10	10, II	20, 706. 53	$a^5F_2\text{–}y^5C^0_3$	(0. 00) 0. 61	(**0. 00**, 0. 25, 0. 50) **0. 25**, 0. 50, 0. 75, ---
173	4, 824. 29	12	12, II	20, 722. 67	$a^5F_3\text{–}y^5G^0_3$	(0. 90) 1. 11	(0. 33, 0. 67, **1. 00**) ---, 0. 58, **0. 92, 1. 25**, 1. 58, ---
179	4, 815. 77	2		20, 759. 34	$a^3D_3\text{–}w^3P^0_2$		
173	4, 815. 62	25	60, I	20. 759. 98	$a^5F_1\text{–}y^5G^0_2$	(**0. 00**, 0. 37) 0. 00, 0. 37, **0. 75***	(**0. 00**, 0. 33) 0. 00, 0. 33, 0. 67
163	4, 815. 05	12	12, II	20, 762. 43	$a^5F_3\text{–}y^5G^0_4$	(0. 00) 0. 85	(**0. 00**, 0. 20, ---) **0. 45**, 0. 65, 0. 85, ---
172	4, 811. 99	1		20, 775. 63	$a^5F_1\text{–}z^5P^0_2$		
177	4, 809. 48	10	8, IV	20, 786. 47	$a^3G_5\text{–}u^3F^0_4$	(0. 00) 1. 07	(**0. 00**, 0. 05, ---) **1. 00**, 1. 05, **1. 10**, ---
180	4, 807. 10	1		20, 796. 77	$a^1D_2\text{–}z^5P^0_3$		
177	4, 806. 68	3		20, 798. 58	$a^3G_4\text{–}u^3F^0_3$		
173	4, 805. 88	12	15, II	20, 802. 05	$a^5F_4\text{–}y^5G^0_4$	(**0. 70**) **1. 20**	(---, 0. 60, **0. 80**) ---, 0. 95, **1. 15, 1. 35**, 1. 55, ---
181	4, 803. 45	3		20, 812. 56	$a^5F_3\text{–}x^3F^0_2$		
	4, 802. 20	1		20, 817. 98			
182	4, 794. 95	4		20, 849. 44	$b^5F_4\text{–}v^3F^0_3$	(0. 00) **1. 35**	(**0. 00**, 0. 17, ---) ---, 1. 42, 1. 58, **1. 75**
179	4, 793. 27	4		20, 856. 76	$a^3D_2\text{–}w^3P^0_1$		
175	4, 793. 18	2		20, 857. 14	$z^5F^0_3\text{–}e^3F_3$		
172	4, 789. 12	5	2, III	20, 874. 86	$a^5F_2\text{–}z^5P^0_2$		
173	4, 788. 99	10	8, II	20, 876. 70	$a^5F_5\text{–}y^5G^0_5$	(0. 61) 1. 25	(---, 0. 53, **0. 67**) ---, 1. 13, **1. 27, 1. 40**, 1. 53, ---
163	4, 784. 94	12	12, II	20, 893. 10	$a^5F_4\text{–}y^5G^0_3$	(0. 00*w*) 0. 79	(**0. 00**, 0. 15, ---) **0. 60**, 0. 75, 0. 90, ---
	4, 783. 43	1		20, 899. 70			
181 183	4, 782. 59	3		20, 903. 35	$\left\{\begin{matrix} a^5F_4\text{–}x^3F^0_3 \\ a^5F_4\text{–}z^5G^0_4 \end{matrix}\right\}$		
	4, 775. 66	1		20, 933. 68			
184	4, 773. 23	0		20, 944. 34	$a^1G_4\text{–}x^3G^0_4$		
173	4, 772. 32	30	80, I	20, 948. 33	$a^5F_2\text{–}y^5G^0_2$	(0. 00) 0. 76*	(**0. 00**, 0. 08, 0. 17) **0. 75**, 0. 83, 0. 92, ---
185	4, 769. 65	2		20, 960. 06	$a^1D_2\text{–}x^3F^0_2$		
186	4, 762. 78	10	8, IV	20, 990. 29	$a^3H_6\text{–}z^3I^0_5$	(0. 00) 1. 01*	(**0. 00**, 0. 03, ---) ---, 0. 90, 0. 93, **0. 97**
182	4, 756. 94	1		21, 016. 04	$b^5F_2\text{–}v^3F^0_2$		
186	4, 753. 06	4	3, V	21, 033. 19	$a^3H_6\text{–}z^3I^0_7$	(0. 00) 1. 07	(**0. 00**, 0. 02, ---) **1. 00**, 1. 02, 1. 05, ---
181	4, 751. 90	3	2, IV	21, 038. 35	$a^5F_2\text{–}x^3F^0_2$	(0. 59) ?	(0. 33, **0. 67**) 0. 33, 0. 67, **1. 00**, 1. 33
187	4, 750. 98	1		21, 042. 44	$a^5F_3\text{–}z^1G^0_4$		
181	4, 749. 39	2		21, 049. 49	$a^5F_3\text{–}x^3F^0_3$		
188	4, 748. 70	1		21, 052. 54	$a^1D_2\text{–}x^3D^0_1$		
189	4, 742. 95	3		21, 078. 06	$b^5F_4\text{–}u^3F^0_3$		
173	4, 739. 48	45	100, I	21, 093. 48	$a^5F_3\text{–}y^5G^0_4$	(0. 00) 0. 84 A1*	(**0. 00**, 0. 10, ---) **0. 85**, 0. 95, 1. 05, ---
	4, 736. 96	2		21, 104. 71			
	4, 735. 10	1		21, 112. 99			

TABLE 3.—*Wave lengths in the arc spectrum of Zr*—Continued

Key No.	λ I. A.	Intensities, temperature class, and notes		Wave No.	Term combinations	Observed Zeeman effects	Theoretical Zeeman effects
		B. S.	King				
190	4, 734. 93	1		21, 113. 75	a^3P_1–$z^5P_1^0$		
191	4, 734. 37	3		21, 116. 24	a^1H_5–$y^1H_5^0$		
192	4, 732. 34	15	15, III	21, 125. 30	a^1D_2–$z^1F_3^0$	(00.0*w*) **0. 61,** 1.07*	(0. 00) 1. 00
193	4, 731. 14	3		21, 130. 66	a^3F_2–$x^3D_1^0$		
175	4, 723. 89	3		21, 163. 09	$z^3F_2^0$–e^3F_2		
	4, 720. 30	1		21, 179. 17			
186	4, 719. 12	10	10, V	21, 184. 48	a^3H_5–$z^3I_6^0$	(0.00) 1.05	(**0. 00,** 0.01, 0.02, ---) **0. 98,** 0.99, 1.00, ---
181	4, 717. 62	8	6, IV	21, 191. 22	a^5F_1–$x^5F_2^0$	(**0, 00,** 0. 70) 0. 00, **0. 70, 1.37**	(**0. 00,** 0. 67) 0. 00, 0. 67, **1. 33**
181	4, 716. 79	2		21, 194. 97	a^5F_3–$x^5F_3^0$		
178	4, 714. 86	1		21, 203. 65	a^5F_2–$x^1F_3^0$		
189	4, 713. 91	1		21, 207. 92	b^3F_3–$u^3F_3^0$		
194	4, 713. 43	5	2, IV	21, 210. 08	a^3H_4–$t^3F_4^0$		
189	4, 711. 91	7	8, V	21, 216. 90	b^3F_4–$u^3F_4^0$	(0. 30) 1. 20	(0. 00) 1. 25
173	4, 710. 08	45	100, I	21, 225. 16	a^5F_4–$y^5G_5^0$	(0. 00) 1. 06	(**0, 00,** 0. 08, 0. 17, ---) **0. 93,** 1. 02, 1. 10, ---
182	4, 707. 78	5	4, V	21, 235. 52	b^3F_3–$e^3F_3^0$	(0. 00) 1. 05*	(0. 00) 1. 08
	4, 704. 73	2		21, 249. 29			
195	4, 703. 59	2		21, 254. 44	a^3P_1–$y^5G_2^0$		
196	4, 702. 20	2		21, 260. 72	a^3G_3–$u^3D_2^0$		
197	4, 700. 83	1		21, 266. 91	c^3P_1–$s^3D_2^0$		
190	4, 700. 18	3		21, 269. 86	a^3P_1–$z^5P_2^0$		
	4, 700. 09	3		21, 270. 25			
183	4, 698. 14	1		21, 279. 08	a^3F_2–$z^3G_3^0$		
193	4, 697. 14	2		21, 283. 62	a^3F_1–$x^3D_1^0$		
197	4, 695. 04	3		21, 293. 14	c^3P_2–$s^3D_3^0$		
190					a^3P_0–$z^5P_1^0$		
193	4, 691. 73	3		21, 308. 15	a^3F_3–$x^3D_2^0$		
183	4, 688. 45	25	40, I	21, 323. 05	a^3F_4–$z^3G_5^0$	(0. 00) 1. 03	(**0. 00,** 0. 05, 0. 10, ---) **1. 00,** 1. 05, 1. 10, ---
173	4, 687. 80	50	150, I	21, 326. 02	a^5F_5–$y^5G_6^0$	(0. 00) 1. 06*	(**0. 00,** 0. 07, 0. 13, ---) **1. 00,** 1. 07, 1. 13, ---
182	4, 686. 57	2		21, 331. 60	b^3F_2–$v^3F_2^0$		
185	4, 684. 25	4	2, V	21, 342. 18	a^1D_2–$z^3F_3^0$		
182	4, 683. 43	10	15, V	21, 345. 91	b^3F_4–$v^3F_4^0$	(0. 00) 1. 08*	(0. 00) 1. 25
181	4, 667. 14	5	4, II	21, 420. 42	a^5F_2–$x^5F_3^0$	(0. 00) 1. 12	(**0. 00,** 0. 08, 0. 17) --- 1. 68, 1. 17, **1. 25**
198	4, 662. 97	2		21, 439. 58	a^1H_5–$u^3G_4^0$		
188	4, 659. 49	4		21, 455. 59	a^1D_2–$x^3D_2^0$		
199	4, 659. 20	2		21, 456. 93	a^3D_2–$t^3F_3^0$		
189	4, 657. 64	6	7, V	21, 464. 11	b^3F_3–$u^3F_3^0$	(0. 00) 1. 07*	(0. 00) 1. 03
196	4, 654. 37	3		21, 479. 19	a^3G_4–$u^3D_3^0$		
200	4, 644. 82	6	8, V	21, 523. 35	a^3D_3–$t^3D_3^0$	(0. 00) **0. 70***	(0. 00) 0. 67
189					b^3F_2–$u^3F_2^0$		
201	4, 640. 38	2		21, 543. 92	a^3P_2–$y^5G_3^0$		
202	4, 640. 12	3	2, V	21, 545. 15	a^3H_4–$x^1G_4^0$		
193	4, 634. 63	3		21, 570. 67	a^5F_4–$z^5D_4^0$		
183	4, 633. 99	30	50, I	21, 573. 67	a^5F_3–$z^5G_4^0$	(0. 00) 0. 98*	(**0. 00,** 0. 03, ---) **0. 95,** 0. 98, 1. 02, ---
189	4, 627. 70	2		21, 602. 99	b^3F_3–$u^3F_4^0$		
203	4, 626. 42	10	12, IV	21, 608. 92	a^3H_5–$z^3H_6^0$	(0. 00) 1. 04*	(0. 00) 1. 03
203	4, 624. 07	1		21, 619. 94	a^3H_5–$z^3H_5^0$		
204	4, 619. 56	0		21, 641. 04	a^3D_2–$y^5S_2^0$		
	4, 613. 35	3	1, IV	21, 670. 17			
187	4, 610. 77	2		21, 682. 29	a^5F_3–$z^1G_4^0$		
205	4, 610. 10	4	2, IV	21, 685. 44	a^3P_1–$x^5F_2^0$		
193	4, 609. 83	3		21, 686. 71	a^5F_1–$x^3D_2^0$		
181	4, 609. 28	3		21, 689. 29	a^5F_3–$x^3F_4^0$		
206	4, 609. 15	3		21, 689. 92	a^3G_4–$y^3H_5^0$		
190	4, 604. 42	10	8, III	21, 712. 18	a^3P_2–$z^5P_3^0$	(0. 00 *w*) 2. 11 A²	(**0. 00,** 0. 17, 0. 33) --- 1. 67, 1. 83, **2. 00**
203	4, 602. 57	12	15, IV	21, 720. 93	a^3H_6–$x^3H_5^0$	(0. 00) 1. 13*	(0. 00) 1. 17
	4, 601. 43	2		21, 726. 33			

TABLE 3.—*Wave lengths in the arc spectrum of Zr*—Continued

Key No.	λ I. A.	Intensities, temperature class, and notes		Wave No.	Term combinations	Observed Zeeman effects	Theoretical Zeeman effects
		B. S.	King				
182	4, 600. 27	3		21, 731. 79	b^3F_3–$v^3F^0_4$		
207	4, 590. 55	10	6, II	21, 777. 80	a^3P_1–$x^3D^0_1$	(1. 00) 0. 49, 1. 47	(1. 00) 0. 50, 1. 50
189	4, 590. 15	3		21, 779. 71	b^3F_2–$u^3F^0_3$		
208	4, 585. 72	2		21, 800. 74	a^1D_2–$w^3D^0_1$		
209	4, 584. 95	2		21, 804. 40	b^3F_2–$w^3D^0_1$		
203	4, 584. 57	1		21, 806. 21	a^3H_4–$x^3H^0_5$		
210	4, 584. 23	4	2, IV?	21, 807. 82	b^3F_3–$u^3D^0_2$		
203	4, 582. 29	5	3, V	21, 817. 05	a^3H_4–$x^3H^0_4$	(0. 00 *w*) 0. 73*	(0. 00) 0. 80
210	4, 576. 20	4	2, V	21, 846. 09	b^3F_2–$u^3D^0_1$	(0. 00) 0. 64	(**0. 00,** 0. 17) 0. 50, 0. 67, **0. 83**
183	4, 575. 52	25	40, I	21, 849. 33	a^3F_2–$z^3G^0_3$	(0. 00) 0. 83*	(**0. 00,** 0. 08, 0. 17) --- 0. 75, 0. 83, **0. 92**
203	4, 574. 94	2		21, 852. 09	a^3H_5–$x^3H^0_5$		
193	4, 572. 85	2		21, 862. 09	a^5F_3–$x^3D^0_3$		
211	4, 570. 59	1		21, 872. 92	a^5F_3–$w^3D^0_2$		
210	4, 565. 45	5	2, V	21, 897. 55	b^3F_4–$u^3D^0_3$	(0. 00) 0. 85	(**0. 00,** 0. 08, ---) **1. 00,** 1. 08, 1. 17, ---
212	4, 562. 54	1		21, 911. 51	a^3D_1–$v^3P^0_0$		
	4, 562. 12	3		21, 913. 51			
	4, 558. 69	3		21, 930. 01			
213	4, 558. 03	3	2, V	21, 933. 04	a^5P_2–$x^3F^0_3$		
206					a^3G_5–$y^3H^0_6$		
211	4, 556. 25	1		21, 941. 74	a^5F_4–$w^3D^0_3$		
209	4, 555. 52	10	8, V	21, 945. 27	b^3F_4–$w^5D^0_4$		
206					a^3G_4–$y^3H^0_5$		
206	4, 555. 12	10	10, V	21, 947. 20	a^3G_5–$y^3H^0_4$	(0. 00) 0. 80*	(**0. 00,** 0. 05, ---) ------ 0. 85, 0. 90, **0. 95**
207	4, 553. 01	10	12, II	21, 957. 36	a^3P_0–$x^3D^0_1$	(0. 00) 0. 51*	(0. 00) 0. 50
207	4, 550. 70	2		21, 968. 42	a^3P_2–$x^3D^0_2$		
214	4, 549. 62	1		21, 973. 73	a^3F_2–$z^3S^0_1$		
188	4, 542. 22	20	20, II	22, 009. 51	a^1D_2–$x^3D^0_3$	(0. 00) 1. 39*	(**0. 00,** 0. 33, 0. 67) --- 1. 33, 167, **2. 00**
208	4, 539. 98	8	4, II	22, 020. 37	a^1D_2–$w^3D^0_2$	(0. 00) 1. 22	(0. 17, **0. 33**) 0. 83, **1. 00, 1. 17,** 1. 33
211	4, 537. 60	1		22, 031. 92	a^5F_1–$w^3D^0_1$		
215	4, 535. 75	25	30, II	22, 040. 90	a^3P_2–$x^1F^0_3$	(0. 00*w*) 0. 67 A1*	(**0. 00,** 0. 50, 1. 00) **0. 00,** 0. 50, 1. 00, ---
216	4, 533. 67	2		22, 051. 02	b^1G_4–$v^1F^0_3$		
213	4, 526. 40	1		22, 086. 47	a^5P_1–$v^3F^0_2$		
193	4, 526. 12	3		22, 087. 83	a^5F_2–$x^3D^0_3$		
217	4, 524. 20	1		22, 097. 21	a^5P_2–$x^3S^0_1$		
211	4, 523. 91	3		22, 098. 60	a^5F_2–$w^3D^0_2$		
218	4, 523. 12	3		22, 102. 48	b^1G_4–$y^1H^0_5$		
219	4, 521. 93	2		22, 108. 29	b^3F_4–$y^3H^0_4$		
212	4, 515. 41	2		22, 140. 20	a^3D_2–$v^3P^0_1$		
220	4, 513. 34	2		22, 150. 36	a^3H_4–$v^3G^0_3$		
221	4, 511. 15	1		22, 161. 11	b^1D_2–$u^3G^0_3$		
222	4, 507. 26	2		22, 180. 23	a^3F_3–$y^1D^0_2$		
207	4, 507. 11	20	30, II	22, 180. 97	a^3P_1–$x^3D^0_2$	(0. 00, 0. 32) **0. 79,** 1. 13*	(**0. 00,** 0. 33) **0. 83,** 1. 17, 150
211	4, 496. 53	2		22, 233. 15	a^5F_3–$w^3D^0_3$		
220	4, 494. 93	3	2, IV	22, 241. 05	a^3H_5–$v^3G^0_4$		
211	4, 492. 80	1		22, 251. 60	a^5F_1–$w^3D^0_2$		
205	4, 491. 55	3	2, IV	22, 257. 78	a^3P_2–$x^3F^0_3$		
	4, 490. 38	3		22, 264. 08			
210	4, 486. 36	2		22, 283. 58	b^3F_3–$u^3D^0_3$		
223	4, 484. 71	1		22, 291. 77	a^3F_3–$z^1F^0_3$		
220	4, 482. 49	3	2, V	22, 302. 81	a^3H_6–$v^3G^0_5$	(0. 00) 1. 12	(**0. 00,** 0. 03, 0. 07, ---) 1. 00, 1. 03, 1. 07, ---
212	4, 480. 77	3	2, V	22, 311. 37	a^3D_3–$r^3P^0_2$	(0. 00) 1. 15	(**0. 00,** 0. 17, 0. 33) **1. 00,** 1. 17, 1. 33, ---
224	4, 478. 45	2		22, 322. 92	a^5F_5–$z^3H^0_5$		
206	4, 470. 55	10	15, III	22, 362. 36	a^3G_5–$y^3H^0_6$	(0. 00) 0. 98 A1*	(**0. 00,** 0. 03, 0. 07, ---) 1. 00, 1. 03, 1. 07, ---
219	4, 470. 31	6	5, IV	22, 363. 56	b^3F_4–$y^3H^0_5$		
224	4, 469. 50	2		22, 367. 61	a^5F_4–$z^3H^0_4$		

TABLE 3.—*Wave lengths in the arc spectrum of Zr*—Continued

Key No.	λ I. A.	Intensities, temperature class, and notes		Wave No.	Term combinations	Observed Zeeman effects	Theoretical Zeeman effects
		B. S.	King				
207	4,468.78	5	3, II	22,370.71	a^3P_2–$x^3D_3^0$	(0.00) 1.16	(0.33, **0.67**) 0.83, **1.17**, **1.50**, 183
225	4,468.22	3		22,374.02	a^5P_3–$w^5D_3^0$		
208	4,466.90	7	10, II	22,380.63	a^1D_2–$w^3D_3^0$	(0.00) 1.44*	(**0.00**, 0.33, 0.67) --- 1.33, 1.67, **2.00**
226	4,462.27	1		22,403.84	a^5P_2–$u^3F_3^0$		
227	4,460.33	1		22,413.60	a^1D_2–$x^1D_2^0$		
228	4,460.00	1		22,415.24	a^3D_1–$u^3P_0^0$		
229	4,459.02	4	2, II	22,420.17	a^3F_4–$y^3D_3^0$		
230 / 231	4,457.92	2		22,425.70	b^1G_4–$u^3G_3^0$ / a^3D_2–$s^3F_2^0$		
225	4,457.42	10 Zr II		22,428.23	a^5P_2–$w^5D_1^0$	(0.00, **1.31**) **1.36**, 2.10	(**0.00**, 0.33) 1.50, 1.83, **2.17**
220	4,456.29	6	3, IV	22,433.90	a^3H_5–$v^3G_4^0$	(0.50) 0.75	(--- 0.67, **0.83**) --- 0.87, **1.03**, **1.20**, 1.37, ---
220	4,455.43	5	2, IV	22,438.23	a^3H_6–$v^3G_4^0$	(0.75) 1.08	(--- 0.75, **1.00**) --- 0.55, **0.80**, **1.05**, 1.30, ---
211	4,451.34	1		22,458.84	a^5F_2–$w^3D_2^0$		
225	4,450.27	7	5, IV	22,464.24	a^5P_1–$w^5D_0^0$	(0.00) 2.49*	(0.00) 2.50
232 / 233	4,448.94	3	2, IV	22,471.00	a^1D_2–$y^3P_1^0$ / a^5P_2–$u^3D_1^0$		
234	4,448.00	3		22,475.75	b^1D_2–$x^1P_1^0$		
219	4,444.33	4	2, V	22,494.30	b^3F_3–$y^3H_4^0$		
235	4,438.04	8	8, II	22,526.17	a^3P_1–$w^3D_1^0$	(0.96) 0.50, 1.43	(1.00) 0.50, 1.50
236	4,436.76	3		22,532.67	a^3D_3–$v^3G_4^0$		
	4,436.08	1		22,536.17			
	4,435.84	2		22,537.34			
	4,435.48	1		22,539.17			
225	4,431.48	8	10, III	22,559.51	a^5P_1–$v^5D_1^0$	(1.01) 1.49, 2.49*	(1.00) 1.50, 2.50
237	4,431.11	3		22,561.40	c^3P_2–$x^1P_1^0$		
232	4,429.09	4	3, III	22,571.68	a^1D_2–$y^3P_2^0$	(0.44) 1.42	(0.50, **1.00**) 0.50, **1.00**, **1.50**, 2.00
238	4,428.86	1		22,572.85	$z^5F_5^0$–f^5F_4		
239	4,428.38	1		22,575.30	b^1D_2–$v^1F_3^0$		
240	4,427.24	6		22,581.12	a^1H_5–$w^1G_4^0$	(0.00) 0.99*	(0.00) 1.00
236	4,424.98	2		22,592.64	a^3D_2–$v^3G_3^0$		
233	4,423.27	1		22,601.37	a^5P_1–$u^3D_1^0$		
225	4,420.45	10	12, III	22,615.79	a^5P_2–$w^5D_2^0$	(0.35, **0.65**) 1.64B*	(0.33, **0.67**) 1.17, **1.50**, **1.83**, 2.17
241	4,420.25	1		22,616.81	a^5F_4–$w^3F_3^0$		
228	4,419.31	1		22,621.62	a^3D_2–$u^3P_1^0$		
241	4,418.25	3		22,627.04	a^5F_3–$w^3F_2^0$		
220	4,417.46	1		22,631.09	a^3H_4–$v^3G_3^0$		
241	4,415.85	5		22,639.34	a^5F_5–$w^3F_4^0$		
237	4,414.89	2		22,644.26	c^3P_1–$x^1P_1^0$		
242	4,414.14	4	2, II	22,648.20	a^5F_4–$y^3D_3^0$		
225	4,413.04	10	12, II	22,653.75	a^5P_3–$w^5D_3^0$	(0.47) 1.57*	(0.17, 0.33, **0.50**) --1.33, **1.50** **1.67**, 1.83, ---
212 / 224	4,411.92	2		22,659.55	a^3D_2–$v^3P_2^0$ / a^5F_3–$z^3H_4^0$		
243	4,411.62	2		22,661.10	c^3P_2–$v^1F_3^0$		
224	4,409.63	3		22,671.31	a^5F_4–$z^3H_5^0$		
244	4,408.32	1		22,678.05	a^3H_4–$s^3F_3^0$		
235	4,402.96	6	4, II	22,705.65	a^3P_0–$w^3D_1^0$		
235	4,400.89	1		22,716.33	a^3P_2–$w^3D_1^0$		
224	4,400.23	7	5, II	22,719.69	a^5F_5–$z^3H_6^0$	(0.00) 0.00*w*	(**0.00**, 0.23, 0.47, ---) **0.00**, 0.23, 0.47, ---
235	4,395.20	7	6, ?	22,745.72	a^3P_1–$w^3D_2^0$		
225	4,394.94	10	8, IV	22,747.08	a^5P_1–$w^5D_2^0$	(**0.00**, 0.97) **0.43**, 1.60	(**0.00**, 1.00) **0.50**, 1.50, 2.50
229	4,394.49	4	2, II	22,749.41	a^5F_3–$y^3D_2^0$		
222	4,394.29	2		22,750.44	a^3F_2–$y^1D_2^0$		
	4,392.73	2 Cb?		22,758.52			
231	4,390.15	2		22,771.88	a^3D_2–$s^3F_3^0$		
231 / 245	4,389.61	2		22,774.69	a^3D_3–$s^3F_2^0$ / a^1D_2–$w^3F_3^0$		
238	4,386.47	2		22,790.98	$z^5F_4^0$–f^5F_5		
	4,382.73	1		22,810.43			

TABLE 3.—*Wave lengths in the arc spectrum of Zr*—Continued

Key No.	λ I. A.	Intensities, temperature class, and notes		Wave No.	Term combinations	Observed Zeeman effects	Theoretical Zeeman effects
		B. S.	King				
238	4,380.75	1		22,820.73	$z^5F^\circ_4$–f^5F_5		
228	4,375.65	1		22,847.32	a^3D_1–$u^3P^\circ_1$		
246	4,373.07	5	2, V	22,860.83	a^5F_5–$x^5G^\circ_4$	(0.00) **2.10**	(**0.00**, 0.35, 0.70, ---) ---2.10 **2.45**, **2.80**
246	4,372.52	2		22,863.73	a^5F_4–$x^5G^\circ_3$		
	4,371.63	1		22,868.43			
212	4,368.41	2 Cb?		22,885.23	a^3D_1–$v^3P^\circ_2$		
225	4,366.45	10	15, II	22,895.51	a^5P_2–$w^5D^\circ_3$	(**0.00**, 0.38, 0.69) **0.80**, 1.15*	(**0.00**, 0.33, 0.67) **0.83**, 1.17, 1.17, 1.50, ---
	4,366.18	1		22,896.92			
	4,364.67	1		22,904.83			
212	4,361.94	2		22,919.16	a^3F_3–$y^3D^\circ_2$		
207	4,360.80	10	15, II	22,925.15	a^3P_2–$x^3D^\circ_3$	(0.00) 1.47*	(**0.00**, 0.17, 0.33) **1.00**, 1.17, 1.33, ---
244	4,359.25	1		22,933.31	a^3H_5–$s^3F^\circ_4$		
235	4,358.74	6	4, II	22,935.98	a^3P_2–$w^3D^\circ_2$	(0.00) **1.24***	(0.33, **0.67**) 0.83, **1.17**, **1.50** 1.83
	4,353.91	4		22,961.43			
	4,350.56	1		22,979.11			
233	4,350.07	4		22,981.69	a^5P_3–$u^5D^\circ_3$		
	4,349.39	1		22,985.29			
241	4,348.93	4	2, IV	22,987.72	a^5F_4–$w^5F^\circ_4$	(0.69) **1.11**	(--- 0.30, **0.40**) --- 1.15, **1.25**, **1.35**, 1.45, ---
	4,348.10	2		22,992.11			
247	4,347.89	25	30, II	22,993.21	a^1G_4–$y^1G^\circ_4$	(**0.00**) **1.01***	(0.00) 1.00
	4,347.37	2		22,995.96			
248	4,347.23	3	2, IV	22,996.70	a^3F_3–$y^3F^\circ_3$		
231	4,346.53	5	4, IV	23,000.41	a^3D_1–$s^3F^\circ_2$	(0.00) **0.76**	(**0.00**, 0.17) 0.50, 0.67, 0.83
241	4,345.58	2		23,005.43	a^3F_1–$w^3F^\circ_2$		
249	4,345.05	1		23,008.24	a^3G_5–$z^3I^\circ_5$		
	4,344.92	1		23,008.92			
238	4,343.40	2		23,016.99	$z^5F^\circ_4$–f^5F_4		
229	4,343.04	4	4, II	23,018.90	a^3F_2–$y^3D^\circ_1$	(0.00) **0.95**	(**0.00**, 0.17) 0.50, 0.67, 0.83
249	4,342.65	1		23,020.95	a^3G_4–$z^3I^\circ_5$		
248	4,341.49	1		23,027.10	a^3F_3–$y^3F^\circ_3$		
225	4,341.13	20	20, II	23,029.00	a^5P_3–$w^5D^\circ_4$	(0.00 *w*) **1.06A**1*	(**0.00**, 0.17, ---) **1.00**, 1.17, 1.33, ---
250	4,338.11	1		23,045.03	a^3G_4–$f^3F^\circ_3$		
245	4,336.11	2		23,055.71	a^1D_2–$w^5F^\circ_3$		
229	4,329.56	3	3, II	23,090.58	a^3F_3–$y^3D^\circ_3$		
246	4,325.44	10	15, II	23,112.56	a^5F_5–$x^5G^\circ_6$		
231	4,324.03	5	4, IV	23,120.10	a^3D_2–$s^3F^\circ_3$	(0.00) **0.95**	(**0.00**, 0.08, 0.17) **0.92**, 1.00, 1.08, ---
251	4,323.90	2		23,120.80	b^3F_2–$y^3P^\circ_2$		
244	4,322.23	0		23,129.73	a^3H_4–$s^3F^\circ_4$		
241	4,321.44	2		23,133.96	a^5F_2–$w^5F^\circ_2$		
242	4,321.17	6	4, II	23,135.41	a^5F_4–$y^5D^\circ_4$		
252	4,319.05	5	3, IV	23,146.76	a^3F_4–$y^1F^\circ_3$	(0.00) **1.12**	(**0.00**, 0.25, ---)---1.50, 1.75, **2.00**
	4,313.98	1		**23,173.95**			
253	4,310.48	1		23,192.76	a^3P_2–$y^3H^\circ_3$		
254	4,309.82	4	3, IV	23,196.31	a^3P_1–$y^3P^\circ_1$	(0.00) **1.44**	(0.00) 1.50
	4,309.10	3		23,200.19			
246	4,307.42	0		23,209.24	a^5F_4–$x^5G^\circ_4$		
255	4,307.22	1		23,210.31	b^3F_2–$w^1D^\circ_2$		
	4,305.03	2		23,222.11			
231 233 254	4,304.68	8	8, III	23,224.00	a^3D_3–$s^3F^\circ_4$ a^3P_2–$u^3D^\circ_3$ a^3P_1–$y^3F^\circ_2$	(0.00) 1.01* (0.00) **1.46***	(**0.00**, 0.08, ---) 1.00, 1.08, 1.17, --- (0.00) 1.50
250	4,303.75	0		23,229.02	a^3G_5–$z^3F^\circ_4$		
238	4,303.38	1		23,231.07	$z^5F^\circ_5$–f^5F_5		
256	4,302.88	15	15, II	23,233.71	a^5F_5–$y^5F^\circ_4$	(0.00) **1.53***	(**0.00**, 0.05, 0.10, ---)---1.50, **1.55**, **1.60**
238	4,302.57	3		23,235.39	$z^5F^\circ_4$–f^5F_3		
250	4,301.58	3		23,240.79	a^3G_4–$z^3F^\circ_4$		
	4,298.92	2		23,255.16			
	4,295.17	2		23,275.46			

TABLE 3.—*Wave lengths in the arc spectrum of Zr*—Continued

Key No.	λ I. A.	Intensities, temperature class, and notes		Wave No.	Term combinations	Observed Zeeman effects	Theoretical Zeeman effects
		B. S.	King				
256	4, 294. 78	18	20, II	23, 277. 58	a^5F_4–$y^5F^0_5$	(0. 00) 1. 51 A[3]*	(**0. 00**, 0. 10, 0. 20, 0. 30) ---1. 45, 1. 55, **1. 65**
241	4, 294. 47	3	2, IV	23, 279. 23	a^5F_3–$w^5F^0_4$		
235	4, 291. 34	6	8, III	23, 296. 21	a^5P_2–$w^5D^0_3$	(0. 00) 1. 47*	(**0. 00**, 0. 17, 0. 33) **1. 00**, 1. 17, 1. 33, ---
254	4, 291. 18	5	5, II	23, 297. 10	a^5P_1–$y^5P^0_2$	(0. 00) 1. 45*	(0. 00) 1. 50
	4, 290. 44	2		23, 301. 11			
257	4, 290. 20	4		23, 302. 42	a^1D_2–$x^3G^0_3$		
250					a^3G_3–$t^5F^0_4$		
242	4, 287. 20	1		23, 318. 72	a^5F_3–$y^5D^0_3$		
229	4, 286. 96	2		23, 320. 03	a^5F_2–$y^5D^0_2$		
258	4, 285. 24	2		23, 329. 37	b^1D_2–$r^1D^0_2$		
259					a^3P_2–$x^1D^0_2$		
	4, 284. 73	3		23, 332. 16			
256	4, 282. 20	15	20, II	23, 345. 94	a^5F_3–$y^5F^0_2$	(0. 00) 1. 54, **1. 77***	(**0. 00**, 0. 25, 0. 50) ---1. 25, 1. 50, **1. 75**
260	4, 282. 03	3		23, 346. 87	$z^5F^0_3$–e^5G_4		
261	4, 280. 31	4		23, 356. 24	a^3H_6–$z^1I^0_6$		
254	4, 276. 71	5	5, III	23, 375. 90	a^3P_0–$y^3P^0_1$	(0. 00) 1. 50	(0. 00) 1. 50
254	4, 274. 76	7	5, III	23, 386. 56	a^3P_2–$y^3P^0_1$	(0. 00) 1. 08	(0. 00) 1. 50
249	4, 272. 25	3		23, 400. 30	a^3G_5–$z^3I^0_6$		
262	4, 269. 62	3		23, 414. 71	c^3P_2–$e^1D^0_2$		
256	4, 268. 01	15	20, II	23, 423. 54	a^5F_2–$y^5F^0_1$	(**0. 00**, 0. 98) 0. 00, 0. 99, **1. 98***	(**0. 00**, 1. 00) 0. 00, 1. 00, **2. 00**
238	4, 267. 30	1		23, 427. 43	$z^5F^0_2$–f^5F_3		
248	4, 265. 75	3		23, 435. 94	a^3F_3–$y^3F^0_4$		
263	4, 265. 13	1		23, 439. 34	b^3F_4–$z^3I^0_5$		
	4, 264. 02	2		23, 445. 45			
	4, 261. 92	1		23, 457. 00			
264	4, 261. 42	4	3, V	23, 459. 78	a^3G_4–$t^3D^0_3$		
246	4, 261. 20	4	4, III	23, 460. 96	a^5F_4–$z^3G^0_5$		
265	4, 260. 77	2		23, 463. 32	b^5F_4–$t^5F^0_5$		
260	4, 260. 38	1		23, 465. 48	$z^5F^0_3$–e^5G_3		
272	4, 258. 32	1		23, 476. 88	c^3P_1–$t^3P^0_2$		
261	4, 256. 44	5	4, III	23, 487. 24	a^3H_5–$z^3I^0_6$	(0. 24) **1. 35**	(0. 00) 1. 50
254					a^3P_2–$y^3P^0_2$		
242	4, 256. 04	2	1, IV	23, 489. 46	a^3F_2–$y^5D^0_3$		
	4, 255. 86	1		23, 490. 42			
271	4, 255. 32	1		23, 493. 42	a^1D_2–$y^5F^0_2$		
270	4, 253. 56	5	4, IV	23, 503. 13	a^5P_3–$y^5P^0_3$	(0. 00) 1. 96 A[3]	(**0. 00**, 0. 17, 0. 33) **1. 33**, 1. 50, 1. 67, ---
265	4, 243. 56	3		23, 558. 51	b^3F_3–$t^3F^0_4$	(0. 00) **1. 30**	(**0. 00**, 0. 42, 0. 83) ---1. 08, 1. 50, **1. 92**
266	4, 242. 61	2		23, 563. 79	a^3G_5–$x^1G^0_4$		
267	4, 242. 01	3	2, IV	23, 567. 12	b^1G_4–$w^1G^0_4$		
248					a^3F_2–$y^3F^0_3$		
256	4, 241. 68	18	80, II	23, 568. 96	a^5F_3–$y^5F^0_4$	(0. 00) 1. 26*	(0. 00) 1. 25
268	4, 241. 43	3 Cb?		23, 570. 34	a^1H_5–$x^1H^0_5$		
256	4, 241. 20	15	50, II	23, 571. 62	a^5F_2–$y^5F^0_2$	(0. 00) 1. 01*	(0. 00) 1. 00
256	4, 240. 35	18	50, II	23, 576. 34	a^5F_1–$y^5F^0_1$	(0. 00) 0. 00*	(0. 00) 0. 00
256	4, 239. 31	25	150, II	23, 582. 13	a^5F_4–$y^5F^0_4$	(0. 00) 1. 32*	(0. 00) 1. 35
	4, 238. 34	3		23, 587. 52			
269	4, 237. 42	6	4, IV	23, 592. 64	a^5P_2–$w^1D^0_2$	(0. 00) 1. 96	(**0. 00**, 0. 17, 0. 33) **1. 33**, 1. 50, 1. 67, ---
238	4, 237. 19	4		23, 593. 92	$z^5F^0_2$–f^5F_2		
248	4, 236. 56	5		23, 597. 43	a^3F_2–$y^3F^0_2$		
270	4, 236. 04	7	6, III	23, 600. 32	a^5P_2–$y^5P^0_1$	(**0. 00**, 0. 62) **1. 24**, 1. 84*	(**0. 00**, 0. 67) **1. 17**, 1. 83, 2. 50
	4, 235. 04	1		23, 605. 89			
273	4, 234. 63	8	7, II	23, 608. 18	a^1D_2–$x^3P^0_1$	(0. 00*w*) 1. 13*	(**0. 00**, 0. 50) **0. 50**, 1. 00, 1. 50
	4, 232. 08	2		23, 622. 40			
256	4, 227. 76	30	200, II	23, 646. 56	a^5F_3–$y^5F^0_3$	(0. 00) 1. 37*	(0. 00) 1. 40
265	4, 225. 49	4		23, 659. 25	b^5F_4–$t^5F^0_4$	(0. 00) 1. 41	(0. 00) 1. 25
229	4, 225. 25	3		23, 660. 58	a^3F_2–$y^3D^0_3$		
274					a^5F_1–$x^3P^0_2$		
260	4, 224. 65	4	2*n*, V	23, 663. 94	$z^5F^0_3$–e^5G_4		

TABLE 3.—*Wave lengths in the arc spectrum of Zr*—Continued

Key No.	λ I. A.	Intensities, temperature class, and notes		Wave No.	Term combinations	Observed Zeeman effects	Theoretical Zeeman effects
		B. S.	King				
274	4, 220. 65	3	2, III	23, 686. 41	a^5F_2–$x^5P^\circ_1$		
275	4, 219. 94	0		23, 690. 40	a^3P_2–$w^3F^\circ_2$		
276	4, 218. 44	6	6, III	23, 698. 79	a^1D_2–$v^3D^\circ_1$	(0. 00) 1. 68	(**0. 00,** 0. 50) 0. 50, 1. 00, **1. 50**
260	4, 217. 25	3		23, 705. 50	$z^5F^\circ_4$–$e^5G^\circ_5$		
264	4, 215. 31	1		23, 716. 41	a^3G_3–$t^3D^\circ_3$		
271					a^1D_2–$y^5F^\circ_3$		
256	4, 213. 86	10	15, III	23, 724. 55	a^5F_1–$y^5F^\circ_2$	(**0. 00,** 0. 98) 0. 00, 0. 99, **2. 00***	(**0. 00,** 1. 00) 0. 00, 1. 00, **2. 00**
270	4, 212. 63	4		23, 731. 49	a^5P_1–$y^5P^\circ_1$		
277	4, 212. 16	1		23, 734. 14	a^5F_4–$v^5D^\circ_3$		
278	4, 211. 34	4		23, 738. 76	a^3D_3–$s^3D^\circ_3$	(0. 00) 1. 41	(0. 00) 1. 33
260	4, 208. 09	3		23, 757. 09	$z^5F^\circ_3$–$e^5G^\circ_4$		
256	4, 201. 45	18	20, III	23, 794. 63	a^5F_2–$y^5F^\circ_3$	(0. 00*w*) 1. 69 A?*	(**0. 00,** 0. 25, 0. 50) 1. 25, 1. 50, **1. 75**
273	4, 199. 08	15	20, III	23, 808. 05	a^1D_2–$x^3P^\circ_2$	(0. 42) 1. 39 B*	(0. 50, **1. 00**) 0. 50, **1. 00, 1. 50,** 2. 00
279	4, 197. 76	2		23, 815. 53	b^3F_2–$w^3P^\circ_2$		
280	4, 196. 14	4		23, 824. 73	a^3G_3–$x^3H^\circ_3$		
270	4, 194. 76	8	10, V	23, 832. 57	a^5P_3–$y^5P^\circ_3$	(0. 00) 1. 66*	(0. 00) 1. 67
269	4, 194. 46	2		23, 834. 27	a^5P_2–$w^1D^\circ_2$		
280	4, 194. 01	3		23, 836. 83	a^3G_4–$x^3H^\circ_3$		
280	4, 192. 10	4		23, 847. 68	a^3G_4–$x^3H^\circ_4$		
265	4, 191. 80	5		23, 849. 38	b^3F_3–$t^3F^\circ_3$	(0. 00) 1. 03	(0. 00) 1. 08
265	4, 187. 56	15	20, III	23, 873. 59	b^3F_2–$t^3F^\circ_2$	(0. 00) 1. 64*	(**0. 00,** 0. 10, ---) 1. 45, 1. 55, **1. 65**
256					a^5F_3–$y^5F^\circ_4$		
270	4, 187. 12	3		23, 876. 06	a^5P_1–$y^5P^\circ_2$	(0. 00) 0. 32*	(**0. 00,** 0. 67) **1. 17,** 1. 83, 2. 50
281	4, 186. 79	3		23, 877. 98	b^5F_4–$t^5D^\circ_3$		
	4, 186. 05	1		23, 882. 20			
282	4, 183. 31	6	10, III	23, 897. 80	a^1D_2–$z^1P^\circ_1$	(**0. 00,** 0. 47) 1. 26, **1. 76***	(0. 00) 1. 00
278	4, 179. 07	1		23, 922. 07	a^3D_2–$s^3D^\circ_1$		
276	4, 173. 13	2		23, 956. 11	a^1D_2–$v^3D^\circ_2$		
269	4, 171. 47	6		23, 965. 64	a^5P_1–$w^1D^\circ_2$	(0. 00, 1. 07) 0. 29*	(**0. 00,** 1. 50) **0. 50,** 1. 00, 2. 50
275	4, 170. 48	1		23, 971. 33	a^3P_2–$w^3F^\circ_3$		
283	4, 169. 67	1		23, 975. 99	a^5F_2–$z^1P^\circ_1$		
278	4, 169. 36	4		23, 977. 77	a^3D_2–$s^3D^\circ_2$		
	4, 168. 45	3		23, 983. 00			
284	4, 166. 51	4		23, 994. 17	b^5F_4–$x^1G^\circ_4$	(0. 00) 1. 35	(---0. 75, **1. 00**) ---0. 75, **1. 00, 1. 25,** 1. 50, ---
256	4, 166. 37	8	10, II	23, 994. 97	a^5F_5–$y^5F^\circ_5$	(0. 00) 1. 47*	(**0. 00,** 0. 05, 0. 10, ---) --- 1. 50, 1. 55, **1. 60**
285	4, 165. 63	1		23, 999. 23	a^3G_4–$w^1F^\circ_3$		
277	4, 159. 54	3		24, 034. 36	a^5F_2–$v^5D^\circ_2$		
265	4, 157. 70	1		24, 044. 99	b^5F_3–$t^5F^\circ_4$		
280	4, 153. 75	3		24, 067. 85	a^3G_3–$x^3H^\circ_3$		
270	4, 152. 64	7+Cb	10, IV	24, 074. 28	a^5P_2–$y^5P^\circ_2$	(0. 00) 1. 43	(**0. 00,** 0. 17, 0. 33) **1. 33,** 1. 50, 1. 67, ---
278	4, 150. 47	1		24, 086. 87	a^3D_2–$s^3D^\circ_3$		
280	4, 147. 36	3		24, 104. 98	a^3G_3–$x^3H^\circ_4$	(0. 00) 1. 08	(**0. 00,** 0. 05, ---) ---0. 85, 0. 90, **0. 95**
278	4, 140. 01	3		24, 147. 76	a^3D_1–$s^3D^\circ_1$	(0. 00) 0. 00*w*	(0. 00) 0. 50
276	4, 135. 68	6	10, II	24, 173. 02	a^1D_2–$v^5D^\circ_3$	(0. 00) 1. 41*	(**0. 00,** 0. 33, 0. 67) ---1. 33, 1. 67, **2. 00**
286	4, 134. 32	4		24, 180. 99	a^3G_4–$v^3G^\circ_3$	(0. 00) 1. 49	(**0. 00,** 0. 30, ---) ---1. 35, **1. 65, 1. 95**
287	4, 133. 70	2		24, 184. 62	a^3D_3–$r^3F^\circ_3$		
288	4, 133. 52	1		24, 185. 67	a^3H_5–$r^3F^\circ_4$		
278	4, 130. 46	2		24, 203. 58	a^3D_1–$s^3D^\circ_2$		
289	4, 128. 30	2		24, 216. 24	$z^5G^\circ_4$–$e^5H^\circ_4$		
290	4, 127. 97	4		24, 218. 18	a^3P_2–$x^3G^\circ_3$		
291					a^3P_1–$y^5F^\circ_2$		
292	4, 121. 67	3		24, 255. 18	b^5F_4–$x^3H^\circ_4$		
285	4, 121. 45	10	30, III	24, 256. 48	a^3G_3–$w^1F^\circ_3$	(0. 00)‡1. 51*	(0. 00) 1. 50
293					a^3P_1–$x^3P^\circ_0$		
281	4, 120. 16	2		24, 264. 07	b^5F_3–$t^3D^\circ_3$		
292	4, 119. 83	4		24, 266. 01	b^5F_4–$x^3H^\circ_4$		
289	4, 110. 66	2		24, 320. 13	$z^5G^\circ_5$–$e^5H^\circ_5$		
294					a^5P_1–$w^3P^\circ_1$		
293	4, 108. 39	8	15, III	24, 333. 62	a^3P_1–$x^3P^\circ_1$	(0. 00) 1. 48*	(0. 00) 1. 50

TABLE 3.—*Wave lengths in the arc spectrum of Zr*—Continued

Key No.	λ I. A.	Intensities, temperature class, and notes		Wave No.	Term combinations	Observed Zeeman effects	Theoretical Zeeman effects
		B. S.	King				
281	4, 107. 50	7	8, V	24, 338. 89	b^3F_3–$t^3D^0_2$	(0. 00) 0. 86*	(**0. 00,** 0. 08, 0. 17) **0. 92,** 1. 00, 1. 08, ---
252	4, 099. 31	4	4, III	24, 387. 51	a^3F_2–$y^1F^0_3$	(0. 00) 1. 70	(**0. 00,** 0. 33, 0. 67) ---1. 00, 1. 33, **1. 67**
295	4, 094. 26	5	3, II?	24, 417. 57	b^3F_4–$w^1F^0_3$	(0.00) 1. 31	(**0.00,** 0. 25, ---) ---, 1. 50, 1. 75, **2. 00**
296	4, 093. 16	3		24, 424. 14	a^3P_1–$v^3D^0_1$	(0. 00, **0.81**) **0. 60,** 1. 50	(1. 00) 0. 50, 1. 50
286	4, 090. 78	6	5, V	24, 438. 34	a^3G_3–$v^3G^0_3$	(0. 00) 0. 50	(0. 00) 0. 75
	4, 088. 20	2		24, 453. 76			
286	4, 087. 68	4	3, II	24, 456. 87	a^3G_5–$v^3G^0_4$	(0. 00) 1. 57	(**0.00,** 0. 15, ---) ---, 1. 50, 1. 65, **1. 80**
286	4, 085. 68	6		24, 468. 84	a^3G_4–$v^3G^0_4$		
287	4, 084. 29	5	4, IV	24, 477. 17	a^3D_3–$r^3F^0_2$	(0. 00) 1. 06*	(**0.00,** 0. 08, ---) **1.00,** 1. 08, 1. 17, ---
281	4, 083. 08	4	4, II	24, 484. 43	b^3F_2–$t^3D^0_1$	(0. 00) 0. 68*	(**0.00,** 0. 17) 0. 50, 0. 67, **0. 83**
297	4, 082. 29	4	3, II	24, 489. 16	a^3F_4–$y^3G^0_3$		
298	4, 081. 22	40	100, II	24, 495. 59	a^5F_5–$x^5D^0_4$	(0. 00*w*) 1. 08A1*	('**0. 00,** 0. 10, ---) **1. 00,** 1. 10, 1. 20, ---
293	4, 078. 31	7	12, II	24, 513. 06	a^3P_0–$x^3P^0_1$	(0. 00) 1. 42*	(0. 00) 1. 50
293	4, 076. 53	5	10, III	24, 523. 75	a^3P_2–$x^3P^0_1$	(0. 00) 1. 13	(0. 00) 1. 50
287	4, 075. 05	4		24, 532. 65	a^3D_2–$r^3F^0_2$		
293	4, 074. 93	6	15, II	24, 533. 40	a^3P_1–$x^3P^0_2$	(0. 00) 1. 50	(0. 00) 1. 50
303	4, 074. 35	1		24, 536. 87	a^1H_5–$q^3F^0_4$		
298	4, 072. 71	30	100, II	24, 546. 75	a^5F_4–$x^5D^0_3$	(0. 00) 1. 14	(**0. 00,** 0. 15, ---) **0. 90,** 1. 05, 1. 20, ---
	4, 069. 53	1		24, 565. 98			
294	4, 068. 71	5	4, II	24, 570. 93	a^5P_1–$w^3P^0_2$	(**0. 00,** 1. 01) 0. 44, 1. 40	(**0. 00,** 1. 00) **0. 50,** 1. 50, 2. 50
298	4, 064. 16	30	100, II	24, 598. 41	a^5F_3–$x^5D^0_2$	(0. 00) 0. 95	(**0. 00,** 0. 25, 0. 50) **0. 75,** 1. 00, 1. 25, ---
296	4, 063. 32	2		24, 603. 51	a^3P_0–$v^3D^0_1$		
	4, 062. 65	4		24, 607. 55			
296	4, 061. 53	10	15, II	24, 614. 33	a^3P_2–$v^3D^0_1$	(**0. 00,** 0. 46) 1. 60	(**0. 00,** 1. 00) 0. 50, 1. 50, **2. 50**
299	4, 060. 58	4	4, IV	24, 620. 09	a^3G_3–$s^3F^0_2$	(0. 00) 0. 93	(**0. 00,** 0. 08, 0. 17) ---, 0. 75, 0. 83, **0. 92**
300	4, 060. 08	3	2, IV	24, 623. 14	a^3P_1–$z^1P^0_1$		
	4, 059. 23	1		24, 628. 29			
301	4, 058. 98	5		24, 629. 82	a^5P_1–$t^3F^0_2$		
291	4, 058. 63	3	3, IV	24, 631. 93	a^3P_2–$y^5F^0_3$	(0. 00) 0. 80	(**0. 00,** 0. 25, 0. 50) **0. 75,** 1. 00, 1. 25, ---
	4, 057. 06	3		24, 641. 47			
272	4, 056. 50	3		24, 644. 87	c^5P_2–$t^3P^0_2$		
286	4, 055. 71	10	20, V	24, 649. 66	a^3G_5–$v^3G^0_5$	(0. 00) 1. 19	(0. 00) 1. 20
292	4, 055. 30	2		24, 652. 16	b^3F_3–$z^3H^0_4$		
298	4, 055. 03	20	60, II	24, 653. 79	a^5F_2–$x^5D^0_1$	(**0. 00,** 0. 48) **0. 48,** 1. 00	(**0. 00,** 0. 50) **0. 50,** 1. 00, 1. 50
302	4, 054. 43	6	10, II	24, 657. 44	a^3F_4–$z^5P^0_3$	(0. 00) 0. 50	(**0. 00,** 0. 42, ---) **0. 00,** 0. 42, 0. 83, ---
286	4, 053. 67	2		24, 662. 07	a^3G_4–$v^3G^0_3$		
	4, 052. 99	3		24, 666. 21			
296	4, 050. 48	5	10, II	24, 681. 48	a^3P_1–$v^3D^0_2$		
299	4, 046. 08	3		24, 708. 32	a^3G_4–$s^3F^0_3$		
298	4, 044. 57	12	25, II	24, 717. 54	a^5F_1–$x^5D^0_0$	(0. 00) 0. 00	(0. 00) 0. 00
293	4, 043. 57	15	30, II	24, 723. 65	a^3P_2–$z^3P^0_2$	(0. 49) 1. 33	(0. 00) 1. 50
304	4, 042. 23	7	10, IV	24, 731. 84	a^5P_3–$y^5S^0_2$	(0. 00) 1. 24	(**0. 00,** 0. 33, 0. 67) **1. 00,** 1. 33, 1. 67, ---
289 / 305	4, 041. 63	4	5, IV	24, 735. 53	$z^5G^0_3$–e^5H_4 / a^3H_6–$y^1H^0_5$	(0. 00) 1. 48	(**0. 00,** 0. 17, ---) ---, 1, 67, 1. 83, **2. 00**
297	4, 035. 89	15	40, II	24, 770. 69	a^3F_4–$y^3G^0_4$	(0. 60) 1. 17	(---, 0. 60, **0. 80**) ---, 0. 85, **1. 05, 1. 25,** 1. 45, ---
	4, 033. 56	2		24, 784. 99			
301	4, 032. 78	3		24, 789. 79	a^5P_2–$t^3F^0_3$		
	4, 032. 47	2		24, 791. 69			
300	4, 030. 75	3	3, IV	24, 802. 62	a^3P_0–$z^1P^0_1$	(0. 00) 0. 86	(0. 00) 1. 00
298	4, 030. 03	15	5, II	24, 806. 63	a^5F_1–$x^5D^0_1$		
300	4, 028. 95	7	15, III	24, 813. 37	a^3P_2–$z^1P^0_1$	(0. 00) 1. 57	(**0. 00,** 0. 50) 1. 00, 1. 50, **2. 00**
	4, 027. 31	2		24, 823. 51			
298	4, 027. 20	20	15, II	24, 824. 03	a^5F_2–$x^5D^0_2$	(0. 98) 0. 73, **1. 23,** 1. 75	(0. 50, **1. 00**) 0. 50, **1. 00, 1. 50,** 2. 00

TABLE 3.—*Wave lengths in the arc spectrum of Zr*—Continued

Key No.	λ I. A.	Intensities, temperature class, and notes		Wave No.	Term combinations	Observed Zeeman effects	Theoretical Zeeman effects
		B. S.	King				
298	4, 024. 92	18	15, II	24, 838. 22	a^5F_3–$x^5D_3^0$	(0. 66) 1. 25	(0. 25, 0. 50, **0. 75**) ---, 1. 00, **1. 25, 1. 50**, 1. 75, ---
298	4, 023. 99	15	30, II	24, 843. 96	a^5F_4–$x^5D_4^0$	(0. 50) 1. 39	(---, 0. 45, **0. 90**) ---, 1. 20, **1. 35, 1. 50**, 1. 65, ---
306	4, 023. 29	2		24, 848. 30	b^3F_2–$e^3P_1^0$		
	4, 023. 04	3		24, 849. 85			
307	4, 021. 01	1		24, 862. 39	$z^5G_5^0$–e^5G_4		
	4, 018. 13	2		24, 880. 20			
308	4, 017. 00	5	8, IV	24, 887. 19	b^3F_4–$z^3G_4^0$	(0. 39) 1. 01	(---, 0. 60, **0. 80**) ---, 0. 85, **1. 05, 1. 25**, 1. 45, ---
289	4, 012. 25	6	12, IV	24, 916. 65	$z^5G_4^0$–e^5H_5	(0. 00) 0. 85	(**0. 00**, 0. 05, ---) **0. 90**, 0. 95, 1. 00, ---
	4, 009. 39	2		24, 934. 43			
309	**4, 007.** 59	8	15, IV	24, 945. 62	a^3H_5–$u^3G_4^0$	(0. 00) 0. 97	(**0. 00**, 0. 02, ---) **0. 97**, 0. 98, 1. 00 ---
307 310	4, 004. 87	4	4*n*, IV	24, 962. 57	$z^5G_6^0$–e^5G_6 a^5P_3–$t^3D_3^0$	(0. 00) 1. 41	(0. 00) 1. 33
299	4, 004. 39	4	4, IV	24, 965. 56	a^3G_3–$s^3F_3^0$	(0. 71) 0. 90	(0. 33, 0. 67, **1. 00**) ---, 0. 42, **0. 75, 1. 08**, 1. 42, ---
304	4, 003. 09	6	12, IV	24, 973. 66	a^5P_2–$y^5S_2^0$	(0. 26) 1. 85	(0. 17, **0. 33**) 1. 67, **1. 83, 2. 00**, 2. 17
298	4, 002. 55	5	8, IV	24, 977. 04	a^5F_1–$x^3D_2^0$		
308	4, 001. 22	2	2, V	24, 985. 32	b^3F_3–$z^3G_3^0$		
311	4, 001. 09	3	4, IV	24, 986. 13	a^3F_4–$z^1F_3^0$		
312	3, 992. 46	1		25, 040. 12	a^3D_2–$u^3G_3^0$		
	3, 992. 05	1		25, 042. 70			
309	3, 989. 50	6	12, V	25, 058. 74	a^3H_6–$u^3G_5^0$	(0. 00) 1. 20	(**0. 00**, 0. 03, ---) **1. 00**, 1. 03, 1. 07, ---
313	3, 989. 29	4	7, III	25, 060. 05	a^3F_3–$y^3G_3^0$		
305 298	3, 988. 68	5	10, IV	25, 063. 88	a^3H_4–$y^1H_5^0$ a^3F_2–$z^5D_1^0$		
302	3, 986. 80	4	5, V	25, 075. 71	a^3F_3–$z^5P_2^0$		
308	3, 986. 14	2		25, 079. 86	b^3F_4–$v^3G_5^0$		
296	3, 984. 75	8	20, III	25, 088. 57	a^3P_2–$v^3D_3^0$	(0. 00) 1. 41	(**0. 00**, 0. 17, 0. 33) **1. 00**, 1. 17, 1. 33, ---
304	3, 982. 16	4	5, V	25, 104. 92	a^5P_1–$y^5S_2^0$		
310 289	3, 981. 59	10	20*n*, IV	25, 108. 53	a^3P_2–$t^3D_1^0$ z^5G_6–e^5H_7	(0. 00) 1. 21	(**0. 00**, 0. 05, ---) **1. 00**, 1. 05, 1. 10, ---
314 289	3, 978. 73	6	30*n*, III	25, 126. 57	b^3F_4–$s^3F_3^0$ $z^5G_5^0$–e^5H_5	(0. 00) 1. 32	(**0. 00**, 0. 17, ---) ---, 1. 42, 1. 58, **1. 75**
	3, 978. 26	3	2, V	25, 129. 53		(0. 00) 0. 94	
315	3, 977. 47	7	15, III	25, 134. 53	a^1G_4–$e^3F_3^0$	(0. 00) 0. 95	(**0. 00**, 0. 08, ---) **0. 75**, 0. 83, 0. 92, ---
298	3, 977. 32	3	3, V	25, 135. 47	a^5F_2–$z^5D_1^0$		
309	3, 976. 17	2		25, 142. 74	a^3H_4–$u^3G_4^0$		
299	3, 975. 29	7	15, IV	25, 148. 31	a^3G_3–$s^3F_4^0$	(0. 60) 1. 10	(**0. 00**, 0. 05, ---) **1. 00**, 1. 05, 1. 10, ---
	3, 974. 20	2		25, 155. 20			
297	3, 973. 51	15	60, II	25, 159. 58	a^3F_3–$y^3G_3^0$	(0. 51) 1. 03	(0. 33, 0. 67, **1. 00**) --- 0. 42, **0. 75, 1. 08, 1. 42**, ---
299	3, 973. 39	3		25, 160. 33	a^3G_4–$s^3F_4^0$		
307 314	3, 972. 30	3	3, V	25, 167. 24	$z^5G_4^0$–e^5G_3 b^3F_3–$s^3F_3^0$		
	3, 970. 45	3		25, 178. 96			
297	3, 968. 25	18	80, II	25, 192. 91	a^3F_4–$y^5G_5^0$	(0. 00) 1. 05	(**0. 00**, 0. 05, ---) **1. 00**, 1. 05, 1. 10, ---
316	3, 966. 65	8	6, II	25, 203. 07	a^3F_4–$x^3F_3^0$	(0. 00) 1. 52	(**0. 00**, 0. 17, ---) --- 1. 42, 1. 58, **1. 75**
307	3, 963. 79	5	2*n*, V	25, 221. 27	$z^5G_5^0$–e^5G_5		
	3, 957. 41	3		25, 261. 90			
	3, 956. 52	3		25, 267. 58			
	3, 955. 81	2		25, 272. 15			
308	3, 955. 64	2		25, 273. 23	b^3F_3–$z^3G_4^0$		
317	3, 952. 87	2		25, 290. 94	c^3P_2–$q^3D_2^0$		
308	3, 951. 33	2		25, 300. 82	b^3F_2–$v^3G_3^0$		
318	3, 941. 62	5	5, IV	25, 363. 13	a^1G_4–$u^3F_3^0$	(0. 00) 0. 91	(**0. 00**, 0. 08, ---) **0. 75**, 0. 83, 0. 92, ---
321 299	3, 933. 18	3	2, V	25, 417. 54	a^3D_2–$r^3D_3^0$ a^3G_2–$s^3F_3^0$		
297	3, 929. 53	30	150, II	25, 441. 15	a^3F_3–$y^3G_4^0$	(0. 00) 1. 03	(**0. 00**, 0. 03, ---) **0. 95**, 0. 98, 1. 02, ---

TABLE 3.—*Wave lengths in the arc spectrum of Zr*—Continued

Key No.	λ I. A.	Intensities, temperature class, and notes		Wave No.	Term combinations	Observed Zeeman effects	Theoretical Zeeman effects
		B. S.	King				
319	3, 927. 41	3		25, 454. 88	a^3D_2–$p^1F_3^0$		
307	3, 926. 78	5	3*n*, V	25, 458. 96	$z^5G_2^0$–e^5G_2	(0. 00) **1. 07**	(0. 00) 1. 15
307					$z^5G_4^0$–e^5G_4		
320	3, 924. 87	3		25, 471. 35	a^3P_1–$z^5D_2^0$		
320	3, 923. 46	3		25, 480. 50	a^3P_0–$z^5D_1^0$		
316	3, 921. 80	20	100, II	25, 491. 30	a^3F_3–$z^3F_3^0$	(0. 00) 1. 81	(**0. 00**, 0. 42, 0. 83) --- 1. 08, 1. 50, **1. 92**
313	3, 916. 64	6		25, 524. 89	a^3F_4–$y^5G_5^0$	(0. 00) 1. 28	(**0. 00**, 0. 02, ---) --- 1. 30, 1. 32, **1. 33**
	3, 906. 14	1		25, 593. 52			
307	3, 901. 49	3		25, 624. 01	$z^5G_3^0$–e^5G_3		
313	3, 900. 51	10		25, 630. 44	a^3F_2–$y^5G_2^0$	(0. 00) 0. 00 *w* A[2]	(0. 33, **0. 67**) 0. 00, **0. 33, 0. 67**, 1. 00
321	3, 898. 54	1		25, 643. 40	a^3D_1–$r^3D_2^0$		
321	3, 897. 65	4	3, V	25, 649. 25	a^3D_3–$r^3D_3^0$	(0. 00) 1. 29	
311	3, 896. 53	6	10, II	25, 656. 62	a^3F_3–$x^1F_3^0$	(0. 00) 1. 06	(0. 08, 0. 17, **0. 25**) 0. 83, 0. 92, **1. 00, 1. 08**, 1. 17, 1. 25
317					e^3P_2–$q^3D_3^0$		
322	3, 893. 84	3		25, 674. 34	a^3G_4–$s^3D_3^0$		
307	3, 892. 02	5	4*n*, IV	25, 686. 35	$z^5G_3^0$–e^5G_3	(0. 00) 1. 09	(0. 00) 0. 92
323	3, 891. 39	20	100, II	25, 690. 50	a^3F_4–$z^1G_4^0$	(0. 63) 1. 15	(--- 0. 75, **1. 00**) --- 0. 75, **1. 00, 1. 25**, 1. 50, ---
316	3, 890. 32	25	125, II	25, 697. 56	a^3F_4–$z^3F_4^0$	(0. 26) 1. 16	(0. 00) 1. 25
	3, 889. 00	3		25, 706. 28			
297	3, 885. 41	20	100, II	25, 730. 02	a^3F_2–$y^3G_3^0$	(0. 00) 1. 00	(**0. 00**, 0. 08, 0. 17) --- 0. 75, 0. 83, **0. 92**
324	3, 882. 39	2		25, 750. 04	a^3P_2–$r^3P_2^0$		
313	3, 879. 04	5	10, I*A*	25, 772. 30	a^3F_3–$y^5G_4^0$	(0. 00) 1. 21	(**0. 00**, 0. 07, ---) --- 1. 22, 1. 28, **1. 35**
325	3, 877. 60	12	40, IV	25, 781. 90	a^1G_4–$z^1H_5^0$	(0. 00) 1. 00	(0. 00) 1. 00
307	3, 872. 18	3		25, 817. 98	$z^5G_3^0$–e^5G_3		
322	3, 871. 38	2		25, 823. 31	a^3G_3–$s^3D_2^0$		
326	3, 864. 33	10	40, ?	25, 870. 41	a^3F_4–$z^3D_3^0$	(0. 00) 1. 19	(**0. 00**, 0. 08, ---) **1. 00**, 1. 08, 1. 17, ---
316	3, 863. 88	20	100, II	25, 873. 41	a^3F_3–$x^3F_3^0$	(0. 00) 1. 08	(0. 00) 1. 08
307	3, 863. 33	4		25, 877. 11	$z^5G_2^0$–e^5G_2		
	3, 860. 65	3		25, 895. 06			
313	3, 849. 26	10	30, II	25, 971. 66	a^3F_2–$y^5G_3^0$	(0. 00) 1. 21	(**0. 00**, 0. 25, 0. 50) --- 0. 92, 1. 17, **1. 42**
326	3, 847. 01	10	30, ?	25, 986. 85	a^3F_3–$z^3D_2^0$	(0. 00) 1. 15	(**0. 00**, 0. 08, 0. 17) **0. 92**, 1. 00, 1. 08, ---
321	3, 845. 45	2		25, 997. 39	a^3D_2–$r^3D_2^0$		
327	3, 839. 12	5		26, 040. 31	e^3P_2–$w^3S_1^0$		
316	3, 835. 96	20	100, II	26, 061. 76	a^3F_2–$x^3F_2^0$	(0. 00) 0. 68	(0. 00) 0. 67
	3, 831. 51	4		26, 092. 02			
328	3, 831. 30	3		26, 093. 45	b^3F_4–$s^3D_3^0$		
	3, 825. 27	6		26, 134. 57			
329	3, 822. 41	12	40, II	26, 154. 11	a^5F_4–$w^5G_4^0$	(0. 00) 0. 76	(**0. 00**, 0. 17) 0. 50, 0. 67, **0. 83**
326					a^3F_2–$z^3D_1^0$		
330	3, 809. 70	2		26, 241. 35	a^3F_4–$w^3D_3^0$		
320	3, 806. 52	2		26, 263. 26	a^3F_3–$w^3G_3^0$		
323	3, 792. 40	4		26, 361. 07	a^3F_3–$z^1G_3^0$	(0. 00) **1. 24**	(**0. 00**, 0. 08, ---) **0. 75**, 0. 83, 0. 92, ---
316	3, 791. 39	12	80, II	26, 368. 09	a^3F_3–$x^3F_4^0$	(0. 00) 1. 37	(**0. 00**, 0. 17, ---) --- 1. 42, 1. 58, **1. 75**
328	3, 791. 07	2		26, 370. 33	b^3F_3–$s^3D_2^0$		
331	3, 784. 86	1		26, 413. 59	a^3D_1–$t^3P_0^0$		
332					a^3G_4–$r^3F_4^0$		
316	3, 780. 53	18	100, II	26, 443. 83	a^3F_2–$x^3F_3^0$	(0. 00) 1. 72	(**0. 00**, 0. 42, 0. 83) --- 1. 08, 1. 50, **1. 92**
328	3, 775. 46	1		26, 479. 33	b^3F_3–$s^3D_3^0$		
333	3, 766. 95	1		26, 539. 14	b^3F_4–$r^3F_4^0$		
326	3, 766. 71	8	60, II	26, 540. 85	a^3F_3–$x^3D_3^0$		
330	3, 765. 18	2		26, 551. 61	a^3F_3–$w^3D_2^0$		
326	3, 764. 38	15	80, II	26, 557. 25	a^3F_2–$x^3D_2^0$	(0. 97) 0. 78, **1. 21**, 1. 67	(0. 50, **1. 00**) 0. 17, **0. 67, 1. 17**, 1. 67
331	3, 754. 79	2		26, 625. 11	a^3D_2–$t^3P_1^0$		
328	3, 754. 08	3		26, 630. 17	b^3F_2–$s^3D_1^0$		

TABLE 3.—*Wave lengths in the arc spectrum of Zr*—Continued

Key No.	λ I. A.	Intensities, temperature class, and notes		Wave No.	Term combinations	Observed Zeeman effects	Theoretical Zeeman effects
		B. S.	King				
334	3,737.40	3	5, IV	26,748.99	a^1D_2–$y^3S^\circ_1$	(0.00) 0.93	(**0.00**, 1.00) **0.00**, 1.00, 2.00
	3,736.50	1		26,755.42			
	3,731.44	1		26,791.69			
333	3,725.75	1		26,832.60	b^3F_4–$r^3F^\circ_4$		
331	3,723.20	1		26,851.04	a^3D_1–$t^3P^\circ_1$		
335	3,714.13	10	30, III	26,916.60	a^3F_4–$w^3F^\circ_3$	(0.00) 1.85	(**0.00**, **0.00**, 0.17, ---) ---1.42, 1.58, **1.75**
333	3,712.94	1		26,925.22	b^3F_3–$r^3F^\circ_3$, b^3F_2–$r^3F^\circ_2$		
336	3,706.63	7	10, III	26,971.05	a^3F_4–$z^3H^\circ_5$	(0.00) 0.00*w*	(**0.00**, **0.00**, 0.22, ---) **0.17**, 0.38, 0.60, ---
	3,695.60	1		27,051.52			
331	3,690.33	1		27,090.14	a^3D_3–$t^3P^\circ_2$		
337	3,688.47	0		27,103.79	a^3F_3–$y^3P^\circ_2$		
	3,685.62	5		27,124.82			
338	3,683.47	6		27,140.61	a^3P_2–$w^3G^\circ_3$		
	3,681.64	1		27,154.14			
339	3,680.37	4	5, III	27,163.47	a^3F_4–$z^3G^\circ_3$		
	3,677.05	2 Cb?		27,188.02			
335	3,663.64	40	300, II	27,287.51	a^3F_4–$w^3F^\circ_4$	(0.38) 1.14	(0.00) **1.25**
335	3,661.20	10	30, III	27,305.62	a^3F_3–$w^3F^\circ_2$		
	3,658.30	2		27,327.34			
336	3,656.88	5	6, III	27,337.96	a^3F_3–$z^3H^\circ_4$		
	3,650.98	4		27,382.11			
	3,650.47	4		27,386.68			
	3,648.39	3		27,401.54			
	3,646.89	6		27,412.84			
340	3,644.50	2		27,430.86	a^3G_3–$u^3G^\circ_4$		
	3,639.56	4 Pb?		27,468.05			
341	3,638.70	5	3, IV	27,474.54	a^3P_1–$y^3S^\circ_1$		
335	3,634.14	15	50, III	27,509.03	a^3F_4–$x^3G^\circ_4$	(0.31) **1.22**	(---0.60, **0.80**) ---0.85, **1.05**, **1.25**, 1.45, ---
342	3,625.39	4		27,575.40	a^3D_3–$t^3G^\circ_4$		
335	3,623.87	45	300, II	27,586.97	a^3F_3–$w^3F^\circ_3$	(0.30) 1.04	(0.00) 1.08
343	3,619.38	4		27,621.18	a^1D_2–$y^1P^\circ_1$		
	3,616.30	3		27,644.70			
341	3,615.09	3		27,653.95	a^3P_0–$y^3S^\circ_1$		
341, 331	3,613.70	7	15, III	27,664.58	a^3P_2–$y^3S^\circ_1$, a^3D_1–$t^3P^\circ_2$		
337	3,612.55	2		27,673.38	a^3F_2–$y^3P^\circ_1$		
	3,609.64	3		27,695.69			
344	3,605.90	3		27,724.45	a^1G_4–$z^3I^\circ_5$		
345, 346	3,602.78	3		27,748.57	a^1G_4–$t^3F^\circ_4$, b^3F_2–$u^3G^\circ_3$		
339	3,601.18	50	400, II	27,760.81	a^3F_4–$z^3G^\circ_3$	(0.00) 1.12*	(**0.00**, **0.00**, 0.05, ---) **1.00**, 1.05, 1.10, ---
347	3,597.42	2		27,789.82	a^1S_0–$w^1P^\circ_1$		
348	3,596.29	2		27,798.55	a^3F_3–$v^3F^\circ_4$		
349	3,594.70	4		27,810.85	c^3F_3–$q^3F^\circ_3$		
	3,593.87	2		27,817.27			
350	3,593.12	2		27,823.06	c^3P_1–$s^3P^\circ_1$		
339	3,591.72	5	2, III	27,833.91	a^3F_3–$x^3G^\circ_3$		
335	3,586.28	25	100, II	27,876.12	a^3F_2–$w^3F^\circ_2$	(0.00) 0.68	(0.00) 0.67
351	3,585.52	2		27,882.03	a^3F_4–$y^5F^\circ_4$		
345	3,577.55	6	15, IV	27,944.12	a^1G_4–$t^3F^\circ_4$	(0.00) 1.04	(---0.75, **1.00**) ---0.75, **1.00**, **1.25**, **1.50**, ---
335	3,575.79	25	100, II	27,957.89	a^3F_3–$w^3F^\circ_4$	(0.00) 1.21	(**0.00**, 0.17, ---) ---1.42, 1.58, **1.75**
352	3,569.46	2		28,007.51	a^3H_4–$q^3D^\circ_3$		
353	3,568.87	5	15, IV	28,012.15	a^1D_2–$x^3S^\circ_1$	(0.42) ?	(**0.00**, 1.00) **0.00**, 1.00, 2.00
354	3,566.10	25	100, II	28,033.86	a^3F_4–$v^3D^\circ_3$	(0.00) 1.11	(**0.00**, 0.08, ---) **1.00**, 1.08, 1.17, ---
355	3,562.48	2		28,062.38	a^1D_2–$u^3F^\circ_2$		
356	3,558.95	4	12, IV	28,090.21	a^1D_2–$v^3F^\circ_3$	(0.00) 0.72	(**0.00**, 0.08, 0.17) ---1.08, 1.17, **1.25**
357	3,552.64	2		28,140.09	a^5F_2–$u^5F^\circ_2$		
355	3,550.46	7	30, III	28,157.35	a^3F_2–$w^3F^\circ_3$	(0.00) 1.26	(**0.00**, 0.42, 0.83) ---1.68, 1.50, **1.92**

TABLE 3.—*Wave lengths in the arc spectrum of Zr*—Continued

Key No.	λ I. A.	Intensities, temperature class, and notes		Wave No.	Term combinations	Observed Zeeman effects	Theoretical Zeeman effects
		B. S.	King				
358	3, 549. 73	5	15, III	28, 163. 14	a^1G_4–$t^3D_3^0$	(0. 00) 0. 00	(**0. 00,** 0. 33, ---) **0. 00,** 0. 33, 0. 67, ---
357	3, 548. 68	2		28, 171. 47	a^5F_3–$u^3F_3^0$		
359	3, 548. 39	2		28, 173. 78	a^3D_1–$q^3D_1^0$		
339	3, 547. 69	25	100, II	28, 179. 33	a^3F_3–$x^3G_4^0$	(0. 00) 1. 25	(**0. 00,** 0. 03, ---) **0. 95,** 0. 98, 1. 02, ---
360	3, 535. 16	8	20, IV	28, 279. 18	a^1G_4–$x^1G_4^0$	(0. 00) 1. 15	(0. 00) 1. 00
351	3, 533. 22	12	60, III	28, 294. 74	a^3F_4–$y^5F_5^0$	(0. 00) 1. 65	(**0. 00,** 0. 15, ---)---1. 70, 1. 85, **2. 00**
	3, 532. 46	2		28, 300. 79			
355	3, 530. 22	6	15, III	28, 318. 83	a^1D_2–$u^3F_3^0$		
	3, 529. 44	2		28, 325. 08			
361	3, 524. 52	2		28, 364. 58	$z^5F_5^0$–f^5G_3		
	3, 524. 26	2		28, 366. 70			
362	3, 523. 63	3		28, 371. 77	a^3F_4–$w^5D_3^0$		
362	3, 522. 18	3		28, 383. 45	a^5F_3–$w^5D_2^0$		
362	3, 520. 30	3		28, 398. 58	a^5F_5–$w^5D_4^0$		
339	3, 519. 60	35	125, II	28, 404. 25	a^3F_2–$x^3G_3^0$	(0. 00) 1. 07	(**0. 00,** 0. 08, 0. 17) --- 0. 75, 0. 83, **0. 92**
	3, 518. 87	1		28, 410. 14			
362	3, 517. 47	3		28, 421. 43	a^5F_2–$w^5D_1^0$		
348	3, 515. 25	1		28, 439. 39	a^5F_3–$v^3F_4^0$		
363	3, 514. 49	2		28, 445. 54	c^3P_2–$p^3D_2^0$		
351	3, 514. 32	3		28, 446. 90	a^3F_2–$y^5F_1^0$		
364	3, 512. 35	1		28, 462. 86	a^5F_2–$u^3D_1^0$		
362	3, 510. 36	2		28, 478. 99	a^5F_1–$w^5D_0^0$		
354	3, 509. 32	25	100, II	28, 487. 43	a^3F_3–$v^3D_2^0$	(0. 00) 1. 10	(**0. 00,** 0. 08, 0. 17) **0. 92,** 1. 00, 1. 08, ---
365	3, 503. 27	2		28, 536. 61	a^3P_2–$y^1P_1^0$		
366	3, 501. 50	7	8, IV	28. 551. 03	a^1G_4–$z^3H_4^0$		
351	3, 501. 33	8	15, III	28, 552. 44	a^3F_3–$y^5F_4^0$		
367	3, 495. 37	4		28, 601. 09	b^3F_3–$v^1D_2^0$		
362	3, 494. 44	4		28, 608. 70	a^5F_2–$w^5D_2^0$		
364	3, 493. 66	3		28, 615. 17	a^5F_1–$u^3D_1^0$		
368	3, 487. 91	3		28, 662. 29	a^1D_2–$u^3D_2^0$		
362	3, 487. 81	3		28, 663. 11	a^5F_2–$w^5D_3^0$		
369	3, 483. 01	7	15, IV	28, 702. 61	a^1G_4–$w^1F_3^0$	(0. 00) 1. 24	(0. 00) 1. 00
354	3, 482. 80	8	20, III	28, 704. 34	a^3F_3–$v^3D_3^0$		
370	3, 482. 13	3		28, 709. 90	a^3F_2–$x^3P_1^0$		
371	3, 478. 78	8	20, III	28, 737. 53	a^3P_1–$x^3S_1^0$	(0. 45) 0. 79	(0. 50) 1. 50, 2. 00
362	3, 477. 64	2		28, 746. 95	a^5F_4–$w^5D_4^0$		
	3, 476. 02	3		28, 760. 35			
372	3, 472. 89	5	4, IV	28, 786. 25	a^3P_2–$v^3F_2^0$		
373	3, 472. 72	2		28, 787. 67	a^3P_1–$u^3F_2^0$		
354	3, 471. 18	25	100, II	28, 800. 43	a^3F_2–$v^3D_1^0$		
361	3, 470. 18	2		28, 808. 73	$z^5F_4^0$–f^5G_4		
351	3, 469. 06	4	4, II	28, 818. 03	a^3F_2–$y^5F_3^0$		
	3, 468. 31	2		28, 824. 26			
374	3, 465. 63	7	10, II	28, 846. 54	a^3F_4–$x^5D_3^0$		
361	3, 464. 30	2		28, 857. 61	$z^5F_3^0$–f^5G_5		
375	3, 461. 09	10	30, II	28, 884. 37	a^1G_4–$v^3G_3^0$	(0. 00) 1. 24	(**0. 00,** 0. 25, ---) ---- 1. 25, 1. 50, **1. 75**
371	3, 457. 19	10	20, II	28, 916. 97	a^3P_0–$x^3S_1^0$	(0. 00) 1. 78	(0. 00) 2. 00
371	3, 455. 90	15	30, II	28, 927. 73	a^3P_2–$x^3S_1^0$	(0. 00) 0. 53	(**0. 00,** 0. 50) **1. 00,** 1. 50, 2. 00
373	3, 449. 91	6	6, IV	28, 977. 99	a^3P_2–$u^3F_3^0$		
	3, 449. 40	2		28, 982. 32			
376	3, 447. 36	30	100, II	28, 999. 44	a^3F_2–$z^1P_1^0$	(0. 00) 0. 59	(**0. 00,** 0. 33) **0. 33,** 0. 67, 1. 00
372	3, 446. 61	15	30, II	29, 005. 73	a^3P_2–$v^3F_3^0$	(0. 00) 0. 79	(**0. 00,** 0. 42, 0. 83) **0. 25,** 0. 67, 1. 08, ---
362	3, 442. 70	1		29, 038. 70	a^5F_3–$w^5D_4^0$		
354	3, 440. 43	12	30, II	29, 057. 84	a^3F_2–$v^3D_2^0$	(1. 00) 0. 00*w*	(0. 50, **1. 00**) 0. 17, **0. 67, 1. 17,** 1. 67
368	3, 430. 94	3		29, 138. 21	a^1D_2–$u^3D_3^0$		
374	3, 430. 29	6	8, II	29, 143. 72	a^3F_4–$x^5D_4^0$		
	3, 430. 02	1		29, 146. 02			
375	3, 426. 93	4		29, 172. 30	a^1G_4–$v^3G_4^0$		

TABLE 3.—*Wave lengths in the arc spectrum of Zr*—Continued

Key No.	λ I. A.	Intensities, temperature class, and notes		Wave No.	Term combinations	Observed Zeeman effects	Theoretical Zeeman effects
		B. S.	King				
361	3,421.42	3		29,219.28	$z^5F_5^5$–f^5G_4		
373	3,419.65	12	20, II	29,234.38	a^3P_2–$u^3F_3^3$	(0.00) 0.74	(**0.00**, 0.42, 0.83) **0.25**, 0.67, 1.08, ---
377	3,417.07	1		29,256.45	a^3P_1–w^5D_2		
	3,416.68	4		29,259.82			
354	3,414.94	2		29,274.78	a^3F_2–$v^3D_3^3$		
374	3,414.66	12	20, II	29,277.13	a^3F_3–$x^5D_3^3$		
361	3,411.78	2		29,301.84	$z^5F_4^4$–f^5G_5		
	3,409.40	2		29,322.33			
378	3,408.54	4		29,329.74	a^5P_2–$r^3D_3^3$		
379	3,401.79	3	3, V	29,387.88	a^3P_1–$u^3D_2^2$		
	3,400.75	2		29,396.90			
361	3,397.92	4	5, V	29,421.37	$z^5F_5^5$–f^5G_6		
	3,389.26	1		29,496.52			
380	3,387.10	2		29,515.33	a^1D_2–$y^5P_1^1$		
374	3,386.90	2		29,517.07	a^3F_3–$x^5D_3^3$		
	3,385.80	5	5, V	29,526.67			
381							
379	3,379.92	7	10, III	29,578.03	$z^5F_4^4$–f^5G_5 / a^3P_2–$u^3D_2^2$		
380	3,370.60	10	20, III	29,659.82	a^1D_2–$y^5P_2^2$	(0.00) 1.38	(0.83, **1.67**) 0.17, **1.00**, 1.83, 2.67
374	3,368.63	5	5, II	29,677.16	a^3F_2–$x^5D_1^1$		
	3,365.00	1		29,709.21			
377	3,363.08	1		29,726.17	a^3P_2–$w^5D_3^3$		
382	3,360.45	15	25, II	29,749.40	a^1D_2–$w^1D_2^2$	(0.00) 1.35	(0.00) 1.00
381	3,355.01	2		29,797.65	$z^5F_5^5$–f^5G_4		
353	3,353.65	12	20, II	29,809.63	a^3F_4–$y^1G_4^4$		
374	3,353.15	3		29,814.17	a^3F_3–$x^5D_4^4$		
384	3,351.23	3		29,831.25	b^3F_3–$t_3P_2^2$		
	3,347.08	1		29,868.23			
381	3,343.71	3 Cb?		29,898.32	$z^5F_2^2$–f^5G_3		
385	3,340.20	2		29,929.72	b^3F_4–$t^3G_4^4$		
	3,334.07	2		29,984.73			
380	3,333.56	6	4, IV	29,989.36	a^1D_2–$y^5P_2^2$		
	3,329.11	3		30,029.49			
379	3,326.43	6		30,053.68	a^3P_2–$u^3D_3^3$		
	3,322.29	6	5, V	30,091.12			
385	3,316.21	5	4, V	30,146.26	b^3F_3–$t^3G_3^3$		
386	3,315.12	3		30,156.18	$z^5G_6^6$–f^5G_6		
	3,310.55	3		30,197.80			
	3,305.90	2		30,240.26			
	3,300.81	1		30,286.88			
385	3,297.64	2		30,315.98	b^3F_2–$t^3G_3^4$		
	3,297.00	2		30,321.87			
386	3,296.73	3		30,324.34	$z^5G_6^6$–f^5G_4		
	3,293.58	2		30,353.34			
387	3,293.45	2		30,354.54	a^1D_2–$w^3P_2^2$		
	3,292.25	1		30,365.60			
388	3,285.18	3		30,431.02	a^3P_2–$y^5P_1^1$		
389	3,282.73	7	15, II	30,453.71	a^3F_4–$w^3G_4^4$		
385	3,281.87	1		30,461.71	b^3F_3–$t^3G_3^3$		
390	3,280.46	2		30,474.80	a^3P_1–$w^1D_2^2$ / $z^5G_4^4$–f^5G_3		
386							
385	3,278.58	1		30,492.26	b^3F_4–$t^3G_4^4$		
391	3,277.38	1		30,503.42	a^3G_5–$q^3F_4^4$		
391	3,276.95	2		30,507.43	a^3G_4–$q^3F_3^3$		
388	3,269.66	12	40, III	30,575.44	a^3P_2–$y^5P_2^2$	(0.00) 1.24	(0.33, **0.67**) **1.17**, **1.50**, 1.83, 2.17
386	3,267.35	3		30,597.04	$z^5G_5^5$–f^5G_3		
392	3,261.06	2		30,656.04	b^3F_2–$q^3D_1^1$		
	3,260.91	1		30,657.45			
390	3,260.11	15	40, III	30,665.00	a^3P_2–$w^1D_2^2$		
393	3,256.00	2		30,703.66	a^1D_2–$t^3F_2^2$		
386	3,254.28	10	15, IV	30,719.94	$z^5G_6^6$–f^5G_5		
389	3,250.42	15	35, III	30,756.46	a^3F_3–$w^3G_3^3$		
386	3,243.98	10	8, V	30,817.50	$z^5G_5^5$–f^5G_5		

TABLE 3.—*Wave lengths in the arc spectrum of Zr*—Continued

Key No.	λ I. A.	Intensities, temperatures class, and notes		Wave No.	Term combinations	Observed Zeeman effects	Theoretical Zeeman effects
		B. S.	King				
394	3, 242. 75	1		30, 829. 16	a^3P_1–$w^3P_1^\circ$		
388	3, 234. 80	5	5, III	30, 904. 92	a^3P_2–$y^3P_2^\circ$		
389	3, 234. 12	30	100, II	30, 911. 42	a^3F_4–$w^3G_3^\circ$	(0. 00) 1. 07	(**0. 00**, 0. 05, ---) **1. 00**, 1. 05, 1. 10, ---
386	3, 233. 11	5	5, V	30, 921. 07	$z^3G_4^\circ$–f^3G_4		
386	3, 225. 47	4		30, 994. 30	$z^3G_3^\circ$–f^3G_3		
386	3, 223. 34	3		31, 014. 78	$z^3G_2^\circ$–f^3G_2		
394	3, 216. 57	3		31, 080. 03	a^3P_1–$v^3P_2^\circ$		
395	3, 212. 57	7	8, III	31, 118. 77	a^1D_2–$t^3D_3^\circ$		
389	3, 212. 02	30	100, II	31, 124. 14	a^3F_3–$w^3G_4^\circ$	(0. 00) 1. 00	(**0. 00**, 0. 03, ---) **0. 95**, 0. 98, 1. 02, ---
395	3, 204. 90	10	12, III	31, 193. 24	a^1D_2–$t^3D_2^\circ$		
394	3, 197. 64	5		31, 269. 92	a^3P_2–$w^3P_2^\circ$		
389	3, 191. 23	25	100, II	31, 326. 85	a^3F_2–$w^3G_3^\circ$	(0. 00) 0. 84	(**0. 00**, 0. 08, 0. 17)---0. 75, 0. 83, **0. 92**
396	3, 191. 05	3		31, 328. 62	a^3P_2–$t^3F_3^\circ$		
386	3, 185. 68	2		31, 381. 41	$z^3G_3^\circ$–f^3G_3		
397	3, 185. 08	3		31, 387. 32	a^1D_2–$v^3P_1^\circ$		
386	3, 182. 37	2		31, 414. 04	$z^3G_4^\circ$–f^3G_5		
386	3, 179. 72	3		31, 440. 24	$z^3G_3^\circ$–f^3G_4		
398	3, 166. 62	2		31, 570. 34	c^3P_2–$o^3D_3^\circ$		
399	3, 162. 23	2		31, 614. 16	a^3P_1–$y^3S_1^\circ$		
400 / 401	3, 157. 82	15	50, III	31, 658. 28	a^1D_2–$w^1F_3^\circ$ / a^3P_1–$v^3P_0^\circ$	(0. 00) 0. 86	(0. 00) 1. 00
402	3, 149. 95	3		31, 746. 43	a^1G_4–$v^1F_3^\circ$		
403	3, 148. 81	10	25, III	31, 748. 86	a^3P_1–$t^3D_1^\circ$		
	3, 146. 30	1		31, 774. 18			
404	3, 143. 94	1		31, 798. 02	a^1G_4–$y^1H_5^\circ$		
	3, 143. 47	1		31, 802. 77			
405	3, 139. 79	10	20, III	31, 840. 04	a^1D_2–$o^3G_3^\circ$		
406	3, 136. 95	12	30, III	31, 858. 85	a^1D_2–$u^3P_1^\circ$	(0. 00) 1. 29	(**0. 00**, 0. 50) **0. 50**, **1. 00**, **1. 50**
397	3, 133. 23	10	20, III	31, 906. 78	a^1D_2–$v^3P_2^\circ$		
403	3, 132. 06	15	50, III	31, 918. 65	a^3P_1–$t^3D_2^\circ$	(0. 00) 1. 00	(**0. 00**, 0. 35) **0. 83**, 1. 17, 1. 50
403	3, 131. 11	12	25, III	31, 928. 33	a^3P_0–$t^3D_1^\circ$	(0. 00) **0. 00***w*	(0. 00) 0. 50
403	3, 130. 05	5	8, III	31, 939. 19	a^3P_2–$t^3D_1^\circ$		
407	3, 121. 95	2		32, 022. 03	a^1D_2–$s^3F_2^\circ$		
403	3, 120. 74	30	125, III	32, 034. 42	a^3P_2–$t^3D_3^\circ$	(0. 00) 1. 19	(**0. 00**, 0. 17, 0. 33) **1. 00**, 1. 17, 1. 33, ---
403	3, 113. 50	8	8, III	32, 108. 81	a^3P_2–$t^3D_2^\circ$		
408	3, 108. 36	8	10, III	32, 162. 01	a^3P_1–$u^3P_0^\circ$		
	3, 101. 06	2		32, 237. 69			
409	3, 099. 65	3	2, V	32, 252. 34	a^3F_1–$s^3F_2^\circ$		
401	3, 095. 82	10	12, III	32, 292. 23	a^3P_0–$v^3P_1^\circ$		
401	3, 094. 79	10	15, III	32, 303. 02	a^3P_2–$v^3P_1^\circ$		
410	3, 093. 29	3	2, III	32, 318. 63	a^3F_4–$u^3F_4^\circ$		
	3, 092. 25	3	2, V	32, 329. 50			
406	3, 090. 44	6	6, III	32, 348. 54	a^1D_2–$u^3P_2^\circ$		
411	3, 085. 34	10	12, III	32, 401. 96	a^3F_3–$v^3F_3^\circ$		
408 / 410	3, 067. 12	4		32, 594. 43	a^3P_1–$u^3P_1^\circ$ / a^3F_3–$u^3F_3^\circ$		
412	3, 066. 74	2		32, 598. 45	a^3F_4–$z^1H_5^\circ$		
401	3, 063. 58	5	8, III	32, 632. 09	a^3P_1–$r^3P_2^\circ$		
413	3, 052. 80	2		32, 747. 37	a^3P_1–$s^3F_2^\circ$		
414	3, 052. 00	2		32, 755. 95	a^3P_2–$v^3G_3^\circ$		
408	3, 050. 33	2		32, 773. 83	a^3P_0–$u^3P_1^\circ$		
408	3, 049. 33	6	6, III	32, 784. 58	a^3P_2–$u^3P_1^\circ$		
401	3, 045. 82	6	10, III	32, 822. 36	a^3P_2–$r^3P_2^\circ$		
410	3, 043. 23	4	3, III	32, 850. 29	a^3F_2–$u^3F_2^\circ$		
415	3, 029. 52	20	300, II	32, 998. 95	a^3F_4–$u^3D_3^\circ$	(0. 00) **1. 11**	(**0. 00**, 0. 08, ---) **1. 00**, 1. 08, 1. 17, ---
408	3, 022. 66	1		33, 073. 81	a^3P_1–$u^3P_2^\circ$		
410	3, 014. 44	5	15, III	33, 164. 02	a^3F_2–$u^3F_2^\circ$		
415	3, 011. 73	20	250, II	33, 193. 86	a^3F_3–$u^3D_2^\circ$	(0. 00) **1. 00**	(**0. 00**, 0. 08, 0. 17) **0. 92**, 1. 00, 1. 08, ---
416	3, 005. 50	5	60, IV	33, 262. 67	a^1G_4–$w^1G_4^\circ$		
408	3, 005. 36	4	40, IV	33, 264. 21	a^3P_2–$u^3P_2^\circ$		
415	2, 985. 36	10	200, II	33, 487. 06	a^3F_2–$u^3D_1^\circ$	(0. 00) 0. 68	(**0. 00**, 0. 17) 0. 50, 0. 67, **0. 83**
415	2, 969. 18	4	40, IV	33, 669. 56	a^3F_3–$u^3D_3^\circ$		

TABLE 3.—*Wave lengths in the arc spectrum of Zr*—Continued

Key No.	λ I. A.	Intensities, temperatures class, and notes		Wave No.	Term combinations	Observed Zeeman effects	Theoretical Zeeman effect
		B. S.	King				
415	2, 960. 86	6	60, IV	33, 764. 14	a^5F_3–$u^5D^0_3$	(0. 75) 1. 32 E_1	(0. 50, **1. 09**) 0. 17, **0. 67, 1. 17, 1. 67**
417					b^3F_2–$p^3D^0_1$		
418	2, 933. 02	1		34, 084. 61	a^3P_2–$s^3D^0_1$		
419	2, 923. 86	4	10, IV	34, 191. 38	a^3F_3–$p^3P^0_2$		
420	2, 916. 23	2	10, IV	34, 280. 85	a^3F_3–$w^1D^0_2$		
	2, 901. 64	2		34, 453. 20			
421	2, 892. 26	6	30, IV	34, 564. 93	a^3F_4–$t^3F^0_3$		
422	2, 889. 15	2		34, 602. 13	a^1D_2–$x^1P^0_1$		
423	2, 880. 83	3	5, V	34, 702. 06	a^1D_2–$v^1F^0_3$		
421	2, 875. 98	12	200, IV	34, 760. 58	a^3F_4–$t^3F^0_4$	(0. 46) 1, 18 E_1	(0. 00) 1. 25
420	2, 868. 48	3		34, 851. 46	a^3F_3–$w^1D^0_2$		
421	2, 860. 85	6	30, IV	34, 944. 41	a^3F_3–$t^3F^0_2$	(0. 00) 1. 46 E_1	(**0. 00**, 0. 42, 0. 83)—1.08, 1.50, **1. 92**
424	2, 857. 97	1	2, V	34, 979. 62	a^3F_4–$t^3D^0_3$		
425	2, 848. 50	6	150, IV	35, 095. 91	a^3F_4–$z^1G^0_4$		
421	2, 837. 23	15	200, IV	35, 235. 31	a^3F_3–$t^3F^0_3$	(0. 00) 0. 96 E_1	(0. 00) 1. 08
426	2, 836. 49	3	4, V	35, 244. 51	a^1D_2–$r^3D^0_3$		
427	2, 831. 33	2		35, 308. 73	a^3F_3–$v^1D^0_2$		
428	2, 829. 80	6	8, IV	35, 327. 82	a^3P_1–$z^1P^0_1$		
429	2, 827. 55	6	8, IV	35, 355. 93	a^3F_4–$z^3H^0_5$		
430	2, 824. 82	3		35, 390. 22	a^3P_1–$r^3D^0_2$		
421	2, 821. 56	6	8, IV	35, 430. 98	a^3F_3–$t^3F^0_4$		
431	2, 819. 56	5	10, IV	35, 456. 11	a^1D_2–$v^1D^0_2$		
432					a^3F_3–$w^3P^0_2$		
428	2, 815. 49	3	2, V	35, 507. 36	a^3P_0–$x^1P^0_1$		
421	2, 814. 91	12	150, IV	35, 514. 67	a^3F_2–$t^3F^0_2$	(0. 00) 0. 60 E_1	(0. 00) 0. 67
428	2, 814. 71	2		35, 517. 20	a^3P_2–$x^1P^0_1$		
433	2, 806. 77	6	12, IV	35, 617. 67	a^3P_2–v^1F^3		
424	2, 798. 30	6		35, 725. 47	a^3F_3–$t^3D^0_2$		
425	2, 795. 14	5	8, V	35, 765. 86	a^3F_3–$z^1G^0_4$		
	2, 793. 40	7	8, V	35, 788. 14			
421	2, 792. 05	10	20, IV	35, 805. 44	a^3F_2–$t^3F^0_3$		
434	2, 790. 14	12		35, 829. 95	a^1D_2–$w^1P^0_1$		
435	2, 786. 90	6		35, 871. 60	a^1D_2–$t^3P^0_1$		
436	2, 777. 64	1		35, 991. 18	a^3F_2–$y^5S^0_2$		
429	2, 774. 03	2		36, 038. 02	a^3F_3–$z^3H^0_4$		
	2, 771. 35	1		36, 072. 87			
	2, 770. 88	1		36, 078. 98			
424	2, 767. 38	4		36, 124. 61	a^3F_2–$t^3D^0_1$		
437					b^3F_2–$o^3D^0_1$		
	2, 766. 50	2		36, 136. 10			
430	2, 764. 68	2		36, 159. 89	a^3P_2–$r^3D^0_3$		
438					a^3P_1–$t^3P^0_0$		
439	2, 763. 01	6		36, 181. 75	a^3P_1–$v^1D^0_2$		
440					a^3F_4–$v^3G^0_5$		
	2, 761. 18	2		36, 205. 72			
441	2, 759. 46	3		36, 228. 29	a^3F_4–$s^3F^0_3$		
439	2, 748. 59	2		36, 371. 56	a^3P_2–$v^1D^0_2$		
437					b^3F_3–$o^3D^0_4$		
440					a^5F_3–$v^3G^0_3$		
	2, 737. 86	5		36, 514. 08			
440	2. 727. 00	5		36, 659. 50	a^3F_2–$v^3G^0_3$		
441	2, 725. 45	8		36, 680. 34	a^3F_4–$s^3F^0_4$	(0. 00) 1. 12 E_1	(0. 00) 1. 25
435	2, 725. 01	2		36, 686. 26	a^1D_2–$t^3P^0_2$		
442	2, 719. 52	4		36, 760. 35	a^3F_2–$w^1F^0_3$		
438	2, 718. 28	4		36, 777. 09	a^3P_0–$t^3P^0_1$		
438	2. 717. 48	5		36, 787. 94	a^3P_2–$t^3P^0_1$		
	2, 709. 76	4		36, 892, 72			
441	2. 709. 33	8		36, 898. 58	a^3F_3–$s^3F^0_3$		
440	2, 706. 15	10		36, 941. 94	a^3F_3–$v^3G^0_3$		
443	2, 701. 83	3		37, 000. 99	a^1D_2–$t^3G^0_3$		
441	2, 692. 91	4		37, 123. 55	a^3F_2–$s^3F^0_3$		
444	2, 687. 74	7		37, 194. 95	a^3F_4–$s^3D^0_3$		
	2, 685. 91	3		37, 220. 29			
445	2, 683. 79	3		37, 249. 67	a^5P_1–$o^5D^0_0$		

TABLE 3.—*Wave lengths in the arc spectrum of Zr*—Continued

Key No.	λ I. A.	Intensities, temperatures class, and notes		Wave No.	Term combinations	Observed Zeeman effects	Theoretical Zeeman effects
		B. S.	King				
	2,681.39	2		37,283.03			
446	2,677.88	1		37,331.89	a^1D_2–$q^3D_2^3$		
441	2,676.54	4		37,350.58	a^3F_3–$s^3F_4^4$		
438	2,672.17	1		37,411.60	a^3P_1–$f^3P_2^2$		
	2,662.78	1		37,543.58			
438	2,658.66	6		37,601.76	a^3P_2–$f^3P_2^2$		
447	2,655.84	3		37,641.68	a^3F_4–$r^3F_3^3$		
	2,649.84	2		37,726.91			
444	2,647.77	4		37,756.40	a^3F_3–$s^3D_2^2$		
444	2,640.13	4		37,865.66	a^3F_3–$s^3D_3^3$		
448	2,636.56	1		37,916.92	a^3P_2–$t^3G_3^3$		
	2,636.38	1		37,919.50			
447	2,635.40	8		37,933.61	a^3F_4–$r^3F_4^4$		
	2,634.56	3		37,945.70			
	2,633.11	1		37,966.60			
	2,630.33	6		38,006.73			
	2,625.98	2		38,069.67			
449	2,625.18	1		38,081.27	a^1D_2–$w^3S_1^1$		
	2,624.83	3		38,086.36			
	2,620.83	5		38,144.48			
450	2,619.81	2		38,159.34	a^5F_2–$w^3S_1^1$		
	2,613.05	2		38,258.04			
463	2,612.18	4		38,270.78	a^1G_4–$u^1F_3^3$		
444					a^3F_3–$s^3D_1^1$		
447	2,609.40	6		38,311.55	a^3F_3–$r^3F_3^3$		
444	2,608.37	3		38,326.68	a^3F_2–$s^3D_2^2$		
451	2,592.39	2		38,562.92	a^3F_4–$v^1F_3^3$		
447	2,592.18	3		38,566.04	a^3F_2–$r^3F_2^2$		
447	2,589.62	5		38,604.17	a^3F_3–$r^3F_4^4$		
452	2,583.64	6		38,693.51	a^3F_4–$u^3G_4^4$		
	2,580.45	2		38,741.34			
	2,579.54	8		38,755.01			
453	2,579.40	1		38,757.11	a^1S_0–$v^1P_1^1$		
454	2,576.08	5		38,807.05	a^3P_1–$w^3S_1^1$		
	2,573.50	1		38,845.95			
452	2,567.44	7		38,937.64	a^3F_4–$u^3G_3^3$		
454	2,564.26	3		38,985.93	a^3P_0–$w^3S_1^1$		
454	2,563.56	4		38,996.57	a^3P_2–$w^3S_1^1$		
	2,561.91	2		39,021.69			
455	2,556.38	6		39,106.09	a^3F_4–$r^3D_3^3$		
	2,554.84	1		39,129.67			
	2,554.30	5		39,137.93			
	2,551.70	2		39,177.81			
455	2,550.50	4		39,196.24	a^3F_3–$r^3D_3^3$		
	2,547.10	2		39,248.56			
452	2,539.62	10		39,364.15	a^3F_3–$u^3G_3^3$		
452	2,538.00	6		39,389.28	a^3F_2–$u^3G_3^3$		
	2,533.98	1		39,451.76			
	2,533.18	2		39,464.22			
	2,527.10	1		39,559.16			
	2,524.84	2		39,594.57			
	2,519.94	4		39,671.55			
451	2,511.56	2		39,803.91	a^3F_2–$v^1F_3^3$		
	2,505.98	4		39,892.53			
	2,504.79	3		39,911.48			
456	2,504.54	2		39,915.46	a^1D_2–$s^3P_2^2$		
	2,495.26	5		40,063.90			
	2,493.73	2		40,088.48			
	2,481.92	1		40,279.22			
	2,481.42	4		40,287.34			
	2,481.22	1		40,290.59			
457	2,478.27	1		40,338.54	a^5F_3–$p^5D_4^4$		
	2,478.06	2		40,341.96			
	2,474.14	2		40,405.97			
	2,474.00	3		40,408.16			
	2,471.96	2		40,441.51			
	2,470.29	1		40,468.84			

TABLE 3.—*Wave lengths in the arc spectrum of Zr*—Continued

Key No.	λ I. A.	Intensities, temperatures class, and notes		Wave No.	Term combinations	Observed Zeeman effects	Theoretical Zeeman effects
		B. S.	King				
458	2,468.03	5		40,505.90	a^3P_1–$s^3P^\circ_1$		
459	2,461.79	2		40,608.56	a^1D_2–$p^3D^\circ_2$		
	2,461.02	4		40,619.61			
458	2,459.84	3		40,640.75	a^3P_1–$s^3P^\circ_2$		
	2,459.27	2		40,650.17			
458	2,456.50	2		40,696.00	a^3P_2–$s^3P^\circ_1$		
	2,454.96	1		40,721.53			
	2,451.97	2		40,771.18			
460	2,450.98	1		40,787.65	a^5F_4–$u^1F^\circ_3$		
	2,449.32	3		40,815.29			
458	2,448.37	4		40,831.12	a^3P_2–$s^3P^\circ_2$		
	2,446.94	1		40,854.99			
	2,445.71	1		40,875.53			
	2,444.04	1		40,903.46			
	2,441.30	8		40,949.36			
	2,440.34	3		40,965.47			
	2,439.49	2		40,979.74			
461	2,437.41	1		41,014.71	a^5P_1–$v^1P^\circ_1$		
	2,434.29	1		41,067.27			
	2,430.54	1		41,130.63			
	2,429.19	4		41,153.48			
	2,428.19	1		41,170.43			
	2,427.82	1		41,176.71			
	2,427.54	1		41,181.45			
462	2,424.89	1		41,226.45	a^1D_2–$u^1F^\circ_3$		
	2,423.76	3		41,245.68			
	2,415.91	2		41,379.69			
	2,415.67	2		41,383.79			
	2,415.58	0		41,385.34			
464	2,414.60	3		41,402.13	a^5P_2–$p^5D^\circ_2$		
	2,413.51	2		41,420.83			
	2,411.92	4		41,448.13			
	2,410.78	1		41,467.73			
	2,407.90	3		41,517.32			
464	2,407.52	1		41,523.88	a^5P_2–$p^5D^\circ_3$		
465	2,407.03	1		41,532.33	a^3F_3–$t^3G^\circ_4$		
466	2,405.52	10		41,558.40	a^3F_4–$q^3D^\circ_3$		
465	2,403.44	5		41,594.36	a^3F_4–$t^3G^\circ_5$		
	2,402.93	4		41,603.19			
	2,402.20	2		41,615.83			
	2,400.81	5		41,639.92			
	2,398.17	3		41,685.75			
	2,397.95	1		41,689.59			
	2,397.70	1		41,693.93			
465	2,397.23	7		41,702.10	a^3F_3–$t^3G^\circ_4$		
	2,396.30	1		41,718.28			
	2,391.88	2		41,795.37			
	2,391.75	3		41,797.64			
	2,391.04	1		41,810.05			
	2,390.15	2		41,825.62			
	2,389.21	8		41,842.07			
466	2,388.00	8		41,863.27	a^3F_3–$q^3D^\circ_2$		
	2,384.84	3		41,918.74			
	2,384.16	12		41,930.69			
	2,381.55	2		41,976.64			
	2,380.55	9		41,994.28			
467	2,378.68	1		42,027.28	a^3F_4–$q^3F^\circ_3$		
467	2,378.25	4		42,034.88	a^3F_4–$q^3F^\circ_4$		
465	2,374.43	10		42,102.50	a^3F_2–$t^3G^\circ_3$		
467	2,372.57	5		42,135.51	a^3F_3–$q^3F^\circ_2$		
	2,372.33	3		42,139.77			
	2,371.70	2		42,150.96			
	2,371.14	1		42,160.92			
	2,370.42	3		42,173.72			
466	2,367.33	8		42,228.76	a^3F_3–$q^3D^\circ_3$		
466	2,363.52	10		42,296.83	a^3F_2–$q^3D^\circ_1$		

TABLE 3.—*Wave lengths in the arc spectrum of Zr*—Continued

Key No.	λ I. A.	Intensities, temperatures class, and notes		Wave No.	Term combinations	Observed Zeeman effects	Theoretical Zeeman effects
		B. S.	King				
	2,363.05	2		42,305.24			
	2,360.41	1		42,352.65			
	2,356.24	1		42,427.50			
466	2,355.90	7		42,433.62	$a^3F_2-q^3D_2^3$		
	2,354.65	1		42,466.97			
	2,349.58	2		42,547.75			
467	2,341.32	3		42,697.85	$a^3F_3-q^3F_3^4$		
467	2,340.87	5		42,706.05	$a^3F_3-q^3F_4^4$		
467					$a^3F_2-q^3F_2^2$		
	2,334.64	1		42,820.01			
	2,330.72	2		42,892.01			
468	2,330.55	1		42,895.14	$a^3F_1-o^3D_1^1$		
	2,321.64	1		43,059.75			
	2,320.78	2		43,075.71			
	2,316.20	1		43,160.87			
468	2,315.56	1		43,172.80	$a^3F_4-o^3D_3^3$		
467	2,310.44	2		43,268.47	$a^3F_2-q^3F_3^3$		
	2,285.25	6		43,745.76			
	2,269.43	5		44,050.28			
	2,253.27	3		44,366.16			
	2,250.73	3		44,416.23			
469	2,248.05	4		44,469.17	$a^3F_4-p^3D_3^3$		
	2,239.19	3		44,645.10			
	2,230.88	5		44,811.39			
	2,224.97	3		44,930.41			
470	2,220.68	5		45,017.20	$a^3F_2-s^3F_2^3$		
469					$a^3F_3-p^3D_3^3$		
469	2,214.63	4		45,140.16	$a^3F_3-p^3D_3^3$		
	2,214.20	5		45,148.93			
469	2,201.69	3		45,405.43	$a^3F_2-p^3D_1^1$		
469	2,192.89	3		45,587.63	$a^3F_2-p^3D_2^2$		
	2,181.50	3		45,725.62			
	2,178.97	5		45,878.82			
	2,173.62	3		45,991.73			
	2,160.23	4		46,276.78			
	2,157.78	5		46,329.32			
	2,149.15	6		46,515.33			
471	2,136.16	7		46,798.15	$a^1D_2-p^1P_1^1$		
	2,119.14	6		47,173.96			
	2,110.53	7		47,366.40			
	2,109.42	4		47,391.31			
	2,108.56	6		47,410.64			
472	2,105.83	5		47,472.10	$a^3F_4-o^3D_1^1$		
	2,103.31	5		47,528.97			
472	2,101.80	5		47,563.11	$a^3F_3-o^3D_3^3$		
472	2,092.88	4		47,765.80	$a^3F_2-o^3D_1^1$		
	2,089.57	5		47,841.45			
	2,088.89	3		47,857.02			

TABLE 4.—*Key to the term combinations of Zr I*

Odd terms \ Even terms	a^1S	a^1P	a^1D	b^1D	a^1F	a^1G	b^1G	a^1H	a^3P	b^3P	c^3P	a^3D	a^3F	b^3F	c^3F	e^3F	a^3G	a^3H	a^5P	a^5D	a^5F	e^5F	f^5F	e^5G	f^5G	e^5H^1
z^1P°	93		282						300				376								283					
y^1P°	160		343						365																	
x^1P°			422	234					428		237															
w^1P°	347		434																							
v^1P°	453		471																461							
z^1D°			34						47				107								29					
y^1D°			116						134				222													
x^1D°			227						259																	
w^1D°			382										420	255					269	38						
v^1D°			431	258					439		262			367							427					
z^1F°			118			76							223													
y^1F°			154			102			167				252	27			46		149							
x^1F°			192			123			215			24	311	67			53	12	77		178					
w^1F°			400			369							442	295			285									
v^1F°			423	239		402	216		433		243	319	451													
u^1F°			462?			463															460					
z^1G°						147							323	71			66				187					
y^1G°						247	50	31					383													
x^1G°						360	135	114					425	284			266	202								
w^1G°						416	267	240																		
v^1G°																										
z^1H°						325	99	81					412													
y^1H°						404	218	191										144								
x^1H°								268										305								
z^1I°								161										261								
z^3S°			106						115				214									49				
y^3S°			334						341																	
x^3S°			353						371	109									217							
w^3S°			449						454		327										450					
z^3P°			83						94												79					
y^3P°			232						254			42	337													
x^3P°			273	19					293		11		370								274					
w^3P°			387						394	152		179	432	279					294							
v^3P°			397						401		150	212		306					324							
u^3P°			406						408		169	228														
t^3P°			435						438		272	331		384												
s^3P°			456						458		350		470													
z^3D°			32						43				108			162					33	110				
y^3D°			124			88			136				229	10					30		119	18				
x^3D°			188						207			23	326	69			63				193					

z^3D°			188						207			23	325	69			65			125										
w^3D°			208						235			36	330	80			73			211										
v^3D°			276						296		13	70	354						127		277									
u^3D°			368						379	128	104		415	210			196	157	233		364									
t^3D°			395			358			403		141	200	424	281			264		310											
s^3D°									418		197	278	444	328			322													
r^3D°			426						430			321	455						378											
q^3D°			446								317	359	466	392				352			457									
p^3D°			459						464		363		469	417							468									
o^3D°											398		472	437					445		9	129			381					
z^3F°			6						25				89			175														
y^3F°			133			86			151				248	8		64	4		39		122									
x^3F°			185			131			205			20	316	65			55	16	78		181									
w^3F°			245						275				335	91			84	51			241									
v^3F°			356			315			372		96	143	411	182			174		213		348									
u^3F°			355			318			373			146	410	189			177		226		357									
t^3F°			393			345	126	111	396			199	421	265	171		250	194	301											
s^3F°			407				166		413			231	441	314			299	244			409									
r^3F°												287	447	333			332	288												
q^3F°								303					467		349		391													
z^3G°			105			57			117				183			87					101									
y^3G°			176						201				297	52			41	2	74		163									
x^3G°			257			184			290				339	97	40		90	56			246									
w^3G°									338				389	155			142	103	170		329									
v^3G°			405			375	159	137	413			236	440	308			286	220												
u^3G°		221					230	198				312	452	346			340	309												
t^3G°			443						448			342	465	385							224									
z^3H°						164							336	95			82	44												
y^3H°														219			206	158	253											
x^3H°						366	145	121					429	292			280	203												
z^3I°						344								263			249	186												
z^5S°									138										22											
y^5S°									399			204	436						304											
z^5P°			180						190			7	302	54			48		68		172									
y^5P°			380						388			168	419	251					270	37										
z^5D°			62						72				130								59	98								
y^5D°			132			92			148				242	15			3		28		125	14								
x^5D°									320				374				113	85	140		298									
w^5D°									377			153		209					225	17	362									
z^5F°			26						35				100								21	112		260	361					
y^5F°			271						291			58	351								256				120					
z^5G°													60								1	156		307	386	289				
y^5G°						139			195				313	61			45	5	75		173				165					

2. THE ZEEMAN EFFECTS

The observed Zeeman effects for the arc lines of Zr, which are entered in column 7 of Table 3, confirm most of the terms given in Tables 1 and 2. As stated above these results are taken from Moore's published observations, from his more recent observations measured and reduced at the National Bureau of Standards, and from observations made with the recently acquired magnet in conjunction with the spectrographs of the National Bureau of Standards. These newest observations are specially marked in the table, an asterisk (*) indicating those made with the concave grating, and the symbol E_1 those made with the quartz prism spectrograph. For comparison with the observed patterns the theoretical Zeeman effects are entered in the last column of Table 3. These have been taken from the Tables of Theoretical Zeeman Effects,[12] by Kiess and Meggers.

Only a few of the observed Zeeman effects are fully resolved, the majority representing blends of the unresolved components of the magnetic patterns. In some instances the type of blending is evident, and this is indicated in the tables by the symbols A^1, A^2, and B, as used by Back.[13] Lines with unresolved but with definitely widened p components are marked with a letter w.

In our paper [14] on the classification of Zr II we cited two lines which are members of both the arc and first spark spectra of Zr, as shown by their Zeeman effects, but which had not been resolved with the spectrographs employed in observing them. To these we add the line at 4,304.68 A. Its wave number is given by three pairs of term combinations, of which two, $a^3D_3 - s^3F_4$ and $a^3P_1 - y^3P_0$, are indicated by the observed pattern (0.00) 1.01, 1.46.

Landé's [15] theory of the anomalous Zeeman effect for weak fields assigns to each spectral term a g value which gives the amount by which the components of a term are separated in the magnetic field. For most of the terms of Zr I the g values appear to be normal, but for several terms the g's are abnormal. This abnormality was detected early in this work for two of the odd terms, $x^3F°$ and $w^3F°$, and in a paper by Meggers and Kiess,[16] was interpreted as indicating a deviation from normality with position in the term diagram. But this view, in the light of the additional data we have obtained, is no longer tenable. These data abundantly illustrate the fact that two terms of approximately the same value, with the same inner quantum number J, and arising from the same electron configuration, will have g values equal to the mean of their theoretical g's. Back [17] was the first to notice this phenomenon for Ca I; subsequently Russell [18] detected instances of it in Ti I, and Shenstone [19] has cited more numerous occurrences of it in Cu I, Cu II, and Ni II. In Table 5 we give the pairs of terms of Zr I which thus affect each other, and in Table 6 we give some of the observed Zeeman patterns resulting from these affected terms, and compare them with patterns calculated with the observed g's according to Landé's rules. There are other terms of Zr I which also exhibit abnormal g's, such as $y^1F_3°$ and $t^3F_4°$, but at

[12] B. S. Jour. Research (RP 23), **1**, p. 641; 1928.
[13] Zeit. für Physik, **15**, p. 206; 1923.
[14] B. S. Jour. Research (RP 255), **5**, p. 1234; 1930.
[15] Zeit. für Physik, **5**, p. 231; 1921; **15**, p. 189; 1923.
[16] J. Opt. Soc. Am. & Rev. Sci. Inst., **12**, p. 443; 1926.
[17] Zeit. für Physik, **33**, p. 581; 1925.
[18] Astrophys. J., **66**, p. 411; 1927.
[19] Phys. Rev., **28**, p. 453; 1926; **29**, p. 384; 1927; **30**, p. 258; 1927.

the present time the observations are not sufficient to show whether the abnormality is produced by a near-by perturbing term of like inner quantum number and electronic origin or by some other cause.

TABLE 5.—*Zr I terms with abnormal g values*

Term	ν	Theoretical g	Observed g	Electron configuration
a^3P_2	4, 186. 11	1. 500	1. 25	$4d^2.5s^2$
a^1D_2	5, 101. 68	1. 000		
b^3F_4	12, 342. 37	1. 250	1. 15	$4d^2.5s$
a^3G_4	12, 760. 66	1. 050		
$z^1G_4^\circ$	26, 931. 35	1. 000	1. 13	$4d^2.5s.5p$
$x^3F_4^\circ$	26, 938. 42	1. 250		
$w^3F_4^\circ$	28, 528. 36	1. 250	1. 15	$4d^2.5s.5p$
$x^3G_4^\circ$	28, 749. 80	1. 050		
$v^3D_1^\circ$	28, 800. 51	0. 500	0. 75	$4d^2.5s.5p$
$z^1P_1^\circ$	28, 999. 46	1. 000		
$y^3P_2^\circ$	34, 761. 52	1. 833	1. 42	$4d^2.5p$
$w^1D_2^\circ$	34, 850. 96	1. 000		
$w^1F_3^\circ$	36, 759. 90	1. 000	0. 87	$4d^2.5p$
$v^3G_3^\circ$	36, 941. 65	0. 750		

TABLE 6.—*Zeeman effects from abnormal g values*

Term combination	λ	Observed Zeeman effect	Calculated Zeeman effect
a^1D_2–$z^3P_2^\circ$	6, 506. 39	(0. 46) 1. 46	(0. 25, **0. 50**) 1. 00, **1. 25, 1. 50**, 1. 75
a^3P_2–$z^3P_2^\circ$	6, 140. 50	(0. 48) 1. 44	
a^1D_2–$y^1D_2^\circ$	5, 664. 55	(0. 51) 1. 69	(0. 25, **0. 50**) 0. 75, **1. 00, 1. 25**, 1. 50
a^3P_1–$y^1D_2^\circ$	5, 385. 14	(0. 45) 1. 10	
a^1D_2–$y^3D_3^\circ$	5, 386. 65	(0. 00) 1. 32	**(0. 00**, 0. 08, 0. 17) 1. 17, 1. 25, 1. 33, 1. 42, **1. 50**
a^3P_2–$y^3D_3^\circ$	5, 133. 42	(0. 00) 1. 23	
a^1D_2–$w^3D_3^\circ$	4, 466. 90	(0. 00) 1. 44	
a^3P_2–$w^3D_3^\circ$	4, 291. 34	(0. 00) 1. 47	
a^1D_2–$x^1F_3^\circ$	4, 732. 34	(0. 00w) **0. 61**, 1. 07	(**0. 00**, 0. 25, 0. 50) **0. 50**, 0. 75, 1. 00, 1. 25, 1. 50
a^3P_2–$x^1F_3^\circ$	4, 535. 75	(0. 00w) 0. 67 A [1]	
a^1D_2–$x^3P_1^\circ$	4, 234. 63	(0. 00w) 1. 13	(**0. 00**, 0. 25) **1. 00**, 1. 25, 1. 50
a^3P_2–$x^3P_1^\circ$	4, 076. 53	(0. 00) 1. 13	
a^1D_2–$v^3D_1^\circ$	4, 218. 44	(0. 00) 1. 68	(**0. 00**, 0. 50) 0. 75, 1. 25, **1. 75**
a^3P_2–$v^3D_1^\circ$	4, 061. 53	(**0. 00**, 0. 46) 1. 60	
a^1D_2–$z^1P_1^\circ$	4, 183. 31	(**0. 00**, 0. 47) 1. 26, **1. 76**	
a^3P_2–$z^1P_1^\circ$	4, 028. 95	(0. 00) 1. 57	
a^1D_2–$x^3P_2^\circ$	4, 199. 08	(0. 42) 1. 39 B	(0. 25, **0. 50**) 1. 00, **1. 25, 1. 50**, 1. 75
a^3P_2–$x^3P_2^\circ$	4, 043. 57	(0. 49) 1. 33	
a^1D_2–$v^3F_3^\circ$	3, 558. 95	(0. 00) 0. 72	(**0. 00**, 0. 17, 0. 33) **0. 75**, 0. 92, 1. 08, 1. 25, **1. 42**
a^3P_2–$v^3F_3^\circ$	3, 446. 61	(0. 00) 0. 79	
a^1D_2–$y^3P_2^\circ$	3, 370. 60	(0. 00) 1. 38	(0. 17, **0. 34**) 1. 08, **1. 25, 1. 42**, 1. 59
a^3P_2–$y^3P_2^\circ$	3, 269. 66	(0. 00) 1. 24	
a^3G_4–$x^3D_3^\circ$	6, 966. 49	(0. 00) 0. 64	(**0. 00**, 0. 18, 0. 37, 0. 55) **0. 60**, 0. 78, 0. 97, 1. 15, 1. 33, 1. 52, 1. 70
b^3F_4–$x^3D_3^\circ$	6, 769. 16	(0. 00w) 0. 72	
a^3G_4–$z^3H_5^\circ$	6, 470. 25	(0. 00) 0. 79	(**0. 00**, 0. 12, 0. 23, 0. 35, 0. 47) **0. 57**, 0. 68, 0. 80, 0. 92, 1. 03, 1. 15, 1. 27, 1. 38, 1. 50
b^3F_4–$z^3H_5^\circ$	6, 299. 72	(0. 00) 0. 78	
a^3G_4–$x^3G_5^\circ$	6, 155. 56	(0. 00) 1. 36	(**0. 00**, 0. 05, 0. 10, 0. 15, 0. 20) **1. 00**, 1. 05, 1. 10, 1. 15, 1. 20, 1. 25, 1. 30, 1. 35, **1. 40**
b^3F_4–$x^3G_5^\circ$	6, 001. 03	(0. 00) 1. 36	
a^3G_4–$w^3G_5^\circ$	5, 155. 46	(0. 00) 1. 30	
b^3F_4–$w^3G_5^\circ$	5, 046. 61	(0. 00) 1. 25	
a^3F_4–$z^1G_4^\circ$	3, 891. 39	(0. 63) 1. 15	(0. 12, 0. 24, 0. 36, **0. 48**) 0. 77, 0. 89, 1. 01, **1. 13, 1. 25**, 1. 37, 1. 49, 1. 61
a^3F_4–$z^3F_4^\circ$	3, 890. 32	(**0. 26**) 1. 16	

TABLE 6.—*Zeeman effects from abnormal g values*—Continued

Term combination	λ	Observed Zeeman effect	Calculated Zeeman effect
a^3F_3–$z^1G_4^\circ$ a^3F_2–$x^3F_3^\circ$	3,792.40 3,791.39	(0.00) 1.24 (0.00) 1.37	(**0.00**, 0.05, 0.09, 0.14) 0.99, 1.04, 1.08, 1.13, 1.18, 1.22, **1.27**
a^3F_4–$w^3F_4^\circ$ a^3F_4–$x^3G_4^\circ$	3,663.64 3,634.14	(0.38) **1.14** (0.31) **1.22**	(0.10, 0.20, 0.30, **0.40**) 0.85, 0.95, 1.05, **1.15**, **1.25**, 1.35, 1.45, 1.55
a^3F_3–$w^3F_3^\circ$ a^3F_3–$x^3G_4^\circ$	3,575.79 3,547.69	(0.00) 1.21 (0.00) 1.25	(**0.00**, 0.07, 0.13, 0.20) 0.95, 1.02, 1.08, 1.15, 1.22, 1.28, **1.35**
a^5P_3–$y^5P_3^\circ$ a^5P_3–$w^1D_3^\circ$	4,253.56 4,237.42	(0.00) 1.96 A [3] (0.00) 1.96	(**0.00**, 0.25, 0.50) 1.17, 1.42, 1.67, 1.92, **2.16**
a^5P_1–$y^5P_2^\circ$ a^5P_1–$w^1D_2^\circ$	4,187.12 4,171.47	(0.00) 0.32 (0.00, 1.07) 0.29	(**0.00**, 1.08) **0.34**, 1.42, 2.50
a^1G_4–$w^1F_3^\circ$ a^1G_4–$v^3G_3^\circ$	3,483.01 3,461.09	(0.00) **1.24** (0.00) **1.24**	(**0.00**, 0.13, 0.26, 0.39) 0.61, 0.74, 0.87, 1.00, 1.13, 1.26, **1.39**

3. THE INTENSITIES

No quantitative measurements of line intensities in the Zr spectra have as yet been published. But the estimates made at the National Bureau of Standards, as described above, and those of King and Miss Carter, are considered sufficiently reliable to illustrate the combination behavior of the terms. Indeed, Russell [20] has shown that King's intensity estimates, based on an extensive series of observations, are quite homogeneous, and are nearly proportional to the square roots of the theoretical intensities. We have, therefore, based the discussion which follows almost entirely on the Mt. Wilson intensities, supplementing them only where necessary with our own estimates.

For many of the Zr I multiplets, and especially those of the quintet system, the intensities appear to follow the requirements of the rules derived independently from quantum theoretical considerations by Russell,[21] by Hönl and Sommerfeld,[22] and by Kronig.[23] According to these rules those lines within a multiplet are strongest which represent a transition for which the change in the inner quantum number J is in the same direction as that of the term quantum number L, lines exhibiting the same ΔJ increasing in intensity with J. Kronig's formulas show further that the total intensities of a triad of multiplets having a common term will differ, that being strongest for which the change ΔL in the term quantum number is in the same direction as the change Δk in the azimuthal quantum number of the current electron.

But there are many Zr I lines which individually show abnormal intensities, and, in the triplet system, there are several multiplets which appear to be in contradiction with the first of the above rules. Most of the individual lines with intensities too high or too low represent combinations of which at least one of the combining terms is perturbed by a near-by term with the same inner quantum number. The perturbing terms also belong, apparently, to the same electron configuration. The effect is entirely analogous to that of the abnormal Zeeman effects described above, two related terms sharing their transition probabilities as well as their g values. All the singlet-

[20] Proc. Nat. Acad. Sci., **11**, p. 322; 1925.
[21] Proc. Nat. Acad. Sci., **11**, p. 314; 1925.
[22] Sitz. Ber. Akad. Wiss. Berlin, p. 141; 1925.
[23] Zeit. für Physik, **31**, p. 885; 1925; **33**, p. 261; 1925.

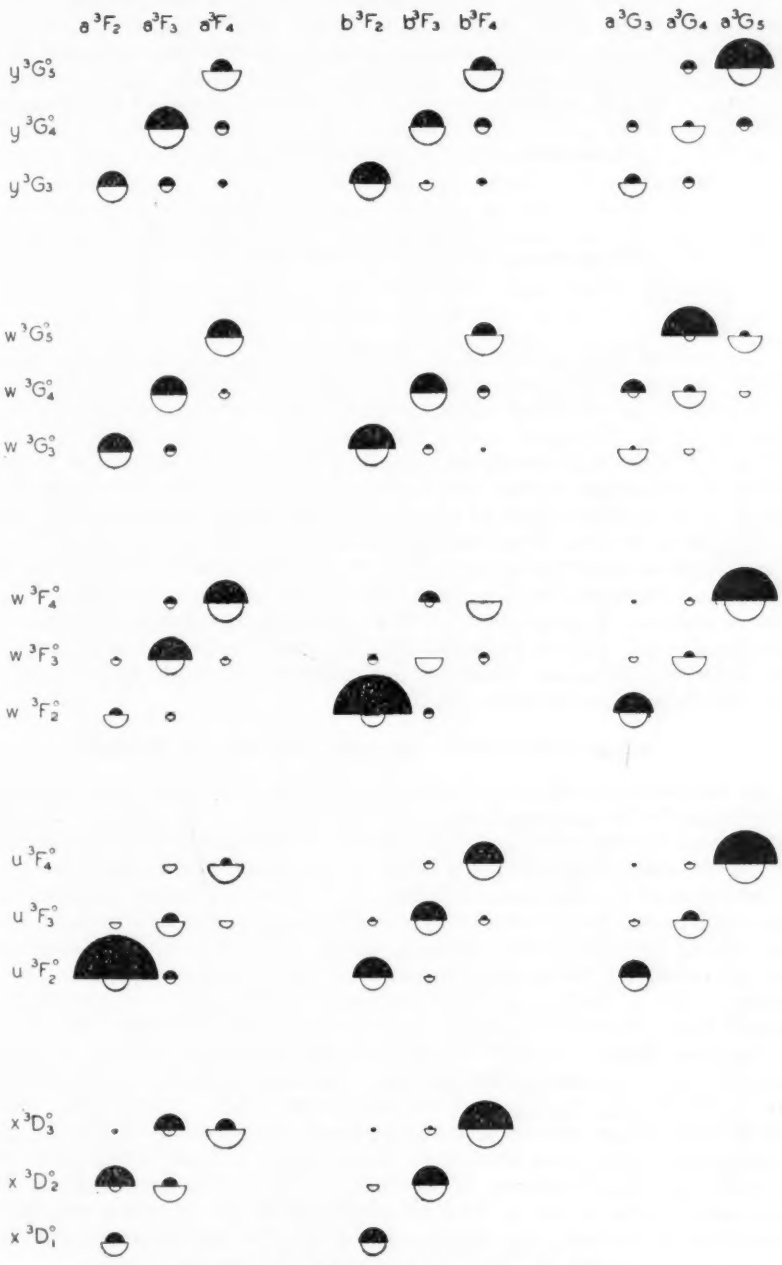

FIGURE 4.—*Abnormal intensities of Zr I*

Black semicircles, observed intensities
Open semicircles, theoretical intensities

quintet intersystem combinations may be thus accounted for. For example, the low term a^1D_2 participates with its companion a^3P_2 in combining with $z^5P°$, $y^5P°$, $z^5D°$, $y^5D°$, $z^5F°$, and $y^5F°$. Again, a^1G and a^5F each combine with high terms of the other system which are undoubtedly perturbed by terms with which they normally combine. The data illustrating this may be summarized as follows:

$$a^1\text{G combines with}\left\{\begin{matrix} y^5\text{D}_3^\circ \\ y^3\text{G}_3^\circ \end{matrix}\right\}\text{perturbed by}\left\{\begin{matrix} y^1\text{F}_3^\circ \\ y^3\text{G}_3^\circ \end{matrix}\right\}$$

$$a^5\text{F combines with}\left\{\begin{matrix} z^1\text{P}_1^\circ \\ z^1\text{D}_2^\circ \\ v^1\text{D}_2^\circ \\ y^1\text{F}_3^\circ \\ x^1\text{F}_3^\circ \\ u^1\text{F}_3^\circ \\ z^1\text{G}_4^\circ \end{matrix}\right\}\text{perturbed by}\left\{\begin{matrix} x^3\text{P}_1^\circ, & v^5\text{D}_1^\circ \\ z^3\text{D}_2^\circ & \\ r^3\text{D}_2^\circ & \\ y^5\text{D}_3^\circ & \\ y^3\text{G}_3^\circ & \\ p^3\text{D}_3^\circ & \\ x^3\text{F}_4^\circ & \end{matrix}\right\}$$

The second type of intensity abnormality is to be found in certain triplet system multiplets resulting from combinations of a common high term with low terms arising from different electron configurations. The effect is displayed most markedly in several multiplets with a^3F and b^3F as final terms, and consists of an inversion of the normal intensity relations within the multiplet; that is, the strongest lines result from combinations of terms of lowest inner quantum numbers. In Figure 4 the data illustrating this effect are shown graphically, the areas of the semicircles being drawn proportional to the intensities, the black ones representing the observed values and the open ones the theoretical values. For comparison the multiplets involving the term a^3G are also shown. It is to be noted that the graph is not intended to show the intensity relations between the different multiplets, but only of the individual lines within a multiplet.

4. INTERPRETATION OF THE OBSERVED TERMS

All the terms which have been observed for Zr I can be accounted for satisfactorily by means of the quantum theory of the atom. According to this theory, the final formulation of which is due to Hund,[24] the terms on which a spectrum is built up represent the resultants of the interaction of the valence electrons of an atom. The neutral Zr atom, atomic No. 40, has 40 electrons outside the nucleus of which 36 form the closed groups of the krypton shell. The 4 remaining electrons are the series or valence electrons, 2 of which are assigned to the 4_3 orbits of the N shell, and 2 to 5_1 orbits of the O shell. The configuration of these electrons is designated by the symbol $4d^2 \cdot 5s^2$. But it can so happen that 3 or all 4 of the valence electrons occupy 4_3 orbits leaving but 1 or none in the 5_1 orbits. In such cases the configurations are symbolically designated as $4d^3 \cdot 5s$ and $4d^4$. The terms which result from these electron configurations are given in Table 7. For comparison with them the terms which have actually been found are given in the third column of the table. Thus it is seen that the low and metastable terms of Zr I all originate in the electron configurations just described, the configuration $4d^2 \cdot 5s^2$ representing the state of minimum energy or the normal state of the neutral atom.

With the absorption of energy by the atom, an electron is removed from one of the configurations just described to an outer orbit. New electron configurations ensue, of which the most conspicuous are those

[24] Linienspektren und periodisches System der Elemente, Julius Springer, Berlin; 1927.

in which one of the original $5s$ or $4d$ electrons is raised to a 5_2 orbit. The configurations containing one $5p$ electron will produce groups of odd terms, as shown in the table, which will combine strongly with the low and metastable terms. Nearly all the terms required by theory for the configurations $4d^2 \cdot 5s \cdot 5p$, $4d^3 \cdot 5p$, and $4d \cdot 5s^2 \cdot 5p$, except some of the singlets, have actually been found for Zr I.

As the energy of the atom increases, the migrating electron will enter the 5_3 and 6_1 orbits and the new configurations will be $4d^2 \cdot 5s \cdot 6s$, $4d^2 \cdot 5s \cdot 5d$, etc. The terms will be even, and will combine with the odd terms of the middle group. Owing to their origin in configurations similar to those giving the low and metastable terms, they will form Rydberg series with the corresponding terms of the low group. As Table 7 shows, only a few of these high, series-forming terms have been identified. The limits of these series will be the low terms of Zr II coming from the configurations $4d^2 \cdot 5s$, $4d^3$, and $4d \cdot 5s^2$, which result when the neutral atom has lost one of its electrons. From our work on the analysis of Zr II are taken the limits given in the last column of Table 7.

TABLE 7.—*Theoretical and observed terms of Zr I*

Electro configuration	Theoretical terms	Observed terms	Limit in Zr II
$4d^2 \cdot 5s^2$	^{3}F ^{3}P ^{1}G ^{1}D ^{1}S	a^3F a^3P a^1G a^1D a^1S	a^4F, a^2F a^4P, a^2P b^2G a^2D a^2S
$4d^3 \cdot 5s$	^{5}F, ^{3}F ^{5}P, ^{3}P ^{3}H, ^{1}H ^{5}G, ^{1}G ^{3}F, ^{1}F ^{3}D, ^{1}D ^{3}P, ^{1}P ^{3}D, ^{1}D	a^5F, b^3F a^5P, b^3P a^3H, a^1H a^3G, b^1G c^3F a^3D, b^1D c^3P	b^4F b^4P a^2H a^2G b^2F b^2D b^2P c^2D
$4d^4$	^{5}D, ^{3}H, ^{3}G, ^{3}F, ^{3}D, ^{3}P, ^{1}I, ^{1}G, ^{1}F, *etc.*	a^5D	
$4d^2 \cdot 5s \cdot 5p$	^{5}G°, ^{5}F°, ^{5}D°, ^{3}G°, ^{3}F°, ^{3}D° ^{5}D°, ^{5}P°, ^{3}S°, ^{3}D°, ^{3}P°, ^{3}S° ^{3}H°, ^{3}G°, ^{3}F°, ^{1}H°, ^{1}G°, ^{1}F° ^{3}G°, ^{3}F°, ^{3}D°, ^{1}G°, ^{1}F°, ^{1}D° ^{3}F°, ^{3}D°, ^{3}P°, ^{1}F°, ^{1}D°, ^{1}P° ^{3}D°, ^{3}P°, ^{3}S°, ^{1}D°, ^{1}P°, ^{1}S° ^{3}P°, ^{1}P°	z^5G°, z^5F°, z^5D°, z^3G°, z^3F°, z^3D° y^5D°, z^5P°, z^5S°, y^3D°, y^3P°, y^3S° x^3H°, u^3G°, z^3F°, z^1H°, x^1G° x^3G°, w^3F°, u^3D°, z^1G°, y^1F° x^3F°, v^3D°, x^3P°, z^1F°, z^1D°, z^1P° x^3D°, z^3P°, z^3S°, y^1D°, y^1P°, v^1P°	a^4F a^4P b^2G a^2F a^2D a^2P a^2S
$4d^3 \cdot 5p$	^{5}G°, ^{5}F°, ^{5}D°, ^{3}G°, ^{3}F°, ^{3}D° ^{5}D°, ^{5}P°, ^{3}S°, ^{3}D°, ^{3}P°, ^{3}S° ^{3}I°, ^{3}H°, ^{3}G°, ^{1}I°, ^{1}H°, ^{1}G° ^{3}H°, ^{3}G°, ^{3}F°, ^{1}H°, ^{1}G°, ^{1}F° ^{3}G°, ^{3}F°, ^{3}D°, ^{1}G°, ^{1}F°, ^{1}D° ^{3}F°, ^{3}D°, ^{3}P°, ^{1}F°, ^{1}D°, ^{1}P° ^{3}D°, ^{3}P°, ^{3}S°, ^{1}D°, ^{1}P°, ^{1}S° ^{3}F°, ^{3}D°, ^{3}P°, ^{1}F°, ^{1}D°, ^{1}P°	y^5G°, y^5F°, x^5D°, y^3G°, y^3F°, w^3D° w^5D°, y^5P°, y^5S°, z^3D°, w^3P°, x^3S° z^3I°, y^3H°, t^3G°, z^1I°, x^1H°, w^1G° z^3H°, v^3G°, s^3F°, y^1H°, y^1G°, v^1F° w^3G°, v^3F°, s^3D°, w^1F°, v^1D° u^3F°, r^3D°, v^3P°, x^1F°, x^1D°, x^1P° p^1D°, s^3P°, w^3S° r^3F°, q^3D°, u^3P°, w^1F°, w^1D°, w^1P°	b^4F b^4P a^2H a^2G b^2F b^2D b^2P c^2D
$4d \cdot 5s^2 \cdot 5p$	^{3}F°, ^{3}D°, ^{3}P°, ^{1}F°, ^{1}D°, ^{1}P°	q^3F°, o^3D°, t^3P°	d^2D
$4d^2 \cdot 5s \cdot 6s$	^{5}F, ^{3}F ^{5}P, ^{3}P ^{3}G, ^{1}G ^{3}F, ^{1}F ^{3}D, ^{1}D ^{3}P, ^{1}P ^{3}S, ^{1}S	e^5F, e^3F	a^4F a^4P b^2G a^2F a^2D a^2P a^2S
$4d^2 \cdot 5s \cdot 5d$	^{5}H, ^{5}G, ^{5}F, ^{5}D, ^{5}P, ^{3}H, ^{3}G, ^{3}F, ^{3}D, ^{3}P ^{3}H, ^{3}G, ^{3}F, ^{3}D, ^{3}P, ^{1}H, ^{1}G, ^{1}F, ^{1}D, ^{1}P ^{5}F, ^{5}D, ^{5}P, ^{3}F, ^{3}D, ^{3}P ^{3}F, ^{3}D, ^{3}P, ^{1}F, ^{1}D, ^{1}P ^{3}I, ^{3}H, ^{3}G, ^{3}F, ^{3}D, ^{1}I, ^{1}H, ^{1}G, ^{1}F, ^{1}D ^{3}G, ^{3}F, ^{3}D, ^{3}P, ^{3}S, ^{1}G, ^{1}F, ^{1}D, ^{1}F, ^{1}S ^{3}D, ^{1}D	e^5H, e^3G	a^4F a^2F a^4P a^2P b^2G a^2D a^2S
$4d^3 \cdot 5p^2$	^{5}G, ^{5}F, ^{5}D, etc.	f^5G	a^3F (Zr III)

There are no definitely established rules for tracing the observed terms of a complex spectrum back to their parent terms in the ion. Therefore, the assignment of the terms to their proper electron configurations is attended with some uncertainty. However, there are certain properties of complex terms and their combinations which give important clues as to their origin. For example, the quintet terms of Zr I can arise only from the addition of s and p electrons to the quartets of Zr II, and similarly, the singlets can arise only from the doublets of Zr. II. The triplets, however, are derived from both doublet and quartet terms. The relative positions of the terms in the term diagram and their separations will, in general, follow those exhibited by the parent terms of the ion. And further, the intensities of the term combinations will indicate the nature of the transitions involved in accordance with Kronig's rule as stated above, those being strongest for which the change ΔL in the term quantum number is the same as the change Δk in the azimuthal quantum number of the series electron.

It was on the basis of these principles that the assignment of the observed terms to their electron configurations was made, as shown in Table 7. The quintets fall into such clearly defined groups that there seems to be no uncertainty in allocating them. Among the triplets and singlets no such unmistakable groupings occur, and the assignments which have been made are admittedly open to revision. However, a partial check on the correctness of these assignments is afforded by the characteristic, noted above, of mutual perturbations exerted on each other by related terms. And conversely, it seems from the data at hand for Zr I, that neighboring terms of the same inner quantum number are unrelated, that is, have different electronic origins, if they fail to exhibit mutual perturbations. A further check on the correctness of the term assignments would be furnished by the application of the irregular doublet law to the Zr I terms and the corresponding terms of Cb II. Progress in the analysis of the first spark spectrum of Cb is not sufficiently advanced, however, to permit this at the present time. In Figures 1, 2, and 3, the terms which have been grouped together in Table 7 are connected with dotted lines.

The origin of the term f^5G is not certain. It lies too close to e^5G, and its combinations are much too strong to consider it as a second series member of the $4d^2 \cdot 5s \cdot md$ configurations. Russell [25] has found an analogous term in Ti I, which, owing to its association with similarly situated ^{5}D and ^{5}F terms, he has assigned to the configuration $3d^2 \cdot 4p^2$ with a^3F of Ti III as limit. We have found no trace of the corresponding D and F terms in Zr I, but because of its position in the term diagram we assign the term f^5G provisionally to the configuration $4d^2 \cdot 5p^2$.

We may now consider the *raies ultimes* of Zr I. In his discussion of the spectra of the elements of the Fe group Russell [26] has pointed out that the *raies ultimes* and resonance lines for the arc spectra originate in the transition $d^{n-2} \cdot s^2 \rightarrow d^{n-2} \cdot s \cdot p$, in which n is the number of electrons outside the argon shell. Except for K and Cr the resonance lines are invariably intersystem combinations of long wave length, whereas the ultimate rays are of much shorter wave length

[25] Astrophys. J., 66, p. 415; 1927. [26] Astrophys. J., 66, p. 212; 1927.

falling generally in the blue or violet. An apparent exception to these rules in the case of Ti I has been shown by Harrison and Engwicht [27] to be unreal. These rules give physical meaning to the empirical rule stated several years ago by Meggers, Kiess, and Walters,[28] and subsequently elaborated by Meggers and Laporte,[29] that the *raies ultimes* originate in the lowest term of the spectrum and result from its combination with a term of the same multiplicity but of L value one unit greater, whereas the resonance lines represent an intersystem combination between the lowest term and a term of higher multiplicity. For Zr I we find that the resonance lines and *raies ultimes* conform to these rules, the former being given by the combination $a^3\mathrm{F}—z^5\mathrm{F}°$, and the latter by $a^3\mathrm{F}—z^3\mathrm{G}°$, of which the principal lines are: 4,688.45, 4,633.99, and 4,575.52 A. These three lines, of Temperature Class I, appear in the fully developed spectrum with intensities much lower than do the neighboring blue lines, 4,687.8 to 4,815.6 A, also of Class I, which were designated by de Gramont [30] as sensitive lines in the visible region for spectrochemical analysis; and they are definitely weaker than the lines 3,601.18, 3,547.69, 3,519.60 A which are among the most intense of the entire arc spectrum and form the main diagonal of the multiplet $a^3\mathrm{F}—x^3\mathrm{G}°$. But on spectrograms obtained at the National Bureau of Standards, of elements containing Zr as a minute impurity, the lines cited above as the ultimate rays prove to be the most sensitive ones, whereas the others, which must be classed as penultimate rays following Russell's [31] terminology, appear much more faintly or not at all. Thus, both the resonance lines and the *raies ultimes* of Zr I result from the electron transition requiring the minimum transfer of energy, and the terms which combine to produce the lines all have $a^4\mathrm{F}$ of Zr II as parent term.

5. SERIES AND IONIZATION POTENTIAL

Only six terms of the third group have been identified combining with odd terms of the middle group. Of these only two, $e^3\mathrm{F}$ and $f^5\mathrm{F}$, form sequences with the low terms $a^3\mathrm{F}$ and $a^5\mathrm{F}$. These sequences represent the migration of an s electron from the O shell to the P shell, and are satisfactorily represented by a simple Rydberg formula, owing to the loose binding of the s electron in its orbits. The $^3\mathrm{F}$ terms will have $a^4\mathrm{F}$ of Zr II as limit, but the $^5\mathrm{F}$ terms will converge to $b^4\mathrm{F}$, the component series of each sequence approaching their different limits in the manner shown by Hund.[32] In Table 8 are the results obtained from six series for the distance between the lowest terms of Zr I and Zr II. The individual determinations are in good agreement and their mean, 56,077 cm^{-1}, is adopted as the value of $a^3\mathrm{F}_2—a^4\mathrm{F}_{1½}$. This represents the work required to remove an s electron from the atom and corresponds to an ionization potential of 6.92 volts.

---

[27] J. Opt. Soc. Am. & Rev. Sci. Inst., **18**, p. 296; 1929.
[28] J. Opt. Soc. Am. & Rev. Sci. Inst., **9**, p. 372; 1924.
[29] J. Opt. Soc. Am. & Rev. Sci. Inst., **11**, p. 460; 1925.
[30] Compt. Rend., **166**, p. 367; 1918.
[31] Astrophys. J., **61**, p. 223; 1925.
[32] Linienspektren, p. 184.

TABLE 8.—*Series limits of Zr I*

Term	a^3F_2	a^3F_3	a^3F_4	a^3F_3	a^3F_4	a^3F_5
Distance from limit, cm^{-1}	56,636	56,226	55,888	54,064	53,787	53,932
Reduction to $a^4F_{1\frac{1}{2}}$, Zr II	−315	−763	−1,323	−2,895	−3,758	−3,300
Reduction to a^3F_2, Zr I	0	+570	+1,241	+5,023	+5,889	+5,540
$a^4F_{1\frac{1}{2}}-a^3F_2$	56,321	56,033	55,806	56,192	55,918	56,192

Mean $(a^4F_{1\frac{1}{2}}-a^3F_2)=56{,}077\ cm^{-1}$
Ionization potential $=56{,}077\times1.2345\times10^{-4}=6.92\ v$

TABLE 9.—*Identification of Fraunhofer lines with Zr*

Observed		Solar			Observed		Solar		
λ	Intensity	λ	Intensity	Identification	λ	Intensity	λ	Intensity	Identification
9,276.94	1	6.92	−1		4,414.14	4	.121	−1	Ti
8,296.54	2	.571	−2		4,390.15	2	.116	−2	
6,994.38	12	.385	−3		4,389.61	2	.644	0	CH
6,853.85	3	.863	−3		4,346.53	5	.563	2	Fe
6,849.29	8	.314	−2 N		4,345.58	2	.608	−1 N	
6,762.38	20	.407	−2		4,325.44	10	.489	−2	
6,160.27	2	.234	−3		4,321.44	2	.424	0 N	
5,984.24	6	.279	−2		4,304.68	8	.724	0	
5,735.70	12	.712	−1	Ca?	4,225.25	3	.220	0	V+
5,555.38	2	.357	−3		4,220.65	3	.654	−1	Sa+
5,545.42	8	.430	−3		4,166.51	4	.534	−2	
5,518.06	2	.069	−2		4,134.32	4	.343	3	Fe
5,487.52	2	.524	−1 N		4,087.68	4	.707	−2	
5,460.71	3	.701	−3 *d* ?		4,053.67	2	.691	−1	
5,407.63	10	.619	−1	Cr+	4,050.48	5	.495	−1	
5,405.13	4	.141	−2		4,028.95	7	.991	−2	
5,280.06	10	.071	−1	Fe	4,007.59	8	.614	−1 *d* ?	Fe
5,243.46	5	.472	−3		4,004.87	4	.919	1	
5,224.94	9	.941	0	Cr Ti	4,001.22	2	.243	−2	
5,223.62	2	.632	−2	Ti	4,001.09	3	.112	0	
5,215.58	2	.577	−2 N		3,989.50	6	.450	−1 N	Ce+
5,165.97	8	.966	−3		3,981.59	10	.622	0	
5,161.01	7	.026	−2	(C−)	3,978.73	6	.777	−2	
5,158.68	6	.665	−3	(C−)	3,976.17	2	.187	−2	
5,145.46	1	.470	0	Ti	3,963.79	5	.806	−2	
5,136.78	3	.802	−2		3,926.78	5	.779	−2	
5,120.44	7	.425	0	Ti	3,901.49	3	.486	−1	
5,105.56	5	.547	4	Fe−Cu	3,892.02	5	.017	−2	Mg?
5,070.27	12	.297	−3	(C−)	3,780.53	18	.518	−1	CN
5,032.42	2	.385	−2 N		3,714.13	10	.158	−2 N	
4,996.35	10	.383	−2		3,656.88	5	.859	−3 N	
4,962.30	5	.294	−2	Sr?	3,612.55	2	.520	−2	
4,933.66	7	.673	−2 *d* ?		3,596.29	2	.314	−3	
4,881.25	8	.269	−3		3,577.55	6	.566	−3	CN
4,789.12	5	.139	−2		3,558.95	4	.985	−3	CN
4,707.78	5	.764	−1	Cr?	3,549.73	5	.766	−3 *d* ?	CN
4,640.12	3	.108	−2	V?	3,548.68	2	.652	−3	CN
4,634.63	3	.607	−2		3,535.16	8	.159	−3 N	
4,624.07	1	.092	−1		3,512.35	1	.382	−2	
4,584.57	1	.559	−3		3,503.27	2	.304	−2 N	
4,582.29	5	.313	0 N		3,494.44	4	.413	−3	
4,574.94	2	.905	−1 *d* ?	La+	3,493.66	3	.696	1	Fe
4,570.59	1	.611	−2 *d* ?		3,487.81	3	.821	−2	
4,539.98	8	0.001	−1 N	V	3,483.01	7	.018	4	Fe
4,513.34	2	.327	−2		3,478.78	8	.786	0	Fe
4,482.49	3	.441	−3		3,476.02	3	.027	−2 N	
4,455.43	5	.452	−2 N	Cr?	3,472.89	5	.905	−2	Cr
4,450.27	7	.237	−2		3,472.72	2	.715	−3 N	
4,448.94	3	.950	−1 N		3,465.63	7	.646	1	Ti+
4,420.25	1	.298	0		3,430.94	3	.956	−2	

TABLE 9.—*Identification of Fraunhofer lines with Zr*—Continued

Observed		Solar			Observed		Solar		
λ	Intensity	λ	Intensity	Identification	λ	Intensity	λ	Intensity	Identification
3,426.93	4	.913	−3	NH	3,243.98	10	4.030	−3 N	
3,416.68	4	.677	0	Fe	3,225.47	4	.463	−1 N	Cb+
3,411.78	2	.752	−2		3,223.34	3	.365	−1	OH
3,409.40	2	.399	−2 N		3,216.57	3	.547	0	
3,408.54	4	.506	−2 *d* ?		3,212.02	30	.006	2	Fe
3,386.90	2	.879	−2		3,185.68	2	.675	0	
3,326.43	6	.424	0	NH	3,185.08	3	.093	−3	
3,316.21	5	.198	−2 *d* ?		3,132.06	15	.056	4	Cr
3,297.64	2	.667	−2		3,121.95	2	.970	−1	
3,293.45	2	.479	−1						
					3,092.25	3	.234	−3	
3,285.18	3	.199	1	−Ce+?	3,085.34	10	.332	1	Fe?
3,261.06	2	.066	−1 *d* ?	Cd	3,052.80	2	.787	0	
3,260.11	15	.146	−2		3,052.00	2	1.987	−2 N	
3,256.00	2	5.983	−3						
3,254.28	10	.262	4	Ti+					

IV. ZIRCONIUM IN THE SUN

In our paper on the first spark spectrum of Zr we showed that many faint lines in the solar spectrum, whose origins are unknown or doubtful, can be accounted for by combinations of terms of Zr II. These include lines which are theoretically possible, but do not appear in laboratory sources in emission. We have carried out a similar survey for Zr I.

The wave lengths of Table 3 have been compared with those of the Fraunhofer lines listed by St. John and his associates in their recent Revision of Rowland's Preliminary Table of Solar Spectrum Wave-Lengths.[33] All coincidences which are not already assigned by them to Zr are given in Table 9. No doubt some of these will prove to be blends, especially those coinciding with lines already assigned to other atomic origins. There are many problems of physics and astrophysics which are based on such characteristics of the absorption lines which appear in the spectra of the sun and stars, as their wave lengths and contours. It is of importance, therefore, to know with certainty the chemical origins of the lines and the extent to which they are affected by blending.

It is a well-established fact that stellar spectra exhibit features that have not been duplicated in the laboratory. For example, more members of the Balmer series have been observed in absorption in the stars than have been observed in absorption or in emission in laboratory sources. And likewise, multiplet lines which appear only faintly or not at all in artificial sources may appear in stellar spectra with intensities revealing higher transition probabilities than those given by the quantum theory, as shown by the recent work of Woolley [34] and of Struve.[35] Many of the Zr I multiplets fail to show their full complement of lines in the laboratory and some which represent permissible transitions do not appear at all. We have calculated the wave lengths of these lines from the terms given above, and have compared them with the solar lines, with the results shown in Table 10.

[33] Carnegie Institution of Washington, Publication No. 396; 1928.
[34] Astrophys. J., **72**, p. 256; 1930.
[35] Astrophys. J., **72**, p. 267; 1930.

Again we recognize the possibility of fortuitous coincidences, but in cases where two or more lines of the same multiplet appear we believe the identifications are real.

TABLE 10.—*Identification of Fraunhofer lines with calculated lines of Zr*

Calculated λ	Solar			Term combination
	λ	Intensity	Identification	
6,224.17	4.206	−3		a^3H_5–$y^1G^0_4$
6,176.48	.463	−3		b^3F_4–$w^3F^0_4$
6,148.67	.668	−2		a^3H_4–$y^1G^0_4$
5,904.19	.208	−3	At m?	b^3F_4–$v^3D^0_3$
5,772.58	.589	−2	At m	b^3F_3–$v^3D^0_3$
5,535.06	.065	−3N		a^5F_2–$z^5S^0_2$
5,466.01	.035	−3N		a^3G_4–$y^1G^0_4$
5,440.96	.984	−2		a^3D_3–$y^1P^0_1$
5,374.90	.895	−3		a^3D_1–$y^1P^0_1$
5,366.43	.428	−1		a^3H_4–$u^3F^0_3$
5,304.42	.438	−3		a^5F_4–$y^1F^0_3$
5,219.90	.887	−3		c^3P_2–$t^3D^0_2$
5,197.40	.376	−3N		c^3P_1–$t^3D^0_2$
5,167.49	.510	5	Fe	c^3P_2–$v^3P^0_1$
5,162.76	.734	−3		a^5F_2–$y^1F^0_3$
5,020.04	.033	2	Ti	a^3H_4–$y^3H^0_5$
4,901.34	.321	−3N		a^5F_2–$z^5P^0_2$
4,848.47	.472	−2	Ti	a^5F_1–$z^5P^0_1$
4,823.06	.086	−3		a^3D_1–$w^1D^0_2$
4,757.33	.325	−2	−Cr?	a^3H_4–$t^3F^0_3$
4,723.30	.349	−2		a^3D_2–$t^3F^0_2$
4,682.98	.962	−2d?		a^3H_5–$x^1G^0_4$
4,673.44	.446	−1N		a^3D_1–$t^3F^0_2$
4,642.56	.593	−1N	Fe	a^5F_2–$z^3D^0_2$
4,398.30	.303	0	Ti+	a^5F_1–$y^3P^0_0$
4,374.62	.619	−1N		a^5F_2–$w^3F^0_2$
4,364.00	3.978	−2		a^3F_3–$w^3F^0_3$
4,229.43	.410	0		a^1G_4–$w^3G^0_4$
4,197.48	.510	−2		a^3F_3–$y^1F^0_3$
4,185.35	.366	−1N	Cr?	a^5F_2–$z^3P^0_2$
4,149.86	.900	−1		a^3H_4–$r^3F^0_3$
4,149.10	.129	0	CN	a^1G_4–$w^3G^0_3$
4,100.54	.510	−2		b^3F_3–$x^1G^0_4$
4,064.23	.215	1	Ti	a^3H_4–$u^3G^0_3$
3,996.88	.859	−2		a^3H_4–$r^1F^0_3$
3,990.56	.569	0Nd?	V	b^3F_3–$v^3P^0_2$
3,979.90	.904	−1		b^3F_2–$w^1F^0_3$
3,968.72	.717	1N		a^3H_5–$u^3G^0_5$
3,947.13	.135	0	Co	a^3F_3–$z^5P^0_3$
3,946.79	.815	−2N		b^3F_2–$u^3P^0_1$
3,923.13	.109	0	Ce+	b^3F_2–$s^3F^0_2$
3,922.02	.022	−1		a^5F_2–$z^5P^0_1$
3,921.40	.430	1	Ti	b^3F_2–$u^3P^0_1$
3,918.54	.575	0		b^3F_3–$s^3F^0_3$
3,908.42	.413	0	Ce+Pr+?	b^3F_4–$s^3F^0_4$
3,870.65	.666	0	CN	b^3F_3–$s^3F^0_3$
3,850.31	.305	−1	CN	b^3F_3–$s^3F^0_4$
3,827.25	.215	−1	CN?	a^3G_4–$r^3F^0_3$
3,811.79	.809	2		a^3F_3–$z^1F^0_3$
3,789.93	.923	−2	CN	a^3G_3–$r^3F^0_3$
3,787.77	.786	0		a^1G_4–$y^3H^0_4$
3,786.54	.524	0		a^3G_5–$r^3F^0_4$
3,751.48	.451	−1N		a^1G_4–$y^3H^0_5$
3,748.83	.801	−2		a^3F_4–$z^3H^0_4$
3,696.76	.754	−2		a^3G_4–$y^1F^0_3$
3,691.38	.396	−3		a^3G_5–$y^1H^0_5$
3,689.73	.701	−3		a^3G_4–$y^1H^0_5$
3,676.83	.815	−3		a^3H_5–$x^1H^0_5$
3,633.30	.309	−3N	Co?	a^3F_3–$x^1D^0_2$
3,625.77	.754	−2		a^3F_2–$y^3P^0_1$

TABLE 10.—*Identification of Fraunhofer lines with calculated lines of Zr*—Contd.

Calculated λ	Solar			Term combination
	λ	Intensity	Identification	
3,612.94	2.942	3	Fe	a^5F_5–$u^3F^\circ_4$
3,606.06	.040	−2	Ti?	a^5F_3–$v^3F^\circ_2$
3,589.98	.969	−1	Mn, CN	b^5F_3–$v^1F^\circ_3$
3,577.72	.746	−3	CN	a^5F_3–$v^5F^\circ_3$
3,568.02	.009	−3	CN	a^5F_4–$u^3F^\circ_4$
3,557.48	.465	−3	CN	a^5F_1–$v^3F^\circ_2$
3,551.68	.660	1	CN–Co	a^5F_4–$v^5F^\circ_4$
3,549.75	.766	−3*d*?	CN	b^5F_3–$v^1F^\circ_3$
3,531.28	.283	−3N		a^5F_3–$u^3F^\circ_4$
3,505.92	.900	0	Ti+?	a^5F_3–$u^3D^\circ_2$
3,504.58	.595	−3		a^3P_0–$y^1P^\circ_1$
3,495.99	.963	−3	CrTi	a^3P_1–$v^3F^\circ_2$
3,483.42	.415	3	Co	a^5F_4–$u^5D^\circ_3$
3,478.39	.367	0	Fe	a^5F_2–$u^3D^\circ_2$
3,476.94	.960	−3		a^5F_2–$v^5F^\circ_3$
3,460.58	.608	−3N		a^5F_2–$w^5D^\circ_4$
3,458.02	.011	−2	Ti?	a^5F_4–$y^5H^\circ_4$
3,449.97	.989	−2*d*?		b^5F_4–$w^1G^\circ_4$
3,448.39	.360	−3N	Co	a^5F_3–$u^5D^\circ_3$
3,427.75	.766	−2N		a^5F_4–$y^5H^\circ_5$
3,426.93	.913	−3	NH	a^1G_4–$v^3G^\circ_4$
3,423.50	.535	−1N	NH	a^5F_3–$y^5H^\circ_4$
3,418.28	.317	−3N		a^5F_5–$y^5H^\circ_6$
3,404.60	.585	0	Pd	b^5F_3–$w^1G^\circ_4$
3,404.44	.449	−3N		a^1G_4–$v^3G^\circ_5$
3,387.43	.419	2	Fe	a^5F_3–$y^5P^\circ_2$
3,384.67	.647	−1	Ti?	a^3G_5–$x^1H^\circ_5$
3,383.28	.314	−2		a^3G_4–$x^1H^\circ_5$
3,383.09	.097	−3N		a^5F_4–$y^5P^\circ_3$
3,350.04	.082	−2N		a^5F_3–$y^5P^\circ_3$
3,344.53	.524	2	Ca–La+	a^5F_1–$y^5P^\circ_2$
3,322.86	.875	1		a^5F_4–$w^5G^\circ_5$
3,322.70	.705	−1		a^5F_2–$x^5D^\circ_3$
3,309.52	.531	2N	Ti–	a^5F_3–$w^5P^\circ_2$
3,280.47	.499	−3N		a^3P_1–$w^1D^\circ_2$
3,255.49	.498	1N	OH	a^5F_5–$x^5H^\circ_5$
3,218.97	.985	−2	Co?	a^5F_4–$x^5H^\circ_5$
3,207.90	.894	−2	Ti	a^5F_1–$v^5P^\circ_0$
3,187.93	.900	−3		a^5F_3–$x^5H^\circ_4$
3,154.40	.421	1		a^5F_3–$v^5G^\circ_4$
3,147.77	.785	1	Fe	a^5F_3–$v^5P^\circ_2$
3,104.58	.572	2N	La+	a^5F_3–$u^5P^\circ_2$
3,081.02	.006	1		a^3F_4–$v^5F^\circ_4$

V. CONCLUSION AND ACKNOWLEDGMENTS

The structure of Zr I as portrayed in the preceding pages beautifully illustrates the effectiveness of the quantum theory of the atom to account for a complex spectrum. Not all the terms postulated by the theory have been established, but there is hardly room for doubt that among the lines of Zr I remaining unclassified or unobserved will be found the clues to the missing terms. Most of the unclassified lines lie in the ultra-violet, and probably result from the binding of an electron in a 4_4 orbit. We have sought for evidence of the terms coming from the $4f$ electron, both in Zr I and in Zr II, but without success, although both Zr III and Zr IV possess groups of lines representing the transition $4f \longrightarrow 4d$. In each of these spectra, however, energy of the order of 15 or 20 volts is required to remove an electron

from a 4_3 orbit to a 4_4 orbit, which is far in excess of that required to ionize the Zr atom.

In conclusion, we take this opportunity to express our thanks to all those who have aided us in the investigations of the Zr spectra described in this and in the preceding papers. To Dr. A. S. King and Miss Carter, to the late Prof. B. E. Moore, and to Prof. H. N. Russell we are particularly indebted for placing at our disposal unpublished observations and results of their investigations. To Mrs. F. J. Stimson, E. Z. Stowell, D. D. Laun, and B. F. Scribner, former and present members of the bureau's staff, we are indebted for the assistance they have given us in making the observations and calculations upon which this work is based.

WASHINGTON, February 12, 1931.

RADIATION FROM METALS BOMBARDED BY LOW-SPEED ELECTRONS

By F. L. Mohler and C. Boeckner

ABSTRACT

A small probe surface at a positive potential in a discharge may draw a current of many amperes per cm² with the potential gradient limited to a thin sheath over the surface. Under such conditions a continuous spectrum is emitted by metal surfaces in caesium, potassium, and helium discharges. With a copper probe at 7 volts in caesium vapor, the intensity J (λ) remains of the same magnitude between 6,200 and 2,400 A with a minimum at 5,800 and a maximum at 3,800. Below 4 volts the spectrum has a high-frequency limit in this range (3,000 A for copper at 2.15 volts). On the assumption that this is analogous to a continuous X-ray spectrum, observed limits indicate work functions of 1.95 volts for Cu, 2.1 for Ag, 1.45 for W (all in caesium vapor). The absolute intensity (except for Ag) agrees within a factor of 2 with values computed from the theoretical equation for intensity of the continuous X-ray spectrum. Efficiency for Cu at 7 volts is estimated as 5×10^{-7}. Comparison with published data on photo-electric effect of radiation from electron bombardment of metals indicates that the magnitude of effects below 10 volts can be explained by this continuous spectrum.

CONTENTS

		Page
I.	Introduction	673
II.	Apparatus	674
III.	Discharge conditions	675
IV.	Location of radiation	675
V.	Observations in various gases	676
VI.	Vapor pressure	676
VII.	Probe current	676
VIII.	Spectral intensity distribution	676
IX.	Intensity and voltage	676
X.	Probe material	678
XI.	Discussion	679

I. INTRODUCTION

There is some experimental evidence that the continuous X-ray spectrum extends on the long wave length side through the visible region. Lillienfeld and Rother [1] have reported a bluish continuous spectrum emitted from the focal spot of an X-ray tube operated at X-ray voltages. Foote, Meggers, and Chenault [2] found a continuous spectrum excited by bombarding metals with 1,000-volt electrons which extended throughout the range of a quartz spectrograph. The numerous studies [3] of the photo-electric effect of the unresolved radiation from metals bombarded by lower-speed electrons include measurements with applied potentials as low as 3 volts. These effects probably come from both continuous radiation and characteristic line emission, and there is little evidence as to which is predominant.

[1] Lillienfeld and Rother, Phys. Zeits., **21**, p. 49; 1920; and correction note p. 360 ib.
[2] Foote, Meggers, and Chenault, J. Opt. Soc. Am., **9**, p. 541; 1924.
[3] Holweck, De la Lumière aux Rayons X; Univ. of France Press.

Presumably a continuous spectrum in the visible could be excited by any potential above a few volts, but we would expect the efficiency at low voltage to be extremely low. It occurred to the authors that an effective means of obtaining high-current density at low voltage would be to use as a target a small probe surface in the highly ionized region of any discharge. Current densities as high as 10 amp's./cm^2 can be obtained at any positive potential below the arcing potential, and with such currents the field produced by the applied potential is limited to a thin sheath over the surface of the order of 10^{-3} cm thick. Thus collisions in the sheath are negligible and electrons strike the surface with their full energy. An obvious complication is that the faint radiation from the metal must be viewed in the presence of a brilliant discharge.

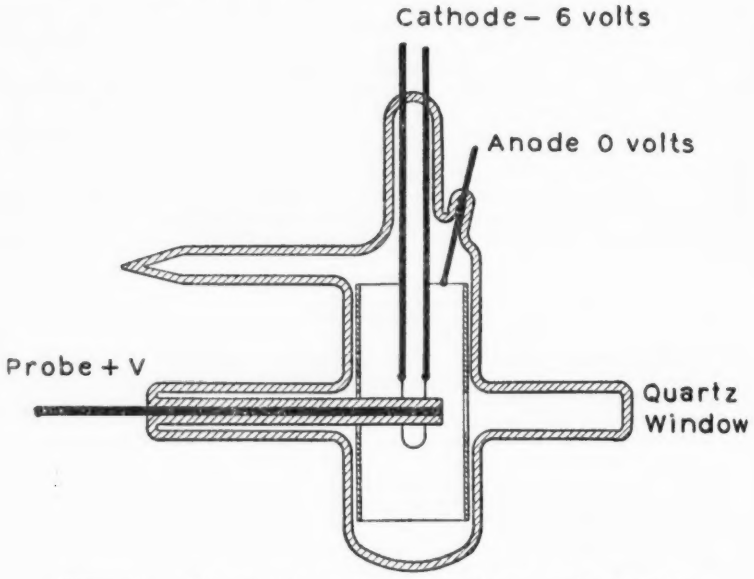

FIGURE 1.—*Type of tube used for observation of probe radiation*

Trial spectrograms of a small wire probe at a positive potential of 7 or 8 volts in a caesium discharge, gave evidence of a continuous spectrum more or less masked in the visible by line emission, but conspicuous in the ultra-violet. This paper reports preliminary experiments on the various factors influencing the intensity of this radiation.

II. APPARATUS

A thermionic discharge was maintained between a cylindrical anode and a hairpin or helical cathode near the center of the cylinder. (Fig. 1.) The probe surface was the end of a heavy wire 1.5 to 3 mm in diameter, the wire being insulated except at the end by a closely fitting glass tube. The insulated wire extended diametrically about two-thirds of the way through the anode cylinder, and the surface was viewed normally through a quartz window and a hole in the side of the cylinder. The image of the surface was focussed by a quartz

fluorite achromat or a quartz water achromat [4] on the slit of the spectrograph.

Roughly quantitative intensity estimates are based on densitometer measurements of several spectra obtained with different exposure times assuming the reciprocity law to hold.

III. DISCHARGE CONDITIONS

Observations have been made with discharges in caesium, potassium, and helium with most of the measurements in caesium. An essential condition for observation of the faint continuous spectrum is the absence of strong emission lines from the discharge in the spectral region studied. In caesium wave lengths less than 3,200 A and between 5,000 and 4,600 A are particularly favorable.

For the caesium discharge, currents of the order of 1 ampere at 5 to 7 volts with pressures between 0.002 and 0.01 mm. were used. Under these conditions most of the space between cathode and anode is at a nearly constant potential slightly positive with respect to the anode. The potential of the space is found from the current voltage characteristics of the probe.[5] As one approaches the space potential from the negative side the electron current increases rapidly, while above the space potential the current remains nearly constant. On a scale of log current versus voltage the negative branch of the curve is a straight line and the slope of the line gives the average energy of the electrons in the space. The intersection of this line and the nearly horizontal positive branch gives the space potential. At positive potentials the current flow is governed by the space charge equation for parallel plate electrodes.

$$I = 2.34 \times 10^{-6} A V^{3/2} / x^2$$

where I is the current in amperes, V is the potential in volts relative to the space, A is the collecting area in cm^2, and x is the sheath thickness or distance normal to the surface to which the applied field is limited. For our conditions I/A was over an ampere so that x was between 10^{-2} and 10^{-3} cm. At some positive potential (5 to 20 volts, depending on the pressure) the sheath breaks down and a brilliant ball of discharge appears on the probe. At any lower potential conditions are favorable for quantitiative measurements. The average electron energy at the sheath surface is given by the semilogarithmic plot (it was always about 0.4 volts in caesium). The potential drop across the sheath is the applied potential minus the space potential. The sum gives the electron energy at the probe surface and to this should be added the work function of the metal surface if it is assumed that radiation takes place within the metal. Unfortunately the work function of a metal surface in a caesium discharge is quite uncertain and may range from 1 to 4 or 5 volts, depending on the temperature and the surface condition. The probes are heated considerably in operation, to visible red heat in extreme cases.

IV. LOCATION OF RADIATION

The probe surface at a positive potential appears bright, but much of this light comes from the thin sheath for the radiation from the dis-

[4] L. and E. Bloch, Rev. Opt. Theor. et Inst., **6**, p. 31; 1927.
[5] Mott-Smith and Langmuir, Phys. Rev., **28**, p. 727; 1926.

charge is enhanced where the electrons are accelerated. The image of a fine wire probe was accurately focussed on the slit of a spectrograph. The width of the continuous spectrum from the wire at a positive potential was equal to the width of the shadow of the wire when the wire was on open circuit and definitely less than the sheath width as measured by the enhanced portion of the spectrum lines. The sheath thickness of the order of 10^{-2} cm was too small to measure accurately, however.

V. OBSERVATIONS IN VARIOUS GASES

The continuous spectrum from probes in potassium and helium discharges is qualitatively similar to that observed in caesium both in intensity and in spectral intensity distribution. Negative results were obtained in a mercury discharge where the scattered light was always sufficient to mask a continuous spectrum of the usual intensity. The observations in helium are difficult but with very pure gas there is little scattered light beyond 2,800 A. Nearly all quantitative measurements were with probes in a caesium discharge.

VI. VAPOR PRESSURE

There is no appreciable variation of the intensity of the probe radiation in a caesium discharge with pressure in the range 0.002 to 0.01 mm. when conditions are adjusted to keep the probe current constant.

VII. PROBE CURRENT

The intensity is nearly proportional to the current. Spectra of equal exposure time of radiation reduced by a grid of 30 per cent transmission and of full radiation with 30 per cent of the initial current show nearly equal densities.

VIII. SPECTRAL INTENSITY DISTRIBUTION

The ultra-violet radiation from a copper probe at +7 volts with a current of 1.4 amp./cm^2 was compared directly with the spectrum of a calibrated tungsten strip lamp in quartz using a quartz spectrograph. Later a similar comparison was made in the visible at 6 volts and 3.1 amp./cm^2 using a 3-prism Zeiss glass spectrograph. Figure 2 gives the results. The intensity $J(\lambda)$ remains of the same magnitude throughout the range covered and other results indicate that there is no marked decrease to 2,300 A. The figure includes a plot of the radiation flux in quanta per unit frequency range per cm.^{2} Ordinates give absolute values for the ultra-violet measurements with the others reduced to the same scale by an arbitrary factor. A questionable correction for scattered radiation has been applied for wave lengths longer than 5,500 A, and beyond 6,000 the curve is extremely uncertain.

IX. INTENSITY AND VOLTAGE

The intensity changes rapidly with voltage, but between 5 and 20 volts there is very little change in the intensity distribution. Below 5 volts the intensity drops off more rapidly in the ultra-violet. Figure 3 shows the relative intensity at 2 and 3 volts as compared

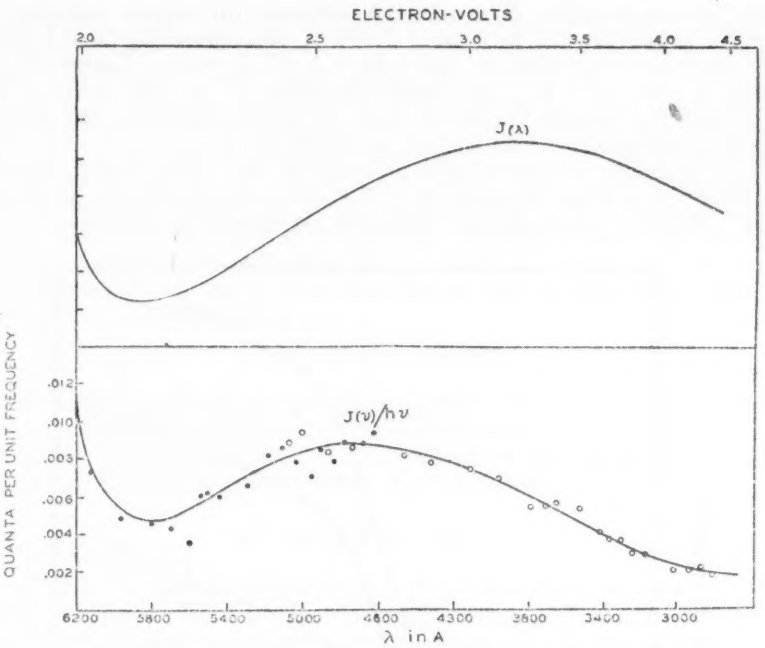

FIGURE 2.—*Intensity distribution of radiation from copper*

Circles and ordinates apply to measurements with 7 volts and 1.4 amperes/cm² while dots give another set of readings multiplied by an arbitrary factor

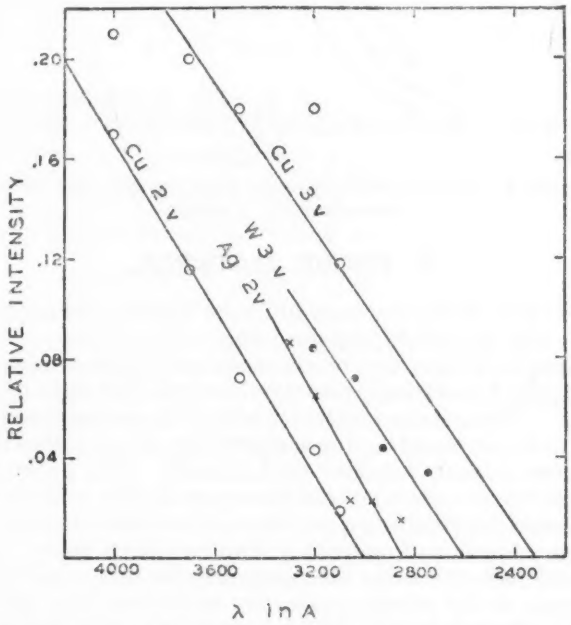

FIGURE 3.—*Relative intensity at low voltages as compared with intensity at 5 volts*

with that at 5 volts. The relative intensity for copper radiation at 2 volts drops toward zero near 3,000 A corresponding to 4.1 volts. The corrected potential V was $1.75+.4=2.15$ volts. Using the relation $h\,\nu_0=e\,(V+W)$, the work function W is 1.95 volts. The threshold for copper radiation with 3-volt electrons is less definite but approximately 1 volt higher, as it should be.

The intensity variation with voltage at any wave length is characterized by a rapid increase up to 7 volts and a slow increase beyond this. Figure 4 shows the isochromats for three wave lenths.

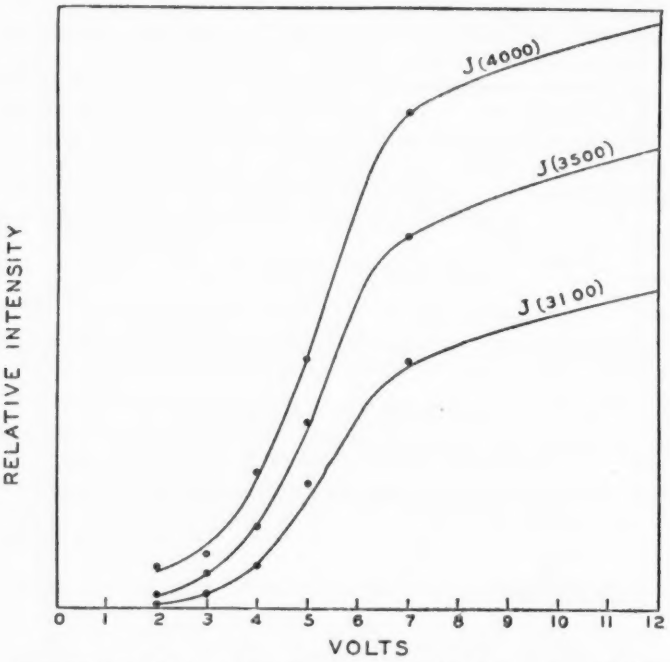

FIGURE 4.—*Relative monochromatic intensity of copper radiation as a function of voltage*

X. PROBE MATERIAL

Comparison of radiation from different metals was made by having two probes side by side in the discharge.

Silver gives radiation five or six times as bright as copper between 2,680 and 3,300 A and nearly twenty-five times as bright between 3,500 and 4,000 A. The relative intensity at 2 volts as compared to that at 5 volts is much the same as for copper (fig. 3) and the threshold at 2,860 A gives a work function of 2.1 volts. The probe surface appeared bright in the vacuum and was coated with a white oxide when air was admitted indicating that the surface was an alloy.

Tungsten radiation is probably two or three times as bright as copper with much the same intensity distribution. Figure 3 includes measurements of the relative intensity at 3.3 volts as compared with 5 volts. The threshold at 2,600 A corresponds to a work function of 1.45 volts.

Platinum was compared with a tungsten surface which was at first slightly oxidized. The tungsten radiation at 7 volts was at first weak and gradually increased under heavy electron bombardment. Finally the platinum radiation at 7 volts was weaker than the tungsten, ranging from 0.5 times tungsten at 3,200 A to 0.3 times tungsten at 2,500 A. At 3 volts applied potential the situation was reversed with the platinum radiation much stronger, particularly in the ultra-violet. The platinum intensity at 3 volts as compared with 7 volts remained about 0.2 between 3,200 and 2,500 A. The tungsten ratio dropped from 0.04 at 3,200 A toward zero near 2,600 A. The result indicates that the platinum has a work function at least a volt or two greater than the tungsten.

XI. DISCUSSION

We have suggested in the introduction that the radiation from probe surfaces is analogous to the continuous X-ray spectrum. In the X-ray range the intensity distribution of radiation from a thick target can be roughly represented by the equation

$$J(\nu)d\nu = c_1 Z(\nu_0 - \nu)d\nu \tag{1}$$

where Z is the atomic number and ν_0 is given by the relation $h\nu_0 = Ve$. The efficiency E[6]; that is, the total radiant energy divided by the electron energy, based on experimental values of c_1 in equation (1), is

$$E = 9.5 \times 10^{-10}\ ZV \text{ (volts)} \tag{2}$$

The isochromatic energy as a function of V is approximately

$$J(\nu) = c_2 Z\ (V - V_0) \tag{3}$$

where V_0 is the threshold value of V.

Kramers[7] has derived the above relations on the basis of the correspondence principle, assuming that a quantum is emitted when the impacting electron makes a transition between hyperbolic orbits in the field of an atomic nucleus. The theoretical constants are nearly identical with the experimental values and equation (1) is given in the form

$$J(\nu)\ \text{(ergs)} = i \times 5 \times 10^{-50}\ Z(\nu_0 - \nu) \tag{4}$$

where i is the number of electrons striking the surface per second.

The above results apply to radiation produced in the metal corrected for absorption. A reduction of our observations to intensities in the metal involves unknown factors. We can assume that radiation takes place at an average depth equal to the mean free path of an electron in the metal. Estimates of this, based on photo-electric properties of thin films, range from 2.7 to 25×10^{-7} cm.[8] Ultra-violet radiation is reduced to $1/e$ in about 20×10^{-7} cm in all the metals used.[9] Thus electrons are stopped at depths from which radiation can emerge and the measured effects probably come from

[6] Int. Crit. Tables, **6**, p. 46.
[7] Kramers, Phil. Mag., **46**, p. 836; 1923.
[8] Gudden, Lichtelektrische Erscheinungen, p. 78. Julius Springer.
[9] Int. Crit. Tables, **5**, p. 248.

electrons of speeds varying from the initial speed to zero. The radiation is modified more or less by absorption but not in order of magnitude. This is qualitatively similar to the case of hard X rays from thick targets.

The intensity measurements for radiation from a copper probe with 1.4 amp. per cm² (0.91×10^{19} electrons /cm²) at 7 volts ($V+W=$ 9.1 volts, $\nu_0=22\times10^{14}$) give a radiation flux at 3,700 A of $J(\nu)=3\times10^{-14}$ ergs per cm² per sec. per unit frequency range. For these conditions equation (4) gives $J(\nu)=1.85\times10^{-14}$ ergs. For radiation of 2-volt electrons at 1 volt from the threshold (4,000 A) both experiment and equation (4) give about one-sixth of the above values.

Assuming $J(\nu)$ at 3,700 to be a mean value over the range ν_0 to 0, the total energy radiated is 66 ergs per cm² per sec. and the efficiency 5×10^{-7}. Equation (2) gives 2.5×10^{-7}.

The above agreements are better than we have any reason to expect. In particular we may question whether it is legitimate to use the atomic number Z in these equations when applied to low-speed electrons.

One can make a qualitative comparison of the intensity we have observed for copper with the intensity reported by Foote, Meggers, and Chenault [10] on the basis of equation (3). They used a current density of about 0.01 amp./cm² at 1,000 volts and photographed the continuous spectrum in about five hours. We used 1.35 amp./cm² at 7 volts applied potential, and the exposure time with a much wider slit was about half an hour. The intensity per unit current was of the order of 50 times greater at 1,000 volts. Equation (3) with $V-V_0$ 5 volts and 1,000 volts gives a ratio of 200.

A rough comparison with the measured photo-electric effect of the radiation produced by low voltage electron bombardment is possible. The photo-electric current from platinum produced by 200 volt copper radiation is 1.5×10^{-6} times the bombarding current.[11] The effect at 5 volts applied potential ($V+W=10$) is perhaps 3×10^{-3} times this.[12] The photo-electric efficiency of quanta between 5 and 10 electron volts may be taken as 2×10^{-3} so that 2.2×10^{-6} quanta per electron are emitted in a range of 1.2×10^{-15} frequency units or 2×10^{-21} quanta per electron per unit frequency range. The average value found in the near ultra-violet was 6×10^{-22}.

The observed radiation process is similar to, but not identical with, the converse of the photo-electric effect. Fowler [13] gives a relation derived by the principle of detailed balance between the probability ϕ of photo-electric ejection of an electron with energy η by a quantum $h\nu$ and the probability ϕ' of emission of $h\nu$ by an electron of energy η assuming both processes governed by the ideal relation

$$h\nu=We+\eta \tag{5}$$

where W is the work function of the metal.

$$\phi=\frac{mc^2\eta}{h^2\nu^2}\phi' \tag{6}$$

[10] Foote, Meggers, and Chenault, J. Opt. Soc. Am., 9, p. 541; 1924.
[11] Bandopadhyaya, Proc. Roy. Soc., A120, p. 46; 1928.
[12] Compton and Thomas, Phys. Rev., 28, p. 601; 1926.
[13] Fowler, Statistical Mechanics, p. 494. Cambridge Press.

It may be permissible to compare the number of electrons of all energies less than η ejected by a frequency ν with the number of quanta of all frequencies less than ν excited by electrons of energy η. From measurements of 2 volt copper radiation we estimate the total radiation to be about 1.3×10^{-7} quanta per electron. An extrapolation of photo-electric data [14] for copper gives the emission by quanta of energy $(W+2)e$ as 10^{-3} electrons per quantum. Equation (6) with values of ν and η appropriate for the radiation measurements gives $\phi=6\times10^{4}\phi'=8\times10^{-3}$ electrons per quantum as compared with 1×10^{-3} observed. The agreement in order of magnitude is interesting in spite of the fact that the equation applies to an ideally simplified case. Equation (6) expresses the balance between photo-electric emission and radiation from electron bombardment from the metal as a whole and not from atoms in the metal in contrast with the X-ray equations.

WASHINGTON, February 14, 1931.

[14] Gudden, Lichtelektrische Erscheinungen, p. 28. Julius Springer.

PIPE-LINE CURRENTS AND SOIL RESISTIVITY AS INDICATORS OF LOCAL CORROSIVE SOIL AREAS

By E. R. Shepard

ABSTRACT

The present tendency in the protection of pipe lines against soil corrosion is away from a uniform coating for the entire length of the line and toward the application of coatings selected with respect to the corrosive character of the soils involved. This calls for a knowledge of varying soil conditions and a means of locating local corrosive soil areas. Such areas, commonly termed "hot spots," are prevalent in many types of soils and it is in these regions that pipe lines suffer the greatest deterioration. The location of such corrosive areas is a matter of considerable importance, both with respect to the selection of coatings for new pipe lines and the reconditioning of old ones.

An extensive investigation on a dozen pipe lines ranging from the gulf coast to southern Kansas revealed an apparent correlation between pipe-line currents, soil resistivity, and corrosion. Galvanic currents of measurable magnitudes were found to be flowing on all pipe lines examined. As a rule, lines were found to be collecting current in areas of normal and high soil resistivity and losing current in areas of low resistivity. Many cases of abrupt loss or discharge of current occurred in soils of unusually low resistivity. In such areas the pipe lines were found to be badly corroded.

Although no direct relation was found to exist between electrical resistivity of soils and their corrosiveness, abrupt changes in resistivity and unusually low resistivity were found to be significant with respect to corrosion. Soils having a resistivity of about 500 ohm-cm or less were invariably found to be highly corrosive. A better relation between resistivity and corrosiveness exists in alkaline than in acid soils.

The technique of surveying pipe lines for galvanic currents is discussed and a piece of apparatus for simply and quickly measuring soil resistivity is described.

CONTENTS

		Page
I.	Introduction	683
II.	Previous investigations	684
III.	Scope of recent investigations	686
IV.	Organization and method of making tests	687
V.	Currents found to be of galvanic origin and related to soil resistivity	688
VI.	Character of galvanic circuits involved in pipe-line currents	688
VII.	Presentation and discussion of data	690
VIII.	Relation of long line currents to corrosion	699
IX.	Relation of electrical resistivity of earth to corrosion	701
X.	Stray currents	702
XI.	Practical significance of data and technique of making measurements	703
	1. Method of measuring line currents	703
	2. Method of measuring soil resistivity	706
XII.	Summary	708

I. INTRODUCTION

The present tendency in the protection of pipe lines against soil corrosion is away from a uniform coating, such as has been applied frequently in the past without regard to soil conditions, and toward

the application of protective coatings which are selected with regard to the corrosiveness of the soil involved. Experience has shown that the deterioration of rolled pipe in many types of soils is so slight as to make it uneconomical to use protective coatings. Other soils are so destructive to pipe materials as to call for the use of the best protective materials and processes available. Intermediate conditions also exist.

Sharp differences in corrosive properties occur from place to place in any one type of soil as well as between types and the problem of detecting such differences becomes a very pertinent and practical one in connection with the coating policy for new lines and the reconditioning of old lines. Several pipe line companies have reported that the proportion of their piping systems subjected to unusually severe soil conditions and, therefore, calling for special protective treatment is very small. Local areas of exceptionally corrosive soil, commonly termed "hot spots," are prevalent over a large proportion of the area traversed by piping systems. Some of these hot spots are of artificial origin, such as salt washes from oil wells, disposal products from manufacturing or refining plants, cinder dumps, etc. However, a great many of the unusually corrosive spots appear to be naturally occurring areas of high salt concentration. As such areas usually can not be identified from surface conditions or even by a visual inspection of the soil, their location by other means becomes a matter of importance. This paper describes a method for locating and outlining the limits of excessively corrosive soil areas along existing pipe lines. It contains a review of the work begun several years ago by K. H. Logan, and a more detailed account of the investigations of the author during the spring and summer of 1930.

II. PREVIOUS INVESTIGATIONS

In 1929 Logan, Putnam, and Rogers published a paper [1] in which they gave the results of measurements of electric currents on oil lines in widely separated sections of the country. As prior to that time the presence of electric currents on pipe lines had usually been attributed to electric railways, the paper was of unusual interest as it showed that such currents could originate from other causes. Although they suggested several possible sources, such as galvanic potentials, condensation of fog on tanks, pumping operations, and magnetic storms, their data seem to justify the conclusion that galvanic potentials were definitely responsible for at least some of the observed currents. More recently Gill and Rogers, who collaborated with Logan on the collection of his data, have extended their tests and presented their findings in a report [2] in which they definitely attribute the observed currents to galvanic action.

While Gill found no striking correlation between corrosion and areas of current discharge on pipe lines, at least two of the lines explored by Logan indicated such a relation. Logan found little if any relation between electrical current flow and water courses; both investigators usually found relatively large currents entering tank farms and pumping stations; also, both found currents circulat-

[1] K. H. Logan, Walter Rogers, J. F. Putnam, Pipe Line Currents, Am. Pet. Inst., D. & P. E. Bull. No. 204, p. 116.

[2] Stanley Gill and Walter Rogers, Electric Currents Carried in Pipe Lines, Oil & Gas J., p. T-158; June 5, 1930.

ing between old and new pipe lines, the latter being the corroding element. Gill found erratic variations in current flow following heavy rains. Neither investigator reported any measurements of earth resistivity in connection with his studies.

Figure 1 shows the results of current flow measurements made by Logan and Putnam on a line of the Standard Oil Co. of California, and later correlated with the corrosion record of the line. To understand the diagram, it is necessary to keep in mind the direction of the flow and the change in magnitude of the current. Thus, the first cross-hatched area lies below a section of pipe along which the current flowed toward the south and decreased in magnitude along the line from north to south. This means that the pipe discharged current along the cross-hatched section. The solid section from *A* to *B* indi-

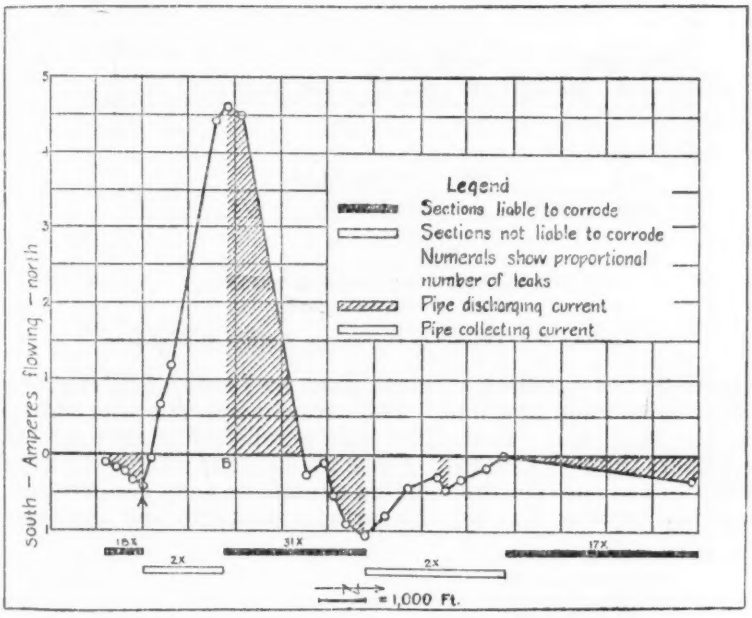

FIGURE 1.—*Association of current discharge and leaks*

cates that, starting at *A* and traveling northward, we find a decreasing current, a reversal, and then an increase in current which reaches a maximum at the point *B*. Between *A* and *B* the pipe is collecting current. The remainder of the diagram is interpreted similarly. The graphs below the line show the corrosion as indicated by the record of leaks. The relation to discharge of current is unmistakable.

Included in the studies of Logan and his associates was 30 miles of a line of the Marland Oil Co. in Oklahoma, in a territory more than 30 miles distant from the nearest electric railway. Measurements in detail on several thousand feet of this line are shown in Figure 2. The frequent changes in direction or magnitude of the current at different points along the line and the gradual change in the magnitude of the current from pipe section to pipe section are clearly indicative of galvanic origin. It will be noted that between the point *A* and

section *EF*, there is a loss of current of 0.97 ampere in a distance of about 1,200 feet. Of this, 0.41 ampere occurs on the first section of about 100 feet, 0.27 ampere entering the section from the south and 0.14 ampere from the north. It is significant that subsequent inspection showed this section to be corroded and other portions of the line to be comparatively good.

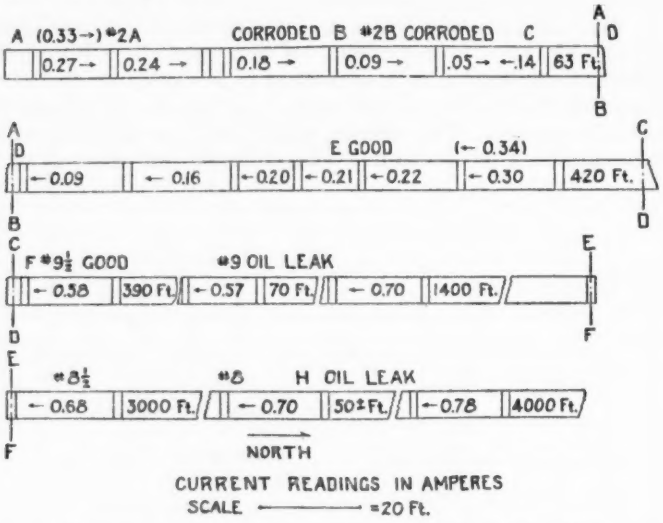

FIGURE 2.—*Details of current on 2 miles of pipe line*

Figure 3 is an excellent example given by Logan of galvanic action between an old and new line. The wrought-iron line was laid earlier than the steel line. Both lines run parallel to each other about 6 feet apart through a marsh. Since we find current flowing from the old line to the new via the metallic circuit, we may assume that the circuit is completed through the earth, or that the new line is anodic

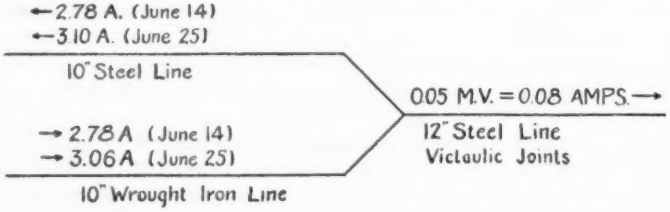

FIGURE 3.—*Galvanic currents between old and new pipe lines*

with respect to the old one. This is in accord with the often expressed theory that corrosion products tend to accelerate corrosion on exposed connected metal structures. It may explain why, in some instances, the original line in a pipe system outlasts those laid subsequently.

III. SCOPE OF RECENT INVESTIGATIONS

Since the work of Logan and others indicated that measurable electric currents, probably of galvanic origin, are to be found on practically all pipe lines, it was deemed worth while to extend the

scope of these investigations under conditions which would permit of examining the pipes for corrosion, to see if any relation exists between such corrosion and line currents. The more recent investigation extended over a period of nearly three months beginning April 1, 1930, and was made on nine pipe lines totaling approximately 60 miles of explored pipe. These ranged in location from the gulf coast through Texas and Oklahoma to southern Kansas.

The National Bureau of Standards solicited cooperation in this work from the pipe-line companies through the American Petroleum Institute. The response was so generous that only a fraction of the offers for assistance could be taken advantage of. In selecting a few pipe lines for examination from among the large number that were available, consideration was given to a number of factors, chief of which were: (1) Conditions for examining corrosion or availability and accuracy of leak record; (2) kind, age, and condition of protective coating; (3) isolation from other lines and from electric railway disturbances; (4) accessibility with respect to working and living conditions. Selections were made with the idea of covering as wide a variety of soils as possible with the minimum of time and travel. Portions of the following lines were explored in the order given:

Lines tested

Line E.—Empire Pipe Line Co.; 8-inch oil line near Perry, Okla.; 10 to 15 years old, bare, being reconditioned while in service.

Line ST.—Sinclair Pipe Line Co.; 8-inch oil line from Burbank to Tonkawa, Okla.; 7 years old, coated with asphalt, being reclaimed.

Line SB.—Sinclair Pipe Line Co.; 6 and 8-inch oil line from Tonkawa to Billings, Okla.; 5 years old, being reclaimed.

Line SK.—Sinclair Pipe Line Co.; 6-inch oil line from Jonesberg to Coffeyville, Kans.; 8 years old, bare, being reconditioned in spots.

Line G.—Gulf Pipe Line Co.; 6-inch oil line from Crosby to Lynchberg, Tex.; 15 years old, bare, some leak data available.

Line P.—Pure Oil Pipe Line Co. of Texas; 8-inch oil line through Spindle Top Gulley, near Beaumont, Tex.; in area known to be highly corrosive.

Line HB.—Humble Pipe Line Co.; 8-inch oil line from Beaumont to Hull, Tex.; 4 years old, thin bituminous coating. No leaks have occurred on this line.

Line HH.—Humble Pipe Line Co.; 12-inch oil line from Hearne to Groesbeck, Tex.; 7 years old, light bituminous coating. No corrosion leaks have occurred on this line.

Line HV.—Humble Pipe Line Co.; 6-inch oil line from Vernon to Swastika, Tex.; 7 years old, light bituminous coating. Recent inspection record and leak record available.

IV. ORGANIZATION AND METHOD OF MAKING TESTS

Assistance rendered by the pipe-line companies consisted of an engineer with his car and one or more helpers, some member of the party being familiar with the location of the line and the roads leading to it. Measurements of current flow on the line were made by observing the potential drop on a 75-foot length of pipe with a very sensitive millivoltmeter. Contacts were made on the line by prodding down to the pipe with a steel bar, then inserting diamond point drill rods in the holes and twisting or tapping these until they made good contact with the pipe. Where reconditioning work was in progress or where pipe was being salvaged measurements were sometimes made after the top of the pipe had been exposed. This was possible at times on lines E, ST, and SB. Where such work was in progress

the procedure was to explore the line for current several miles in advance of the operations and then to inspect the pipe for corrosion after it was taken out of the ground. In the first three lines examined the work of uncovering the top of the pipe was pushed several miles ahead of any other operation, thus permitting access to the surface of the pipe before electrical conditions on the line were greatly disturbed. Measurements of the electrical resistivity of the soil were made in the field by a direct-current method, the details of which are described later.

V. CURRENTS FOUND TO BE OF GALVANIC ORIGIN AND RELATED TO SOIL RESISTIVITY

It was evident soon after starting the work that the currents observed on line E were largely of galvanic origin. Small variations at any one point were attributed to distant interurban electric lines, but abrupt changes in magnitude from point to point along the line indicated that the currents originated at the pipe surface. Currents were found to be flowing into certain sections of the pipe line from both directions and away from other sections in both directions. Moreover, these currents remained substantially constant day after day, except for the small stray fluctuations referred to. A more detailed study showed that as a rule the current accumulated on the pipe gradually over a considerable length and discharged abruptly over relatively short sections of the pipe line.

A study of the soil along the line, including electrical resistivity measurements, showed that invariably the areas of abrupt discharge were in soils of low resistivity, while the areas of collection or little change were in soils of normal or high resistivity. When the pipe came out of the ground and was cleaned, additional measurements of soil resistivity were made and these revealed a striking relation to the observed corrosion, the pitting and rusting being most severe in soil areas of unusually low resistivity. Here, then, was a three-way correlation between line currents, soil conductivity, and corrosion. As the work progressed to other lines these relations were found to hold true quite generally; in some instances the correlation was striking, while in others it was less definite.

VI. CHARACTER OF GALVANIC CIRCUITS INVOLVED IN PIPE LINE CURRENTS

Before discussing the data in detail we will describe the manner in which galvanic currents are built up to produce measurable currents on pipe lines and in so doing will adhere to the generally accepted electrochemical theory of corrosion.

Among the possible sources of electromotive force by which galvanic currents on pipe lines are generated we may list the following static potential differences:

1. Potential differences between bright iron and mill scale.
2. Potential differences between different points on the pipe due to strains, inequalities, impurities, etc. Usually of the order of millivolts.
3. Potential differences between different kinds of pipe or between new and old pipe.

4. Potential differences resulting from soil differences. These may be local in character, such as occur in irregular or nonhomogeneous earth, or more extensive, such as between different kinds of soils. All degrees of soil differences are possible, ranging from minute irregularities to major differences in extensive soil areas. In this group must also be included differences in moisture content, also differences in oxygen and in salt concentrations.

Many of the galvanic potentials listed above are local in their action. Abrasions, strains, discontinuity of mill scale, impurities, and similar conditions tend to establish galvanic currents which are local in character and usually affect a relatively small portion of the pipe surface. Likewise the action resulting from concentration cells is local, but may be more frequent in occurrence. Figure 4 is intended to illustrate local action where a relatively small fraction of the pipe area is undergoing corrosion. The electric circuits are small in extent because of the plentiful supply of cathodic pipe surface adjacent to the corroding areas. As the anodic area becomes larger the current in the earth increases and appreciable amounts of current are found at points more remote from the anode. This condition, illustrated in Figure 5, will produce measurable currents on the pipe line, or "long line" currents. The extent of such circuits depends upon the length of pipe so affected and the proportion of pipe within the affected area which is actually undergoing corrosion, or in other words, from which current is being discharged.

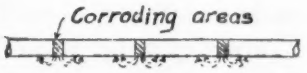

FIGURE 4.—*Galvanic currents on pipe, in which the affected area is relatively small and in which no long line currents are produced*

In Figure 6 the entire surface of the pipe within a corrosive area or "hot spot" is shown to be discharging current. This may not actually occur in practice, but the proportion of the pipe area undergoing corrosion, and, therefore, from which current is leaving, is often very great in such soil areas. This current returns in sweeping streamlines through the earth to the pipe, the density diminishing with increasing distance from the point of origin. The magnitude of the current on the pipe at any point is shown by the current curve. A current flow from east to west is plotted above the base line, while a flow from west to east is plotted below the base line. It will be seen that on approaching the corrosive area from either direction the magnitude of the pipe-line current increases and that throughout the corrosive area the current is decreasing. An ascending slope in the current curve from left to right represents a discharge of current from the pipe, while a descending slope from left to right represents a

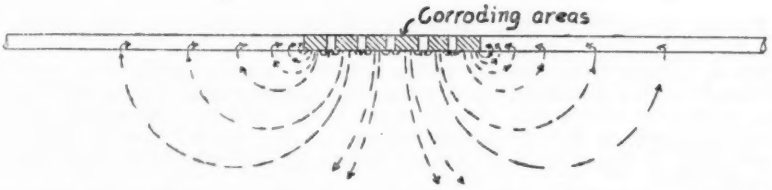

FIGURE 5.—*Galvanic currents on pipe, in which the affected area is relatively large and in which long line currents are produced*

collection of current. This is true both above and below the base line. It is, of course, also understood that a discharge of current from a pipe is usually accompanied by corrosion while a collection of current is not.

VII. PRESENTATION AND DISCUSSION OF DATA

Line E.—The soil and topography in Noble County, Okla., through which line E extends, is so similar to that in Payne County, for which a report of the United States Bureau of Soils is available, that we will quote that report as applicable to the case at hand:

> Payne County lies within the great plains province, as defined by the Bureau of Soils. The upland soils are derived principally from rocks of the Permian and Pennsylvania divisions of the Carboniferous. * * * The soils residual from the Permian Red Bed prevailingly partake of the color of the parent rocks and are classified in the Vernon Series. The other important soil series, the Kirkland, coming from Permian rocks, is brown in color rather than red. Its difference in color is probably due to the long period of time during which it has been subject to weathering. In the areas of red soils the topography is more rolling, the bedrock is much nearer the surface and the soil is more subject to erosion than in the areas of brown soil, where the topography is gently sloping or nearly level. * * *
>
> In texture the residual upland soils range from fine sandy loams to clay, with loam and fine and very fine sandy loams predominating. The subsoils are characteristically much heavier than the soils. The latter are generally mellow and friable, while the subsoils range from stiff and plastic to moderately friable, and even when friable are usually compact.

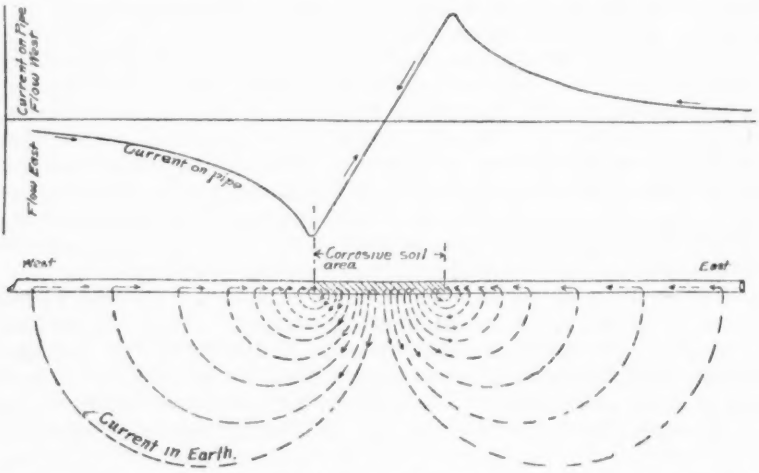

FIGURE 6.—*Effect of localized corrosive soil areas on production of line currents*

A survey of galvanic long-line currents was made over approximately 9 miles of this line. Five reversals were discovered. The maximum current observed was 1.5 amperes. Figure 7 shows the current flow on the line and the earth resistivity along a typical 18,000-foot section. The current flow is plotted in accordance with the explanation of Figure 6. It will be seen that two reversals occur in this section. Earth resistivity in ohm-centimeters is plotted as

ordinates from the base line. Values greater than 7,000 ohm-centimeters are not shown, but are roughly indicated by the slope of the resistivity curve.

The resistivity of the soil along this line varies sharply over a wide range. For the sandy loams which predominate it is from 3,000 to 12,000 ohm-centimeters. Many irregular outcrops and pockets of red coarse clay and of yellowish and whitish clays occur, and these range in resistivity from 2,000 to less than 400 ohm-centimeters. Black bottom loams and clays range around 1,000 ohm-centimeters and sometimes lower. In some sections the soil is quite deep and uniform, and where this condition is found the pipe showed little if any evidence of corrosion. In other regions where the soil is broken by outcrops of heavy red coarse clay, alkali soil, and other types of irregular soils, the location of the corroded sections of the pipe coincided in a striking manner with the irregular and low resistance soils. These bad areas were not always in low ground, but often occurred

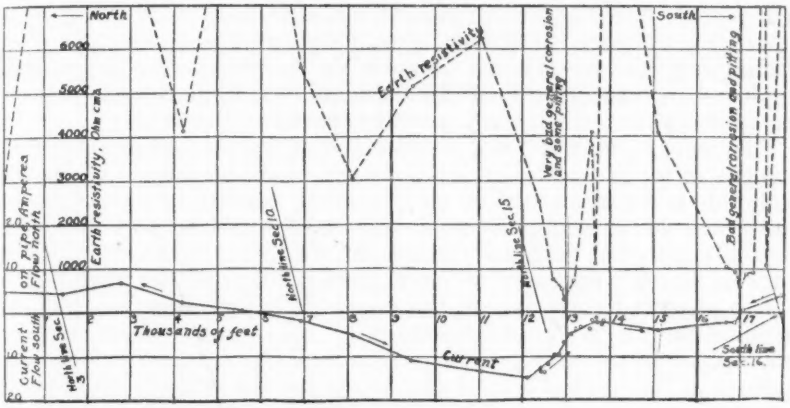

FIGURE 7.—*Line E; electric currents and soil resistivity along 8-inch oil line, Noble County, Okla.*

on the slopes and higher elevations. Soils of the Permian group are likely to contain alkali salts, and it is probably the presence of such salts in relatively high concentrations that produces the low resistivities encountered.

In Figure 7 will be seen two zones, one at 13,000 and the other at 17,000 feet, in which abrupt discharge of current takes place, and both of these coincide with areas of unusually low soil resistivity. An inspection of the pipe when it was uncovered and placed on skids for reconditioning showed a heavy encrustation of rust for several hundred feet in the vicinity of station 13,000. Some pitting was also in evidence, but it was not acute. At station 17,000, for a distance of about 75 feet, the pipe was deeply pitted. The presence of two leak clamps indicated that failures had previously occurred. The shape of the current curve between 6,000 and 13,000 feet bears a strong likeness to the corresponding portion of the theoretical curve shown in Figure 6. It is quite evident that the current discharging from the pipe between 12,000 and 14,000 feet is returning to the line between 6,000 and 21,000 feet. Some of the current curves in Figures 8, 11, 12, and 14, show an even more striking resemblance to the

theoretical curve. The variable character of the soil is indicated in the following table which shows conditions at station 17,000 in greater detail than are given in Figure 7.

TABLE 1.—*Variations in soil resistivity, line E*

Station	Resistivity	Condition of pipe
	Ohm-cm	
16700	1,071	Fair.
16850	966	Do.
16925	2,016	Do.
17000	546	Very bad (leak clamp).
17010	370	Do.
17100	906	Bad.
17200	891	Do.
17250	658	Very bad.
17350	1,176	Bad.
17800	9,360	Good.

In addition to the fairly extensive areas of low soil resistivity shown in Figure 7, there are innumerable small outcrops or pockets, sometimes only a few feet in extent. In such places the amount of current discharging from the pipe was too small to be detected by the methods employed in measuring long-line currents, but their corrosive nature was quite evident when the pipe was exposed and cleaned.

The curve in Figure 7 is not presented as a complete picture of the changes in earth resistivity in that area. At the time this line was explored no rapid method of making earth resistivity measurements was available, consequently such tests were made only at infrequent intervals except at points of abrupt current discharge where the character of the soil appeared to have some relation to the current flow and to observed corrosion on the pipe. It is probable that at intermediate points in the high-resistance soils many small areas of relatively low resistivity exist. This was found to be true on other sections of line E that were being reconditioned prior to starting the current survey, and, therefore, on sections where no current flow data were obtained, but on which a careful comparison was made between corrosion and earth resistivity. In some of these sections corrosion was most erratic, being severe for a few feet or on one or two joints of pipe, and entirely absent on others. It was in such regions that the numerous and erratic areas of low-resistance soil occurred, and these coincided with the badly corroded sections of the pipe line.

There was a general belief among those associated with the repair of the pipe line that oil leaks were responsible for much if not most of the corrosion, and a casual inspection of the line would certainly lead one to this opinion. However, a careful examination of the soil and measurements of its resistivity showed that most of the barren spots where grass did not grow were of a different soil, having a low resistivity, and were not the result of oil leaks. This fact was demonstrated repeatedly, both along the line and at some distance from it. There is sometimes the question of which came first, the leak or the corrosion. Where a leak clamp is found it may be assumed that a bad soil condition caused the failure and is responsible for any other corrosion in that vicinity. But where a collar leak is found, accompanied by corrosion on the downhill side only, the evidence is rather convincing for the oil theory. It is not the intent in this discussion to overthrow this theory of corrosion as it seems to be a universally accepted one. It

does appear, however, that at times it may be greatly overworked. Such an effect, if confirmed, might be caused by local differences in oxygen concentration brought about by the presence of oil.

Line ST.—The soil through which this line extended is of a much more uniform and homogeneous character than that on line E, 30 miles to the south. This condition and the presence of a bituminous coating in a fair state of preservation probably account for the relatively small currents that were found on the line, the maximum values of which were about 0.5 ampere. Although several current reversals were observed, there was only one point where the current discharge was of sufficient magnitude and density to indicate the possibility of corrosion. This was on a rocky hillside at a point where a seep or swampy outcrop existed and where a loss of 0.2 ampere occurred in a distance of 100 feet. The soil resistivity was about 1,800 ohm-cm. The pipe was examined upon removal and found to have failed

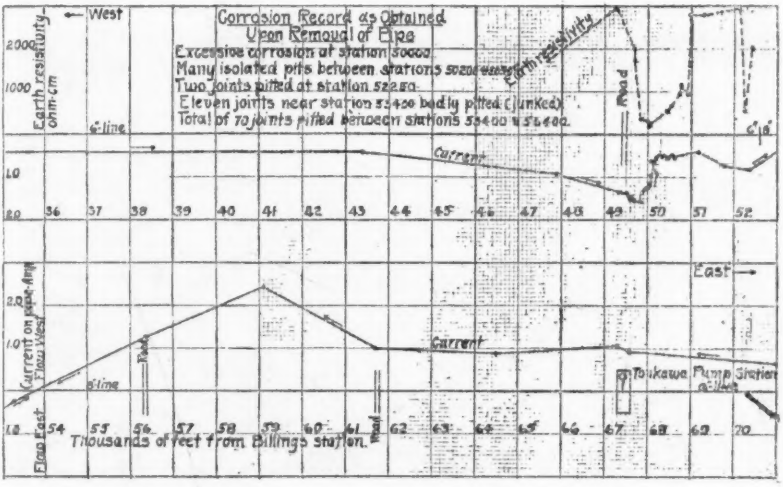

FIGURE 8.—*Line SB; electric currents and soil resistivity along 6 and 8 inch oil line, Noble and Kay Counties, Okla.*

completely at one point. Many pits from 0.2 to 0.3 inch deep were observed. The pits were very sharp and regular and filled with a yellow product of corrosion at the top, and with black oxide in the bottom. Although acute at points, corrosion had occurred on only a small fraction of the pipe surface.

In this case the soil resistivity did not tie in so well as in others where bad corrosion has been found. In fact, it is the only case involved in this investigation where severe corrosion was observed in soil other than that of unusually low resistivity. Generally, the soil in the hilly region where this springy outcrop occurred has a resistivity of from 5,000 to 12,000 ohm-cm. At the point in question the values were from 1,500 to 2,000 ohm-cm, or considerably lower than soils immediately adjacent. Perhaps relative resistivity rather than the absolute value is an important factor in the corrosion problem in some soils.

Line SB.—Figure 8 shows the long-line galvanic currents on about 7 miles of this line, part of which lies within the area of the Three-

Sands oil field. The field extends roughly from the road at 49,400 to the road at 61,700. Salt water from the wells has overflowed portions of this field and is probably responsible for the severely corrosive conditions observed.

The most abrupt discharge of current observed throughout the investigation occurred in the vicinity of station 50000, and this was accompanied by a drop in soil resistivity from the normal values in this region of about 3,000 ohm-cm to less than 200 ohm-cm. The pipe at this location was practically destroyed as shown in Figure 9. The extent of damage at other points, as reported by the company engineers, is indicated in Figure 8.

Because of the condition of the ground at the time of test and the difficulty of locating the line through the oil field, only a few readings were made between stations 53000 and 62000. It is unfortunate that no data on soil resistivity are available in this territory. At the time

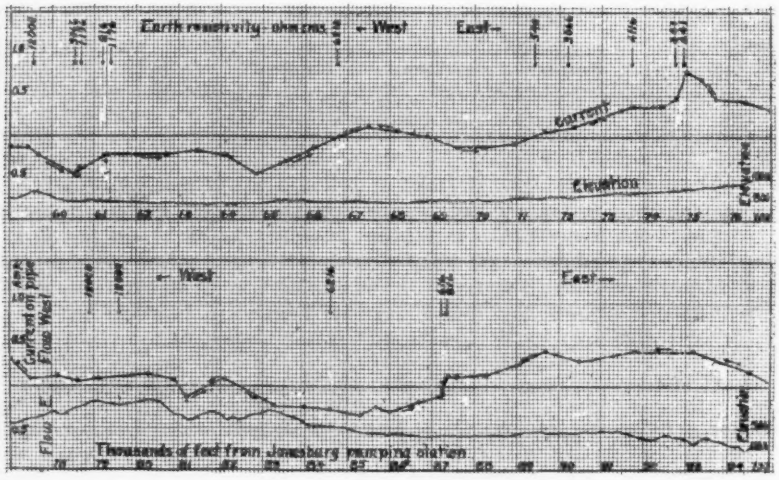

FIGURE 10.—*Line SK; electric currents and soil resistivity along 6-inch oil line, Jonesburg to Coffeyville, Kans.*

the measurements were made it was supposed that the line made contact with other pipes in the oil field and that the large loss in current was due to current interchange at such points. However, the engineers who were on the ground at the time the pipe was removed reported that no such contacts existed. As salt water has been discharged from the wells in this oil field at different locations from time to time, it is not probable that the line currents and soil resistivities here recorded have always prevailed during the life of the pipe. It is not reasonable, therefore, to expect too close a correlation between the observed corrosion and present electrical conditions.

Line SK.—This line runs through a rather flat region in which farm and grazing lands predominate. Low ranges of hills at intervals of several miles occur as shown by the profile in Figure 10. For the most part the soil is a black, or brown silty loam. The subsoil is often yellowish or gray clay.

Figure 10 shows the results of a current-flow survey over a 7-mile stretch of the line. The soil resistivity at a few points is given in

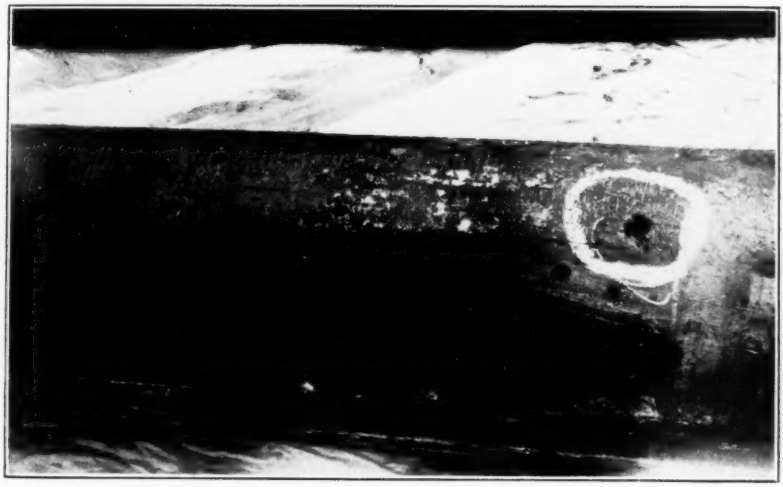

FIGURE 9.—*Pipe removed from line SB, at station 50000*

figures. Six reversals of current were observed and three points of concentrated discharge. At the time the tests were made, the pipe was exposed for reconditioning at station 60600 and was found to be badly corroded. It will be seen that a rather sharp discharge of current takes place at this point and onto 61300. The earth resistivitity is also relatively low, being around 1,000 ohm-cm, whereas the normal values of resistivity range from 3,000 to 12,000 ohm-cm. Two other points of abrupt discharge occur at stations 74900 and at 87300. It will be seen that both of these are associated with abnormally low earth resistivity. These two locations were cited for inspection and repair, and later the following report was received from one of the engineers of the pipe-line company:

> Our line in Kansas has a heavy red rust with some pitting. Your discovery of loss of current at the points where you recommended reconditioning saved this pipe because in a short time it would probably have corroded out.

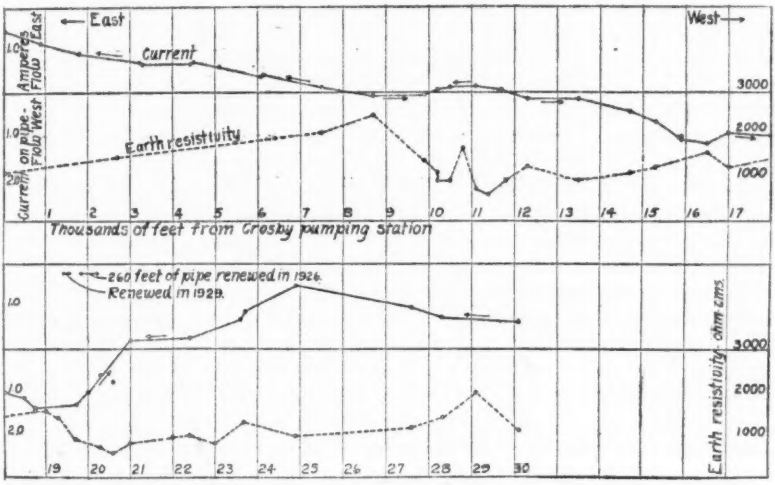

FIGURE 11.—*Line G; electric currents and soil resistivity along 6-inch oil line Harris County, Tex.*

The interesting and significant thing about this line as well as most of the other lines explored, is the erratic changes in soil resistivity in regions where surface conditions appear to be uniform.

Line G.—This line lies in the coastal plain at an elevation of about 45 feet above sea level. The topography and vegetation appear to be uniform throughout the 6-mile stretch explored. The top soil is black loam and the subsoil varies from a bluish gray clay shot with red, to a light yellow clay shot with red. Even under the apparently uniform conditions prevailing along this line the earth resistivity was found to vary from about 600 to 2,500 ohm-cm.

The results of current flow and resistivity measurements are given in Figure 11. The east end of the line for a distance of about 2 miles is collecting current and delivering it to the Crosby pumping station and tank farm, the current entering the station being about 1.5 amperes.

Two low points in the resistivity curve exist, but only one is accompanied by a heavy discharge of current. A loss of 1.5 amperes occurs

between stations 19750 and 21000, and this area includes the lowest soil resistivities encountered. In 1926 a stretch of several hundred feet of pipe was replaced in this section. The small section renewed in 1929 may also fall within the area of heavy discharge, but as no measurements were made between 18750 and 19750, the shape of the current curve between those points is not definitely known. No other renewals than those shown have been made on this portion of the line, but leak clamps have been installed at a few points.

Line P.—Spindle Top Gulley is well known by the pipe line companies as a region of extremely corrosive soil. The measurements recorded in Figure 12 were made along an 8-inch line which runs

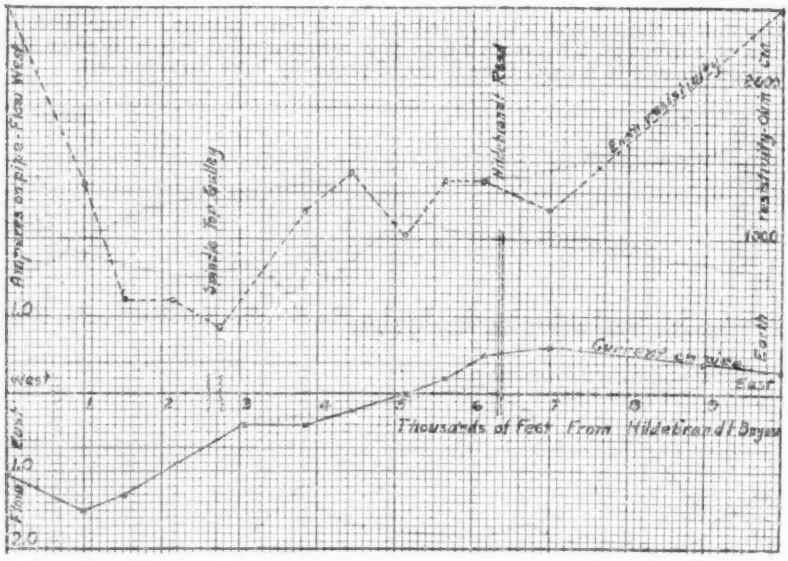

FIGURE 12.—*Line P; electric currents and soil resistivity along 8-inch oil line through Spindle Top Gulley*

through that territory. Engineers of the company state that the worst corrosion has occurred between stations 2000 and 3000 as shown in Figure 12. It will be seen that this is also the region of highest current discharge and lowest soil resistivity. The correlation between current discharge, soil resistivity, and corrosion is therefore striking.

In this case, however, there appears to be a better correlation between soil resistivity and corrosion than between current discharge and corrosion. Loss of current occurs at a fairly uniform density over several thousand feet of pipe, but replacements have been made only in the region of unusually low resistivity.

Line HB.—This line lies in the low lands of the coastal plain and runs through rice fields, open pasture land, and pine and oak woods. The soil is a heavy black clay loam for the most part, underlaid with yellow or gray mottled clay. Pockets of silty clay occur at some points and heavy muck is encountered in a few locations. The water table was found to be near the surface in some of the pasture lands, although the top soil was very dry. The soil resistivity was com-

paratively uniform, ranging from about 1,000 to 3,000 ohm cm., except in a few locations where silty soils of a much higher resistivity were encountered. Relatively small currents were found on this line and no points at which concentrated discharge took place. The greatest loss in current occurred in flooded rice fields where it was impracticable to trace the discharge in detail. As the measurements on this line reveal no line currents of appreciable magnitude and no areas of low resistivity they confirm in a general way the good record of no corrosion trouble whatsoever during the 4-year life of the line.

Line HH.—Figure 13 shows the results of measurements on line HH, which runs through a rolling country of scrub oak woods and farm lands, the elevation being 400 to 500 feet above sea level. The soil on the uplands is largely yellow sand having a very high electrical resistivity. In the lower and farm lands the silty and sandy top soils are underlain with a heavy yellow clay having a relatively low resistivity. The depth to this subsoil is quite variable. Outcrops of it occur in many places, but for the most part it is below pipe depth. Erratic soil resistances at pipe depth are due to variations in the depth of this clay below the ground surface.

A very satisfactory correlation between current discharge and earth resistivity is shown in Figure 13. Two points of unusually high current discharge are shown at stations 216000 and 221500, and at both locations the earth resistivity drops to abnormally low values. Both of these points are in corn fields. In the first the corn was yellow and sickly, showing the effect of the clay outcrop. In the other place the corn was green and rank because of sufficient good soil over the clay subsoil. The pipe was uncovered at the edge of the field at station 221500 and found to be pitted to a depth of 0.15 inch. Many pits 0.1 inch deep were found. Because of the growing crop no inspections were made at station 216000.

The regions of low resistivity at station 162000 and 168000 are also accompanied by loss of current from the pipe line, but the density of discharge is relatively small. An inspection of the pipe at station 162000 revealed no extensive corrosion.

The large current of 5.3 amperes on the south end of the line is entering the Hearne tank farm. The collection on the line near the tank farm is very dense as indicated by the steep slope of the curve.

Line HV.—The soil through which this line runs is of a chocolate-brown color and very uniform in appearance. Its resistivity ranges from about 500 to 2,000 ohm-cm. The correlation between current discharge and soil resistivity, as shown in Figure 14, is perhaps more striking than on any of the other lines. At many of the points where loss of current is shown, trouble from corrosion had been experienced. Leaks had been repaired at 157700, 159800, and 204850. New pipe had recently been installed at 193700 and at 201200.

The heavy loss of current shown at 162500 was probably a temporary condition. One and two days prior to the tests very heavy rains had occurred, following a prolonged drought. This rain had not penetrated to the pipe level except where the trench had been newly made or backfilled. The location in question is at the site of an old booster station where several months prior to the tests the main had been uncovered for the purpose of removing various connections. No new pipe had been installed, but about 200 feet of trench had

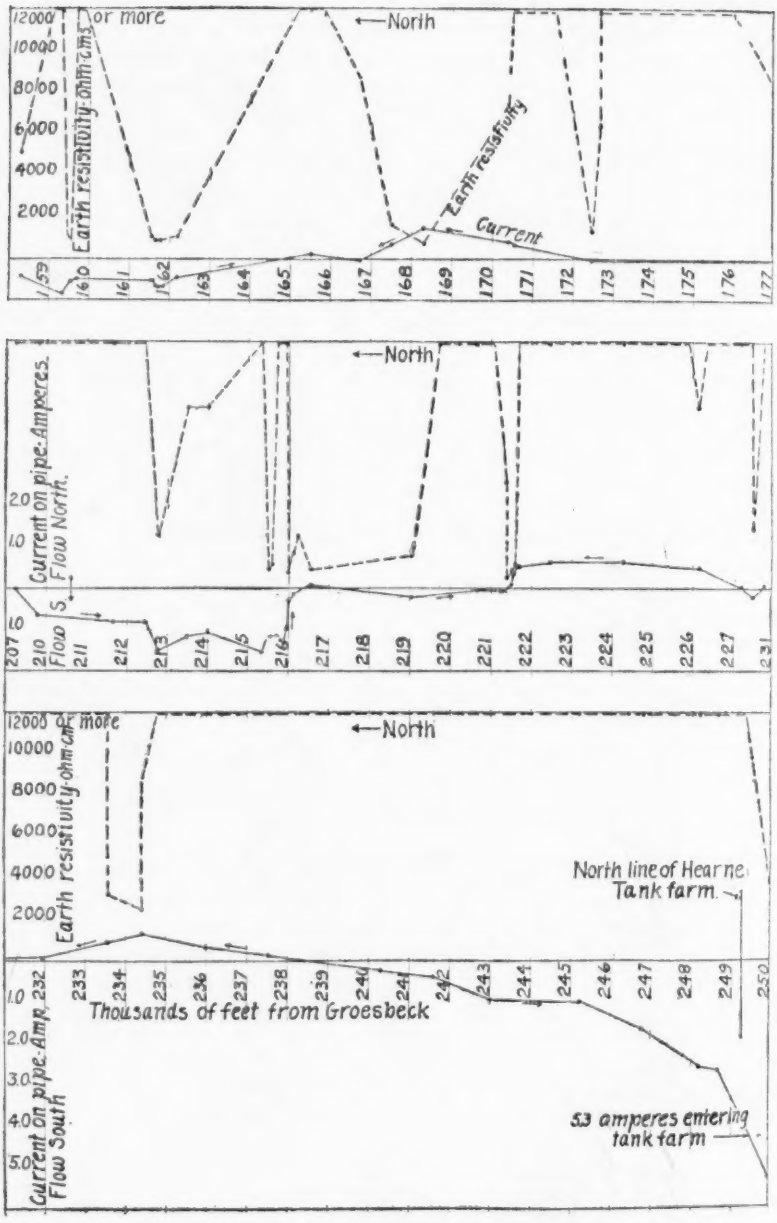

FIGURE 13.—*Line HH; electric currents and soil resistivity along 12-inch oil line, Groesbeck to Hearne, Tex.*

been opened up and backfilled. The heavy rains had penetrated to the pipe in this area but not in adjacent areas. It seems probable that this condition is in some way responsible for the abrupt loss of current at that point. Similar conditions exist at stations 193700 and 201200. These locations are further complicated by the presence of new pipe. However, at these two locations unusually low-earth resistivities were encountered and as measurements of resistivity were always made outside of the trench area the newly filled trenches can not account for the low values observed.

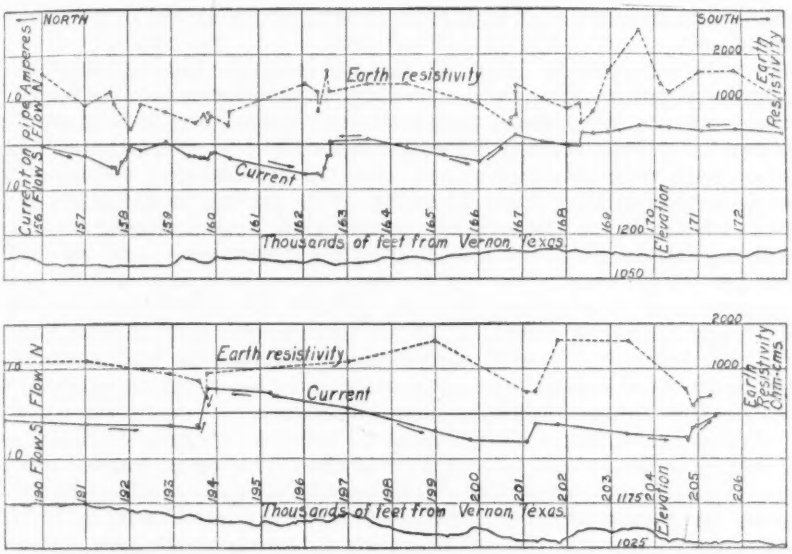

FIGURE 14.—*Line HV; electric currents and soil resistivity along 6-inch oil line, Archer County, Tex.*

VIII. RELATION OF LONG-LINE CURRENTS TO CORROSION

The correlation between loss of current and corrosion which has been shown to exist on pipe lines, at once raises many questions as to the actual relation between these factors and the real significance of such currents. It is possible that the long-line currents represent the effects of local galvanic action on the surface of the pipe as shown in Figure 5, or they may be the result of potential differences between pipe surfaces in two widely separated soils. Although potential differences of steel amounting to several tenths of a volt can be obtained in the laboratory between a concentrated alkaline solution and a neutral solution, the potential difference in different soils in any territory is usually less than 0.1 volt. It seems more probable that the currents are the residual results of local action as shown in Figure 5. The theory is supported by the fact that almost without exception currents are found entering tank farms rather than leaving them. If such currents were generated by differences in soil areas one would not expect to find them always flowing toward the tanks. It appears, therefore, that the currents flowing toward tank farms are the result of a difference of potential between the pipe line and the tank bottoms.

This may be a difference in metals or a difference in oxygen supply. The latter supposition appears to be the more reasonable.

That currents entering tank farms must have a negligible influence on the corrosion of tank bottoms is shown by the following simple calculation. A tank 117 feet in diameter has an area of approximately 10,700 square feet. At 100 per cent anodic efficiency a current of one ampere will carry into solution 20 pounds of iron in one year, or, when discharging from an area of 1 square foot, will produce a penetration to a depth of about one-half inch per year. Assuming a discharge of 5 amperes from a 117-foot tank, which is a little greater than the maximum discharge rate so far discovered, there would be a penetration of only about 0.000233 inch per year.

As corrosion usually takes the form of irregular pitting rather than of uniform penetration, it is necessary to employ a pitting factor if we are to estimate the pit penetration corresponding to a given loss of weight. Data on the bureau's 8-year-old corrosion specimens show pitting factors ranging from about 2 to more than 40, the more common values being from 10 to 20. The pitting factor is the ratio of the maximum to the average penetration. Assuming in this case a pitting factor of 15, the maximum pit penetration would be 0.0035 inch per year. Such a rate of corrosion would require over 70 years to puncture a ¼-inch tank bottom. While this calculation is necessarily speculative, it serves to show that line currents should have a negligible effect on the corrosion of tanks and station equipment, and that such corrosion as occurs on tank bottoms must be charged to local, rather than to long-line galvanic action.

Similar calculations with respect to areas of current discharge on pipe lines indicate that a large part of the corrosion in some locations can be accounted for by the action associated with the long line currents. In Figure 13 at station 221500 there is a loss of current of one-half ampere from a 12-inch line in a distance of 50 feet. This is equivalent to 0.003 ampere per square foot or to an average penetration of 0.0015 inch per year. Assuming again a pitting factor of 15, we arrive at a yearly penetration of 0.0225 inch or approximately a 10-year life. As this pipe is now seven years old and has not failed, and as the calculated depth of pitting agrees closely with the pitting actually observed, it would seem that the extent of the corrosion occurring at such particularly corrosive spots is roughly indicated by the density of the current leaving the pipe.

This does not mean that unconnected short pieces of pipe placed in these areas would not experience severe corrosion. It simply means that the highly concentrated current discharge from the pitting areas finds an easier return path by way of remote earth and the pipe line, than by short crowded circuits to immediately adjacent cathodic areas, such as would necessarily be the case with short pieces. Such action would probably retard the rate of corrosion somewhat, particularly under conditions where a relatively large proportion of the pipe is affected. In soils where the pitting factor is large or when a relatively small proportion of the pipe is affected, it is probable that short nipples will show about the same rate of corrosion as the line itself.

Line currents are, perhaps, more suggestive of the locations of corrosive areas than they are of the degree of the corrosion in any given area. Acute corrosion is not associated with pipe-line currents, except at points of exceptionally dense discharge. Moderate rates of

discharge such as those shown in Figure 7 do not in themselves produce excessive corrosion, although they may be associated with and point to acute areas. In Figure 7 the rate of discharge at station 13000 and also at 17000 is approximately 1.8 amperes per thousand feet of 8-inch line. This is equivalent to 0.00086 ampere per square foot or to an average penetration of 0.00043 inch per year. Assuming again a pitting factor of 15 we arrive at a yearly penetration of 0.0064 inch or approximately a 40-year life. As the pipe line at both of the points under discussion was corroded very much worse than the above figures would indicate, it is evident that the line current as measured represents only a fraction of the action taking place at the points of greatest discharge.

The magnitude of line currents is undoubtedly a function of the extent of the corrosive areas with which they are associated. A local hot spot of only a few feet in extent may cause rapid corrosion and yet not be accompanied by line currents of measureable magnitude. Conversely, corrosive areas of considerable extent will usually be accompanied by relatively large line currents. The magnitude of a line current appears, therefore, to be a better measure of the total amount of corrosion in progress in the discharging zone than it is of the rate of corrosion in that zone. Another factor affecting the size of line currents, as well as their rate of discharge, is the character of the corrosion with which they are associated. If the corrosion is uniform the current entering a discharging zone will be a better measure of the total corrosion involved than if only a fraction of the pipe surface is affected. An example of this latter condition is to be found on line ST, previously referred to, where acute corrosion in the form of deep isolated pits occurred, but where the loss of current was relatively small. No general quantitative interpretation, therefore, can be placed on either the size or the rate of discharge of line currents although experience in any given territory may eventually lead to some such interpretation.

IX. RELATION OF ELECTRICAL RESISTIVITY OF EARTH TO CORROSION

While it has been generally recognized that the electrical resistivity of earth is one factor in the corrosion problem, its full significance is so masked by a host of other factors as to make its relation to the problem difficult of analysis. A review of the foregoing data on long-line currents will show that wherever the soil resistivity drops to about 500 ohm-cm, or lower, there is a sharp loss of current and pronounced pitting. Smaller values of current-density discharge occur in areas where the soil resistivity is 600 to 1,500 ohm-cm, but as a rule the corrosion in such areas has not been acute. Illustrative of this is Figure 12, where the discharge zone coincides with a soil resistivity of about 1,300 ohm-cm or lower, but where destructive corrosion has occurred only where the resistivity is 600 ohm-cm or lower. In Figure 14 there is a rather sharp line at 500 ohm-cm below which practically all of the corrosion trouble experienced on that line has occurred. In only one instance throughout the entire investigation was severe pitting encountered in any but soils of low resistivity. This condition was discussed under line ST.

Various methods for determining the corrosiveness of soils have been proposed from time to time, most of which involve resistivity in

one form or another. None of these methods, however, are applicable to all soils, although some of them may apply roughly to soils of some particular type or even to several types. Although the most corrosive soils, as indicated by the tests of the National Bureau of Standards on buried specimens, are soils of low resistivity, severe corrosion has also occurred in some soils of relatively high resistivity. No satisfactory relation between earth resistivity and corrosiveness has been found which is applicable to all soils. However, a recent study of 22 of the soils in which the National Bureau of Standards has test specimens buried and on which six or eight year corrosion data were available at the time of the study, indicates that electrical conductivity is a rough index of the corrosiveness of alkaline soils or those in which the pH value is greater than 7.0. For acid soils, or those having a pH value less than 7.0, no such relation appears to exist, although it is possible that abrupt changes in conductivity in any one territory are indicative of a corrosive area. While it is not probable that a conductivity scale can be used as an index of corrosion for all soils, it is true that abnormally low resistivities in any type of soil are indicative of corrosiveness.

X. STRAY CURRENTS

On some of the pipe lines stray currents of measurable magnitudes were observed, but these did not seriously interfere with properly evaluating the galvanic component. Twenty-four hour smoked chart records showed these disturbances to be characteristic of interurban electric traction lines, and most pronounced during the night hours. Figure 15 (*a*) is the record of the current flow on an 8-inch oil line near Perry, Okla. The all-day average value of the current is 1.16 amperes. Peaks occur at 4.45, 5.50, and 6.35 p. m. Other disturbances occur throughout the night, with a fairly steady current during the working period of the day, between 8 a. m. and 4.30 p. m. Figure 15 (*b*) shows a chart taken on the same line on a different day. The peaks have about the same displacement from each other as those in Figure 15 (*a*) but occur at different times. The irregularity shown on the chart about 10 a. m. is the result of starting the record at that time and removing it the next day at 9.15 a. m.

Figure 16 (*a*) shows the current flow on an 8-inch oil line near Ponca City, Okla. Only slight disturbances resulting from stray currents were detected. These were not large enough to interfere with obtaining consistent results, throughout the working portion of the day.

Figure 16 (*b*) is surprising in that it shows the same kind of disturbance on a 12-inch oil line near Hearne, Tex., as occurred at Perry, Okla., some hundreds of miles distant. During the working portion of the day the disturbances are not serious.

A thorough canvas of the electric traction schedules in Oklahoma indicated that these disturbances originated near Tulsa, where large trains of cars are assembled by electric locomotives and moved from the oil fields. The large number of oil and gas lines extending from the Tulsa district to other parts of the State and into Texas are no doubt responsible for carrying the stray currents such great distances. The currents shown on the accompanying charts are of no practical significance, so far as corrosion is concerned, but may be objectionable on pipe lines near the power stations where they originate. In some sections they may also be of sufficient magnitude to interfere seriously with a study of galvanic long line currents.

a *b*

FIGURE 15.—*Twenty-four-hour records of current on 8-inch oil line near Perry, Okla.*

a, April 9, 1930; *b*, April 10, 1930.

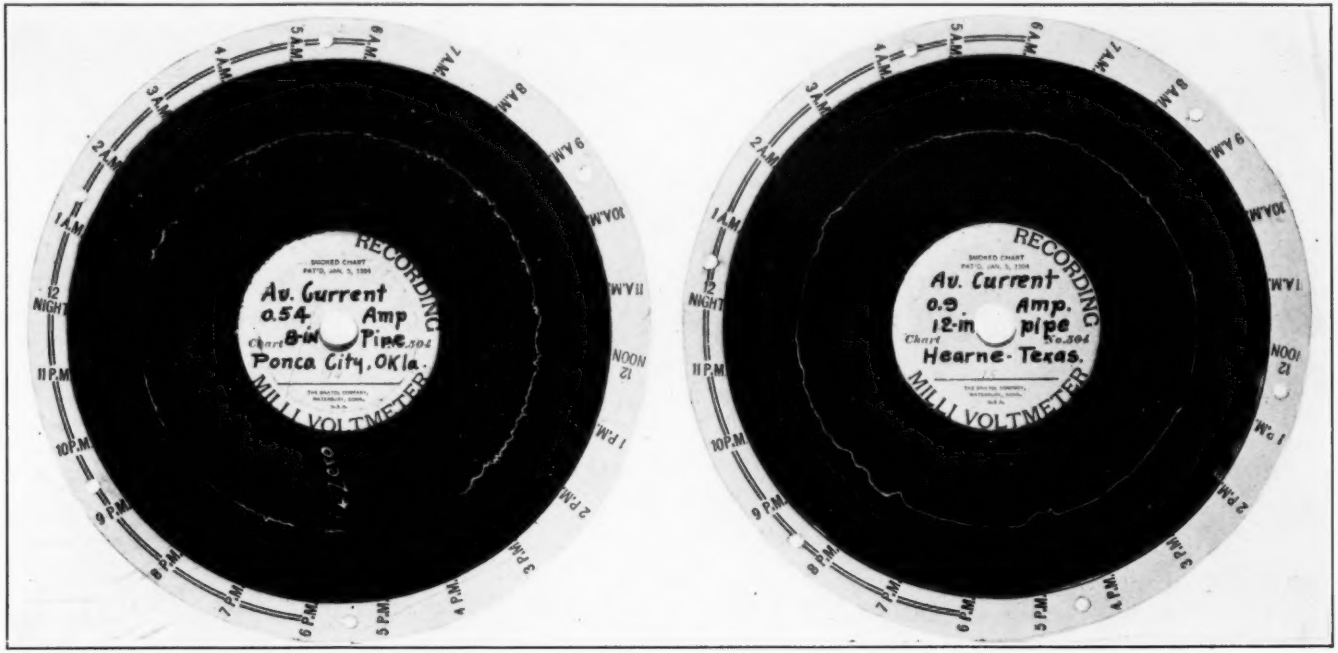

a *b*

FIGURE 16.—*Twenty-four-hour records of current on oil lines*

a, Near Ponca City, Okla.; *b*, near Hearne, Tex.

Other causes for observed variations in pipe line currents at any one point are not fully understood. One observer in California claims that he has good evidence to show that such variations are the result of static electricity produced by the action of the wind as it blows across ranges of hills. Magnetic storms are another possible source of variations.

XI. PRACTICAL SIGNIFICANCE OF DATA AND TECHNIQUE OF MAKING MEASUREMENTS

The significance of the correlations shown in this study are quite apparent to those who are concerned with the construction and protection of pipe lines. It has already been stated that the most recent tendency in pipe-line protection is toward the idea of selecting a coating to meet the particular requirements involved and away from a standard or uniform covering throughout the length of a line, irrespective of the character of the soil. The data herein justify this trend and suggest a practical means of carrying it into practice. They also support recent contentions [3] that destructive corrosion of pipe lines is largely confined to local bad soil areas or "hot spots" of comparatively small extent. It can not be expected that the methods of survey here described are equally applicable to all types of soil. In some areas like the flat lands of the gulf coast the soil is so uniform that no useful information may be obtained from the measurement of line currents. However, in most rolling territory or where soil conditions are more variable, the study of line currents and soil resistivity affords a helpful means of locating the most corrosive soils. On existing lines both kinds of measurements are possible, while for projected lines or where, for any reason, current flow measurements are impracticable, it will be necessary to resort to the resistivity tests alone. For the benefit of those wishing to employ or experiment with these methods of soil survey a brief description will be given of the technique and apparatus employed in the investigations here reported.

1. METHOD OF MEASURING LINE CURRENTS

In using the current-flow method for locating corrosive areas measurements should be made at intervals of one-eighth to one-quarter mile, and when one of these sections shows a pronounced loss of current it should be further subdivided until the exact point where the current is leaving is located. Earth resistivity tests can then be made to ascertain the extent of the corrosive soil area.

The greatest problem involved in measuring pipe-line currents by the potential-drop method is that of making good electrical contact with the pipe. The potential differences to be measured are usually less than 1 mv and this calls for a meter of high-volt sensitivity and, therefore, low resistance. Any resistance introduced into the circuit at the points of contact with the pipe will, therefore, affect the accuracy of the measurements. As rust is a poor conductor or even an insulator it is necessary to get through the rust film and make contact with the solid metal of the pipe. Unless the pipe is uncovered, this is best accomplished by prodding or driving a bar to the top of the pipe and then inserting in the hole thus made a hardened steel point or drill. By turning or tapping the drill a good contact can usually

[3] Chas. Fitzgerald, Corrosion and Pipe Line Coverings, Am. Pet. Inst., D. & P. E. Bulletin No. 204, p. 126. I. A. Denison, Soil Characteristics and Corrosion, Oil & Gas J.; June 5, 1930.

be secured with but little difficulty. It is very important that the rod meet the pipe squarely on top where it will not creep down the side of the pipe when tapped with a hammer. More time is usually consumed in attempting to get good contact in a hole which is off center than is required to put down a new hole.

A low resistance millivoltmeter having a full scale range of 1 mv is well adapted to this use. Both Gill and Putnam have successfully used a portable potentiometer. A standard millivoltmeter of the range indicated and having a resistance of about 3.4 ohms was employed in the work here described.

A standard test length of from 50 to 100 feet should be employed, and this distance can be indicated on one of the leads of the voltmeter which can then be used in lieu of a tape. Where the current is so large that the standard test length gives a deflection beyond the range of the meter, the section can be halved or otherwise subdivided. In fact it is a good practice to subdivide every test section or to make two independent measurements at each point on reconnaissance work. This procedure will enable the observer to catch any error resulting from high resistance joints in the pipe line or from poor contacts. Screw couplings in pipe lines usually have the same resistance per foot as the solid pipe, but occasional ones of abornomally high resistance are encountered and these must be guarded against. It is, of course, necessary to make correction for the resistance of the voltmeter leads. This correction can be combined with the other constants involved to arrive at a conversion factor by which the current can be easily computed from the meter reading.

Let

W = weight of pipe in pounds per foot.
L = length of test section in feet,
R = resistance of voltmeter in ohms.
r = resistance of leads in ohms.
s = resistivity of pipe material in microhms per pound-foot. For steel pipe, National Tube Co. tables, 1913, give $s=215.8$. For wrought-iron pipe, Byers' table weights give $s=209.3$.
e = reading on meter in millivolts.

Then, the current in amperes will be

$$i=\frac{1{,}000\ W\ (R+r)}{R\ s\ L}\times e \qquad (1)$$

For the following constants:

$W=28.55$ pounds (8-inch steel pipe).
$L=75$ feet.
$R=3.4$ ohms.
$r=0.35$ ohm (85 feet of No. 16 lamp cord).
$s=215.8$ (steel pipe).

$$i=\frac{1{,}000\times 28.55\times 3.75}{3.4\times 215.8\times 75}\times e=1.95\ e.$$

In like manner the conversion factor for any set of conditions can be derived.

The sample data sheet shown on opposite page was submitted by one of the pipe line companies which assisted in this investigation and which has since carried on an independent study of line currents and soil resistivity along its own lines with considerable success.

---------- Line ---------- Date ---------- Graph No. ------ F. D. ---------- page ---- sec. ----

Sketch showing features of line under investigation.

[X=direction of current. Y=meter scale used. Size and length of leads ----------]

Location		Current flow				Soil resistance				Soil	Remarks
From	To	X	Y	M. 100 feet	Amp.	Line top	Depth	e	KR		

2. METHOD OF MEASURING SOIL RESISTIVITY

When accurate results are desired it is customary to measure the resistance of earth and other electrolytes with alternating current, in order to avoid polarization and other effects inherent in methods employing direct current. However, by employing a suitable range of current density and voltage, and by taking readings immediately after the circuit is closed or before polarization has set in to any great extent, it is possible in most soils to obtain by direct-current measurement results closely approximating the actual resistance of the medium.

Because of the extreme simplicity of the direct-current equipment and the greater speed with which it can be used in the field this method was employed in making soil resistance tests in this investigation. The first apparatus consisted of a rectangular cell made of insulating material and provided with metal end plates. This cell was 1 inch square in section and 2.54 inches long, between the end plates. In such a cell, which has a cross section of 6.45 cm^2 and a length of 6.45 cm. the actual resistance in ohms of a prism of earth between the end plates is numerically equal to the resistivity of the earth in ohm-centimeter. The resistivity of a medium is the resistance in ohms between two parallel faces of a centimeter cube of that medium.

This cell was packed full of earth and connected in series with two dry cells and a small pocket voltmeter. The deflection on the voltmeter was observed immediately after pressing the key or before polarization had greatly diminished the reading. The resistivity of the earth was then calculated from the constants of the apparatus.

As the work progressed and the significance of earth resistivity became more apparent, the need for a more rapid method of making these tests was seen. Accordingly, two metal tipped oak rods were constructed with the voltmeter mounted on one and a small flash light battery on the other, as shown in Figure 17. Wires leading from the metal ferrules, through channels in the rods to the voltmeter and battery, respectively, and a connection between the battery and meter completed the test set. These rods are pushed into the earth to any desired depth and a reading obtained by pressing the voltmeter key. The resistance in ohms between the electrodes is then calculated as before. To obtain the resistivity of the earth the constant for the apparatus must be known. This constant depends on the area and shape of the metal electrodes and distance between them and can be obtained by calibrating them in a medium of known resistivity. The resistance between the tips of the rods shown in the figure is practically independent of the distance between them, provided it is about 8 inches (20 cm) or more. More recent development work on this piece of apparatus has shown that iron electrodes develop less polarization than brass or copper electrodes, although more care must be exercised in keeping them bright and free from rust. Since with iron or other ordinary base metal electrodes polarization is largely a cathode effect, it can be reduced still further by making the cathode much larger than the anode, thereby decreasing the current density on the cathode. A low-resistance meter, such as a milliammeter is found to be preferable to a high-resistance volt-

FIGURE 17.—*Apparatus for measuring electrical resistivity of earth*

UNIV. OF MICH.

meter, as with the former practically the full voltage of the test battery is applied between the electrodes, irrespective of the meter reading, while with the latter a large part of the battery voltage is consumed within the meter itself. This is particularly objectionable in low-resistance soils where a large deflection on the meter is recorded, and, therefore, where the potential between the electrodes is correspondingly small and polarization effects are relatively large.

An instrument of the following description has been found to give satisfactory results and gives values of the resistivity of sodium chloride solutions ranging from 100 to 10,000 ohm-cm with an accuracy of about 6 per cent as compared to a.c. bridge determinations. The anode is an iron cone of one-half inch (12.8 mm) base and one-quarter inch (6.3 mm) height. The cathode, also of iron, is a frustrum of a cone 2⅝ inches (6.7 cm) long, ¾-inch (1.9 cm) lower base, ⅛-inch (3 mm) upper base. The point is ground or turned on a 1/16-inch (1.5 mm) radius. A three-volt battery of two flash-light dry cells is used, the positive pole being connected through a switch to the smaller electrode or anode. A milliammeter having ranges of 25 and of 100 m. a. is employed, the 25 m. a. range is good for resistivities down to about 370 ohm-cm while the 100 m. a. range is good for resistivities between 400 and 100 ohm-cm. The scale of the meter can be graduated directly in ohm-centimeter. A multiplier coil is also included in the meter by which the voltage of the battery can be checked from time to time. The calibration constant for such an instrument is approximately 3; that is, the soil resistivity in ohm-centimeters is equal numerically to three times the measured resistance between the electrodes when they are separated in the earth about 8 inches (20 cm), or more.

This apparatus permits of making frequent and rapid tests of earth resistivity along a pipe line or along a projected pipe line. Although it is not claimed that absolute values of resistivity are obtained with this apparatus, the results are sufficiently accurate for all practical purposes, provided the soil is not too dry. It is important to test the earth at pipe level and where there is sufficient moisture to afford nearly maximum conductivity. Measurements should not be made in dry soil as they will mean nothing, even though an indication on the meter is obtained. Damp soil which will pack in the hand will usually show a conductivity approaching that of a saturated condition. It is therefore necessary to confine measurements to wet, or at least to damp soil. Access to the desired depth can be obtained by driving a steel bar to make a hole or by using a soil auger. Where the ground is not too hard a depth of 18 inches or 2 feet can be attained by removing the top soil with a shovel and pushing the rods into the soft earth.

The intervals at which such tests should be made will depend upon the character of the soil and, perhaps, many other factors. To be sure that no extensive hot spots are missed, it may be necessary in some locations to make tests at intervals of 100 feet or less, while in other areas the vegetation and topography may be depended on to a large extent to indicate the character of the soil.

XII. SUMMARY

1. Much of the soil which is exceptionally corrosive to ferrous materials exists in the form of naturally occurring outcrops or pockets in which the soluble salt content is abnormally high. Although relatively small in extent, such areas account for a large proportion of the corrosion on underground pipe systems. The predetermination of these corrosive areas is a matter of great importance to the pipe owners, both from the standpoint of protecting new lines and the reconditioning of old ones.

2. Practically all pipe lines carry galvanic electric currents of measurable magnitudes and these bear a worthwhile relation to both corrosion and the electrical resistivity of the soil.

3. In general, galvanic electric currents collect on pipe lines in regions of normal or high-soil resistivity and discharge from the lines in relatively small areas of low-soil resistivity.

4. At points of abrupt discharge and abnormally low-resistivity corrosion is most severe.

5. Soil resistivities of about 500 ohm-cm or less are usually indicative of severe corrosion. Above about 1,000 ohm-cm there appears to be little relation between resistivity and corrosion.

6. The measurement of pipe-line currents and soil resistivity offers a helpful means of locating exceptionally corrosive soil areas.

WASHINGTON, February 7, 1931.

TWO NEW CRYSTALLINE DIFRUCTOSE ANHYDRIDES FROM HYDROLYZED INULIN

By Richard F. Jackson and Emma McDonald

ABSTRACT

Hydrolyzed inulin has previously been shown by Jackson and Goergen (RP79) to contain about 5 per cent of a group of nonreducing difructoses, one of which was isolated in crystalline form and found to be a difructose anhydride of $[\alpha]_D^{20} = +27.0$. The mother liquors from which this substance had crystallized ultimately yielded by crystallization from alcoholic solution a second crystalline substance, designated difructose anhydride II, and a third, difructose anhydride III.

Difructose anhydride II crystallizes in truncated prisms, frequently having a hexagonal cross section, melts at 198° C., and has a $[\alpha]_D^{20}$ of +13.85. It is hydrolyzed solely to fructose.

Difructose anhydride III crystallizes from alcohol in the form of bipyramids, melts at 162° C., and has a $[\alpha]_D^{20}$ of +135.64. It is hydrolyzed to fructose by 0.2 N H_2SO_4 at 100° C., showing evidence of an intermediate product of hydrolysis.

From the 5 per cent of nonreducing substance in hydrolyzed inulin three crystalline difructose anhydrides have now been isolated, whose mean rotatory power (+58.8) agrees with that of the mixture (+55) as originally isolated. This indicates that the mixture contained the three sugars in approximately equal proportions.

The evidence accumulated in this and in pevious articles indicates that inulin has a molecular weight approximating 18,000.

CONTENTS

		Page
I.	Introductory	709
II.	Isolation of two new crystalline difructose anhydrides	710
III.	Difructose anhydride II	711
IV.	Difructose anhydride III	711
V.	Discussion	711
VI.	The molecular weight of inulin	712
VII.	Experimental	713
	1. Purification and analysis of difructose anhydride II	713
	2. Hydrolysis of difructose anhydride II	714
	3. Purification and analysis of difructose anhydride III	714
	4. Hydrolysis of difructose anhydride III	715
VIII.	Acknowledgment	715

I. INTRODUCTORY

In a study of the hydrolysis of dahlia inulin in aqueous solution with sulphuric acid Jackson and Goergen [1] showed that the products of hydrolysis consisted of about 92 per cent fructose, 3 per cent aldose, and 5 per cent of a group of nonreducing difructoses. The present authors [2] in continuation of the study found that hydrolyzed inulin prepared from a wide variety of plants other than the dahlia

[1] B. S. Jour. Research, 3 (RP 79), p. 27; 1929.
[2] B. S. Jour. Research, 5 (RP 251), p. 1151; 1930.

also possessed approximately the same composition with respect to the analytically determinable constituents and that extensive fractional crystallization failed to alter the composition essentially. It was stated in the latter article that evidence was already at hand which indicated that the group of nonreducing disaccharides consisted of no less than three isomeric difructoses. From this fact the authors were able to compute the order of magnitude of the molecular weight of inulin. This evidence will be presented in the present article.

Jackson and Goergen isolated the nonreducing portion of hydrolyzed inulin and found that the substances in the resulting aqueous solution possessed a $[\alpha]_D^{20} = +55$. Upon acetylation of the mixture, a portion, about 30 per cent, crystallized and was found to be the hexa-acetate of a difructose anhydride. The acetate showed a $[\alpha]_D^{20} = +0.54$ in chloroform and the free sugar $+27.0$ in water. This sugar was designated difructose anhydride I.

II. ISOLATION OF TWO NEW CRYSTALLINE DIFRUCTOSE ANHYDRIDES

Remaining from the experimental material of Jackson and Goergen was a quantity of the mother liquors from which difructose anhydride I hexa-acetate had been separated. The substances dissolved in these mother liquors had a specific rotation of about $+35$ and a molecular weight corresponding to the hexa-acetate of a disaccharide. All efforts to induce crystallization had proved futile. A large portion of it was consequently deacetylated in order that experiments might be made with the mixture of free sugars. The resulting sugar mixture had a specific rotation of about $+70$. It was considered possible that even after removal of the greater part of the first sugar there might remain two additional sugars. Efforts were accordingly made to effect a separation by some method of fractional extraction. The expedient which appeared to be most promising was a method of separation by means of insoluble compounds which, it was found, the sugars formed with lime. It was planned to carry out the precipitation fractionally in the hope of separating the respective sugars. A portion was accordingly evaporated in vacuo in order to carry out this project. However, during the evaporation a crystallization of one of the constituents unexpectedly occurred and rendered elaboration of the original plan unnecessary.

At the completion of the crystallization the crystals were collected on a filter, and although deposited from a solution having a $[\alpha]_D$ of about 70 showed a $[\alpha]_D$ of only $+13$. This indicated the presence of still another disaccharide in the solution. The verification of this indication came very suddenly, for the filtrate from the crystals above mentioned became turbid within a few minutes after passing the filter and within a few hours had deposited an abundant quantity of crystalline material which appeared under the microscope to have a very different character from either of the two sugars previously isolated. The crude crystals showed a $[\alpha]_D = +133.9$.

The sugar of lower rotatory power will be referred to as difructose anhydride II; that of higher rotatory power as difructose anhydride III.

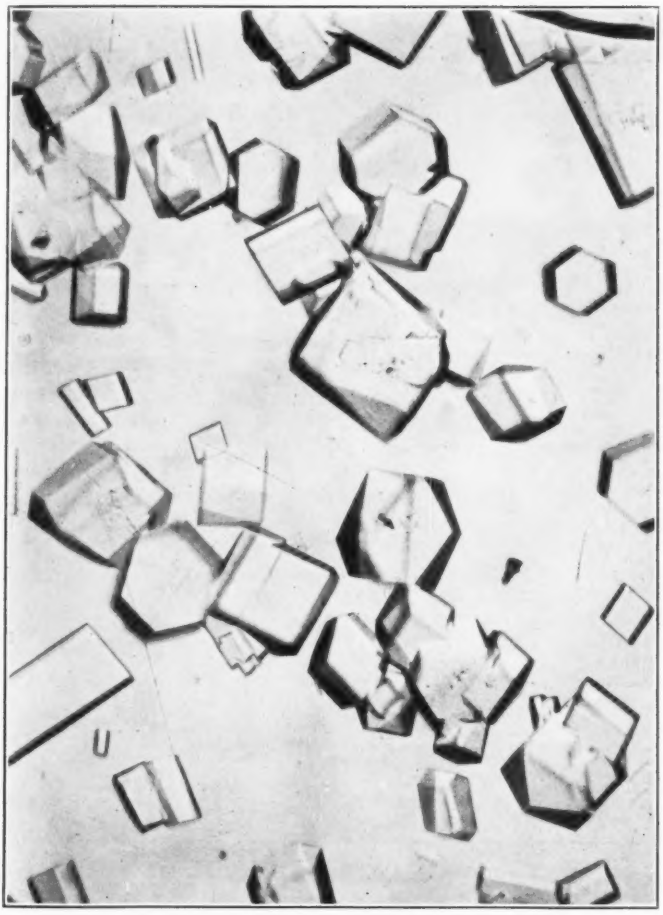

FIGURE 1.—*Difructose anhydride II*
(Crystallized from aqueous solution.)

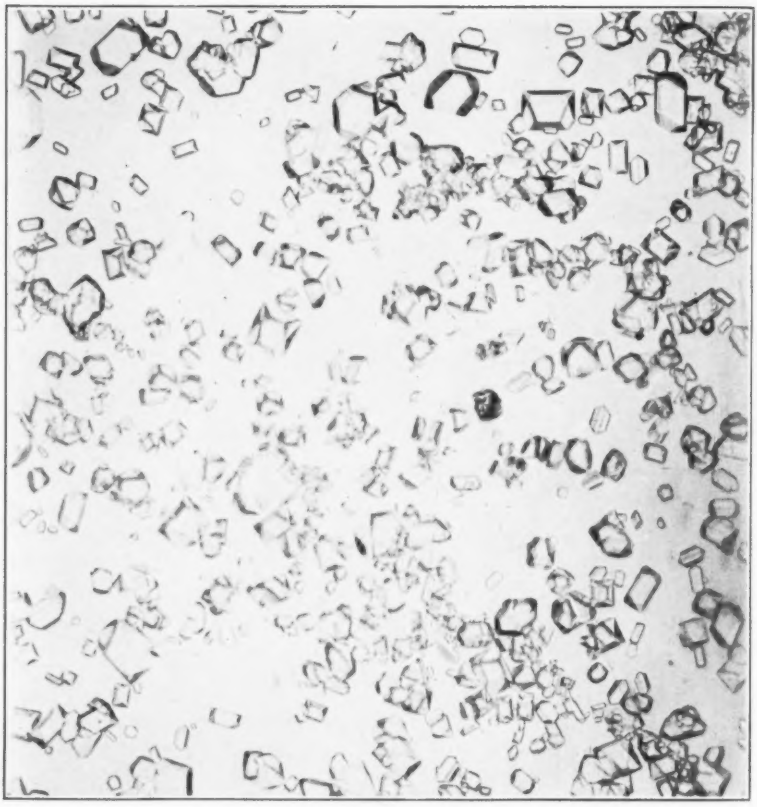

FIGURE 2.—*Difructose anhydride III*
(Crystallized from alcholic solution.)

III. DIFRUCTOSE ANHYDRIDE II

This sugar crystallizes from alcoholic or aqueous solution in the form of truncated prisms (fig. 1) frequently having a hexagonal cross section. It is only slightly soluble in hot absolute alcohol, but may be conveniently crystallized from 95 per cent alcohol by dissolving in a large volume of solvent and evaporating the excess. In water it has an approximate solubility of but 32 per cent. The purified substance exhibited a $[\alpha]_D^{20} = +13.85$ in aqueous solution and a melting point of 198° C. Its ultimate analysis and its molecular weight, determined by the depression of the freezing point of water, indicated that it was the anhydride of a disaccharide and had the empirical formula, $C_{12}H_{20}O_{10}$. Upon hydrolysis the sugar yielded only fructose. It was, therefore, a difructose anhydride isomeric with the difructose anhydride I described by Jackson and Goergen. Acetylation with acetic anhydride and sodium acetate produced a sirup, but all efforts to induce crystallization proved unsuccessful.

IV. DIFRUCTOSE ANHYDRIDE III

The third difructose anhydride crystallizes from absolute alcohol usually is well-formed bipyramids (fig. 2), but occasionally in elongated prisms. Despite the fact that it was the last of the group to make its appearance in crystalline form, it proved to be the most readily crystallized one of the three, once crystals for seeding had become available. After repeated recrystallization the purified substance showed a $[\alpha]_D^{20} = +135.64$ in water and a melting point of 162° C. The combustion analysis and a molecular weight determination by the freezing-point method indicated a disaccharide of the formula $C_{12}H_{20}O_{10}$.

When treated with 0.20 *N* H_2SO_4 for 110 minutes at 100° C. it was 80 per cent hydrolyzed, the final product of hydrolysis consisting solely of fructose. It was, therefore, a third difructose anhydride isomeric with the two previously described. The polariscopic evidence seemed to indicate that an intermediate product of lower rotatory power than the original sugar was formed during hydrolysis. This could conceivably be ascribed to the addition of a single molecule of water. The resulting product would not necessarily acquire reducing properties if, for example, one of the hexose residues in the original substance were an anhydrofructose. The explanation, however, must await further experiments on the structure of the disaccharide.

The sugar crystallizes readily from aqueous solution in which it has a solubility of but 38 per cent.

Acetylation with acetic anyhdride and sodium acetate yielded a positively rotating sirup from which we have as yet been unable to obtain crystalline material.

V. DISCUSSION

From the nonreducing material which constitutes about 5 per cent of the products of hydrolysis of inulin we have now isolated in crystalline form the three difructose anhydrides whose properties are summarized in Table 1.

TABLE 1.—*Properties of the isomeric difructose anhydrides*

	I	II	III
$[\alpha]_D^{20}$ (water)	+27.0	+13.85	+135.64
Melting point	164	198	162
Crystalline form	Thin plates.	Truncated prisms.	Bipyramids.
Molecular weight (calculated 324)	307	310	308
Approximate solubility in water [1]	32	32	38

[1] Expressed as grams of sugar in 100 gs. of solution at 20°C.

The three sugars resemble each other in respect of their great resistance to hydrolytic action and their strikingly low solubility in water. They differ in rotatory power, melting point, and crystalline structure. It seems probable that they are closely related in chemical structure, a problem which will engage our attention in continuation of the study of inulin.

Jackson and Goergen after isolating the nonreducing portion of hydrolyzed inulin determined its specific rotation with a fair degree of approximation. The value which they found, namely, +55, was probably slightly lower than the true value, since the product was inevitably contaminated by impurities introduced during the processes of isolation. The mean value of the measured specific rotations of the three respective difructose anhydrides (that is, +27.0, +13.8, and +135.6) which have subsequently been isolated and purified is +58.8. This relatively close agreement with the rotation of the mixture makes it appear probable that these three sugars occur in the mixture in equal proportions and that their summation accounts for the total nonreducing residue. This conclusion is further corroborated by the fact that the mother liquors after the removal of the greater part of the first disaccharide in the form of its acetate contained a mixture of the second and third disaccharides showing a specific rotation of +69.3. The complete removal of the first disaccharide would yield a mixture of mean rotation +74.7. Moreover, Jackson and Goergen obtained the acetate of the first disaccharide in about 30 per cent yield, which suggests that it is one-third of the total substance. Thus the preponderance of evidence seems to indicate that the 5 per cent of nonreducing residue from hydrolyzed inulin consists solely of these three sugars occurring in equal proportions. We hope further to establish this conclusion by effecting a more nearly quantitative separation of the constituents.

VI. THE MOLECULAR WEIGHT OF INULIN

The molecular weight of inulin was discussed by us in a previous article.[3] Basing our conclusions on a clear indication of the existence of these three difructose anhydrides we showed by simple arithmetical reasoning that a 5.2 per cent nonreducing portion of hydrolyzed inulin,

[3] See footnote 2, p. 709.

which consisted of three disaccharides, predicated a whole molecule composed in average of no less than 111 hexose residues and having a molecular weight of approximately 18,000. The fundamental basis upon which that calculation rests, namely, the existence of the three isomeric disaccharides, is now definitely established.

Our conclusion was, however, not entirely free from assumptions, since it was suggested as a possibility that the three disaccharides might have existed in the original inulin molecule as a single difructose group and that the isomerism might have been introduced by different modes of cleavage from the rest of the inulin molecule. This possibility can now probably be eliminated, for, in general, when competitive reactions, such as the hypothetical one which we have suggested, occur, one of the possible reactions usually predominates. Since there is apparently no predominance of any one of the three isomers, it is probable that the reactions by which the disaccharides are released are not competitive. It is our view, therefore, that the difructose groupings present in the inulin molecule are the same as in the sugars which we have isolated, except for the readily hydrolyzable points of contact. Probably a knowledge of the structure of the disaccharides will at some later period contribute to a final solution of the question.

The value calculated in the previous article is merely the average molecular weight of inulin prepared in the usual way by crystallization from aqueous solution. It is not our conception that inulin is a single polysaccharide of definite composition. It is rather a group of polysaccharides of very similar properties, but varying in number of hexose residues. Our analyses show extreme variations in the disaccharide content of nearly 20 per cent from the mean. While much of this variation may be ascribed to the uncertainties of a difficult analysis, there can be no doubt that real variation in composition occurs. It will be of interest to examine the more soluble polysaccharides and to determine at what point in the scale of complexity the difructose anhydrides appear.

VII. EXPERIMENTAL

1. PURIFICATION AND ANALYSIS OF DIFRUCTOSE ANHYDRIDE II

The material which served as a starting point for the present series of experiments was a mixture of sirupy acetates prepared by Jackson and Goergen [4] from the nonreducing portion of hydrolyzed inulin. The crystalline hexa-acetate of difructose anhydride I had been in great part removed by crystallization from alcoholic solution, but even after two years' standing no other substance appeared in crystalline form. It had been previously shown by Jackson and Goergen that the substances in this sirup had a molecular weight corresponding to the hexa-acetate of a disaccharide and a specific rotation of about +31.

A portion of this sirup was deacetylated by warming gently with an aqueous solution of $Ba(OH)_2$ until the sirup was completely dissolved and allowing it to remain in alkaline solution over night.

[4] See footnote 1, p. 709.

The barium was then removed by adding the calculated amount of H_2SO_4. The aqueous solution was evaporated and the solvent displaced by absolute alcohol. The resulting solution was evaporated to a thick sirup for the purpose of attempting a fractional separation of the respective lime compounds, but during the evaporation an abundant crystallization of one of the constituents of the mixture occurred. This was collected and was found to have a specific rotation of +14.8. After three recrystallizations from absolute alcohol the rotation was 13.85 and remained unaltered by further treatment. The purified crystals were dried in a vacuum chamber heated to about 70° to constant weight. *Anal.* Calcd. for $C_{12}H_{20}O_{10}$: C, 44.42; H, 6.22. Found: C, 44.7 ± 0.5; H, 6.0 ± 0.1. (If calculated for $C_{12}H_{22}O_{11}$: C, 42.1; H, 6.5.) *Mol. wt.* Subs., 0.4744, 0.8398: water, 21.9989, 25.4810; Δ T, 0.127°, 0.201°. Calcd.: 324. Found: 316, 305. (A pure cane sugar solution gave approximately the same percentage error as the mean of these determinations under the experimental conditions. Calcd., 342. Found, 328.) *Rotation.* $[\alpha]_D^{20}$ in $H_2O = +13.85$ ($c = 8.993$, $\alpha = +7.20°$, saccharimeter, 2-dm tube), $[\alpha]_{5,461}^{20} = +16.30$ ($\alpha = +2.931°$, circular), and $[\alpha]_{5,780}^{20} = +14.46$ ($\alpha = +2.600°$, circular). *Melting point*, 198° C. (uncorrected).

2. HYDROLYSIS OF DIFRUCTOSE ANHYDRIDE II

A 5.0 ml solution, containing 201.2 mg of the second difructose anhydride (=40.24 mg per ml) and sufficient H_2SO_4 to make it 0.20 *N*, was maintained at 100° C. for 100 minutes. Upon analysis it was found to contain 28.1 mg of total reducing sugar per ml (Scales' method) and 28.9 mg of fructose per ml (Nyns' method). The hydrolyzed solution in a micropolariscope tube (calculated to a 2 dm length) gave a saccharimeter reading at 20° C. of −14.1°. By correcting the observed rotation for the rotation of the disaccharide which remained unhydrolyzed we obtained the rotation of the hydrolytic products. This, calculated for fructose, yielded the value 28.7 mg per ml. In the period of 100 minutes' digestion the disaccharide was 64 per cent hydrolyzed. The agreement between total reducing sugar and the fructose calculated in two independent ways indicates that fructose is the sole product of hydrolysis.

3. PURIFICATION AND ANALYSIS OF DIFRUCTOSE ANHYDRIDE III

Previous to the preparation of the second difructose in quantity a number of small portions had been filtered from the mixture of sugars. The substances in the mother liquor showed a specific rotation of about +81, indicating the presence of another sugar of high rotatory power. Immediately after the filtration of one of the larger portions this substance crystallized spontaneously in the filtrate while the filtration was still in progress. When the seed crystals became available it proved to be a simple matter to induce crystallization from any of the fractions in which it was present. It is the most readily crystallizable member of the group. Even from an alcoholic solution of the mixture of sugars in the original nonreducing residue from hydrolyzed inulin it crystallizes slowly. The crude crystals showed a specific rotation of +133.90. After four recrystallizations it acquired a rotation of +135.64° which remained unaltered upon further treatment. (*Anal.* Calcd. for $C_{12}H_{20}O_{10}$: C, 44.42; H, 6.22.

Found: C, 44.9 ± 0.5; H, 6.3 ± 0.1. *Mol. wt.*, Subs., 0.4004: water, 24.9018; Δ T, 0.097. Calcd.: 324. Found: 309. (Under the same experimental conditions a solution of pure cane sugar showed the same divergence from the calculated value.) *Rotation.* $[\alpha]_D^{20}$ in H_2O = +135.64 (c = 7.847, α = +61.49°, saccharimeter, 2 dm tube), $[\alpha]_{5.461}^{20}$ = +160.51 (α = +25.191°, circular), and $[\alpha]_{5.780}^{20}$ = +142.23 (α = +22.322°, circular). *Melting point*, 162° C. (uncorrected.)

4. HYDROLYSIS OF DIFRUCTOSE ANHYDRIDE III

A 5.0 milliliter solution containing 308 mg of the third difructose anhydride (=61.6 mg per milliliter and sufficient H_2SO_4 to make it 0.20 N was hydrolyzed at 100° C. for 110 minutes. Upon analysis it was found to contain 54.8 mg total reducing sugar per milliliter (Scales' method) and 56.2 mg fructose per milliliter (Nyns' method). Hydrolysis estimated from reducing sugar analysis was, therefore, about 81 per cent complete. The hydrolyzed solution in a 2 dm column gave a saccharimeter reading at 20° C. of −25.1°. Upon correcting for the rotation of the unhydrolyzed sugar and converting the resulting polarization to weight of fructose the very discordant value of 64.8 mg was obtained. The experiment was repeated with 61.14 mg per milliliter and a period of 135 minutes digestion at 100° C. Total reducing sugar per milliliter, 57.0 mg; fructose (Nyns), 56.7 mg; fructose by corrected polarization, 64.2 mg. Hydrolysis was computed from the reducing sugar analysis to be 84 per cent complete. The concordance between the total reducing sugar and the fructose by the very selective Nyns' method shows that fructose is the only product of complete hydrolysis. The discordance between the true fructose and the fructose by corrected polarization is probably to be ascribed to an intermediate stage of hydrolysis. The correction for the unhydrolyzed sugar involved the assumption that its rotation was unaltered. On account of its high rotatory power the correction amounted to nearly 40 per cent of the observed rotation. If the calculation is reversed and the specific rotation of the nonreducing portion is calculated the values +60 and +66 are obtained, respectively, in the two experiments. There are many other indications of the presence of an intermediate product of hydrolysis which at present are too vague to merit description but which will engage our attention in continuation of the present study.

A portion of the hydrolyzed solution was neutralized with $Ba(OH)_2$ and treated with phenylhydrazine acetate. The resulting crystals after recrystallization gave the correct melting point (204° C.) for glucosazone.

Considering the molecular weight determination, the carbon analysis, and the fact that fructose is the only reducing sugar formed after 80 per cent hydrolysis, we conclude that the substance under discussion is a third difructose anhydride.

VIII. ACKNOWLEDGMENT

The authors desire to express their appreciation of the assistance rendered by F. P. Phelps, who prepared the photographs of the crystals of the disaccharides and by M. J. Proffitt and J. A. Bogan, who extracted the large quantity of inulin which was required.

WASHINGTON, January 6, 1931.

MEASUREMENT OF FIBER DIAMETERS BY THE DIFFRACTION METHOD

By H. J. McNicholas and H. J. Curtis

ABSTRACT

The classification of wool fibers into standard grades is based entirely on the average diameter of the fibers. The diffraction of light by a bundle of parallel fibers was employed by Thomas Young in 1824 in a simple ingenious instrument for the rapid direct measurement of average diameter, but no thorough investigation has ever been made of the practical possibilities of this method in the routine grading of wool.

In the present paper a new construction of Young's instrument (the eriometer) is described, and a critical study is made of the accuracy and adaptability of the instrument in the averaging of a wide range of diameters as distributed in a group of fibers. Sources of error and limitations of the method are discussed.

It is found that the eriometer average is in excellent agreement with comparable data obtained with the microscope. The method affords considerable opportunity for the further development of instruments to include additional features desirable in the study of wool or other textile fibers.

CONTENTS

	Page
I. Introduction	717
II. Description and theory of the eriometer	719
III. Calibration and performance	723
1. Calibration of the eriometer scale	723
2. Effect of irregularities in form and arrangement of the fibers	725
3. Dispersion of diameters in wool samples	725
4. Precision and accuracy of measurements	731
IV. Discussion and conclusions	733

I. INTRODUCTION

The average diameter[1] of wool fibers is a dominant dimensional characteristic of the material immediately affecting its value for manufacturing purposes. In the establishment of the United States standards[2] for wool and wool top the average diameter of the fibers is the sole basis for the classification. Sets of these standards are in general use in the wool industry; they define the official scale of quality in this country in terms of which the wool grader gives numerical expression to his results.

In present commercial practice the routine grading of wool is done by men of long experience in the industry who by merely handling

[1] The term "average diameter" is somewhat loosely applied in this connection, for wool fibers are not always circular in cross section, but may exhibit a considerable degree of irregularity in contour. We employ the term, following customary usage, for the average projected width of the fibers as obtained by microscopic methods or by direct measurement of enlarged images projected on a screen. It is also the quantity observed by direct visual inspection.

[2] Official Standards of the United States for Grades of Wool and Wool Top, U. S. Department of Agriculture, Service and Regulatory Announcements, No. 100; issued Aug. 3, 1926.

and observing the material assign it intuitively to its proper grade. There is no suitable instrument available for the rapid, convenient, and accurate evaluation of wool on the established basis. Various microscopic and optical projection methods have been employed in the laboratory for measuring the diameter of wool and other textile fibers. Such methods are slow and cumbersome, however, requiring a large number of diameter determinations on individual fibers to obtain a reliable basis for grading.

A simple, rapid optical method for direct measurement of the average diameter of a group of fibers was devised by Thomas Young[3] in 1824, but no thorough investigation has ever been made of the possibilities of this method in the routine grading of wool. Young's method is based on the phenomenon of diffraction, which is manifested when a light source of small dimensions is viewed through a bundle of fibers which are arranged approximately parallel to one another. Under these conditions a banded light distribution is seen extending laterally and symmetrically on opposite sides of the source in directions perpendicular to the axes of the fibers. From the theory of diffraction a known relation exists between the separation of the bands and the average diameter of the fibers. Young called his instrument the eriometer, from its utility in measuring the fibers of wool. He recommended its use for agricultural purposes and indicated how a tolerable approximation to the value of wool might be obtained from its readings. Young also applied his method to the study of other materials, measuring the average size of particles in milk, blood, barley smut, and dust.

Several instruments embodying the principle of this method have been applied since with moderate success by Pijper,[4] Bergansius,[5] Millar,[6] and Emmons [7] in the measurement of the average size of blood cells under different pathological conditions. Young's method and instrument are again brought to the attention of the textile industry in a recent article by Ewles,[8] but no experimental data are given on the performance of the instrument.

In the present paper a new design of the eriometer is described. The theory of the method is fully explained and some theoretical and experimental data are included on the accuracy of the instrument and on its ability to collect into a single averaged result the effect of a wide variation in projected diameters as distributed in a group of fibers. Some advantages and disadvantages of the method are considered in relation to its further development and application.

It is beyond the scope of the present paper to discuss general aspects of the problem of wool classification or the qualifications of different measures which have been suggested as a basis for grading. In a more complete evaluation of wool quality by scientific measurements [9] various physical and chemical attributes of the fiber must undoubtedly be taken into consideration. No single property of the fiber alone may be expected to yield an accurate index to the value of all types of wool for different trade purposes. One important factor

[3] Miscellaneous Works of Thomas Young, **1**, p. 343; 1855.
[4] Lancet, Lond, **2**, p. 367; 1924.
[5] Pflüger's Archiv., **112**, p., 118; 1921.
[6] Proc. Roy. Soc. London, **99B**, p. 264; 1926.
[7] Quarterly J. Medicine, **21**, p. 83; 1927.
[8] J. Textile Sci., **2**, p. 101; 1928.
[9] A comprehensive survey of research in this field is given by S. G. Barker in Wool, A Study of the Fiber, September, 1929. Published by H. M. Stationery Office, London.

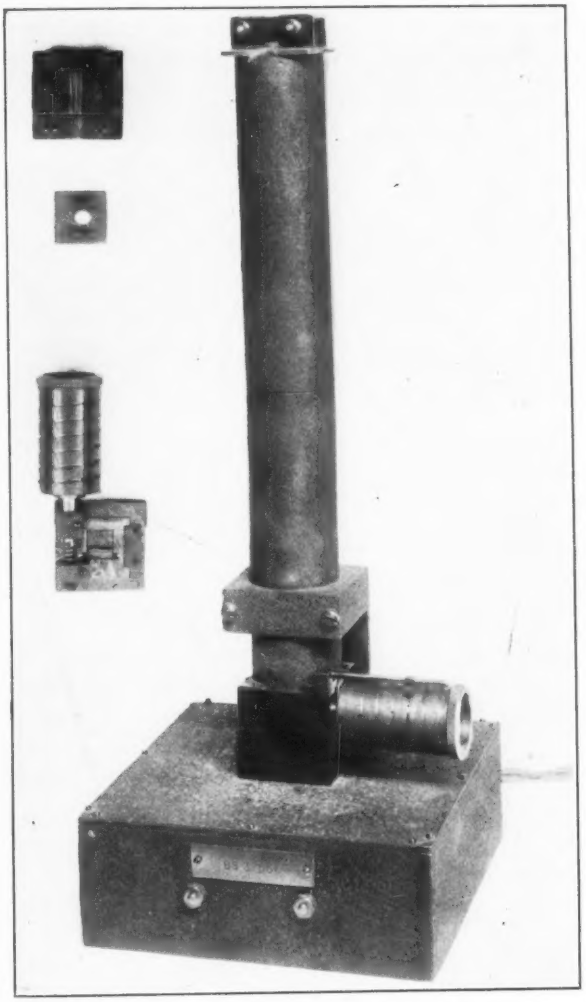

FIGURE 1.—*Photograph of the criometer, with views showing the construction of the slit and the mounting of the fibers*

may be mentioned in this connection because of its general bearing on the subject at hand.

It is well known that all dimensional characteristics of the fibers, such as diameter, staple length, crimpiness, cross-sectional area, and contour, each exhibit a wide range of variation within any sample of the material. Our object for measurement is not a single quantity invariant throughout a given sample but is always a wide range of values occurring with variable frequency distribution from sample to sample. If it so happens that this distribution of values for a given property shows no definite central tendency, or concentration, about a single point on the scale of values, then it is evident that no single value, such as the average, can adequately represent the distribution. By itself, the average may have little significance unless supplemented by a measure of variation. A consignment of wool with a high degree of variability and irregularity in certain dimensional properties may not be as suitable for some manufacturing purposes as another consignment with more nearly uniform properties, although both may average the same. The work of Potsdamer and Schenker[10] indicates that a more reliable and significant procedure for grading on the diameter basis is by comparison of the diameter distribution of the unknown sample with known distributions represented by the set of standards.

In the development of methods and instruments for measuring dimensional properties of the fibers it is therefore of considerable importance to provide, if possible, for rapid and easy determinations of distribution. With the microscope a laborious diameter distribution analysis must precede the determination of the average. It will be shown in the present paper that the diffraction method with the particular instrument herein described provides a rapid direct measure of the arithmetical average along with a definite indication of variation. With further development of instruments based on this method it appears possible to obtain in addition a quantitative expression for the variation.

II. DESCRIPTION AND THEORY OF THE ERIOMETER

A photograph of the eriometer is reproduced in Figure 1 with views illustrating the mounting of the fibers and other items of the construction. The design and operation of the instrument will be explained with reference to the diagrams in Figure 2.

At the lower end of an upright observation tube is a rectangular slit *S1* approximately 1 mm wide and 15 mm long. This slit is illuminated through a ground glass diffusion screen by four 10-watt Mazda lamps mounted in a white-lined box which forms the base of the instrument. The narrow illuminated slit serves as a uniform line-source of light for the observation of the diffraction phenomena.

At the top of the tube is a circular aperture 6 mm in diameter over which a group of fibers may be mounted and arranged approximately parallel to the slit. To assist in this adjustment the sample holder may be rotated about the axis of the observation tube.

Looking through the fibers at the illuminated slit one sees then a series of bright diffraction bands separated by narrow darker intervals.

[10] The Melliand, **1**, pp. 1665, 1776; 1930.

These bands are arranged parallel to the slit and are extended laterally and symmetrically on both sides. It will be shown presently that the spread of these bands, or more specifically, the distance from the center of the bright slit to the first dark band on either side, is—to a close approximation—inversely proportional to the average diameter of the fibers.

For the purpose of measuring this distance the slit is actually made up in three parts, as shown in Figure 1. By means of a screw of known pitch the short outer parts of the slit (approximately 1 mm in length) may be displaced, simultaneously and laterally, relative to the central stationary part, until they are lined up with the center of the first dark band. This displacement, or its reciprocal value, is then read directly

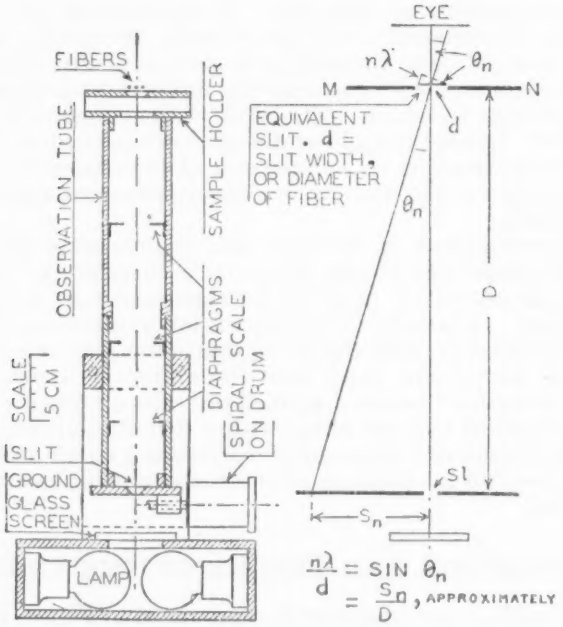

FIGURE 2.—*Diagram of eriometer*

from a spiral scale on the drum. The use of the ground glass diffusion screen provides for the uniform illumination of the displaced as well as the stationary portions of the slit.

Diaphragms are inserted in the observation tube to avoid oblique reflection of light from the walls of the tube to the eye, so that the diffraction bands are thereby observed on a uniformly dark field of view.

The formation of the bands may be explained as follows by application of well-known optical principles. We consider first the diffraction effects for a single straight fiber of uniform diameter, or for any small element of fiber length in a large group of fibers.

In Figure 2 let *Sl* represent a cross section of the slit-source and *d* the diameter of a fiber element. The length axes of the slit and fiber are parallel and the perpendicular distance between them is *D*. For the purpose of this exposition we need consider only the dif-

fraction effects in a plane which is perpendicular to the fiber element and intersects both this element and the slit. Let this plane be the plane of the paper.

Light from the slit is partially obstructed by the fiber giving rise to diffraction and interference phenomena. By Babinet's principle[11] the effects observed will be exactly the same if the arrangement is inverted by replacing the fiber with a slit in an opaque screen MN, the slit having exactly the same width as the fiber.[12] In certain directions θ_n from the equivalent slit there will be destructive interference of all secondary wave trains originating at different points across the slit.[13] These directions are given (fig. 2) by $\sin \theta_n = n\lambda/d$, where $n = 1, 2, 3$, etc., is the order of the diffraction band and λ is the wave length of light. In directions with intermediate values of θ reinforcement of secondary wave trains will occur. We may assume for the moment that the source of light is strictly homogeneous with respect to wave length.

The undeviated light passing the equivalent slit, or fiber, is received by the lens of the eye and brought to a focus on the retina, forming a real image of the source—the illuminated slit, Sl. The diffracted light is brought to a focus in like manner as a series of maxima and minima of illumination. This retinal pattern is projected outward, or seen, in the plane of Sl. The center of the first dark band, for $n = 1$, will appear at a distance s_1 from the center of the slit. The angle θ_1 is always so small that the sine may be replaced by the tangent, giving

$$d = \frac{\lambda D}{s_1} = \frac{C}{s_1} \tag{1}$$

where $C = \lambda D$ is the constant of the instrument.

In a group of fibers, all members approximately parallel to the slit, different fiber elements will generally vary in diameter and will simultaneously intercept different portions of the light beam entering the eye. Applying Babinet's principle again, we invert this arrangement, replacing the fibers by a group of equivalent slits in the opaque screen MN (fig. 2). The length axes of these slits are only approximately parallel to one another and are not uniformly spaced in the plane MN, so that there is no precise geometrical relationship between all elements of slit length in the group; consequently, there can be no definite phase relations between secondary wave trains originating at different slit elements and propagated in any given direction; no optical effects are observed, therefore, which may be ascribed to the mutual interference of wave trains from different slit elements. We may regard each slit element, or fiber element, as acting independently of all other elements to form its own diffraction pattern of the source, and equation (1) may be applied separately for each element.

---

[11] Wood, Phys. Optics, 2d ed., p. 238.

[12] This is analogous to the principle of the optical diffraction grating in which spectra of the same character and in the same position are observed no matter whether the grating consists of black lines on a white ground or white lines on a black ground.

[13] The initial phases of the light vibrations may be regarded as the same at all points in the plane of the equivalent slit. Let a direction of propagation θ_n (fig. 2) be chosen such that the phase difference between secondary wave trains originating, respectively, at the center and either edge of the slit is a whole number n of half-wave lengths. Then the slit width may be subdivided into $2n$ equal parts and pairs of wave trains from corresponding points in adjacent subdivisions, points always separated by the width of a subdivision, will differ in phase by one-half wave length and consequently will mutually destroy each other. Hence, the resultant intensity of propagation in the chosen direction is zero. There will always be a pair of directions, positive and negative, respectively, for which the condition is fulfilled for any given value of n.

We see that the diffraction pattern of each fiber element will be superposed on the patterns of all other elements, and the observed intensity distribution along the set of diffraction bands is the result of the simple addition of many separate effects arising from all fiber elements which partially intercept the beam of light in its passage from the source to the aperture of the eye. If the elements are very nearly uniform in diameter there will be a corresponding degree of coincidence of these patterns and, therefore, a maximum definition of the bands. Because of the variation in diameter, however, from fiber to fiber and along the length of each fiber, the elemental patterns are spread or contracted laterally in accordance with the variation in diameter. This effect tends to smooth out the distribution of light intensity and reduces the definition of the bands. The effect is particularly noticeable in the fusion of maxima and minima of higher orders (for $n=2, 3,$ etc.). The distribution of light in the band system, as observed for a bundle of fibers, thus bears a relation to the uniformity of the fibers as well as to their average diameter.

Corresponding to the case of a single fiber element, of a given diameter, we now take the position of the first minimum of intensity in the band system as a measure of the average diameter of the group of fibers. This presupposes, of course, by equation (1), that the observed position of the first minimum of intensity for the group of fibers is the harmonic mean of the positions for all elementary fiber lengths in the group. Denoting mean values by a bar over the corresponding letter, we have

$$\bar{d}=\frac{C}{\bar{s}_1}=\frac{C}{m}\sum_m \frac{1}{s_{1,m}} \tag{2}$$

In this equation m represents the number of a fiber element and the summation is taken over the total observed length of fiber in the sample. This is the averaging process automatically performed by the instrument. Later tests will show how well the instrument fulfills its intended purpose.

It is shown by the preceding equations that the constant of the eriometer depends on the wave length, or wave-length composition, of the source of light. When white light is used in the illumination of the slit, the diffraction bands are, therefore, colored at the edges because of the small dispersion in the angle of diffraction corresponding to the finite wave-length range of the source. This effect does not interfere greatly with the use of the instrument when settings are made only on the first dark band. It does contribute, however, to the general diffuseness of the light distribution and to the uncertainty in settings of the eriometer scale. A monochromatic source of known wave length, if of sufficient intensity, would be an advantage undoubtedly and would yield an absolute measure of average diameter, for then the value of C would be completely determined from the known construction of the instrument.

In the present initial study of the diffraction method unnecessary complications in the construction of the apparatus were avoided. Some experiments were made with a red light filter between the source and the slit of the instrument, but the resulting intensity of the diffraction bands was not sufficient for precise or comfortable readings. It is believed that a more intense source of white light combined with a suitable high-transmission red or green filter would be a distinct

improvement and would serve all purposes as well as a more strictly monochromatic but more expensive source, such as the green spectral line of the mercury-vapor arc. When unfiltered white light is used, as with the present instrument, the choice of an effective average wave length for the source is somewhat arbitrary and uncertain. Hence, the constant C is best determined for this instrument by measurements made on fine wires or fibers of uniform and known diameter.

The distance D from the slit to the fibers is normally 30 cm. For very fine fibers, however, the spread of the diffraction bands is so great that the first dark band may cover the greater part of the field of view; moreover, the intensity of the adjacent bright bands is much reduced under these circumstances so that it may prove very difficult to set precisely on the center of the first dark band. Hence, the observation tube is made in two parts (fig. 1), so that a length of 15 cm. is readily removable. Then D is reduced by one-half, giving $d = C/2s_1$.

III. CALIBRATION AND PERFORMANCE

1. CALIBRATION OF THE ERIOMETER SCALE

To determine the constant of the eriometer and to obtain pertinent data on the performance of the instrument, comparative measurements were made with the eriometer and with a microscope on fine wires and various textile fibers. For these measurements samples were prepared by mounting 5 to 10 fibers, or wires, parallel to one another and streched taut across an aperture in the center of a cardboard form. (Fig. 1.) The ends of the fibers were held by soft wax. This cardboard form was properly mounted on the sample holder of the eriometer and secured in place by a little soft wax. These samples could be used with either instrument, inserted or removed as desired, without disturbing the arrangement of the fibers.

The microscope used in this work gave a magnification of approximately 100 diameters, and was equipped with a micrometer eyepiece. It may be recalled that the result obtained with the eriometer is the average diameter of such fiber lengths only which extend across the aperture of the eye. Hence, to obtain comparable data with the microscope, individual diameter measurements were made at intervals of 0.5 mm along the length of each textile fiber and covering a total length of approximately 5 mm. The mean of the individual determinations for all the fibers was taken as the average diameter of the sample. Inasmuch as the wire samples are very uniform in diameter, the range of uncertainty in the average as determined with the microscope is estimated to be within a few tenths of a micron. These samples were also very carefully measured with the eriometer, several determinations of the mean displacement $\bar{s}_1$ being made at different times, each determination representing 10 settings of the eriometer scale. Two determinations (10 settings each) of each textile sample were made.

The mean of all determinations for each sample with the eriometer is represented by a single point in Figure 3 and there compared with the microscope average. The microscope averages, expressed in microns, are plotted against the reciprocal mean scale readings of the eriometer; that is, against the values of $1/\bar{s}_1$ in equation (2). The straight line passes through the origin of coordinates and its slope

gives the required constant of the eriometer. After the constant was thus determined the micron scale for the eriometer was added to the chart.

With d expressed in microns and s_1 in millimeters, the numerical value of C is 167. From the definition $C=\lambda D$, with $D=300$ mm, the effective wave length of the source is found to be 0.56μ. This wave length falls, as it should, well within the region of high spectral luminosity of the source, and thus serves as a rough check on the correctness of the calibration.

In determining the slope of the calibration line consideration was given only to the wire samples and to two of the textile samples

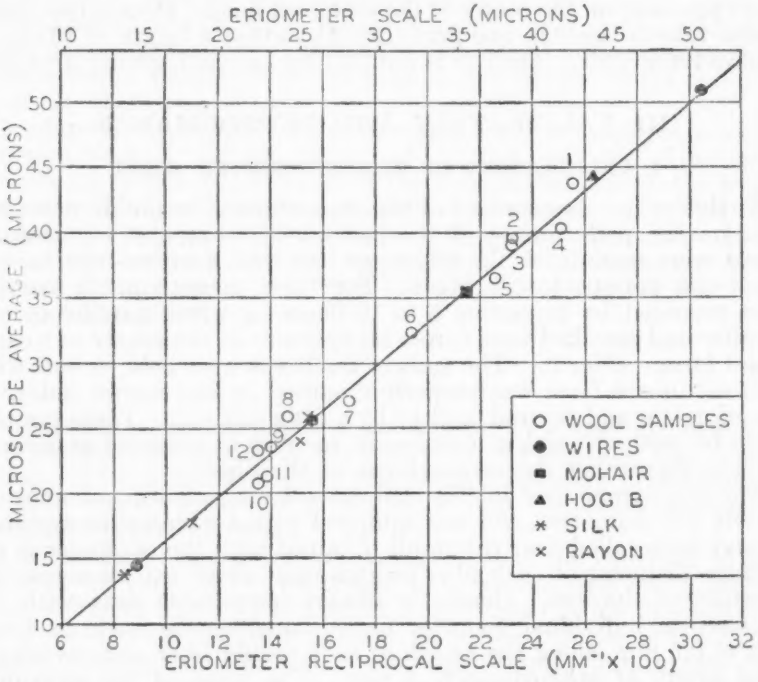

FIGURE 3.—*Comparison of eriometer readings with microscope averages*

(mohair and hog bristles) which were shown by the microscope to be very uniform in diameter and moreover filled in an open range of diameters between the wire samples. A wide range of diameter variation within a sample introduces uncertainties in the microscope average because of the limited number of individual diameter determinations made. Also the precision of the eriometer readings is slightly reduced under these conditions because of the poorer definition of the bands.

Each wool sample is composed of 10 fibers chosen at random from a single grade of the United States standards for wool top. One sample from each of the 12 grades was measured. These samples were chosen mainly for convenience because they provided wool-fiber groups of progressively varying average diameter. No attempt is made in this paper to study the standards as such. The data on the

wool samples were given no weight whatever in the determination of the constant of the eriometer. They will be used in later discussions of performance.

All measurements with both instruments on the textile fibers were made under constant atmospheric conditions of temperature and relative humidity in order to avoid any appreciable changes in diameter, particularly of wool, accompanying changes in moisture content of the material during the measurements. It is known that wool is extremely hygroscopic, and its diameter changes appreciably with moderate changes in moisture content.

2. EFFECT OF IRREGULARITIES IN FORM AND ARRANGEMENT OF THE FIBERS

In the development of the theory of the eriometer it was assumed that all fiber elements were parallel to the slit source of light. The diffraction phenomena were then discussed in their relation only to the diameter, or variation in diameter, of the fiber elements. The effect of the wave-length composition of the source, being constant, was of relatively small importance in the measurements, and only necessitated a calibration of the instrument by some independent method of observation. In the present section the theoretical discussion is extended to include the effect of varying orientation of the fiber elements from the previously assumed condition of parallelism.

In practical applications of the instrument it would be difficult and very inconvenient to fulfill closely this condition of parallelism within a large group of fibers. Some of the fibers may be in contact with adjacent fibers or crossing at one or more points; moreover, some of the finer grades of wool often exhibit a considerable degree of crimpiness in form so that the observed portion of the fiber length may be somewhat wave like in appearance unless particular care is taken to pull the fibers taut across the aperture in the sample holder; but if this operation is not performed with considerable care there is danger of stretching the fibers and thus appreciably reducing their normal cross section. It is therefore imperative to obtain some information on the effect of such irregularities in form and arrangement on the measurement of average diameter.

In the following theoretical discussion of the problem, the fiber elements of a group are assumed to be all the same in diameter, but may be oriented at varying angles with the slit source of light. In respect to the actual variation in diameter within a given group of fibers we may regard the uniform diameter assumed in the calculations as the average diameter of the group; then, providing there is no marked degree of correlation between the diameter of fiber elements and their orientation, the computations will give, at least approximately, the effect of orientation alone on the experimental determination of the average.

Let us consider first two perfectly straight fibers, or fiber elements, one of which is strictly parallel to the slit and the other inclined at an acute angle α. The diffraction bands are always arranged parallel to the slit, but exhibit their normal separation only along a line perpendicular to the axis of the fiber. Hence, as illustrated in Figure 4 (*A*), the two sets of diffraction bands can not be coincident. The set corresponding to the fiber making an angle α with the slit is displaced

laterally along the line OA by an amount Δs relative to the normal set, the displacement being always toward the slit (negative direction with respect to s). If the vertical lines in the figure represent the centers of the dark bands, then

$$-\Delta s_1 = s_1(1-\cos\ a) \tag{3}$$

The fractional error e in the measurement of the diameter of the inclined fiber is obtained from equations (1) and (3): Thus

$$e=\frac{\Delta d}{d}=-\frac{\Delta s_1}{s_1}=1-\cos\ a \tag{4}$$

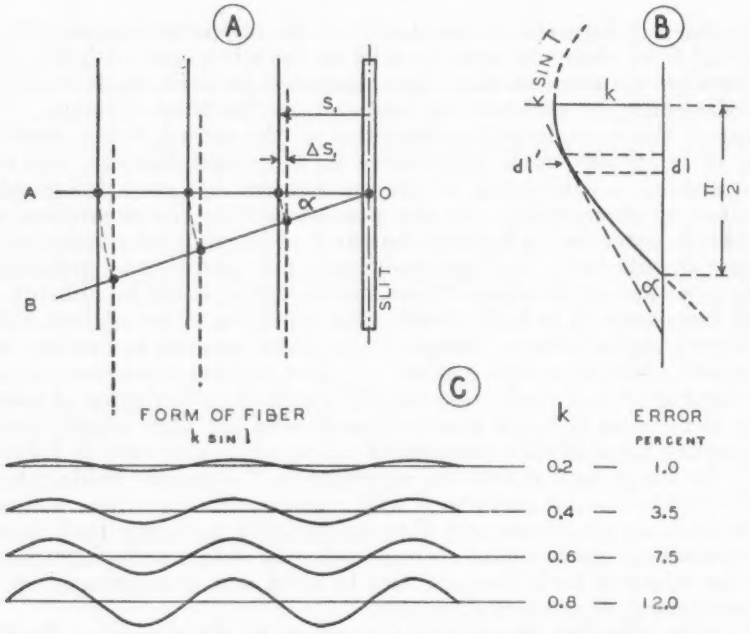

FIGURE 4.—*Effect of irregularities in form and arrangement of the fibers*

The error is an even function of a so that plus and minus values of a are equivalent. If the fiber makes an angle of either $\pm 12°$ with the slit then the error in its measurement is $+2$ per cent. For angles of $\pm 8°$ the corresponding error is about $+1$ per cent.

Equation (3) was verified experimentally for $a=12°$ by carefully mounting four straight mohair fibers parallel to one another on a cardboard form and providing an arrangement whereby the fibers could be set easily either parallel or at 12° to the slit. A series of 60 scale settings was made with the fibers alternately parallel and inclined to the slit. The average scale reading for the inclined fibers was found to be 2 per cent lower than that for the parallel condition. The precision of a single determination with the eriometer is such that a large number of successive scale settings are necessary to determine this difference.

It is not very difficult to mount a bundle of straight fibers so that the condition of parallelism is fulfilled to a sufficient approximation to make the residual error negligible.

Let us now calculate the error in the measurement of crimped fibers whose elements of length make continuously varying angles with the slit. For the purpose of calculation let the projection of each fiber be sinusoidal in form, as illustrated in Figure 4 (*C*). A suitable variation in form, to simulate varying degrees of crimpiness, is obtained by a factor k. The form of the fiber is thus expressed by the function $k \sin l$.

The error in the separate measurement of any fiber element, if this measurement were possible, would be given by equation (4). We now require the average value $\bar{e}$ of this error function taken over a quarter period of the sinusoidal variation in form of the fiber. Referring again to Figure 4 (*A*) we recall that s_1 is the position of the first minimum of intensity for a fiber element which is strictly parallel to the slit, and Δs_1 is the linear displacement of this minimum resulting from a given angular displacement of this element. The calculation of the average error for the quarter period involves the same assumptions which were made previously in the derivation of equation (2); and the total effect, for a group of fibers, is the result of the superposition of many separate effects arising from a large number of quarter periods, each of which is assumed to be of exactly the same form and, hence, acts in exactly the same way. We may regard the total number of quarter periods as so large that the effect of a fractional remnant may be disregarded. The error for the group of fibers is thus given by the error for a single quarter period.

A quarter period of variation in the form of the fiber is shown in Figure 4 (*B*). The error e due to any fiber element is properly weighted when multiplied by the element length dl'. Let $dl = dl' \cos \alpha$ be the projection of dl' on a line parallel to the slit (axis for description of form of fiber). Then the resultant error $\bar{e}$, representing the joint effect of all fiber elements in the quarter period, is given [14] by the equation

$$\bar{e} = \frac{\int_0^{\pi/2} (1 - \cos \alpha) \sec \alpha \, dl}{\int_0^{\pi/2} \sec \alpha \, dl} = 1 - \frac{\pi}{2 \int_0^{\pi/2} \sec \alpha \, dl} \tag{5}$$

From the relation $\tan \alpha = d\,(k \sin l)/dl = k \cos l$ we may express $\sec \alpha$ in terms of l, after which the equation readily reduces to the form

$$\bar{e} = 1 - \frac{\pi}{2\sqrt{1+k^2}} \cdot \frac{1}{E\left(\frac{\pi}{2}, K\right)} \tag{6}$$

where $K = k/\sqrt{1+k^2}$, and $E\left(\frac{\pi}{2}, K\right)$ is the complete elliptic integral of

[14] The average value of a function $f(x)$ with a set of weights $g(x)$ is the ratio of the integral of $f(x)\,g(x)$ to the integral of $g(x)$, the integrations being taken over the range of x for which the average of $f(x)$ is required.

the second kind. The value of this integral, for various values of K, may be read directly from tables [15] of the elliptic functions.

In this manner the numerical data in Figure 4 (C) were obtained. Each datum is the theoretical percentage error in a diameter measurement with the eriometer for a single fiber, or for a group of fibers, when each fiber of the group has the corresponding form ($k \sin l$, with k constant) depicted in the figure. It may be noted that no particular length unit is involved in the mathematical description of these forms; hence, any form may be uniformly contracted or expanded at will so that any desired number of quarter periods may be included within the fixed aperture area of the eriometer. In this way a given form may be made to match as closely as possible the actual projected configuration of a given fiber. Furthermore, the degree of contraction or expansion may be varied at will to match different fibers in a given sample or different portions of the same fiber. The only requirement in this respect which has been imposed on the above calculations is that the contraction or expansion shall be uniform in all directions in the plane of the aperture so that the geometrical form of the theoretical fiber is not changed. If different forms (different values of k, or different functional forms) are used to represent different members of a given group of fibers, then the resultant error would be found as a mean value of the properly weighted theoretical errors applying to the different forms used.

The preceding computations show that the resultant effect of all irregularities in the orientation of the fibers is a contraction of the band system toward the central bright slit; so that the error is always in the same sense, giving values which are always too large.

Several experiments were performed in an attempt to obtain a partial check on the magnitude of these theoretical errors. In each of these experiments four characteristically crimped fibers were selected from one of the finer grades of wool top and mounted with wax on a cardboard form. The average diameter was determined with high precision by making a large number of settings of the eriometer scale. The sample holder was then removed from the instrument and the fibers straightened approximately, taking care not to stretch the fibers appreciably during this operation. The measurement of average diameter was then repeated and the percentage difference computed. The results all showed a definite decrease in the value of the average diameter measured after the fibers had been straightened. This decrease varied from 5 per cent to nearly zero, however, even though the irregularities in the fibers, as originally mounted, appeared very much the same in each experiment.

In consideration of these results it should be borne in mind that the straightening operation may involve some rotation and untwisting of fibers with noncircular cross section so that the average projected diameter might be altered in this process. Furthermore, it is probable that the tendency toward crimpiness is greatest for fiber lengths of smallest diameter; this tendency would off-set the orientation error, so that the measured effect would be less than that calculated on the assumption that there was no correlation between diameter and orientation of fiber elements. Again, it is evident that no set of crimped fibers will actually assume such a regular sinusoidal varia-

[15] Peirce, "A Short Table of Integrals," 2d ed., p. 121.

tion in form as depicted in Figure 4 (*C*). Some of the mounted fibers may be quite wave like in appearance over a small portion of their total length, but twisted in an adjacent portion so that their projection in the line of sight is straight. This latter portion of the total fiber length would contribute no appreciable error due to its form. On the whole, judging from a visual comparison of irregularities in the mounted fibers with the theoretical forms shown in Figure 4 (*C*), it appears that the theoretical errors are somewhat too large so that the effect may be exaggerated in the theoretical discussion. It is difficult to obtain an adequate experimental confirmation of the theory. In 6 successive mountings of badly crimped fibers the average experimental error was only 3 per cent. It would not be difficult to straighten such fibers approximately so that the residual experimental error in their measurement would be insignificant.

In regard to overlapping and crossing of the fibers it is evident that these irregularities should be avoided as much as possible. Although the effect at the intersection of two crossed fibers is negligible, the crossing in itself implies a varying orientation. Overlapping of two approximately parallel fibers is equivalent to one very much wider fiber and, hence, must increase the observed average. Some experiments were performed in which it was attempted to mount two uniform mohair fibers side by side in close contact but not overlapping, so that the instrument would indicate the combined thickness of the two fibers. It was found, however, that the contact was never close enough to effect the looked-for change in the separation of the bands. Apparently there is no danger of any appreciable error from this cause in the measurement of wool or other textile fibers.

From the results of these studies of irregularities in orientation it is advisable to use reasonable care in the arrangement of the fibers so that they lie approximately parallel to one another with a minimum of crossing and overlapping. If the fibers show a high degree of crimpiness in form, some error in the measurement may be expected, although experiment has shown that the effect is not serious. It is doubtful, in view of later considerations of diameter distribution and accuracy requirements, if errors arising from casual irregularities in mounting can be regarded as a serious disadvantage of the method.

3. DISPERSION OF DIAMETERS IN WOOL SAMPLES

An analysis of data obtained on the wool samples will illustrate the wide range and varied distribution of diameters, which are averaged in a single determination with the eriometer.

Each wool sample consisted of 10 fibers carefully mounted parallel to one another. The width of each bundle was from 4 to 5 mm, and 10 individual diameter measurements with the microscope were made on each fiber at intervals of 0.5 mm along its length. Thus 100 individual diameter measurements were made on each sample, covering an area approximately 5 mm square. This area fully covered the aperture of the eye when the bundle was measured with the eriometer.

The diameter-frequency distribution in each wool sample is represented by one of the curves in Figure 5. In this figure the abscissae represent percentage deviations from the mean of 100 diameters. The computed deviations have been grouped into classes, each class

covering a range of 6 per cent. The number of cases falling within a given class is represented by an ordinate erected on the mid-class value. The points thus determined are connected by straight lines forming a frequency polygon, or roughly, a frequency curve.

It may be emphasized that these frequency curves do not represent directly the variation in diameter between different fibers of a group; they are intended to illustrate only the range and distribution of diameters among fiber elements as actually presented to the instrument for averaging. The diameter variation along the length of the fibers is often less than the variation between fibers, so that a sample containing a few fibers of approximately the same diameter, but quite

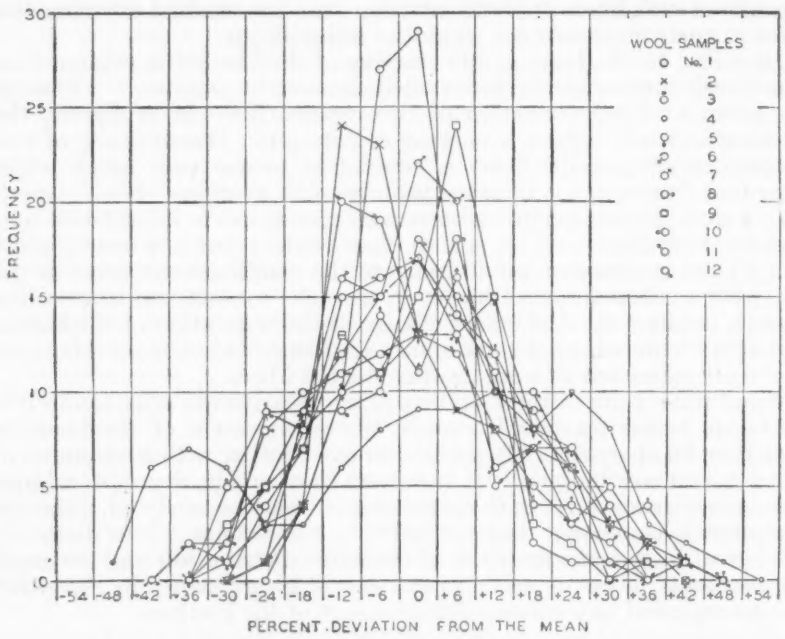

FIGURE 5.—*Diameter-frequency distribution in wool samples (100 observations on each sample; class interval 6 per cent)*

different from the average diameter of the group, would show a definite maximum at a corresponding distance from the center of the diagram. The number of fibers in the sample measured is too small to be fully representative of the total population of fibers in the larger sample from which the fibers were taken. These considerations explain some of the observed irregularities in diameter distribution as exemplified, for instance, by sample No. 4; but it is undoubtedly quite possible to have irregular curves as shown representing true diameter distributions in large commercial samples.

A small degree of skewness may be noted in the general trend of these diameter distributions, showing a tendency in these samples for exceptionally large diameters to occur more frequently than the opposite extreme. The diameter composition is nearly the same for the majority of these samples, regardless of the progressive variation in average diameter.

If the diameters of the fiber elements are grouped very closely about their average value then the sets of diffraction bands corresponding, respectively, to individual elements are also all nearly coincident and a maximum definition of the observed bands is attained. With textile fibers, however, there is always a considerable dispersion of diameters which tends to smooth out the maxima and minima of light distribution and thereby decrease the definition of the bands. This effect is therefore a definite indication of the dispersion of diameters in the sample. In Section IV it will be indicated how a quantitative measure of the dispersion might be obtained. As the range of diameters increases, and particularly, if the distribution curve is broad and flat, settings of the eriometer scale become increasingly difficult and uncertain. The instrument is thus limited in its range of application. Not every possible diameter distribution may be averaged with the instrument. Definite reliable settings were readily obtained, however, with all the wool samples whose diameter distribution curves are given in Figure 5.

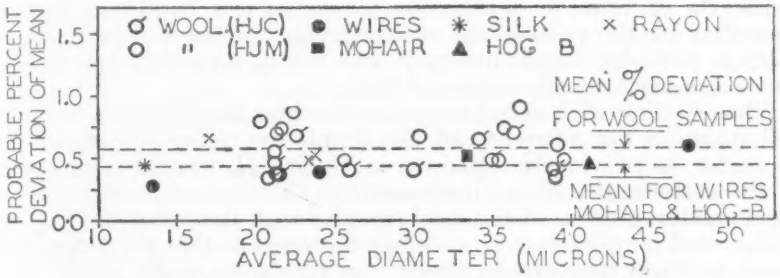

FIGURE 6.—*Precision of measurements with the eriometer*

4. PRECISION AND ACCURACY OF MEASUREMENTS

In the following discussion of the precision of measurements a single standard determination of average diameter with the eriometer is defined as the result derived by equation (2) when $\bar{s}_1$ is the mean of 10 consecutive settings of the eriometer scale. For the purpose of expressing the precision, the probable percentage deviation[16] of this mean scale setting was computed for each determination of average diameter. By the relation $\Delta s/s = -\Delta d/d$ (equation (4)), these deviations are also the probable percentage deviations of single standard determinations of average diameter.

The data are given in Figure 6. It is shown that there is no consistent change in the precision of measurements over the entire range of average diameters covered by these observations; furthermore, there is only a small decrease in precision, as the dispersion of diameters in the sample increases markedly in passing from the very uniform wire and textile samples to the most nonuniform samples of wool. The probable percentage deviation of a single standard determination is, roughly, 0.5 per cent for the wool samples and decreases only slightly for the wires and other textile samples of nearly uniform diameter. Assuming no constant sources of error in the method or

[16] Probable percentage deviation of the mean of 10 observations is given by the product 0.0282 Σ (residuals). Merriman "Method of Least Squares" 8th ed., p. 93 and Table 4. (Short formula.)

instrument, and the normal law for symmetrical distribution of successive scale settings about the mean, these data on precision may be interpreted as follows: In a single standard determination of the average diameter of a wool sample the chances are even that the observed value will be within ± 0.5 per cent of the true value, and it is almost certain that the observed value will not differ from the true value by more than ± 2 per cent.

We may recall at this point that each value given (fig. 3) for the average diameter of a wool sample, as measured with the eriometer, is the mean of two determinations, each by a different observer. It is of interest to note that no consistent difference was found between the two sets of data, corresponding, respectively, to the two different observers. The average difference, taken without regard to sign, between corresponding values for the two observers was 1.2 per cent. It appears, therefore, that there is no considerable personal factor in these measurements. One may expect some consistent variation between the average scale settings of individual members of a group of observers, because of the colored edges of the diffraction bands; the criterion for settings on the center of a band may depend somewhat on the color-vision characteristics of the observer. This effect is probably small, however, and would be eliminated by the use of a monochromatic source of light.

When dealing with broad irregular diameter distributions one may well question the adequacy of the simple averaging process of the eriometer, as previously explained in Section II. Some information on the performance of the instrument in this respect is gained from the diameter analysis of the wool samples with the microscope.

The wool samples were all carefully mounted so that no appreciable errors in their measurement with the eriometer could result from residual irregularities in orientation. Assuming no significant errors in the individual diameter determinations with the microscope, and that a truly representative average is obtained from the 100 individual determinations on each sample, then the accuracy of the averaging process of the eriometer may be adjudged by the grouping of points for the wool samples about the calibration line in Figure 3.

We find here no consistent differences between the averages obtained with the eriometer and the microscope. Sample numbers are attached to the points in Figure 3 and to corresponding distribution curves in Figure 5. By comparison, for a given sample, of the departure from the calibration line with the spread or flatness of the corresponding distribution curve, we see that these departures are not definitely correlated with the character of the diameter distribution. Thus, the average diameter of samples 4, 3, and 12, which show the broadest and flattest distribution curves, do not depart farther or consistently in direction from the calibration line than samples 1, 7, or 2, which show the greatest concentration of diameters about the mean. Samples 11 and 2, with the same type of distribution curve, fall on opposite sides of the calibration line. Such variations as found between results with the two instruments are not inconsistent with the precision of the eriometer (fig. 6) and with the dispersion of diameters in the samples.

The average diameter measured with the eriometer compares very favorably with the microscope average. The differences observed are not greater than 2μ. Although the microscope is undoubtedly

the more accurate for nearly uniform samples, such as the wires, it is probable that in the case of the nonuniform textile fibers the eriometer yields an average value which is more accurate than the microscope average, for 10 individual determinations over a 5 mm length of a nonuniform fiber may not adequately gage the fiber.

IV. DISCUSSION AND CONCLUSIONS

The most commendable feature of the diffraction method is its ability to combine into a single averaged result the effect of a wide range of projected diameters as distributed in a group of fibers (or particles). For many purposes this gives the instrument unquestionable advantage over every form of micrometer which measures only a single interval at once. An average obtained in a few minutes with the eriometer may require an hour or more to duplicate with a microscope; moreover, the method averages the continuous diameter variation along the entire length of fiber under observation, and not, as in any microscopic method, the diameters at a limited number of points.

It should be emphasized, however, as previously noted, that the method is not suitable for averaging all possible diameter distributions. It is inherent in the method that the range of diameters must not be too large combined with a frequency distribution curve which is flat or very irregular. For best results there should be a pronounced concentration of diameters about a single class.

Off-setting this limitation it may be remarked that whenever the method does fail to function, any practical significance which may be attached to the average diameter must be small. In an application of the eriometer to the grading of wools a sample which is not sufficiently uniform in diameter to permit a reading to be obtained with the instrument is also, by the same token, not representative of any one class of wools or even a narrow range of classes.

Aside from the somewhat uncertain effect of gross irregularities in the mounting of the fibers, it is believed that the precision and accuracy attained in the measurements are sufficient for practical applications of the method. When one considers that the diameters in a sample of wool may vary over a range of 100 per cent, and may be distributed within this range in a variety of different ways, it would seem that higher degrees of precision and accuracy in the measurement of the average could have no particular significance from the point of view of the utility of the material for any manufacturing purpose. It is, perhaps, only in a desire to distinguish sharply between limits arbitrarily set for different grades that greater refinement in the measurements may be considered desirable.

By the use of a monochromatic source of light, or a narrow spectral range in filtered white light, a definite characteristic wave length may be assigned to the source and an absolute measurement thereby obtained. Thus the eriometer is readily made independent of calibration in terms of another instrument.

The most serious disadvantage of the present instrument is its inability to cover a larger area of the sample, or greater total length and number of fibers, in a single determination. A few fibers chosen at random from a large sample may exhibit a very erratic diameter distribution which is not truly characteristic of the material; and if the

fibers are not straight and approximately circular in cross section it is conceivable that the distribution or average of projected diameters may depend in this case to a small degree on the mounting of the fibers. It would obviously be desirable if measurements could be made directly on a more fully representative sample of the material.

As stated in the introduction, it is also desirable that the determination of the average be supplemented by a suitable measure of variation. It has been shown how a qualitative indication of variation is provided in the present instrument by the appearance of the diffraction bands. We recall that the contrast between the maxima and minima of intensity distribution decreases with increased dispersion of diameters in the sample. It is possible that a measurement of the intensity distribution along the system of diffraction bands would yield pertinent information and quantitative expression of the essential features of the actual frequency distribution of diameters in the sample. The sample could be arranged so that equal lengths of individual fibers are always included in the measurements, and the results could then be interpreted as a measure of the variation between fibers rather than between fiber elements as depicted in Figure 5. The intensity distribution curve would also provide for greater precision in the determination of the position of minimum or maximum intensity and the average diameter derived therefrom.

These desirable features of the diffraction method could readily be incorporated in a more complex and costly construction of the instrument. To cover a larger area of the sample we may replace the lens of the eye, with its small aperture, by a lens of any desired aperture over which the parallel bundle of fibers could be spread and mounted, as before. The diffracted light may then be brought to a focus on a screen and the diffraction pattern viewed directly; or better, the pattern may be formed in the focal plane of a suitable eyepiece. Various devices may then be employed to obtain a measure of the angular separation of the bands. Some micrometer arrangement is necessary either to shift the bands across a fixed mark in the field of view, or to move a pointer across the stationary system of bands. If the intensity distribution is to be obtained, the eyepiece may be replaced by a suitable form of radiometer, employing either visual, photo-electric, or thermoelectric methods for measuring and recording relative variations in intensity.

From the results of the present investigation it is believed that the diffraction method offers considerable opportunity for the further development of instruments which would prove very useful in the textile field. Such instruments, however, would require a more bulky, delicate, and costly construction than the present instrument, and may require more care and skill in their operation. The instrument herein described will serve many purposes for which only a direct average diameter is required for a small group of fibers. Extensions to larger samples may be made if desired by averaging many small specimens properly selected from the larger sample. The simplicity of construction and operation and its portability commend this instrument not only for use in the laboratory, but also for extended application in the field.

WASHINGTON, January 26, 1931.

WIND PRESSURE ON A MODEL OF A MILL BUILDING

By Hugh L. Dryden and George C. Hill

ABSTRACT

This paper describes some measurements of the distribution of wind pressure over a model of a mill building, carried out in the 10-foot wind tunnel of the National Bureau of Standards. The results for three wind speeds show little scale effect, and it is believed that the results are directly applicable to a full-scale building of the same shape. Tests were made with a plain roof of 20° pitch, and also with a monitor ventilator on the ridge of the roof. Three wind directions were used, one normal to a side wall, one normal to an end wall, and one at 45°. The effect of the ground was simulated by the use of a long platform on which the model was mounted.

The detailed results can not well be abstracted. The maximum average loads were obtained with the wind at 45°, and in many cases fairly large areas were subjected to loads as great as twice the average load on the whole face. The loads on the roof of the monitor were greater than those on the roof of the main building. The greater part of the model was subject to pressures lower than the static pressure, and for most circumstances all faces except the windward one would be subject to outward forces.

CONTENTS

		Page
I.	Introduction	735
II.	Apparatus	738
III.	General procedure	741
IV.	Reduction of observations	741
V.	Results	742
VI.	Discussion	753
VII.	Numerical examples	754
VIII.	Scale effect	755
IX.	Conclusion	755

I. INTRODUCTION

In Scientific Paper No. 523 and Research Paper No. 221 of the National Bureau of Standards, a general discussion has been given of the wind-pressure problem and of the results of some model experiments on the distribution of pressure over a tall building and over two circular cylinders in a uniform and steady wind. The second paper also gives some pressure measurements on a full-size chimney in natural winds. The present paper represents an extension of this work to a model of a mill or factory type of building.

The reader is referred to the earlier papers for the background necessary to understand the application of the results of model experiments to estimates of wind pressure on the full-scale structure in the natural wind. Some of the explanatory material found in those papers is here repeated so that the method of expressing the results of the measurements may be clear. It will, perhaps, be best at this point to again review briefly the conventional method of presenting aerodynamic data.

When an air stream blows against an object, the pressure, p, at any point on its surface may be regarded as consisting of two parts—the static pressure,[1] p_s, which in a natural wind is the barometric pressure; and the excess, $p-p_s$, caused by the presence of the object. This excess, $p-p_s$, arises solely from the motion of the air with reference to the model. It will be called simply the wind pressure, and will be denoted by p_w. If there is no wind or no object present, then $p=p_s$ everywhere, and the wind pressure is everywhere zero. The wind pressure may be either positive or negative or zero; that is, p, which by definition of p_w is equal to p_s+p_w, may be either greater or less than p_s or equal to it.

In the comparison of wind pressures carrying the negative sign, the lower numerical value corresponds to the higher absolute pressure. Thus -0.2 is a higher pressure than -0.4 (just as 10° below zero is a higher temperature than 20° below zero). p_w is the quantity usually measured, corresponding to the common practice of using "gauge" pressure in dealing with pressures in steam boilers, compressed air tanks, etc., rather than absolute pressure. Dimensional reasoning teaches that p_w will be given by an expression of the form

$$p_w/q=f\left(\frac{VL\rho}{\mu}\right)$$

where q is the velocity pressure ($\frac{1}{2}\rho V^2$), ρ the air density, V the wind speed, μ the viscosity of the air, and L a linear dimension fixing the scale. The expression applies only to geometrically similar bodies. The wind pressure, p_w, could be measured in any convenient units, but there are advantages in using the velocity pressure, $q=\frac{1}{2}\rho V^2$, as the unit. In the first place p_w/q is in many cases[2] independent of the wind speed and the size of model, so that from a single value of it for any given shape of body the pressure at the corresponding point on a similar body of any size at any wind speed can be readily computed with the aid of a table of velocity pressures. In many other cases the variation of p_w/q with the Reynolds number $\frac{VL\rho}{\mu}$ is small. The ratio is a pure number independent of the units used so long as the pressures are all measured in the same units.

The engineer is in most cases more directly concerned with the resulting forces than with the pressures themselves and their distribution. These resulting forces always involve the pressure acting on the opposite sides of the surface or object. In the case of a hollow object, such as a building, which is open to the outside at various places, air currents are set up within the building, and there is a distribution of wind pressure over the interior as well as the exterior surfaces of the walls. At any point of the wall the force per unit area tending to move the wall normal to itself equals the difference between the wind pressure on the two sides and is in the direction from the higher toward the lower pressure. Little is known at the present time as to the distribution of wind pressure over the interior

[1] The term static pressure is used to indicate the pressure which would be measured by a pressure gauge moving with the air and, therefore, "static" with respect to the air. In actual practice the measurement is made by means of holes in the side of a closed tube, the axis of which is parallel to the wind direction. The form of the tube is such that the air flows smoothly past the holes.

[2] B. S. Sci. Paper No. 523, Bull., **20**, p. 697.

walls of actual buildings in high winds and in the presentation of data for the distribution over the exterior it is commonly assumed that the interior is at a constant pressure equal to the static pressure, p_s; that is, p_w is zero for the interior. If the pressure on the interior is constant, it has no effect on the resultant force tending to overturn the building, no matter what its value.

By definition, p_s is the same at every point of the surface and, hence, it contributes nothing to the resulting forces and may be ignored in the computations. The force on any element, dA, is equal to pdA and acts in the direction of the normal to the surface.[3] If θ is the angle made by the surface element dA, with the wind direction, s, then the component of force in that direction, F_s is given by $\int\int p\,dA \sin\theta$. Since p_s is constant and for closed surfaces $\int\int dA \sin\theta = 0$, the force coefficient for closed surfaces is also given by $\int\int p_w dA \sin\theta$. Dividing by q, we have $\frac{F_s}{q} = \int\int \frac{p_w}{q}\, dA \sin\theta$. It is found convenient to divide this expression by the area of projection, A_p, of the body on a plane normal to the direction, s. The quotient $F_s/A_p q$ is called the force coefficient.[4] It is the average force per unit projected area divided by the velocity pressure; that is, the ratio of the effective resultant pressure on the total projected area to the velocity pressure. The force in any particular case is obtained by multiplying the force coefficient by the projected area and by the velocity pressure.

For the convenience of the reader, the relation between the indicated speeds, as measured by 3-cup and 4-cup United States Weather Bureau anemometers, and the true speed is given in Table 1, and the velocity pressures at various true speeds for air of standard density are given in Table 2.

TABLE 1.—*Indicated wind speeds by Robinson cup anemometers* [a]

True speed (miles per hour)	Indicated speed, old 4-cup standard	Indicated speed, new 3-cup standard	True speed (miles per hour)	Indicated speed, old 4-cup standard	Indicated speed, new 3-cup standard
5	5	5	60	78	63
10	11	10	65	85	68
15	17	15	70	91	73
20	23	20	75	98	79
25	30	25	80	105	84
30	37	31	85	112	89
35	44	36	90	118	95
40	50	41	95	125	100
45	57	47	100	132	105
50	64	52	105	138	111
55	71	57	110	145	116

[a] Before Jan. 1, 1928, the U. S. Weather Bureau used the 4-cup instrument; after that date, the 3-cup.

[3] Excluding frictional effects, which are of importance only in special cases.
[4] The terms, resistance coefficient, drag coefficient, shape coefficient, are also used.

TABLE 2.—*Velocity pressures at several wind speeds*

True wind speed (miles per hour)	Velocity pressure	True wind speed (miles per hour)	Velocity pressure
	Lbs./ft.²		*Lbs./ft.²*
5	0.064	65	10.81
10	.256	70	12.53
15	.575	75	14.39
20	1.023	80	16.37
25	1.600	85	18.48
30	2.302	90	20.72
35	3.133	95	23.08
40	4.092	100	25.58
45	5.179	105	28.20
50	6.394	110	30.95
55	7.737	115	33.83
60	9.208	120	36.83

NOTE.—Velocity pressure in lbs./ft.^{2}=0.001189 $(V\times\frac{22}{15})^2$ where V is the true speed in miles per hour, and the density is that at 15° C., 760 mm. Hg.

II. APPARATUS

Figure 1 is a photograph of the model, which is 48 inches long, 24 inches wide, and 6 inches high to the lower edge of the roof. The roof, having a 20° pitch, measures 12.76 inches from the lower edge to the peak. There is no overhang of the roof. The monitor ventilator is 29 inches long, 1.6 inches high, 6 inches wide, and its roof has a pitch of 20° and an overhang of 0.1 inch. The model is made of aluminum plates one-quarter inch thick. For purpose of reference the faces are designated as shown in Figures 2 and 3. Face *A* of the model has 44 holes drilled in it, face *B* 177 holes, face *F* 72 holes, face *AA* 22 holes, face *BB* 55 holes and face *FF* 18 holes. The arrangement and location of the holes are shown in Figures 2 and 3.

The holes or pressure stations were prepared as follows: A hole approximately 0.25 inch in diameter was drilled and tapped at each station. A hollow cylindrical threaded plug about five-eighths inch long and closed at one end was screwed into the hole and the closed end carefully worked down so as to make it flush with the outer surface of the model. After polishing, a small hole approximately 0.040 inch in diameter was drilled along the axis of the plug from the outside face inward. By means of rubber tubing, connection through the interior of the model could then be made from each station to the pressure gauge.

The various plates of which the model is made are held together by screws. The bottom plate has a large circular hole through which the pressure tubes pass to the manometer. When testing the model with the monitor ventilator in place a rectangular piece was removed from the roof of the main model under the ventilator to accommodate the pressure tubes.

The wind stream was supplied by the 10-foot wind tunnel, which is described in Scientific Paper No. 523. The method of measuring wind speed, and the pressure gauge used for measuring pressures at the stations on the model were described in the same paper. In the present tests speeds up to about 55 miles per hour were used.

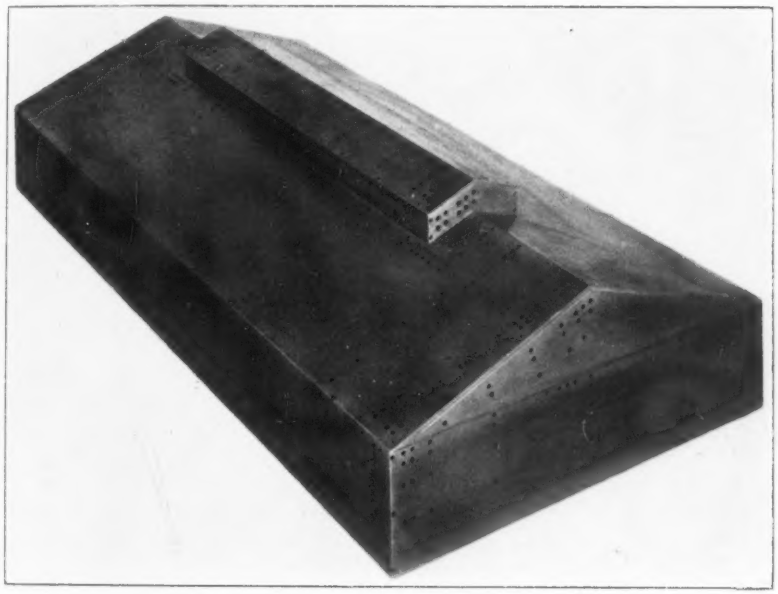

FIGURE 1.—*The model with monitor ventilator*

The dark circles are the ¼-inch plugs in which the 0.04-inch holes are drilled

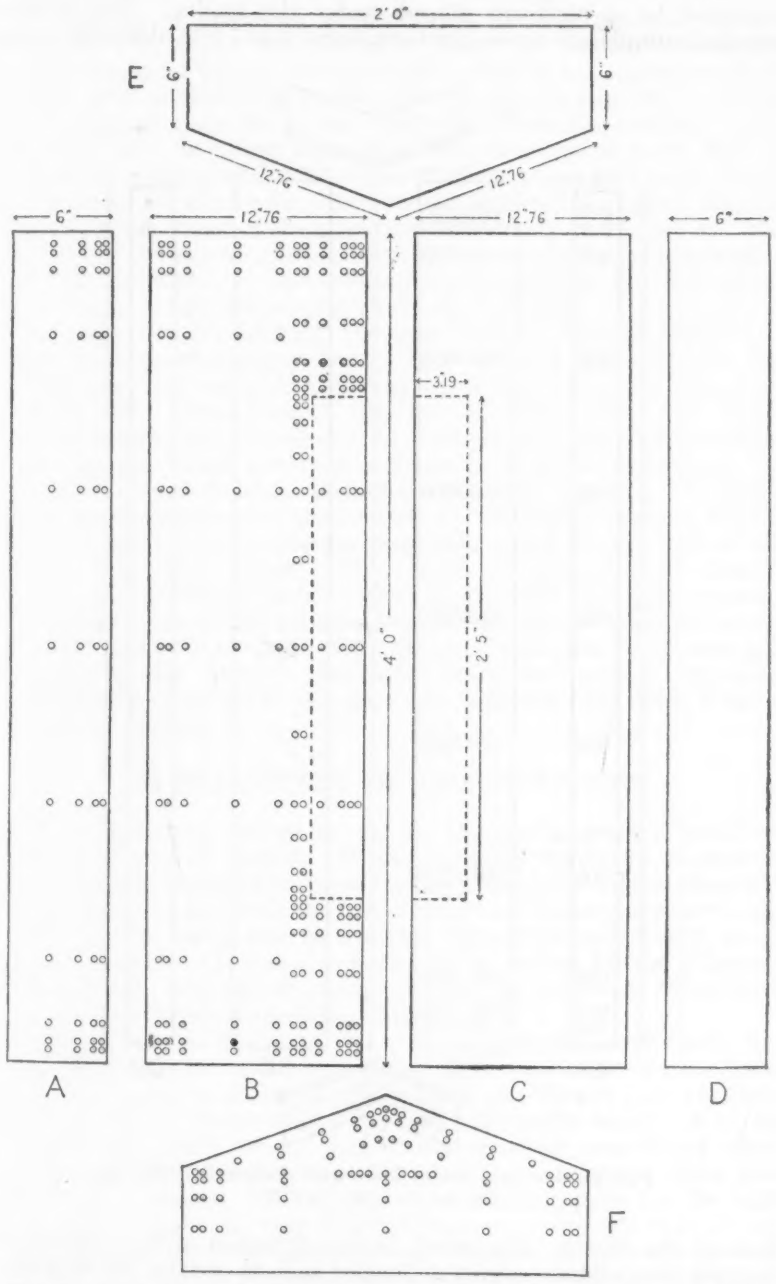

FIGURE 2.—*Location of holes and designation of faces for the model without the monitor ventilator*

The effect of the ground on which an actual building stands was simulated by a platform placed under the model. The platform extended completely across the tunnel and was 5 feet above the tunnel

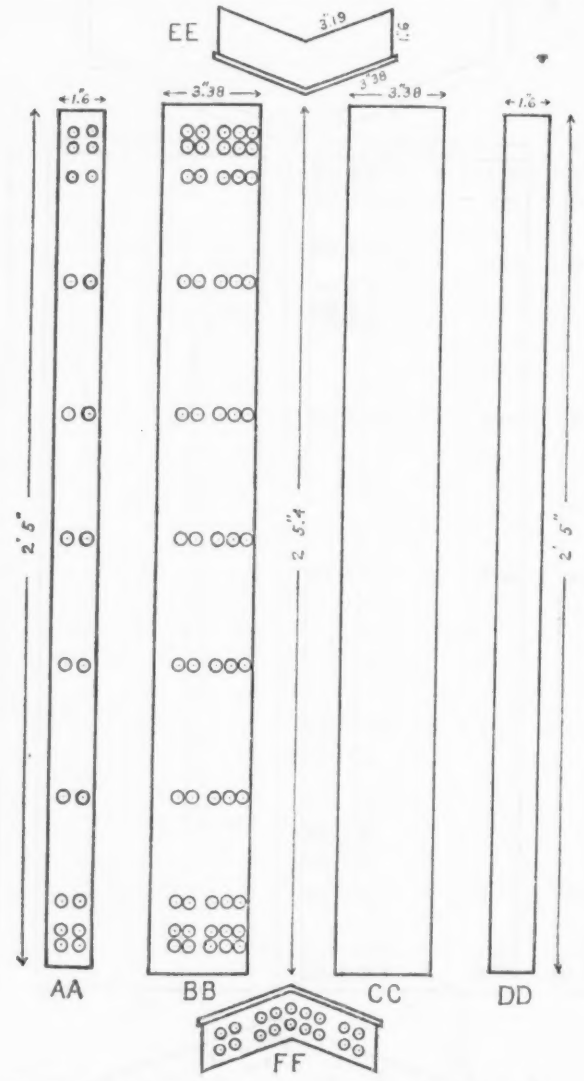

FIGURE 3.—*Location of holes and designation of faces for the monitor ventilator*

floor at the center. Its length in the direction of the wind was 15 feet and its upstream edge was beveled so as to reduce the disturbance produced by it. The wind speed was uniform to within less than 2 inches of the platform.

III. GENERAL PROCEDURE

The tests to be described were divided into two groups. In the first group the model was tested without the monitor ventilator. The data required for the complete distrubution at a given angle to the wind were obtained by turning the model through 180°. In the second group of tests the model was tested with the monitor ventilator attached. In these tests only the distribution over faces *B* and *C* and over the monitor ventilator was measured, as it was believed that the presence of the monitor ventilator would not affect the distribution or the value of the pressure on faces *A*, *D*, *E*, and *F*. The model rested directly on the platform and a scale of angles was marked off on this platform. A thin strip of wood nailed to the floor at the back of the model prevented the wind from sliding it.

The procedure for making the observations was as follows: 12 pressure stations were connected to 12 tubes of a multiple-tube manometer, the reservoir of the manometer being connected to a small hole in a static plate located 12½ feet upstream from the model. When the wind speed was steady, an observer read the 12 tubes of the multiple gauge, which gave the differences in pressure between the holes at the surface of the model and the reference pressure. Readings were taken for speeds of approximately 47, 60, and 80 feet per second. Then 12 more pressure stations were taken and so on until all the available holes were tested. The model was then turned through 180° and the necessary holes tested to give the complete pressure distribution. The entire process was carried out for wind directions of 0°, 45°, and 90°, an angle of 0° denoting that the wind was perpendicular to the ridge of the roof. Next the monitor ventilator was attached and tested in the same way together with faces *B* and *C* of the main building.

IV. REDUCTION OF OBSERVATIONS

The results finally desired are p_w, the changes in pressure produced by the presence of the model. It was necessary, therefore, to measure the difference in pressure between the reference pressure and the static pressure in the tunnel (with the model removed) at the place previously occupied by the model and to add this value with proper sign to the observed pressure. It was also necessary to correct for the difference in wind speed between the place where the reference Pitot-static tube was located and the position of the model.

The procedure in reducing the observations was as follows: The gauge readings observed on the multiple-tube manometer were reduced to absolute pressure differences in pounds per square foot and were then expressed as fractions of the velocity pressure indicated by the reference Pitot-static tube. The two corrections mentioned above were then applied and the values at each station for the three wind speeds were averaged. At any one station the values for the three speeds were, in general, very nearly the same; rarely did that for any one speed differ from the mean by more than 0.02. The designation of faces is indicated in Figures 2 and 3 which show the model with the four walls opened out at 90° and the roof pressed down on the same horizontal plane. When the wind blows normal to face *A* the model is said to be at 0° to the wind. Rotating the model clockwise, as

viewed from above, through 90° so that face F is normal to the wind gives the position designated as 90°. The angle 45° is, of course, midway between these two positions.

V. RESULTS

The results are represented in the form of contour maps (figs. 4 to 12), the contour interval being one-tenth of the velocity pressure. At all points of any one contour p_w has the same value. When p_w is positive (sign not printed) p exceeds p_s, when it is negative p is less than p_s.

The average value of p_w/q on each face was computed by a process of graphical integration, namely, by measuring the area between adjacent contour lines, multiplying the area by the arithmetic mean of the pressures for the two contours, summing for the entire face, and dividing by the area of the face. The results of this computation are shown in Table 3. The force on any face (assuming the pressure in the interior to be equal to the static pressure, p_s) may be obtained by multiplying the average value of p_w/q by the area of the face and by the velocity pressure q.

The direction of the force on any face is normal to that face. To obtain the resultant force on the building it is necessary to resolve the forces parallel to the directions of three axes of reference. The system shown in Figure 13, fixed with respect to the model and turning with it, has been adopted. Since the areas of the various faces of the model are not equal, the force components can not be obtained by adding values of the average pressures, but the pressures must be weighted in proportion to the areas of the faces. The computation is made in two steps. The values of p_w/q are first multiplied by the cosines of the angles between the normal to the face and the axes of references to give what may be called the X, Y, and Z components of p_w/q or F/qA. These values are shown in Tables 4 and 5, together with the areas of the faces relative to face A. The component of the force in the direction of the Y axis, for example, may be obtained by multiplying the values tabulated under Y by the area of the face, and by the velocity pressure.

TABLE 3.—*The average values of p_w/q on each face of model*

Face	Without monitor ventilator			With monitor ventilator		
	0°	45°	90°	0°	45°	90°
A	+0.498	+0.255	−0.354	+0.498	+0.255	−0.354
B	−.381	−.441	−.381	−.238	−.245	−.340
C	−.863	−.774	−.381	−.584	−.691	−.340
D	−.518	−.517	−.354	−.518	−.517	−.354
E	−.620	−.449	−.205	−.620	−.449	−.205
F	−.620	+.372	+.615	−.620	+.372	+.615
AA				+.441	+.180	−.197
BB				−1.026	−1.312	−.251
CC				−.560	−1.370	−.251
DD				−.488	−.938	−.197
EE				−.913	−.762	−.250
FF				−.913	−.160	−.850

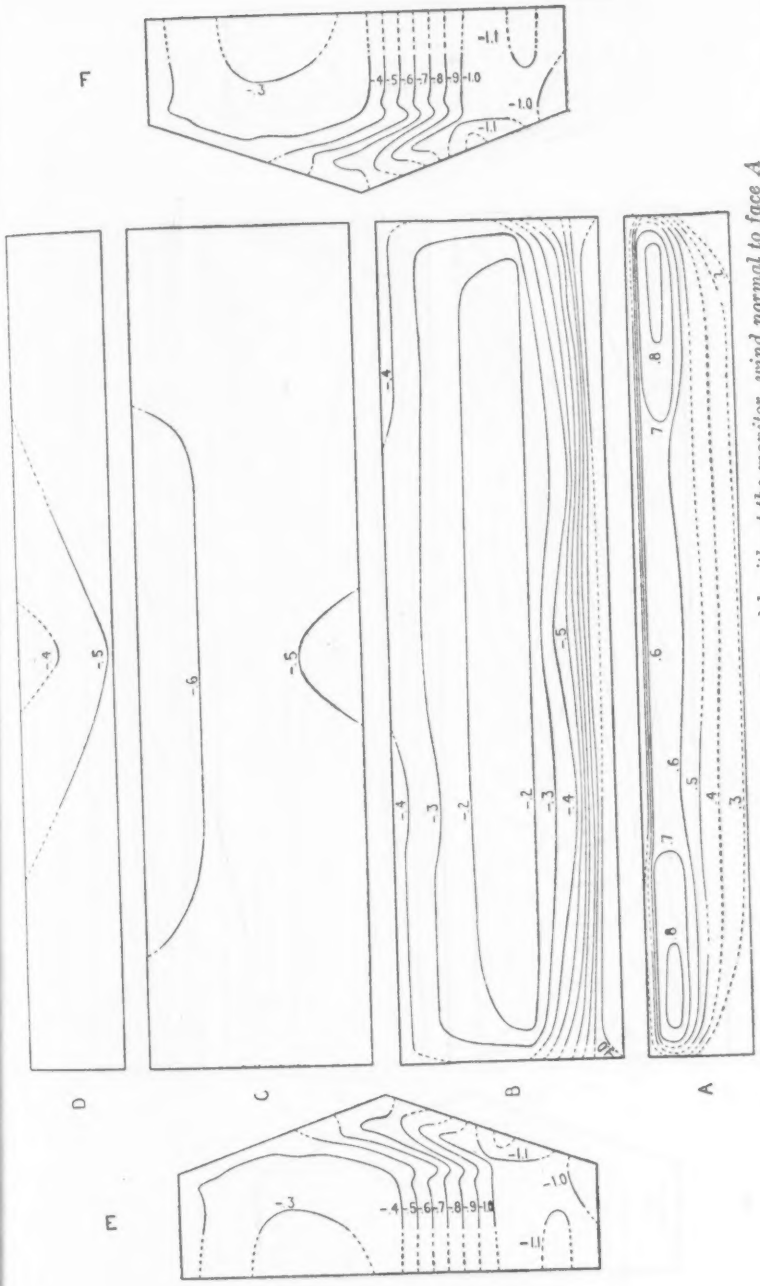

FIGURE 4.—*Distribution of pressure over the model without the monitor, wind normal to face A*

The pressures are measured from the static pressure as base, and expressed as ratios to the velocity pressure. Minus signs denote that the pressure is lower than the static pressure

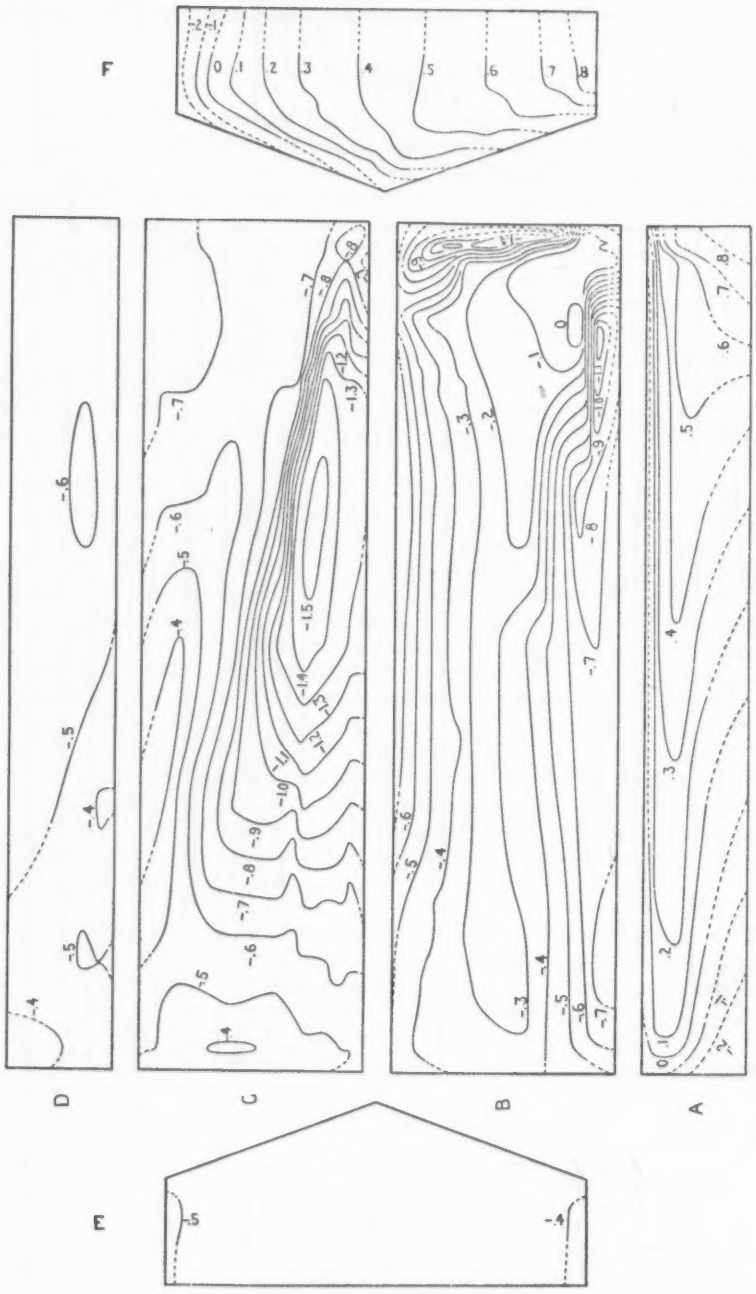

FIGURE 5.—*Distribution of pressure over the model without the monitor, wind at 45° to faces A and F*

See legend of Figure 4

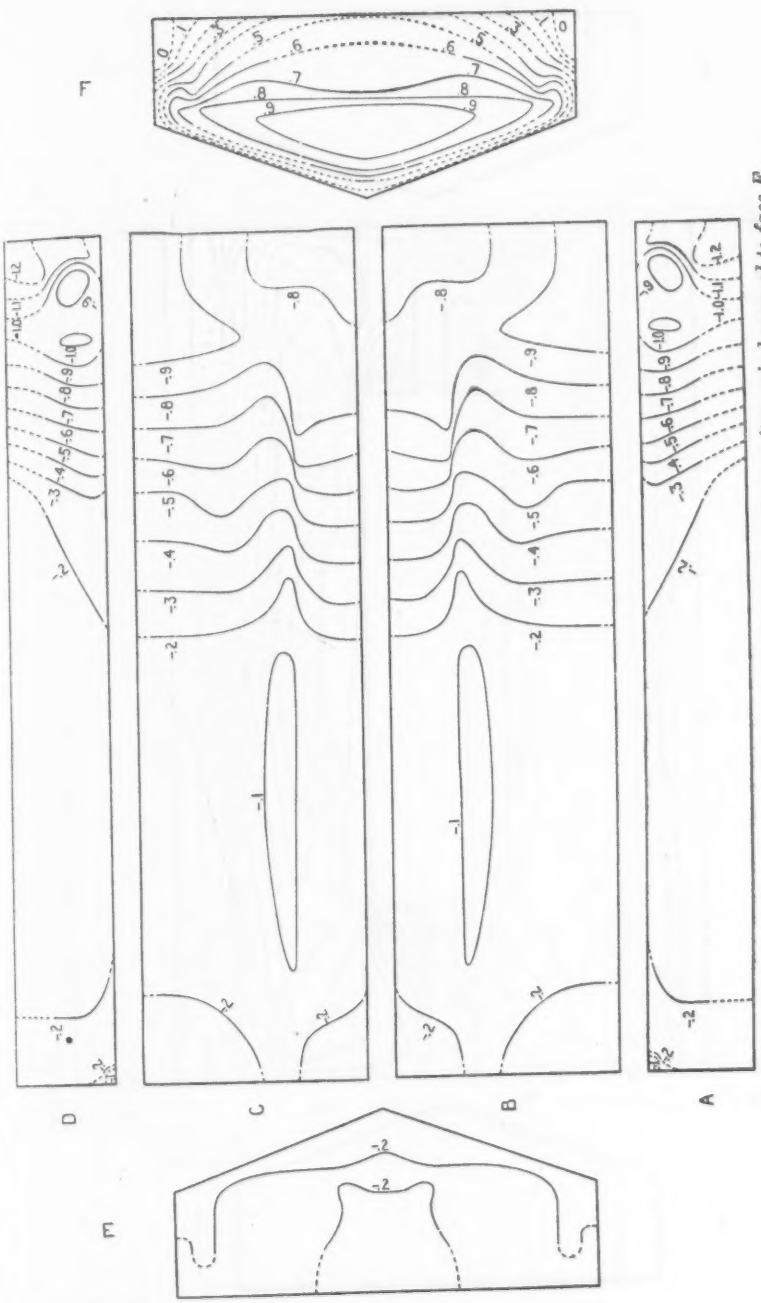

FIGURE 6.—*Distribution of pressure over the model without the monitor, wind normal to face F*

See legend of Figure 4

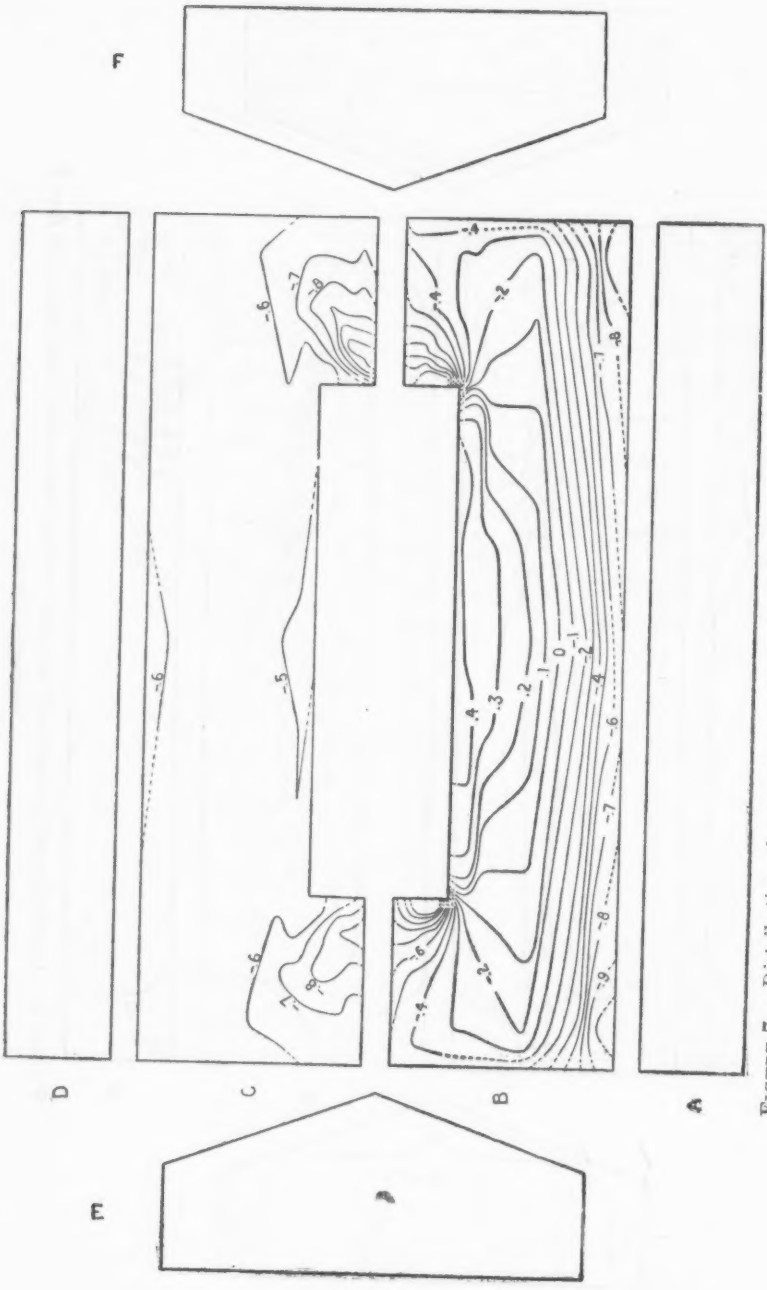

FIGURE 7.—*Distribution of pressure over the model with the monitor, wind normal to face A*

See legend of Figure 4. See also Figure 10

See legend of Figure 4. See also Figure 10

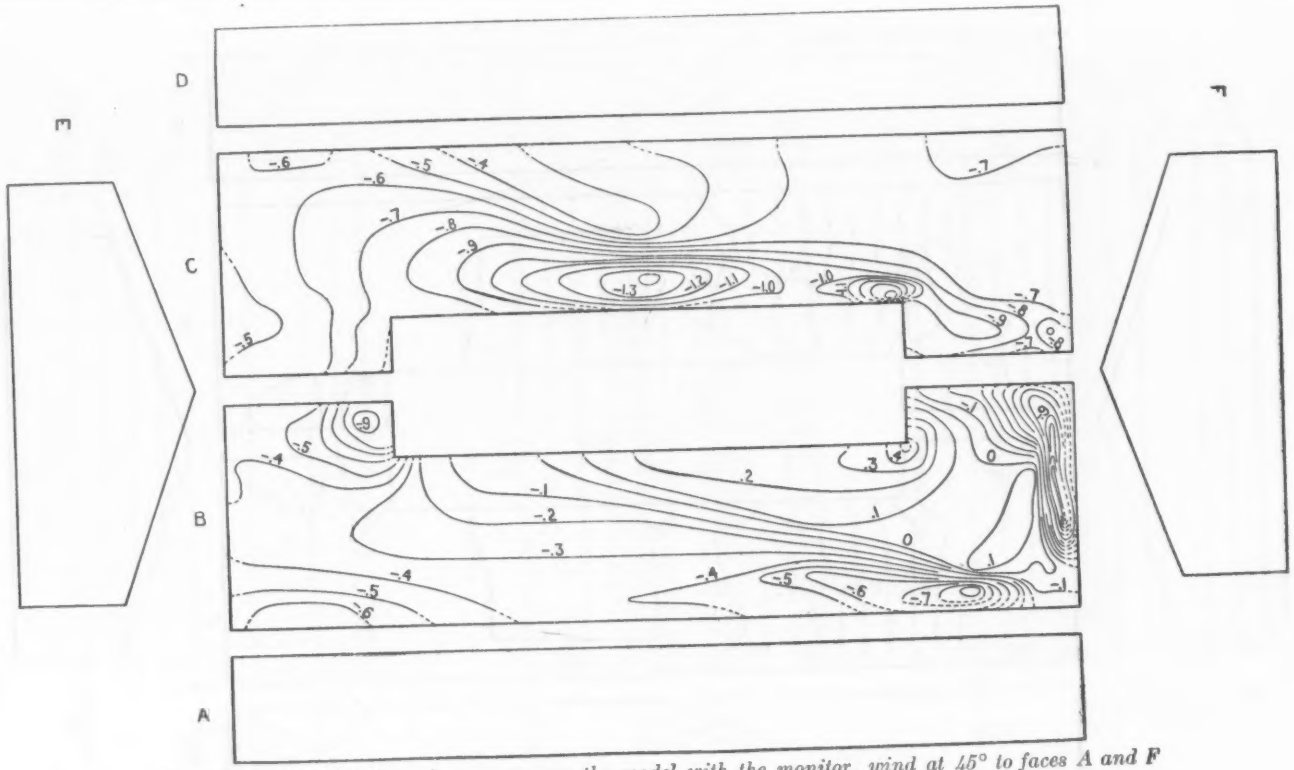

FIGURE 8.—*Distribution of pressure over the model with the monitor, wind at 45° to faces A and F*

See legend of Figure 4. See also Figure 11

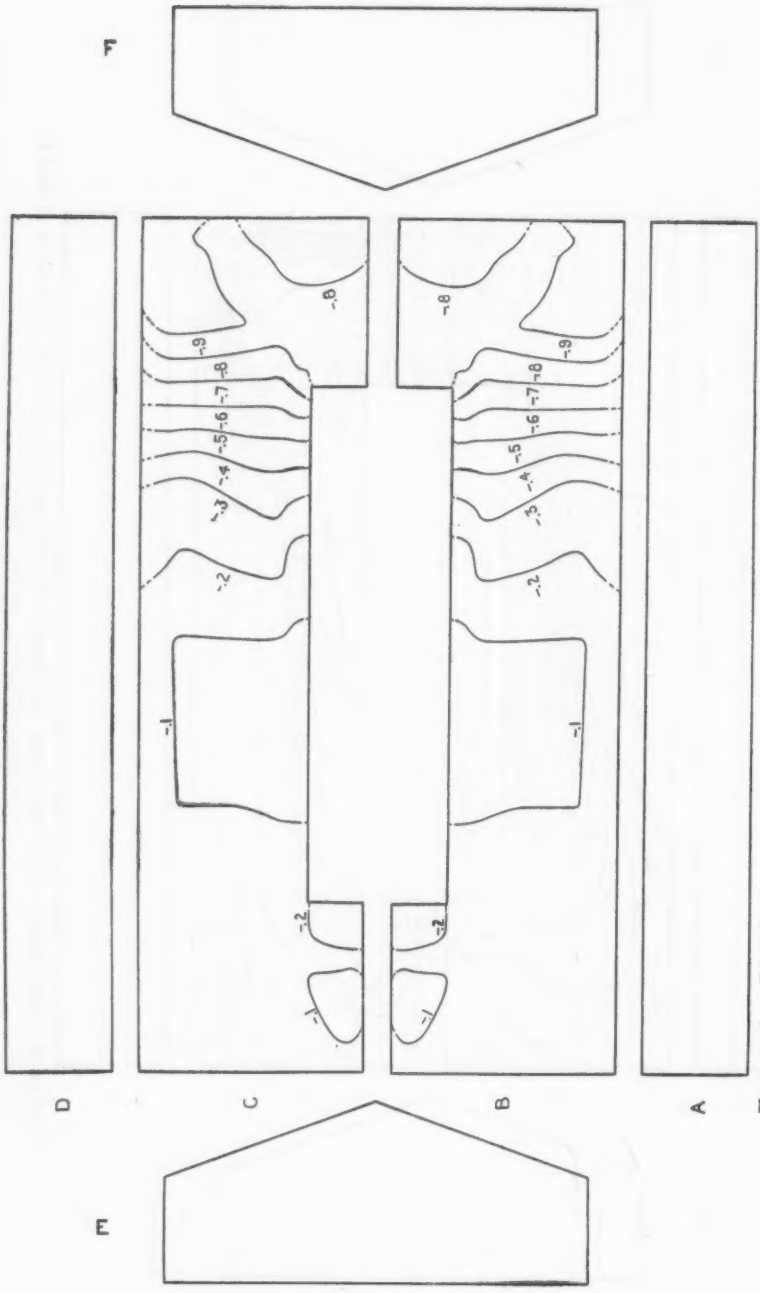

FIGURE 9.—*Distribution of pressure over the model with the monitor, wind normal to face*
See legend of Figure 4. See also Figure 12

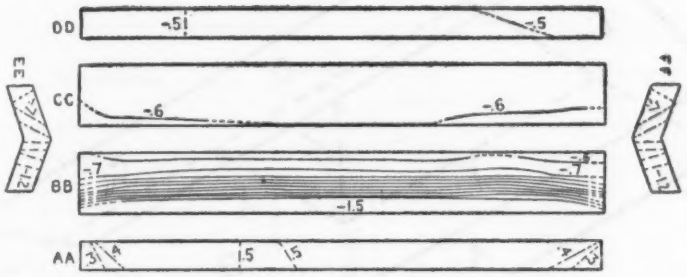

FIGURE 10.—*Distribution of pressure over the monitor, wind normal to face A*

See legend of Figure 4. See also Figure 7

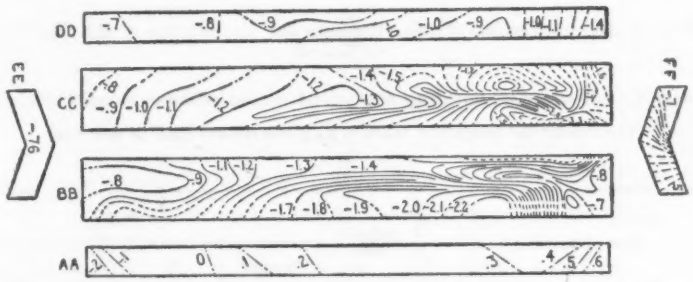

FIGURE 11.—*Distribution of pressure over the monitor, wind at 45° to faces A and F*

See legend of Figure 4. See also Figure 8

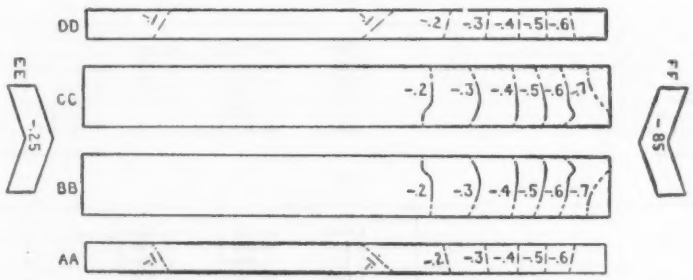

FIGURE 12.—*Distribution of pressure over the monitor, wind normal to face F*

See legend of Figure 4. See also Figure 9

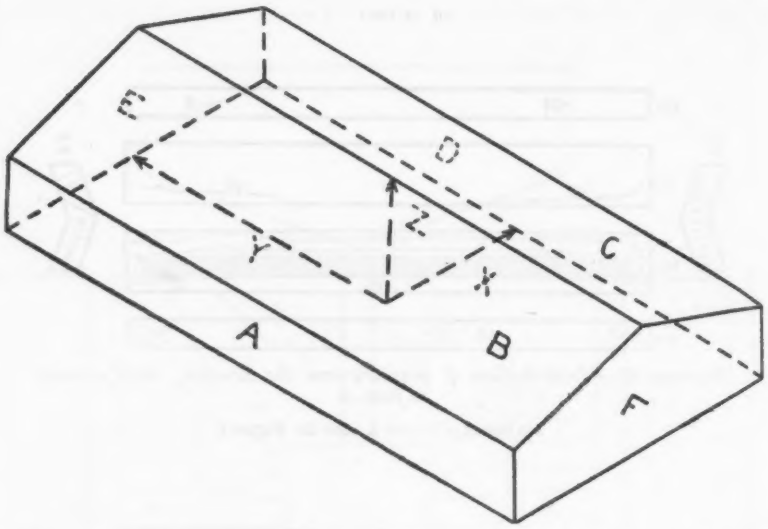

FIGURE 13.—*Direction of reference axes for components of the total force coefficient*

TABLE 4.—*Model mill building at various angles without monitor ventilator*

[The average and component values of p_w/q, and relative areas for each face]

0°

Face of model	Relative area	p_w/q			
		Normal	X	Y	Z
A	1.000	+0.498	+0.498		
B	2.127	−.381	−.130		+0.358
C	2.127	−.563	+.191		+.529
D	1.000	−.518	+.518		
E	.681	−.620		+0.620	
F	.681	−.620		−.620	0

45°

A	1.000	+.255	+.255		
B	2.127	−.441	−.150		+.415
C	2.127	−.774	+.263		+.728
D	1.000	−.517	+.517		
E	.681	−.449		+.449	
F	.681	+.372		+.372	

90°

A	1.000	−.354	−.354		
B	2.127	−.381	−.130		+.358
C	2.127	−.381	+.130		+.358
D	1.000	−.354	+.354		
E	.681	−.265		+.265	
F	.681	+.615		+.615	

TABLE 5.—*Model mill building at various angles with monitor ventilator*

[The average and component values of p_w/q and the relative areas for each face]

0°

Face of model	Relative area	p_w/q			
		Normal	X	Y	Z
A	1.000	+0.498	+0.498		
B	1.805	−.238	−.081		+0.224
AA	.161	+.441	+.441		
BB	.346	−1.026	−.351		+.965
CC	.346	−.560	+.192		+.526
DD	.161	−.488	+.488		
C	1.805	−.584	+.200		+.549
D	1.000	−.518	+.518		
E	.681	−.620		+0.620	
EE	.033	−.913		+.913	
FF	.033	−.913		−.913	
F	.681	−.620		−.620	

45°

A	1.000	+.255	+.255		
B	1.805	−.245	−.083		+.230
AA	.161	+.180	+.180		
BB	.346	−1.312	−.446		+1.234
CC	.346	−1.370	+.466		+1.288
DD	.161	−.938	+.938		
C	1.805	−.691	+.235		+.650
D	1.000	−.517	+.517		
E	.681	−.449		+.449	
EE	.033	−.762		+.762	
FF	.033	−.160		−.160	
F	.681	+.372		+.372	

90°

A	1.000	−.354	−.354		
B	1.805	−.340	−.116		+.320
AA	.161	−.197	−.197		
BB	.346	−.251	−.086		+.236
CC	.346	−.251	+.086		+.236
DD	.161	−.197	+.197		
C	1.805	−.340	+.116		+.320
D	1.000	−.354	+.354		
E	.681	−.205		+.205	
EE	.033	−.250		+.250	
FF	.033	−.850		−.850	
F	.681	+.615		+.615	

TABLE 6.—*Illustration of the computation to give the resultant value of the X, Y, and Z components of the force coefficient for the complete model with monitor ventilator, wind direction 0°*

X component of p_w/q		Y component of p_w/q		Z component of p_w/q	
Face	p_wA/q	Face	p_wA/q	Face	p_wA/q
A	1.000(+0.498) = +0.498	E	0.681(+0.620) = +0.422	B	1.805(+0.224) = +0.404
B	1.805(− .081) = − .146	EE	.033(+ .913) = + .031	BB	.346(+ .965) = + .334
AA	.161(+ .441) = + .441	FF	.033(− .913) = − .031	CC	.346(+ .526) = + .182
BB	.346(− .351) = − .121	F	.681(− .620) = − .422	C	1.805(+ .549) = + .990
CC	.346(+ .192) = + .066		0		+1.910
DD	.161(+ .488) = + .079				
C	1.805(+ .200) = + .361				
D	1.000(+ .518) = + .518				
	+1.696				
Total relative area projected on YZ plane		Total relative area projected on XZ plane		Total relative area projected on XY plane	
A	1.000×1.000=1.000	E	0.681×1.000=0.681	B	1.805×0.940=1.696
B	1.805× .342= .617	EE	.033×1.000= .033	BB	.346× .940= .325
AA	.161×1.000= .161		.714	CC	.346× .940= .325
BB	.346× .342= .118			C	1.805× .940=1.696
	1.896				4.042
Average $F_x/A_{yz}q = \frac{1.696}{1.896} = +0.894$		Average $F_y/A_{xz}q = \frac{0}{0.714} = 0$		Average $F_z/A_{xy}q = \frac{1.910}{4.042} = +0.472$	

TABLE 7.—*The three components of the force coefficients for the entire model*

	Without monitor ventilator			With monitor ventilator		
	0°	45°	90°	0°	45°	90°
$\frac{F_x}{A_{yz}q}$	0.664	0.587	0.000	0.894	0.651	0.000
$\frac{F_y}{A_{xz}q}$	.000	.821	.820	.000	.811	.755
$\frac{F_z}{A_{xy}q}$	.472	.608	.381	.472	.608	.326

The second step is illustrated at length for one case in Table 6. The X, Y, and Z components of the average p_w/q for each face are multiplied by the area of the face relative to face A and the results summed. The areas of projection of the model on the YZ, XZ, and XY planes relative to the area of face A are then computed and the results of the summations are divided by the appropriate areas of projection to give the force coefficients for the X, Y, and Z directions. The components of the total force are denoted by F_x, F_y, and F_z and the actual areas of projection on the YZ, XZ, and XY planes by A_{yz}, A_{xz}, and A_{xy}. The final results for the whole model are given in Table 7.

VI. DISCUSSION

Some of the more striking features of the distribution will be described for purposes of emphasis.

Referring to Figure 4 for 0° (wind normal to face A), the distribution is substantially symmetrical with respect to the XZ plane. The pressure was measured at all of the stations on faces A, B, C, D, and F, but no measurements were made on face E, the results shown for this face being a copy of those for face F. Attention is called to the fact that the lowest pressures occur near the upstream edges of faces B, E, and F and that the pressure rises toward the rear. For face B it then falls again. The pressures over faces C and D show only small gradients. The highest pressures are on the windward face, A, but the largest forces are outward and are found on the end faces, where the average p_w is $-0.62\ q$.

At 45° (fig. 5) the windward faces, A and F, show the highest pressures near the upstream corner, and the pressure falls toward the rear, finally reaching values below the static pressure. The lee faces, D and E, again show nearly uniform values. The distributions over faces B and C illustrate the necessity of having a large number of stations if the distribution is to be accurately determined. The minimum pressures are found near the upstream corner of face B and near the ridge of the roof in face C. The largest force is outward and is found on face C, the average p_w on this face being $-0.77\ q$, but over a fairly large area, p_w, is lower than $-1.3\ q$, and hence that area is subject to forces per unit area nearly double the average for the face.

At 90° (fig. 6) the largest force occurs on the windward face F, the average pressure being $p_w = 0.62\ q$. The lowest pressures on faces A, B, C, and D are again concentrated near the upstream edges and appreciable areas are subject to loads approaching and somewhat exceeding twice the average loading.

A comparison of Figure 7 with Figure 4 shows that when the monitor is placed on the model (the wind being normal to face A) the distribution on face B is greatly modified. The lowest pressure is still near the junction of the roof and the wall, but the pressure changes fairly rapidly to a value of $p_w = 0.2\ q$ near the center and then more slowly to $p_w = 0.4\ q$ near the monitor. There is a great concentration of the contour lines at the corner of the monitor, the pressure changing rapidly from $p_w = 0.2\ q$ to $-1.0\ q$ as the corner is turned. The force on face B is reduced in magnitude by the presence of the monitor, the average pressure changing from $p_w = -0.38\ q$ to $-0.24\ q$.

The effect of the monitor on the distribution on face C at 0° is not so great. The principal change is the building up of a region of reduced pressure between the ends of the monitor and the ends of the building. The effect of these regions is to increase the force on the face by a small amount.

Comparing Figure 8 with Figure 5, with the wind at 45° the effect of the monitor is again to cause the absolute pressure over a considerable area of face B to be greater than the static pressure. The concentrated low pressures near the upstream edges are changed very little. There is a marked reduction in the force on face B, but the existence of the low pressure regions immediately adjacent to high pressure regions represents a rather severe type of loading. The force on face C also is reduced by the presence of the monitor.

The effect of the monitor at 90° (figs. 6 and 9) is very small. It is especially to be noted that the monitor does not in this case build up a region of increased pressure on the windward side.

Figure 10 shows the distribution over the monitor at 0°. The pressure on the windward face is nearly uniform and but little greater than the pressure on the roof of the main building adjacent to it. (Fig. 7.) The pressure on the lee faces of the monitor is nearly constant. The end faces *EE* and *FF* are subject to fairly large forces, the average pressure being $p_w = -0.91\ q$, but the greatest force is on face *BB* where the average pressure is $p_w = -1.03\ q$. The lowest pressures on face *BB* occur near the upstream edge.

At 45°, the pressures on the vertical faces of the monitor (fig. 11) follow in a general way the pressures on the adjacent parts of the roof. Faces *BB* and *CC*, however, show very complicated distributions. The forces on both faces are quite high, $p_w = -1.31\ q$ and $-1.37\ q$, and a minimum pressure of $p_w = -3.3\ q$ is observed on face *CC*. This is the lowest pressure which we have ever observed in measurements of wind pressure. Rather large areas are subject to pressures lower than $p_w = -2.0\ q$.

At 90° (fig. 12) the distribution over the monitor follows in a remarkable way the distribution over the main roof of the building. The most astonishing fact is that the windward face *FF* is subject to a pressure lower than the static pressure. It appears that the air deflected by the front face of the building is swept entirely clear of the monitor.

VII. NUMERICAL EXAMPLES

In order to illustrate the method of utilizing the data, a few numerical examples will be given for an angle of 45° for the complete model with the monitor. It will be assumed that the wind speed is 98 miles per hour as recorded by a Robinson 4-cup anemometer. Table 1 gives the true speed as 75 miles per hour and Table 2 gives the velocity pressure at this true speed as 14.39 lbs./ft.^{2} From Table 7, the *X* force coefficient is 0.651, the *Y* force coefficient 0.811, the *Z* force coefficient 0.608, and, hence, the resultant force on the building may be found by combining a pressure of 9.37 lbs./ft.^{2} on the area of projection on the *YZ* plane, a pressure of 11.70 lbs./ft.^{2} on the area of projection on the *XZ* plane, and a pressure of 8.75 lbs./ft.^{2} on the area of projection on the *XY* plane.

If it is desired to compute the resultant load on an individual face, some estimate must be made of the pressure within the building. By studying the diagrams and considering the probable location of windows and other openings, it appears that the pressure within the building might be anything from $p_w = 0.8\ q$ to $p_w = -1.4\ q$. Table 3 gives the values of p_w/q on the outer surfaces of the building. For example, for face *CC* at 45° with the monitor ventilator, the value given is $p_w = -1.37\ q$ corresponding to an upward force of 19.7 lbs./ft.^{2} at a true speed of 75 miles per hour. If the pressure within the building were $p_w = -1.4\ q$ caused by an open window in the monitor face *DD* (fig. 11), the average pressure on the face would be $p_w = +0.03\ q$, corresponding to a downward force of 0.4 lbs./ft.^{2} at a true speed of 75 miles per hour. If the pressure within the building were $p_w = +0.8\ q$ the differential pressure would be $p_w = -2.17\ q$, corresponding to an upward force of 31.2 lbs./ft.^{2}

VIII. SCALE EFFECT

As previously stated, measurements were made at three speeds, approximately 47, 60, and 80 feet per second. The ratios of the observed wind pressure to the velocity pressure for the three speeds were, in general, in very good agreement, the departure of a single observation from the mean of the three rarely exceeding 0.02. In a few instances in regions where the pressure gradient was very steep and the pressure was unsteady, there were systematic changes with speed. The number of such stations and the area represented by them is so small, however, as to be of no importance in computing the force coefficient. Over the range of speeds covered by the tests, the observations indicate that the scale effect is small.

It is the judgment of the authors that the results obtained on the model can be applied directly to full-scale structures without causing errors of any consequence. At present, this judgment can not be proved experimentally in a direct manner. It is based on studies of the available information, including actual experiments on bodies of many types, and under widely different conditions. The mechanism of scale effect is gradually becoming understood, and the reason for the large scale effect on bodies of rounded form, such as spheres, cylinders, and airship hulls is found in the development of the boundary layer theory. From the same reasoning, it is believed that the scale effect on bodies with sharp edges can not be very large, and is probably absent altogether. The engineer must accept the judgment of the aerodynamical physicist on this point unless he is willing to qualify as an expert in aerodynamics by study and experimentation.

IX. CONCLUSION

The experiments described in the paper show the distribution of pressure over a model mill building, with and without a monitor, when resting on a plane surface with the wind blowing parallel to the surface and at 0°, 45°, and 90° to the end of the building. The greatest wind loading occurred when the wind was at 45° to the walls. The loads on the roof of the monitor were greater than those on the roof of the main building, and were directed outwardly. The loads on appreciable areas of a face were often as great as twice the average over the entire face.

WASHINGTON, February 14, 1931.

STABILIZATION OF BORIC ACID BUFFERS BY AERATION

By Edna H. Fawcett and S. F. Acree

ABSTRACT

This paper describes a method of stabilizing the commonly used $M/20$ boric acid-$M/20$ potassium chloride-sodium hydroxide buffer mixtures by aerating them with ordinary fresh air until they reach a state of equilibrium with atmospheric CO_2.

A series of buffers ranging from pH 7.8 to pH 11.65 were prepared, and their values determined electrometrically. These buffers were then aerated until no further change in pH could be detected on repeating the electrode tests.

A table is given showing the initial pH readings and the changes in pH at different intervals of time during the aeration process.

Curves were plotted both from the initial and from the final series of readings, and are shown in a text figure.

Air-stable $M/20$ buffer standards of any desired pH may be prepared by adding the required volumes of $N/5$ NaOH read from the "equilibrium curve" to 50 ml portions of the $M/5$ H_3BO_3-KCl buffer mixture, diluting to 200 ml and aerating the resulting solutions for the periods of time shown to be necessary. From 2 to 6 days are required to reach equilibrium according to the pH of the $M/20$ buffer.

The alkaline limit for air-stable $M/20$ boric acid buffers is pH 9.4.

The ionization constant of boric acid was calculated from the data and found to be $Ka=0.75\times10^{-9}$.

CONTENTS

		Page
I.	Introduction	757
II.	Method of pH measurement	758
III.	Preparation of solutions	758
IV.	Method of aeration	759
V.	Calculation of the ionization or activity constant of boric acid	762
VI.	Summary	763

I. INTRODUCTION

The need for stable buffers for colorimetric pH measurements in the alkaline range, pH 8 to 10, suggested the possibility of stabilizing the usual $M/20$ boric acid-$M/20$ potassium chloride-sodium hydroxide buffer mixtures, which have been found unsatisfactory in general practice because of their change in the acid direction upon standing. Since preliminary observations [1] had shown this change to be due to the action of atmospheric CO_2 and since it is impossible to prepare any carbonate-free buffer mixture in the alkaline range which would not be so affected, it was suggested by us earlier to add calculated mixtures of alkali-carbonate-bicarbonate to keep the buffer air stable at a given pH or to aerate it completely during the pH adjustment. The attempt, has, therefore, been made to bring a series of boric acid buffers covering the above range into equilibrium with the CO_2 of the air by aeration. The buffers were desired for use as pH standards,

[1] This series: Fawcett, Edna H., and Acree, S. F., J. Bact., **17**, p. 163-204; 1929. Acree, S. F., and Fawcett, Edna H., J. Ind. Eng. Chem., **2**, p. 78-99; 1930.

and especially for experiments to be reported in another article on the salt errors or changes in activities of indicators and buffers as the latter are diluted from $M/1$ to $M/10{,}000$.

II. METHOD OF pH MEASUREMENT

All pH determinations were made on the Acree double hydrogen electrode by using as a standard a $M/10$ sodium acid phthalate solution which had been carefully checked against a calomel cell. The readings were sharp in nearly every determination made and accurately reproducible. Only in the case of the last two or three buffers at the alkaline end of the series was there any tendency for the readings to "run down" owing to driving out of CO_2 under partial pressure by the rapidly bubbling hydrogen, and this change was not more than about 1 mv. in 10 minutes after equilibrium had been reached. Five minute readings, therefore, were accepted in these cases, since we have found this amount of time sufficient for attaining equilibrium with this apparatus when the electrodes are fully saturated in the beginning.

The initial pH curve for the unaerated solutions was extended beyond the usual range for boric acid buffer-standards in order to determine the limit of the buffering power of boric acid against carbonates in equilibrium with atmospheric CO_2 by aeration and at the same time determine how far in the alkaline direction a series of air-stable buffers might be prepared by this method.

III. PREPARATION OF SOLUTIONS

The buffers used in preparing the solutions were C. P. chemicals recrystallized as stated in Tables 1 and 2. The $N/5$ sodium hydroxide was carefully compared with a standard sample of potassium-acid phthalate furnished by the National Bureau of Standards. Two different samples of boric acid (designated as 1 and 2) and two different samples of potassium chloride (likewise designated as 1 and 2) were recrystallized three different times, the different recrystallizations being designated as *a*, *b* and *c*. $M/5$ solutions of these compounds were made up from the different crops of crystals for use in determining the effect of the number of recrystallizations on the pH values. Solution labeled 1 *b*, for example, is made from sample 1 of boric acid and sample 1 of potassium chloride, each recrystallized twice (*b*). The $M/20$ borate buffers were then made up by adding graded volumes of $N/5$ sodium hydroxide to 50 ml portions of any of these solutions as desired and diluting to 200 ml. Double distilled, CO_2-free, pH 7 water was used in making all these solutions. Table 1 shows agreement, in the few comparative tests made, between pH readings on buffer mixtures representing the different samples of salts in the various stages of purification, but with additions of equal quantities of the $N/5$ NaOH. The pH values for the $M/5$ boric acid-potassium chloride solutions without added alkali were determined with isohydric indicators and in one instance also with the hydrogen electrode. Colorimetric and electrometric values agree as closely as can be expected of such weakly acid solutions and further confirm the purity of the chemicals. The isohydric indicator method is better than the electrometric procedure for such cases.[2]

[2] Fawcett and Acree, J. Bact., **17**, p. 163; 1929. J. Ind. Eng. Chem., Anal. ed., **2**, p. 78; 1930.

TABLE 1.—*Agreement in pH Values of Solutions of Different Samples of Boric Acid and Potassium Chloride*

Samples	Recrystallized	ml M/5 NaOH	Color pH	ml N/5 NaOH	Electric pH
1-*a*	Once	15	8.7		
1-*b*	Twice	15	8.7	40	9.61
2-*b*	do	15	8.7		
2-*c*	Three times	15	8.7	40.	9.62
1-*a*	Once	None.	5.0	None.	4.87 to 5.18
1-*b*	Twice	None.	5.0		
2-*b*	do	None.	4.8		
2-*c*	Three times	None.	4.8		

Table 2 and curve *A* in Figure 1 give the pH values of the series of unaerated *M*/20 buffers prepared from solutions 1–*a*, 1–*b*, and 2–*c* (series I, II, and III). The pH readings fall somewhat lower in every instance than the values given by another worker and shown in curve *C* of Figure 1.[3]

IV. METHOD OF AERATION

The graded series of boric acid solutions were aerated in the following way: A stream of fresh air from the pressure cock was led through (1) a side arm flask filled with absorbent cotton to remove possible dust or grease from the air and (2) through a flask of distilled water to take up moisture and lessen evaporation of the buffer, and thence into the aeration bottle containing the buffer solution through which it was allowed to bubble freely. The level of the liquid in the bottle was marked and the loss, which was small, was made up from time to time by addition of pure distilled water. Table 2 shows the change in pH on aeration at different points on the curve and the length of time required to bring the buffers to air-equilibrium. In Series I checks were made daily in order to ascertain how long aeration would have to be carried on to accomplish this result. In Series II determinations were not made until the fourth day with subsequent checks to discover any further change. It will be noted that the more alkaline the buffer the greater the change in pH and also that the changes and attainment of equilibrium are very slow at the alkaline end of the series after the first rapid falling off has taken place. The fact that the "equilibrium" pH curve tends to become nearly a straight line at 50 ml buffer to 50 ml alkali in contrast to the very rapid rise at this point in the other curve giving initial measurements on the unaerated solution (see fig. 1) shows that boric acid reaches its practical limit as a buffer for carbonates in this region; that is, at about pH 9.4.

[3] Clark and Lubs, J. Bact., **2**, pp. 1, 109, 191; 1917. Clark, Determination of Hydrogen Ions. Williams & Wilkins, Baltimore.

TABLE 2.—*Change of pH of M/20 boric acid buffers upon aeration*

Series I (COMMERCIAL BUFFERS ONCE RECRYTSALLIZED, 1-*a*)

No. of ml M/5 NaOH to 50 ml M/5 H_3BO_3—KCl	Initial pH of M/20 buffers	pH readings after aeration				
		1 day	2 days	3 days	4 days	5 days
3	7.80	7.78	7.76	7.78		
15	8.63	8.55	8.52	8.53	8.53	
25	9.03	8.96	8.88	8.85	8.84	
40	9.64	9.45	9.30	9.22	9.13	9.10
47	10.01	9.63	9.36		9.26	9.26

Series II (COMMERCIAL BUFFERS TWICE RECRYSTALLIZED, 1-*b*)

No. of ml M/5 NaOH to 50 ml M/5 H_3BO_3—KI	Initial pH of M/20 buffers	pH readings after aeration						pH readings after standing	
		4 days	5 days	6 days	8 days	11 days	17 days	Time elapsed	pH
								Weeks	
5	8.01	7.95				7.96		3	7.97
15	8.67		8.55		8.55			2	8.54
25	9.00		8.72?			8.85		3	8.86
35	9.37		9.02			9.05		3	9.06
40	9.61		9.14		9.14			2	9.15
47	10.00		9.24			9.24		6	9.24
50	10.37	9.32	9.34	9.31			9.24	6	
52	11.03	9.39	9.38	9.34			9.29	6	
55	11.30	9.43	9.39	9.38			9.34	6	9.36
60	11.65	9.53	9.49	9.43			9.37	6	9.40

Series III (COMMERCIAL BUFFERS RECRYSTALLIZED THREE TIMES, 2-*c*)

No. of ml M/5 NaOH to 50 ml M/5 H_3BO_3—KCl	Initial pH of M/20 buffers	pH readings after aeration			pH after standing		pH on further aeration	
		2 days	3 days	5 days	Time elapsed	pH	Time aerated	pH
					Weeks		*Hours*	
8.6	8.29	8.21			6	8.28	18	[1] 8.24
11.75	8.50		8.43		6	8.47	18	[1] 8.40
16.25	8.71	[1] [2] 8.6			6	8.64		
23.00	8.97	[1] [2] 8.8			6	8.83		
32.00	9.28			[2] 9.0	6	9.04	3	[1] 8.99
44.25	9.82			[2] 9.2	6	9.25	18	9.28
60.00	11.51			[2] 9.4	6	9.46	18	9.36

[1] Aerated with a porous alundum thimble.
[2] These readings were made colorimetrically against color standards prepared the same day from buffers which had been checked two days previously.

Hydrogen electrode measurements were made on this entire series with two exceptions after the buffers had stood for varying periods of time in Pyrex bottles closed with rather poorly fitting ground-glass stoppers. The last column in Table 2 shows how great a degree of stability these aerated buffers possess and indicates the practicability of the method.

Series III, Table 2, represents an attempt to prepare a set of aerated boric acid buffers graded in steps of 0.2 pH from pH 8.2 to pH 9.4 by the use of curve *B*. (Fig. 1.) The amounts of *M*/5 NaOH given in column 1 were read from this curve (*B*) and added

to the H_3BO_3-KCl mixture (2−c) as in Series I and II. The pH readings obtained after aeration and given in columns 3, 4, and 5 show that the desired values can be easily obtained by this method. These data are all the more valuable because Series III was prepared from different samples of chemicals and the readings on the unaerated (column 2) and aerated buffers fit in to curves *A* and *B* plotted originally from Series II as is shown in the figure.

The variations from the even intervals found in the last two columns are due partly, no doubt, to experimental error in making quantitative

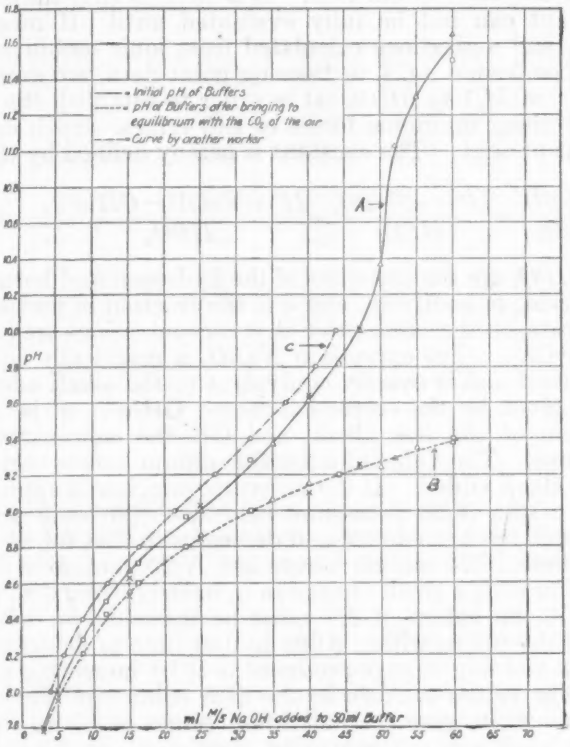
Initial pH of Buffers
pH of Buffers after bringing to equilibrium with the CO_2 of the air
Curve by another worker
A
B
C
pH
ml M/5 NaOH added to 50ml Buffer

Figure 1

× ---------- Series I, Table 2.
△ ---------- Series II, Table 2.
□ ---------- Series III, Table 2.

measurements either in preparing the buffer mixtures or at the electrode, but may also be partially explained by a difference in temperature, which is not corrected for in the colorimetric readings, or to variation in barometric pressure which would affect slightly the amount of CO_2 dissolved in the solutions and hence the pH. It is also probable that the buffers had not completely reached equilibrium in some instances and hence changed in the acid direction on further aeration as the figures in the last column seem to show with one exception. In any case the changes are far less than those taking place in unaerated buffers in this pH range. A carefully prepared

set of color standards containing thymol blue which had stood six weeks showed no perceptible change when compared with a fresh set made from the same buffers.

V. CALCULATION OF THE IONIZATION OR ACTIVITY CONSTANT OF BORIC ACID

The above pH measurements on the unaerated solutions can be used to calculate the ionization constant of boric acid within 5 per cent under the stated conditions. It is obvious that the exact ionization constant can not be fully evaluated until pH measurements, viscosities, and ionizations calculated from ionic mobilities and conductivities or from e. m. f. or freezing point data, are determined for solutions from $M/1$ to $M/10{,}000$ in order to establish the magnitude of the disturbing interionic forces or salt errors. Such data are not available at present. The constant is hereby defined by the equation

$$Ka=\frac{H^+\times B\bar{O}_2}{HBO_2}=\frac{H^+\times \alpha NaBO_2}{HBO_2}=\frac{H^+\alpha(\mathrm{NaOH}-OH/\alpha')}{HBO_2}$$ in which H^+, $B\bar{O}_2$, and HBO_2 are the activities of the hydrogen and borate ions and free boric acid, respectively, and α is the fraction of ionization of the sodium borate, on the assumption that concentrations are proportional to the activities. The expression $NaBO_2$ is practically equivalent to the alkali used and is exactly equivalent to the alkali added less the free alkali given by the correction factor OH/α'. α' is the fraction of ionization of the free alkali, and OH the concentration of the hydroxyl ions. The value of α for the sodium borate varies with the amount of alkali added. If the isohydric principle is applied, α is the ionization of the $N/20$ potassium chloride-$N/20$ boric acid solution when no alkali has been added and decreases to that for an $N/10$ solution when both $N/20$ sodium borate and $N/20$ potassium chloride are present. For such a small change in α, namely, from 0.83 to approximately 0.77, the values of H^+ must be measured to within 1 or 2 per cent or the pH to within 0.005 to 0.01 unit to determine the real value of Ka and any change produced in it by increasing salt concentration. The values of Ka/α in the fifth column of Table 3 are not constant enough to give the individual values of Ka to within 1 per cent. The work was not controlled closely enough for this purpose, but rather for practical uses to within 0.02 to 0.03 pH unit. We see, however, that the values of Ka/α show a maximum variation up and down of about 7 or 8 per cent and a mean deviation of 3 or 4 per cent from an average of 1×10^{-9}. In calculating the values of Ka/α in column 5 the actual experimental data were used, and it was assumed that the weight of the boric acid used should require 50 ml. of alkali for exact neutralization. If the data for $NaBO_2$ and HBO_2 are taken from the smooth curve A of Figure 1 the values of Ka/α given in column 6 are slightly lower than those in column 5. The values for Ka/α are calculated from curve C and are given in column 7 for comparison. It would seem from inspection of the data in column 5 that the value of Ka/α lies between 0.9 and 1×10^{-9}. A few calculations have shown that the amount of alkali required to give any desired pH will vary 5 per cent with use of these two constants in the ionization equation given above. This is larger than the experimental

error, and it would seem that a value around 0.95×10^{-9} is to be preferred. As the average value of α in this range is about 0.80 we can use $Ka=0.75\times10^{-9}$ for the present.

TABLE 3.—*Ionization constant of boric acid*

pH	H^+	$NaBO_2$	HBO_2	$10^{+9}\times Ka/\alpha$ from—		
				Actual data	Smooth Curve A	Curve C
7.8						0.887
8.0	10×10^{-9}	0.005	0.04575	1.110	1.056	.870
8.2	6.31×10^{-9}	.00725	.04350	1.070	1.060	.841
8.3	5.13×10^{-9}	.00860	.04215	1.065		
8.4	3.98×10^{-9}	.01016	.04059	1.015	1.001	.821
8.5	3.16×10^{-9}	.01175	.03900	.971		
8.6	2.51×10^{-9}	.0137	.03705	.948	.918	.793
8.8	1.585×10^{-9}	.0185	.03225	.931	.910	.773
9.0	1.000×10^{-9}	.0250	.02575	1.000	.934	.748
9.2	6.31×10^{-10}	.0306	.02015	.995	.927	.723
9.28	5.25×10^{-10}	.032	.01875	.933		
9.4	3.98×10^{-10}	.0356	.01515	.984	.885	.708
9.6	2.51×10^{-10}	.03975	.01100	.974	.882	.704
9.8	1.585×10^{-10}	.0436	.00715	1.080	.966	.703
9.82	1.515×10^{-10}	.04425	.00650	1.040		
10.00	1.000×10^{-10}	.047	.00375	(1.26)	1.027	.718
Average Ka/α				1.02×10^{-9}	0.96×10^{-9}	0.78×10^{-9}
If $\alpha=0.8$, Ka				0.8×10^{-9}	0.75×10^{-9}	0.62×10^{-9}

VI. SUMMARY

The commonly used $M/20$ boric acid-$M/20$ potassium chloride-sodium hydroxide buffer mixtures can be stabilized by aerating them with ordinary fresh air until they reach a state of approximate equilibrium with atmospheric CO_2.

Air-stable $M/20$ buffer standards of any desired pH may be prepared with an accuracy within 0.05 pH by adding the required volumes of $N/5$ NaOH read from the "equilibrium curve" to 50 ml portions of the $M/5$ H_3BO_3-KCl buffer mixture, diluting to 200 ml and aerating the resulting solutions for the periods of time shown to be necessary. From 2 to 6 days are required to reach equilibrium according to the pH of the $M/20$ buffer. With the position of the equilibrium curve B now established, air-stable buffers of desired pH values can be prepared quickly by trial use of calculated bicarbonate-carbonate mixtures, or of pure carbon dioxide gas or of air under pressure sprayed into the liquid through an alundum thimble, followed by brief aeration with normal air.

The practical alkaline limit for air-stable $M/20$ boric acid buffers is about pH 9.4.

The ionization constant of boric acid was calculated from the data and found to be about $Ka=0.75\times10-^{9}$.

WASHINGTON, February 7, 1931.